Seismic Design of Core-Wall Systems for Multi-Storey Timber Buildings

By

Andrew J. M. Dunbar

Supervised by Professor Andrew H. Buchanan and

Professor Stefano Pampanin

A thesis submitted in partial fulfilment of the requirements for the

Degree of Master of Engineering in Earthquake Engineering

Department of Civil and Natural Resources Engineering

University of Canterbury

Private Bag 4800

Christchurch, New Zealand

February 2014

ABSTRACT

This thesis discusses the results of experimental tests on two post-tensioned timber core-walls, tested under bi-directional quasi-static seismic loading. The half-scale two-storey test specimens included a stair with half-flight landings.

Multi-storey timber structures are becoming increasingly desirable for architects and building owners due to their aesthetic and environmental benefits. In addition, there is increasing public pressure to have low damage structural systems with minimal business interruption after a moderate to severe seismic event.

Timber has been used extensively for low-rise residential structures in the past, but has been utilised much less for multi-storey structures, traditionally limited to residential type building layouts which use light timber framing and include many walls to form a lateral load resisting system. This is undesirable for multi-storey commercial buildings which need large open spaces providing building owners with versatility in their desired floor plan. The use of Cross-Laminated Timber (CLT) panels for multi-storey timber buildings is gaining popularity throughout the world, especially for residential construction.

Previous experimental testing has been done on the in-plane behaviour of single and coupled post-tensioned timber walls at the University of Canterbury and elsewhere. However, there has been very little research done on the 3D behaviour of timber walls that are orthogonal to each other and no research to date into post-tensioned CLT walls.

The “high seismic option” consisted of full height post-tensioned CLT walls coupled with energy dissipating U-shaped Flexural Plates (UFPs) attached at the vertical joints between coupled wall panels and between wall panels and the steel corner columns. An alternative “low seismic option” consisted of post-tensioned CLT panels connected by screws, to provide a semi-rigid connection, allowing relative movement between the panels, producing some level of frictional energy dissipation.

ACKNOWLEDGEMENTS

I would like to start by acknowledging the Department of Civil and Natural Resources Engineering, for the opportunities presented to me throughout my undergraduate and post-graduate studies. Specifically, I would like to thank my supervisors Prof. Andy Buchanan, Prof. Stefano Pampanin and, who have enabled me to partake in cutting-edge research. I would also like to thank Dr. David Carradine who started out as my primary supervisor.

To technical staff, Russel McConchie, Gavin Keats, Peter Coursey and John Maley, your technical ideas, tempered with practicality, have greatly contributed to the advancement of my research. I have valued your practical input and good humour.

The financial support of the Structural Timber Innovation Company (STIC) and Jim Rutherford, for providing the Ada Rutherford scholarship in Architectural Engineering, is gratefully recognized. Without the support of STIC, Jim and the University of Canterbury our experimental program would not have been possible.

Finally I would like to thank family, especially my Mother, Father and Brother, whom supported and encouraged me throughout my university studies. To my partner Jamie, thank you for your love, support and baking that kept me going through this thesis.

CONTENTS

LIST OF FIGURES

LIST OF TABLES

1 INTRODUCTION

1.1 Overview

Multi-storey timber structures are becoming increasingly desirable for architects and building owners due to their aesthetic and environmental benefits. In addition, there is increasing public pressure to have low damage structural systems with minimal business interruption after a moderate to severe seismic event.

Timber has been used extensively for low-rise residential structures in the past, but has been utilised much less for multi-storey structures. The use of timber in multi-storey construction has traditionally been limited to residential type building layouts which include many walls to form a lateral load resisting system. In Europe and North America, cross-laminated timber (CLT) is increasingly being used for houses and apartments, with buildings up to 9-storeys. A similar CLT apartment building has also been constructed in Melbourne to 10-storeys. The structural layouts associated with apartment and residential type structures are not suitable for the New Zealand market, where multi-storey commercial buildings are usually characterised by large open spaces. This provides building owners with versatility in their desired floor plan.

The post-tensioned timber structural system (Pres-Lam) provides a viable solution to achieving multi-storey timber buildings with large open spaces. The Pres-Lam system was adapted from concrete to timber by the University of Canterbury (Palermo et al. 2005) in a research program lead by the Structural Timber Innovation Company (STIC) research consortium. This system utilises prefabricated timber beam, column and wall elements connected by un-bonded post-tensioned steel tendons and dissipater devices. The Pres-Lam system allows there to be large displacements and ductility with minimal residual damage. This is achieved by "controlled rocking" at critical sections in the structure, in which all inelastic action is concentrated, such as at the base of a wall or beam-column joint. The timber elements remain elastic, while un-bonded post-tensioned tendons supply the restoring force. Energy dissipation is achieved by replaceable dissipation devices.

As part of this research, options will be provided for architects and engineers to utilise timber walls around stairwells and lift shafts. To date, little research has been done on timber stairwell and lift shaft cores (especially for the Pres-Lam system) and how they are incorporated into the lateral load resisting system of a structure. Commonly in multi-storey commercial buildings, the stairwell and lift-shaft cores are used as the main lateral load resisting elements.

This thesis focuses on practical issues in implementing timber core walls as opposed to obtaining a seismically optimal solution. The design recommendations are based on the quasi-static tests on two 1/2 scale test specimens. Design guidance for a simple case-study building is provided.

1.2 Research motivation and objectives

The key objective of this research is to provide structural engineers and architects with options for CLT walls used around stairwells and lift shafts. To achieve the overall objective, it is considered necessary to investigate the following points:

1. Architects' preferred layouts of stairwells and lift shafts.
2. The structural options for straight walls, L-shaped walls, and C-shaped walls and core walls.
3. The recommended structural analysis methods for these walls.
4. The best arrangements for locating and anchoring post-tensioning tendons in CLT walls.
5. The options for connections between walls and foundations, between coupled walls and connecting dissipation devices.
6. Options for timber stairs and landings, and their fixings.

1.3 Thesis outline

Chapter 2 provides the research background for this thesis. Current research for CLT systems from Europe and North America are investigated and some disadvantages of this system are described. The Pres-Lam system from development to continuing research is described. A number of real building cases were investigated with the aim of determining common trends in the structural layouts of multi-storey buildings.

Chapter 3 summarises the general design procedure of post-tensioned CLT walls with and without energy dissipation devices. The geometry, connection details, and material properties of the High Seismic and Low Seismic test specimens are described. Furthermore, the stairs and landings, and the loading beams, are also detailed.

Chapter 4 outlines the construction of the High Seismic and Low Seismic test specimens. The general construction of the two test specimens is described in addition to the components associated with each specimen.

Chapter 5 describes the experimental testing procedure of the two test specimens. The details of the test apparatus and loading protocols are given.

Chapter 6 provides the test results for the High Seismic and Low Seismic specimens. The global response of the system is shown along with the behaviour of the post-tensioning strand, wall panels, and loading beams. Observed damaged for each test specimen is described.

Chapter 7 shows simplified analytical models used to predict the response of the High Seismic and Low Seismic specimens. These models were refined based on the experimental results.

Chapter 8 provides design guidance for implementing post-tensioned CLT core-walls. A case-study building is designed with a Low Seismic system and a High Seismic system using displacement-based design and the design procedure outlined in Chapter 3.

In Chapter 9, the thesis is concluded and recommendations for future research are made. In addition, design guidance is provided for building designers.

2 LITERATURE REVIEW

2.1 Light Timber Frame Construction

Traditionally, light timber frame construction has been the main construction method for Timber structures in New Zealand. It is extensively used for residential low-rise buildings, up to three or four storeys. In this system, many walls and partitions are required to form the lateral load resisting system. The walls consist of plywood or particle board sheeting nailed or screwed to sawn timber joists. The design of these systems is most commonly through the use of prescriptive codes for buildings up to 2 storeys (NZS3604:2011). Figure 2-1 shows two light timber frame buildings, one under construction and one completed.

Figure 2-1: Traditional timber construction for a) a typical residential building and b) the old parliament building in Wellington built 1876

Experimental studies examining the behaviour of plywood shear walls were undertaken by Deam (1997). This study, among others, showed that plywood shear walls worked well in terms of collapse prevention of a building during an earthquake. Some level of ductility is achieved with plywood shear walls, although stiffness degradation and pinching in the hysteretic behaviour is observed, as can be seen in Figure 2-2. In addition to this, residual deformation is likely to occur, which would result in costly repairs.

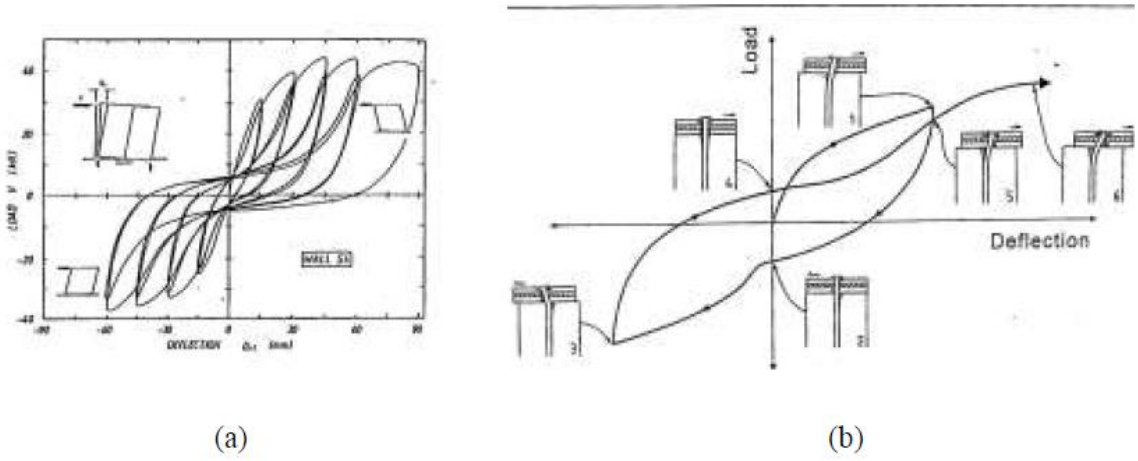

Figure 2-2: Typical hysteretic behaviour of plywood shearwalls (Deam, 1997)

2.2 Performance-Based Design

Seismic events around the world (Northridge 1994 and Kobe 1995) and, more recently, in New Zealand (Darfield 2010 and Christchurch 2011) have highlighted the necessity for a shift towards more performance-based structural engineering. Performance-based seismic design explicitly determines how a building is likely to perform, given the potential hazard it is likely to experience. Performance-based design incorporates uncertainties in the level of the potential hazard and the probability of occurrence of an event over the life of the building. It also enables building owners and designers to gain a realistic understanding of the risk of casualties, occupancy interruption and business downtime that may result from a moderate or large seismic event. In contrast to prescriptive design approaches, where a building can be designed following a set of prescribed guidelines, performance-based design provides a systematic methodology for assessing the performance capability of a building. It can be used to verify the equivalent performance of alternatives, deliver standard performance at a reduced cost, or confirm higher performance needed for critical facilities such as Hospitals (Applied Technology Council (2006)). Generally, structures in Christchurch exposed to the Darfield 2010 and Christchurch 2011 events satisfied primary life safety objectives. However, many buildings were badly damaged, requiring costly and timely repairs and, in many cases, demolition. The post-earthquake costs that are associated with these earthquakes are being deemed unacceptable by building and business owners (Hare et al. 2012). Recommendations were made following the Northridge and Kobe earthquakes to move towards a performance-based design philosophy (SEAOC, 1995). The performance-based objective matrix, (Figure 2-3), outlines the proposed shift in performance levels. Under current design standards for a design level earthquake (1/475 year), a building must prevent loss of life, but it is accepted that it would

be damaged beyond repair. The proposed shift in objectives demands for a structure to be operational with only minor repairable damage following the design level earthquake, and provide life safety following the maximum credible earthquake.

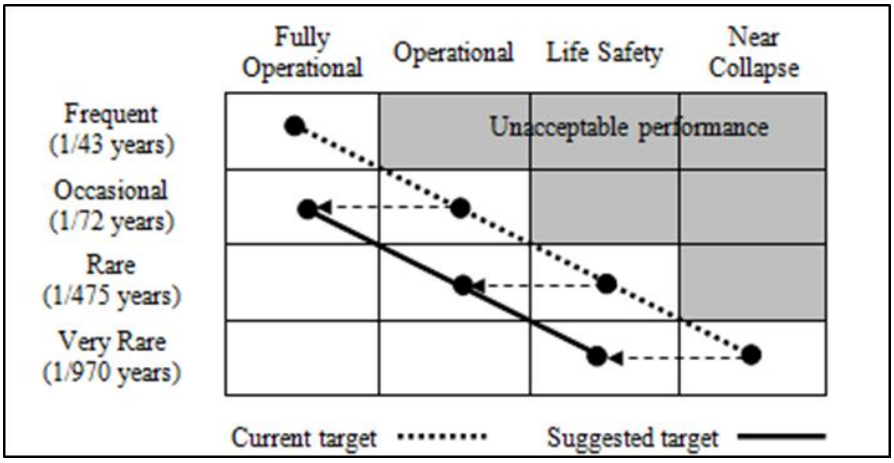

Figure 2-3: Performance-based seismic engineering design objective matrix (after SEAOC, 1995)

The research outlined in this document investigated timber walls using a performance-based frame-work. Emphasis was placed on providing solutions that will incur minimal business downtime and reduce the need for extensive repairs or demolition following a moderate or large seismic event (Pampanin et al. 2002).

2.3 PRESSS Technology

Technology developed in the precast concrete industry under the PREcast Seismic Structural System (PRESSS) program at the University of California, San Diego (Priestley 1996, Conley et al. 2002), has enabled new solutions for a damage avoidance structural system. Frame and Wall systems were developed with a focus on inelastic deformation at member joints with a number of connection details. One connection type, the Hybrid connection, consists of partially un-bonded mild steel reinforcement and un-bonded post-tensioning tendons. Energy dissipaters increase ductility and seismic energy absorption of the structure, reducing the displacement demand on the system. The combination of re-centering and energy dissipation is illustrated in Figure 2-4 for a beam column joint (Palermo et al. 2005). The bi-linear elastic response of the tendons and the inelastic response of the dissipaters act together to produce a "flag shaped" hysteresis associated with rocking systems.

The PRESSS system allows there to be large displacements with minimal residual damage. This is achieved by "controlled rocking" at critical sections in the structure, in which all inelastic action is concentrated, such as at the base of a wall. Therefore, the system can be designed such that under large displacements, a brittle failure mechanism will not be activated. The controlled rocking behaviour,

coupled with Displacement Based Design procedures, can provide the designer with a high degree of control over displacements in the structure. This means the designer has a high level of understanding of the performance of the structure and, as damage is related to displacements, what level of damage will occur (Priestley, 1997).

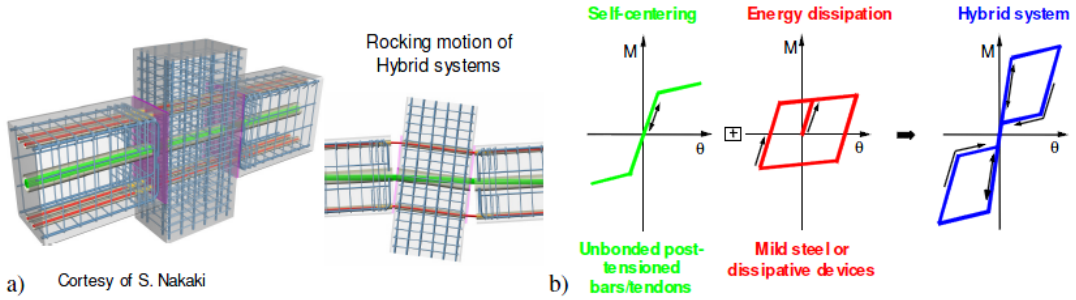

Figure 2-4: a) Cyclic response of "controlled rocking", b) the idealised "Flag-shape" hysteresis (NZS3101:2006)

Recent analytical research by Henry (2011) at the University of Auckland investigated the behaviour of concrete PRESSS walls in a core configuration. Experimental testing on single post-tensioned concrete walls was also performed. Investigation was made into wall systems with precast walls, and end columns with energy dissipating O-connectors which consist of oval-shaped flexural plates that dissipate energy through flexural yielding. A finite element model was developed (Figure 2-5) that captured the cyclic behaviour of the core system observed during experimental testing of the single walls. The model was used to investigate design parameters including the relative quantities of post-tensioning and energy dissipation.

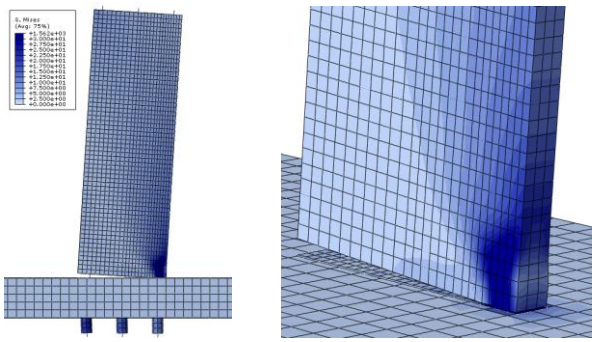

Figure 2-5: Displaced shape of the 3D FEM of a simple concrete wall at maximum lateral displacement alongside the plotted stress profile (Henry, 2011)

A number of new buildings have been constructed using PRESSS technology since the original study. Namely the Endoscopy Building in Christchurch, as part of the Southern Cross Hospital, and the Victoria University building in Wellington. These two buildings are shown in Figure 2-6.

a) b)

Figure 2-6: Real building applications of PRESSS technology; a) Endoscopy Building in Christchurch, b) MacDiarmid Building in Wellington

2.4 PRES-LAM Technology

The PRESSS system was adapted from concrete to timber by the University of Canterbury (Palermo et al. 2005) in a research program led by the Structural Timber Innovation Company (STIC) research consortium. The system, referred to as Pres-Lam, utilises prefabricated Laminated Veneer Lumber (LVL) beam, column, and wall elements connected by un-bonded post-tensioned steel tendons and dissipater devices. LVL is an engineered wood product in which logs are peeled into thin veneers and glued together. This process increases the strength of the timber such that it can compete with concrete as a building material. The axial load applied to the elements by the un-bonded post-tensioned strands and mild steel reinforcement provides moment resisting connections and re-centering capability. Large moment connections can be achieved without the use of hundreds of mechanical fasteners. In addition, the Pres-Lam system allows there to be large displacements with minimal residual damage due to the "controlled rocking" at critical sections.

Feasibility studies (Smith, 2008) and experimental testing at the University of Canterbury under the STIC research programme have included a number of beam-column, single wall and coupled wall sub-assemblies with a range of different dissipater devices (shown in Figure 2-7a) (Iqbal 2010, Iqbal et al. 2010, Palermo et al. 2005, Smith 2006). In addition to the sub-assembly tests, quasi-static testing of a 2/3rd scale two storey building (Newcombe et al. 2010) was performed (Figure 2-7b). The structural system of the building utilised post-tensioned frames in one direction and rocking walls in the other.

Following testing, the building was dismantled and reconstructed as a two storey building that now serves as the STIC office. This structure has been instrumented, and the seismic performance of the structure was analysed following the Christchurch 2011 earthquake and the subsequent aftershock sequence (Smith et al. 2012)

a)

b)

Figure 2-7: Experimental tests performed at the University of Canterbury on (a) coupled wall sub-assembly (Iqbal 2010) and (b) a 2/3rd scale post-tensioned timber building (Newcombe et al. 2010)

Investigation into improving the seismic performance of LVL post-tensioned walls was done by Iqbal, 2010. In this study, LVL walls coupled with energy dissipating U-shaped Flexural Plates (UFPs) were tested, as seen in Figure 2-7a. The hysteretic behaviour of these walls, with a number of different arrangements of UFPs, as well as a post-tensioned only solution is shown in Figure 2-8. The bi-linear backbone of the hysteresis is provided by the post-tensioning which remains in the elastic range. The area inside the hysteretic loops is contributed by the yielding of the UFPs providing an amount of energy dissipation.

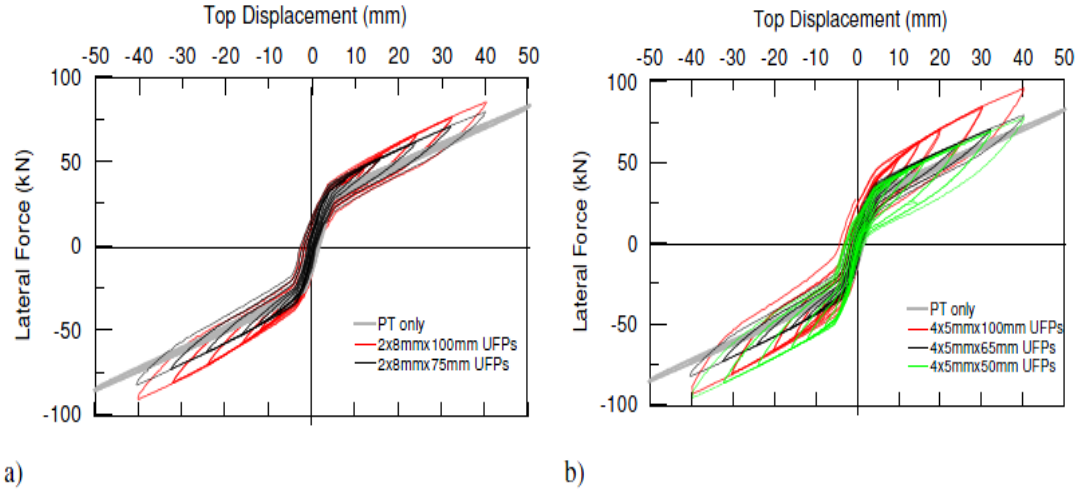

Figure 2-8: Hysteretic comparison between different UFP configurations and post-tensioning only (Iqbal, 2010)

Research is continuing in at the University of Canterbury into the optimisation of Pres-Lam walls and frames (Sarti et al. 2013) and the secondary effects on the floor diaphragm (Moroder et al. 2013). Displacement compatibility between rocking elements in the Pres-Lam system has been seen as a potential issue. A two-bay post-tensioned timber frame, as shown in Figure 2-9, was tested by applying quasi-static seismic loading through a timber floor diaphragm (Moroder et al. 2013). This study found that the presence of the floor diaphragm had little effect on the behaviour of the frame. In addition to this, the flexibility of the timber floor elements and the connections were able to accommodate the elongation of the frame, resulting in no noticeable damage.

Further research is being completed investigating the effect different configurations of post-tensioned walls and connections have on simulated floor diaphragms (Moroder et al. 2014). Research into Pres-Lam walls with Column-Wall-Column configurations have also been investigated (Sarti et. al. 2014). This system comprises of a central post-tensioned wall with boundary columns that support the floor diaphragm and were coupled with UFP devices to provide energy dissipation.

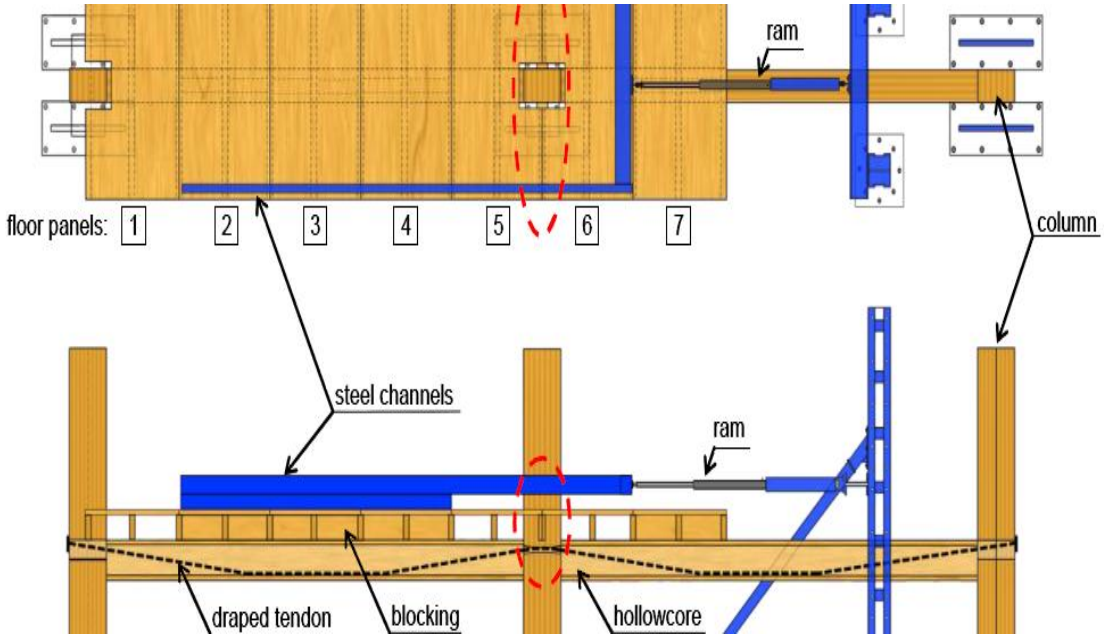

Figure 2-9: Test setup of a 2 bay frame with floor panels (Moroder et al. 2013)

2.5 Cross Laminated Timber Systems

Cross-Laminated Timber (CLT) is an engineered timber product that is gaining popularity throughout the world. CLT was first developed in Austria and Germany and has been used for residential and non-residential applications in Europe (Popovski et al. 2010) and more recently in Australasia. Figure 2-10a shows the Stadthaus building, which at the time it was constructed in 2009 was the tallest CLT building in the world. Figure 2-10b shows the Lend lease building in Melbourne which, at 10 storeys, is now the tallest CLT building. CLT is made by a number of manufacturers in Europe and the first New Zealand manufacturer XLam Ltd has recently begun producing CLT panels in Nelson. The panels are constructed using planed-sawn boards. The boards are arranged in layers which are rotated 90º to the previous layer and then glued, usually using polyurethane adhesive. The panels can be made to a variety of thicknesses (up to 300mm or more) and can be produced in panels of up to 3.5m by 15m.

Figure 2-10: a) the Stradthaus 9-storey building in London, constructed from CLT and b) the 10-storey Lend Lease building, Melbourne

The primary construction method using CLT panels is platform construction (Figure 2-11b), with the panels connected by mechanical fasteners. Platform construction is a method whereby a structure is built up a single storey at a time. The walls are positioned on the floor below and then a new floor, or 'platform', is constructed on top of the walls. This method is more common as opposed to balloon construction, where multi-storey walls are erected at once (Figure 2-11a).

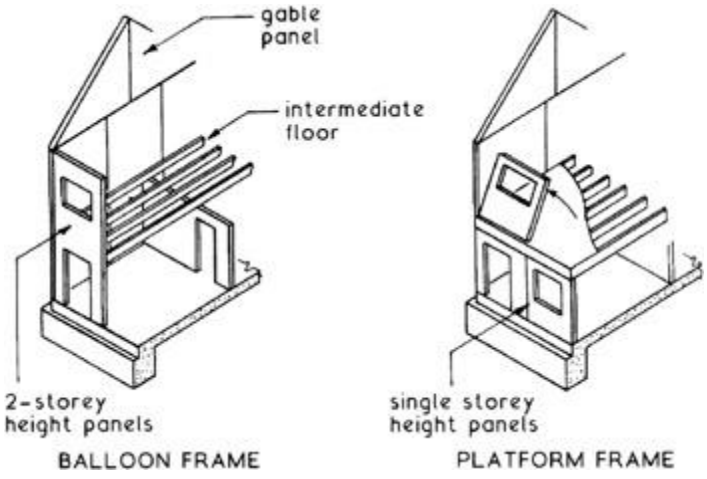

a) b)

Figure 2-11: Typical construction methods, a) balloon frame construction, b) platform frame construction

a) b)

Figure 2-12: a) An interior view of the tallest CLT building in the world, located in Melbourne, b) a CLT stairwell from the Stradthaus building, London

In some cases, the traditional CLT structural system does not provide an acceptable solution for multi-storey buildings due to the large number of load resisting walls that are required. The Lend Lease building (Figure 2-12a) located in Melbourne, at 10 storeys, is the tallest CLT building in the world. It can be seen that the lateral load resisting system has been achieved by using many structural walls throughout the floor plan. For commercial buildings in particular, it is desirable to have large open floor spaces. However, in these CLT systems, many internal walls are required, which interrupts the useable floor space. Although the CLT system is well suited for residential applications, for the above reason, there is a reluctance to incorporate CLT systems into commercial structures.

The largest study to date investigating the seismic behaviour of CLT panels with mechanical fasteners was the SOFIE project conducted by the Trees and Timber Institute of Italy in collaboration with Japanese researchers. The testing programme of the SOFIE project included in-plane cyclic tests on CLT wall panels (Ceccotti et al. 2006), pseudo-dynamic tests on a one-storey specimen, and shake table tests (at Japans E-Defence Laboratory) of full-scale three and seven-storey CLT buildings (Ceccotti and Follesa (2006), Ceccotti (2008)). The three-storey (Figure 2-13) and seven-storey (Figure 2-14) structures were able to withstand several strong earthquake records, including that from Kobe (1995), without significant structural damage (Quenneville and Morris (2007)). The 3 storey house as shown in Figure 2-13(b) was tested with three floor plan configurations. Two were symmetric and one asymmetric. Small steel angles were used to resist the shear forces and uplift of the panels such as those

shown in Figure 2-13(a). Shake table tests were performed on the three configurations with scaled ground motions from the Kobe, El Centro, Nocera Umbra earthquake records. Following the conclusion of the tests, the building had been through approximately 15 destructive earthquakes with little to no damage. It was noted that re-centring behaviour was observed.

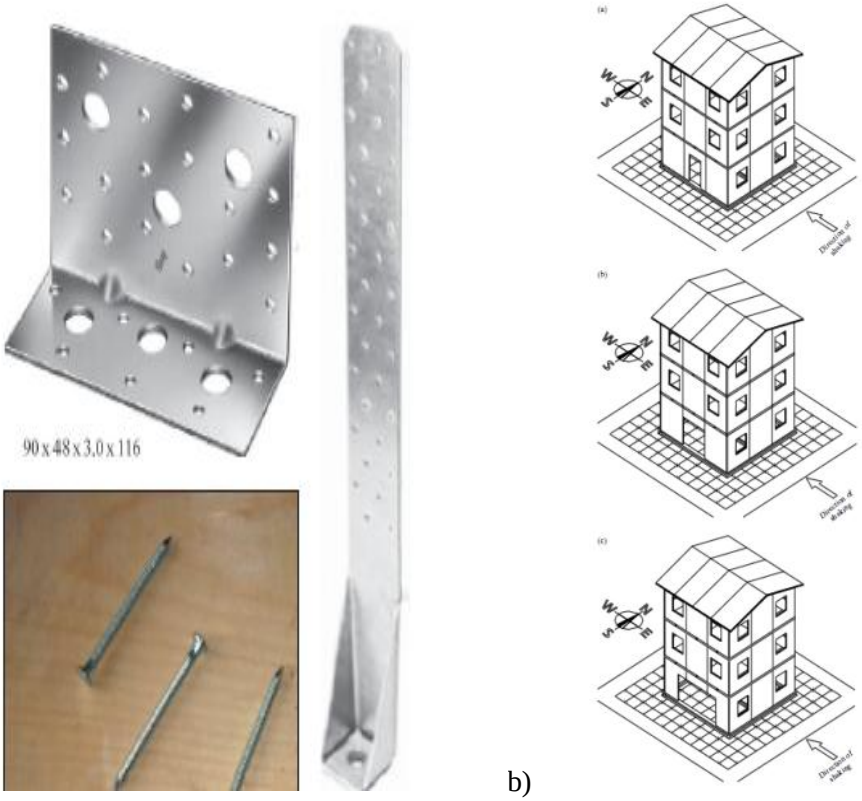

a) b)

Figure 2-13: a) Typical steel shear angles and hold-downs used in the SOFIE project and b) 3 storey house tested with 3 different configurations (Ceccotti et al. 2008)

As mentioned previously, a full scale seven storey CLT building was also tested under the SOFIE programme (Figure 2-14). The structure behaved very well when subjected to a number of different ground motion records (Ceccotti 2008). No damage to the CLT panels was observed after any of the tests. However, some of the shear angle brackets and hold-downs, similar to Figure 2-13(a), needed to be repositioned. The building was able to be de-constructed and shipped back to Italy, demonstrating the recyclability of the CLT panels. Although the building had very little damage, the maximum accelerations within the building from the Kobe input were up to 4g (Quenneville and Morris (2007)). Accelerations of this magnitude would endanger the lives of the building occupants.

Figure 2-14: Seven-storey CLT building tested under the SOFIE Project on the E-Defence shake table in Japan (Ceccotti et al. 2006)

Research by Popovski and Karacabeyli (2011) conducted at FPInnovations in Canada, investigated the seismic performance of CLT panels. A variety of panel and fastener layouts were investigated, as shown in Figure 2-15. Although a variety of layouts were tested, all of the test specimens involved in-plane walls; no L or C shaped configurations were investigated. A typical test set up is shown in Figure 2-16 (Popovski et al. 2010). The wall configurations were subjected to either monotonic or cyclic loading.

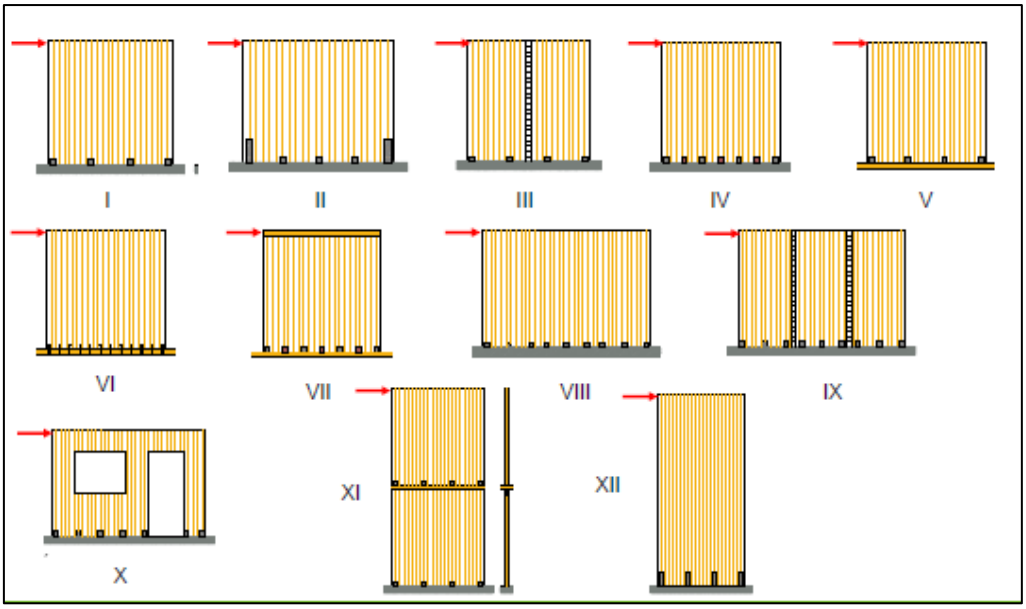

Figure 2-15: CLT wall configurations that were tested under cyclic loading at FPInnovations (Popovski and Karacabeyli (2011))

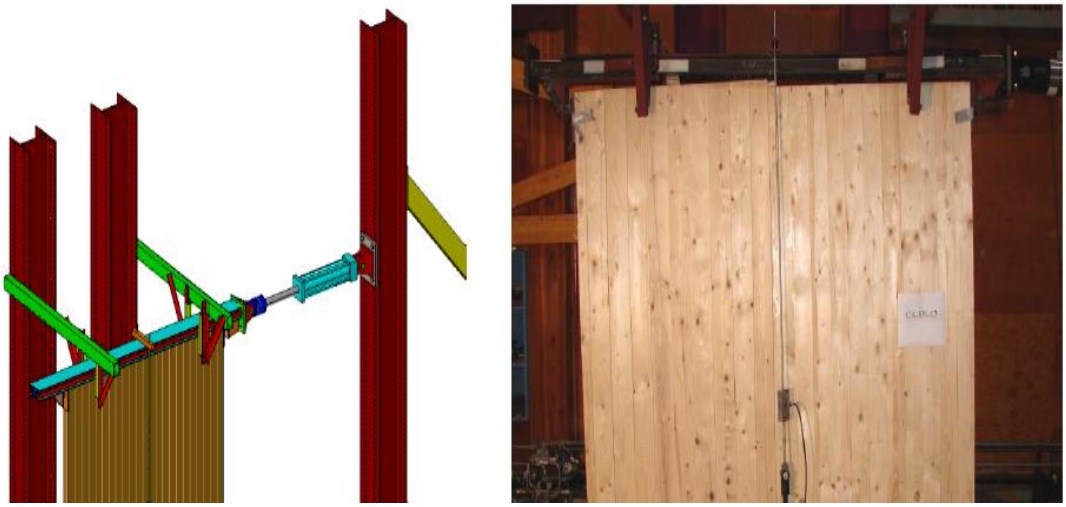

Figure 2-16: a) Sketch of the test setup used for CLT walls, b) one CLT wall configuration similar to setup III from Figure 2-13 during testing (Popovski et al. 2010)

The performance of each specimen was determined and the results of two of the test specimens loaded cyclically are shown. Figure 2-17(a) shows the performance of a panel with no additional axial load and Figure 2-17(b) shows the performance of a panel with additional axial load. The results of these tests showed that CLT wall panels can achieve acceptable seismic performance when mechanical fasteners are used. It was stated by the authors that the wall configurations achieved an adequate level of ductility. In addition to ductility, energy dissipation due to the deformation of the fasteners was achieved, given

by the area enclosed under the hysteresis loops. Re-centering properties were observed only for the specimens with additional axial load (Figure 2-17b). The additional axial load could be provided by post-tensioning the wall panels vertically.

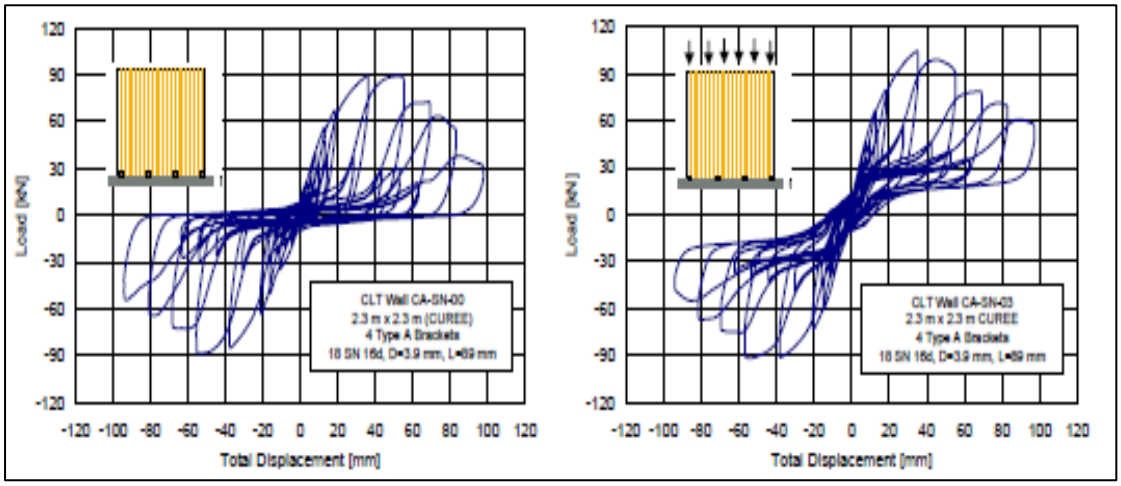

a) b)

Figure 2-17: Results of two CLT walls of configuration I (Figure 2-15), (a) hysteretic behaviour of a wall with no additional axial load, (b) hysteresis for CLT wall panel tested with additional axial load (Popovski and Karacabeyli (2011))

In these systems, the CLT panels behave as a rigid body with almost all the deformation occurring in the mechanical fasteners, more specifically in the nails and screws rather than the steel brackets. Similar fasteners that were used in the SOFIE project described above were used in these tests. Typical damage to nail brackets as a result of testing can be seen in Figure 2-18. Some minor crushing and damage to the CLT panel, around where the nail brackets were attached, was also observed.

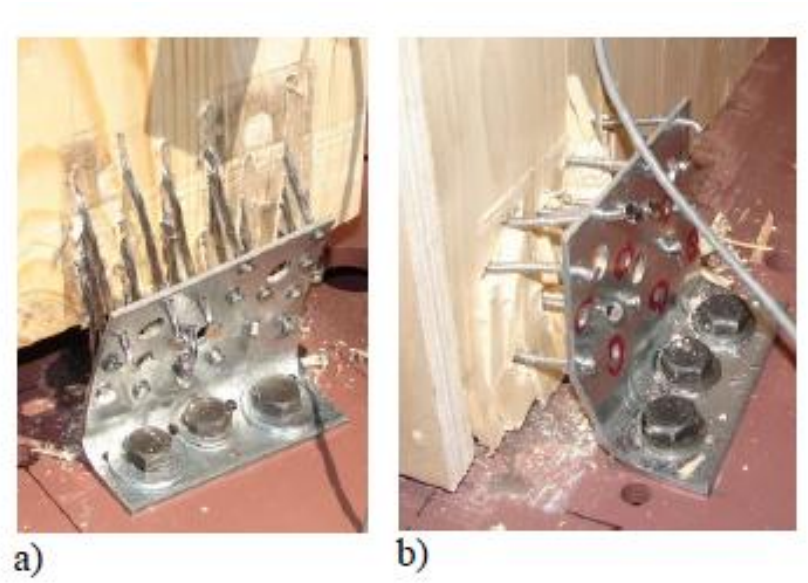

Figure 2-18: Typical damage to angle brackets and fasteners a) during testing, b) following testing (Popovski et al. 2010)

It was reported that the quasi-static tests on CLT wall panels showed that CLT structures can have adequate seismic performance when nails or screws are used with steel angle brackets. The use of hold-downs with nails, on each end of the wall, improves its seismic performance. Diagonally placed long screws to connect the CLT walls to the floor below were not recommended in seismic prone areas due to less ductile wall behaviour. The use of vertical joints in longer walls can be an effective solution not only to reduce the wall stiffness, and thus reduce the seismic input load, but also to improve the wall deformation capabilities.

FPInnovations investigated the behaviour of a two-storey CLT house under bi-directional loading (Figure 2-19). The house was constructed in the traditional manner using screws and steel brackets connecting wall and floor panels in a platform type construction. The internal layout of the walls provided some eccentricity of the centre of stiffness with a large opening along one side of the lower level.

Figure 2-19: 2 storey CLT house tested at FPInnovations

While, at the time of writing, results of these tests are yet to be published, preliminary results were discussed with visiting PhD student Igor Gavric who was involved in the testing. In-plane walls were said to behave in a similar manner to that in Figure 2-17, while the connections between perpendicular walls behaved manly as rigid connections. Complimentary research to this (Gavric et al. 2012) has been done, investigating the strength and deformation characteristics of typical connections between CLT panels. This research differs from that of Popovski and Karacabeyli (2011), as monotonic and cyclic tests were performed on panels connected orthogonally as well as in-plane panels. The results of these tests showed that step joint or half lap connections (Figure 20a) had a higher stiffness than that of spline joints (Figure 20b). It was also found that sufficient spacing, end distances, edge distances, and panel thickness were required to prevent brittle failures of connections between orthogonally connected panels.

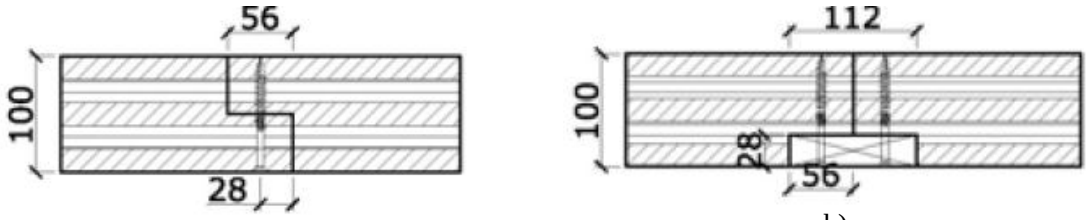

a) b)

Figure 2-20: Connections between in-plane panels, a) step or half-lap joint, b) spline joint (Follesa et al. 2010)

It is reported by various authors that experimental testing on CLT wall configurations showed that CLT structures can have adequate seismic performance when nails or screws are used with steel angle

brackets. This definition of adequate seismic performance in this case is debatable. The hysteretic behaviour of the system is influenced heavily by the behaviour of the mechanical fasteners at the base or edges of the wall panels. From Figure 2-17, which shows typical hysteretic behaviour of nail type connections, it can be seen that there is a very significant amount of stiffness and strength degradation. For large displacement cycles, large amounts of slip appears to have occurred as the shear fasteners have pulled out from the CLT panels and provide little resistance to further displacement cycles. Typical damage to these types of fasteners is shown in Figure 2-18, where the nails have withdrawn from the timber and yielded. Therefore, following a large earthquake, the structural system would be left with greatly reduced strength and stiffness capacities.

2.6 Existing Buildings and Architectural Layouts

Many buildings have differing arrangements of stair and lift-shaft cores. A number of real building cases were investigated with the aim of determining common trends. A sample of stairwell and lift-shaft cores is shown in Figure 2-21. Figure 2-21b, c and d, show a similar layout with a single stair and single lift separated by a long structural wall. The layout in Figure 2-21a differs slightly in that it has a single stair with a double lift, enclosed in a lobby with a mix of structural and non-structural walls. All the stairs in these layouts are half-height stairs with a mid-floor landing, so that there is only one means of escape in each stair core.

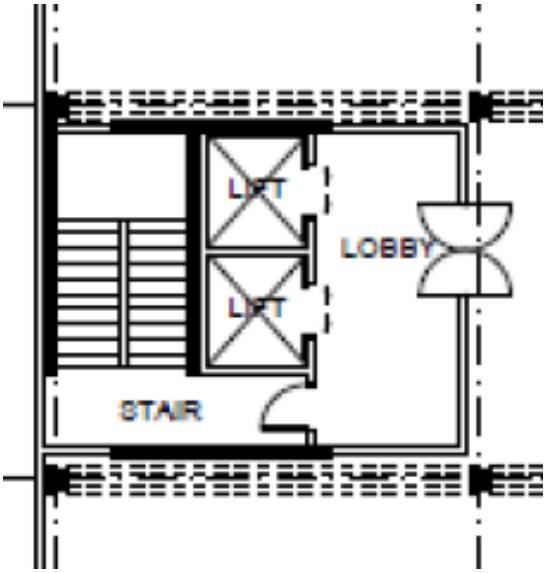

a)

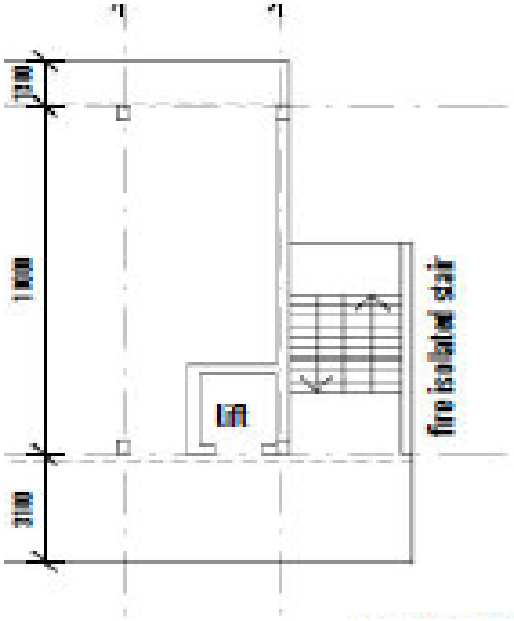

b)

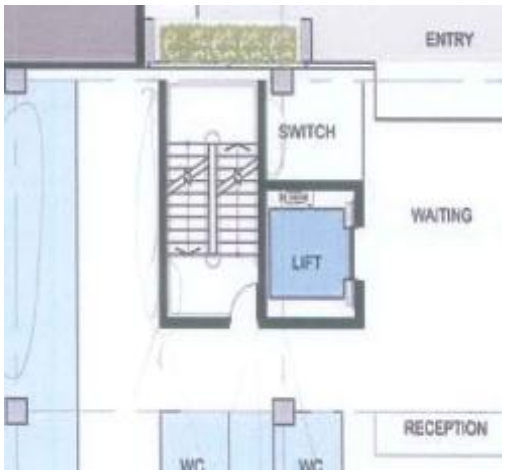

c)

d)

Figure 2-21: Architectural layouts of stair and lift shaft configurations

Figure 2-22 shows the architectural layout of a building with separate stair and lift cores. In this case, solid structural walls enclose the double lifts with a combination of structural and non-structural walls used for the stairwell. Similarly to Figure 2-21, the layout shown in Figure 2-22 also has half-storey stair flights with a mid-storey landing.

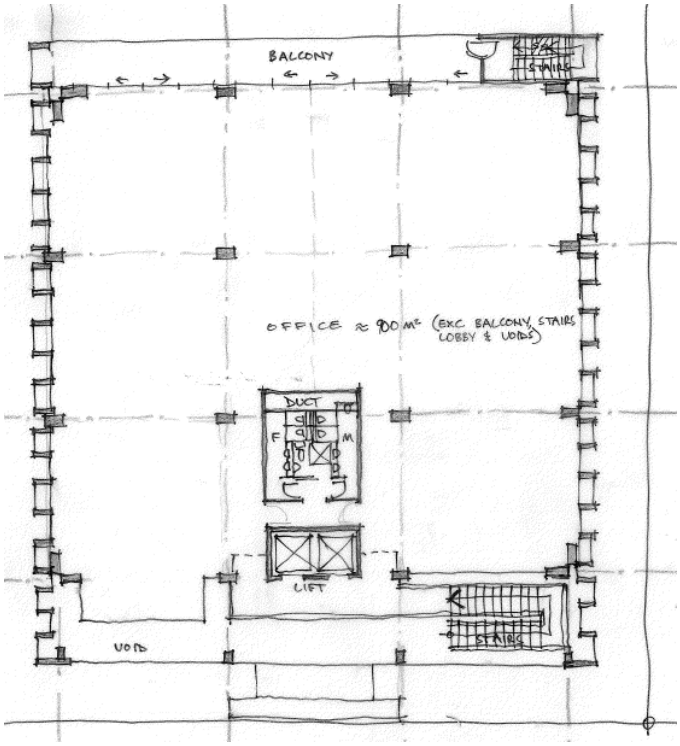

Figure 2-22: Architectural layout of a conceptual multi-storey timber building with separate stairs and lifts

The floor layouts shown in Figure 2-21 and 2-22 are primarily for medium-rise structures less than 10 storeys. A theoretical study into the feasibility of high rise timber buildings was produced by mgb et al. 2012. This study proposes high-rise timber buildings 10, 20 and even 30 storeys high. Three floor plans from this study from the, 'up to 12 storeys' and '20 storeys' examples are shown in Figure 2-23. The three floor plans shown all contain a set of "scissor stairs" and double lifts, along with a single service shaft. Figure 2-23a displays a reinforced concrete option which requires fewer walls than the timber options shown in Figure 2-23b and c. All the stairs in Figure 2-23 are full-storey-height stairs in a "scissor stair" configuration, such that there are two separate means of escape in one stair core.

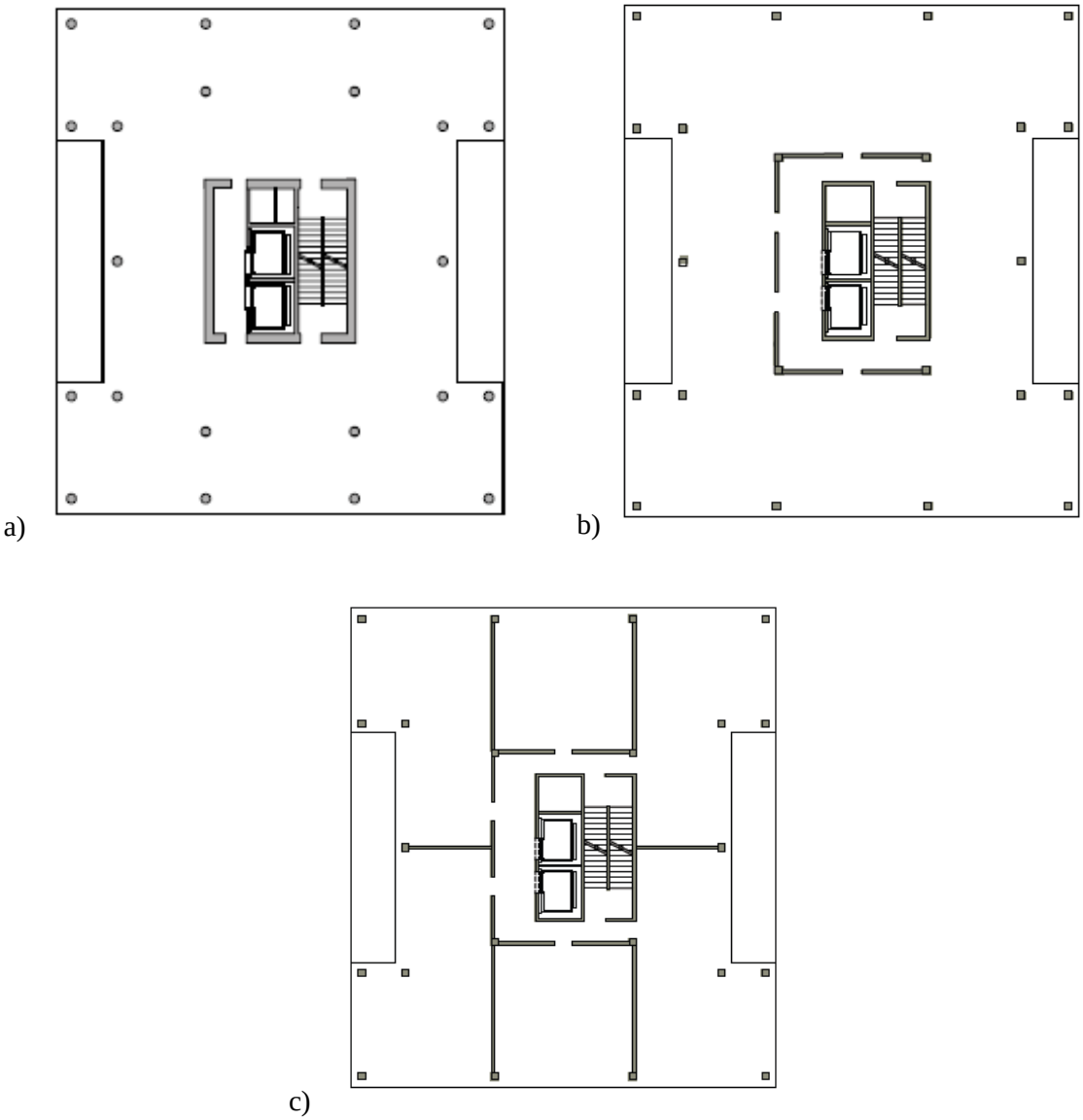

Figure 2-23: Architectural floor plans from the Tall Wood study for a) and b) up to 12 storeys, c) up to 20 storeys (mgb et al. 2012)

In looking at a number of different architectural plans, it can be concluded that there is not one solution that is always used. However, there are some common features. There is usually an off-centre doorway providing access to the stairwell, and the general shape of the stairwell is commonly a rectangular shape with long structural walls separating the stairs and the liftshaft(s).

2.7 Summary of Review

In the research conducted at the University of Canterbury, single and coupled timber walls loaded in plane are well understood. However, there has been little investigation into how the Pres-Lam system

could be incorporated into timber walls of a different shapes, such as for the purpose of stairwell and lift shaft cores. A PRESSS concrete core has been investigation by Henry (2011) at the University of Auckland. However, the system was only investigated analytically and no experimental testing was performed.

The use of CLT is steadily growing in Europe and North America, and is gaining traction in New Zealand. To date, the primary construction method for CLT panels is to use mechanical fasteners such as the connectors mentioned above. At the time of writing there has been no research into the incorporation of CLT into the Pres-Lam system. Many of the buildings constructed using CLT to date have required many internal structural walls to form the lateral load resisting system. Traditional CLT structures have been shown to have good seismic performance, achieving ductility and some energy dissipation through mechanical fasteners. However, stiffness degradation and pinching is observed in the hysteretic behaviour for these types of systems.

This research intends to show that, by using CLT in the Pres-Lam system, a more versatile building layout will be achievable. This research investigates ways in which this can be achieved. A versatile CLT Pres-Lam system may help to increase use of CLT in multi-storey commercial buildings, while providing a low damage seismic system.

3 DESIGN OF TEST SPECIMENS

3.1 General Description

To investigate the seismic performance of post-tensioned core-wall systems, two test specimens were designed; one aimed at a high seismicity region and another aimed at a low seismicity region. Each specimen was a two storey ½ scale stairwell core. The High Seismic test specimen comprised of post-tensioned rocking CLT walls coupled with energy dissipating U-shaped Flexural Plates (UFPs). Steel SHS columns were situated in the corners of the core. The UFP devices were attached between wall panels and the steel SHS corner columns. The Low Seismic specimen had the same layout as the high seismicity specimen. However, in place of SHS corner columns and dissipater devices, horizontal screws were used to connect perpendicular panels.

The layout of this specimen consisted of a rectangular tube with two sets of coupled walls in the longitudinal direction and two sets of single walls, one with doorway openings, in the transverse direction. The two specimens included a half-flight stair case with landings within the core. The components of the specimens were pre-fabricated off site and then erected in the laboratory.

3.1.1 High Seismic

The lateral load resisting system of the High Seismic specimen was comprised of post-tensioned rocking CLT walls coupled with energy dissipation devices. Energy dissipaters were used in the form of U-shaped Flexural Plates (UFPs) attached between wall panels and the corner columns. The corner columns were steel, square hollow sections.

Beams representing the floor slab were connected to the walls, such that there were two beams running in the long direction and short direction of the stairwell. The beams represent gravity and drag beams respectively and are part of the floor diaphragm. The loading beams were connected to the corner columns. The post-tensioned wall panels were in contact with the corner columns, such that the load was transferred from the columns to the walls by friction. The objective of applying the load through the columns and then into the walls was to minimise deformations of the flooring system. As the walls rock, one end of the walls will uplift. However, as the loading beams were not connected directly into the walls, the flooring system was isolated from the uplift. Therefore, as the walls rock, the loading beams, and hence floor slab, remain level.

3.1.2 Low Seismic

The primary objective of the low seismicity test was to investigate how the rocking system would perform with simple screwed connections. Horizontal screws were used to connect perpendicular panels. The screws connect the panels with a semi-rigid connection, such that when the walls rocked, there was relative movement between the wall panels. The relative movement causes deformation in the screws which act as ductile fuses and result in some energy dissipation.

For the Low Seismic specimen there were no corner columns. Therefore the beams were connected directly into the walls by idealised pin connections. As a result of this, the beams were subjected to vertical displacements due to the uplift of the walls.

3.2 Geometry of Test Set-up

The layout of the High and Low seismicity test specimens was adapted from a preliminary design of a multi-storey building on Kilmore Street in Christchurch produced by Wilson and Hill Architects. The tested stairwell represents the highlighted box in Figure 3-1. The seismic actions were not taken from this building.

Figure 3-1: Architectural floor plan of the prototype stairwell system, Wilson and Hill Architects

The plan geometry was the same for the Low Seismic specimen and for the High Seismic specimen such that a direct comparison could be made. The cores were rectangular in shape with overall outside dimensions of 3.4m long and 1.875m wide. The total wall height was 3.75 m, including two floor levels

with an inter-storey height of 1.5m. This represents a full scale three storey building with inter-storey height of 3m. The orientation of the core is shown in Figure 3-2.

Access to the inside of the core was by a doorway at each level situated in the North-East corner of the core. At half-scale the doorway was 1.1m high and 0.45m wide. Coupled walls make up the North and South sides, and single walls, with and without openings, make up the East and West sides respectively

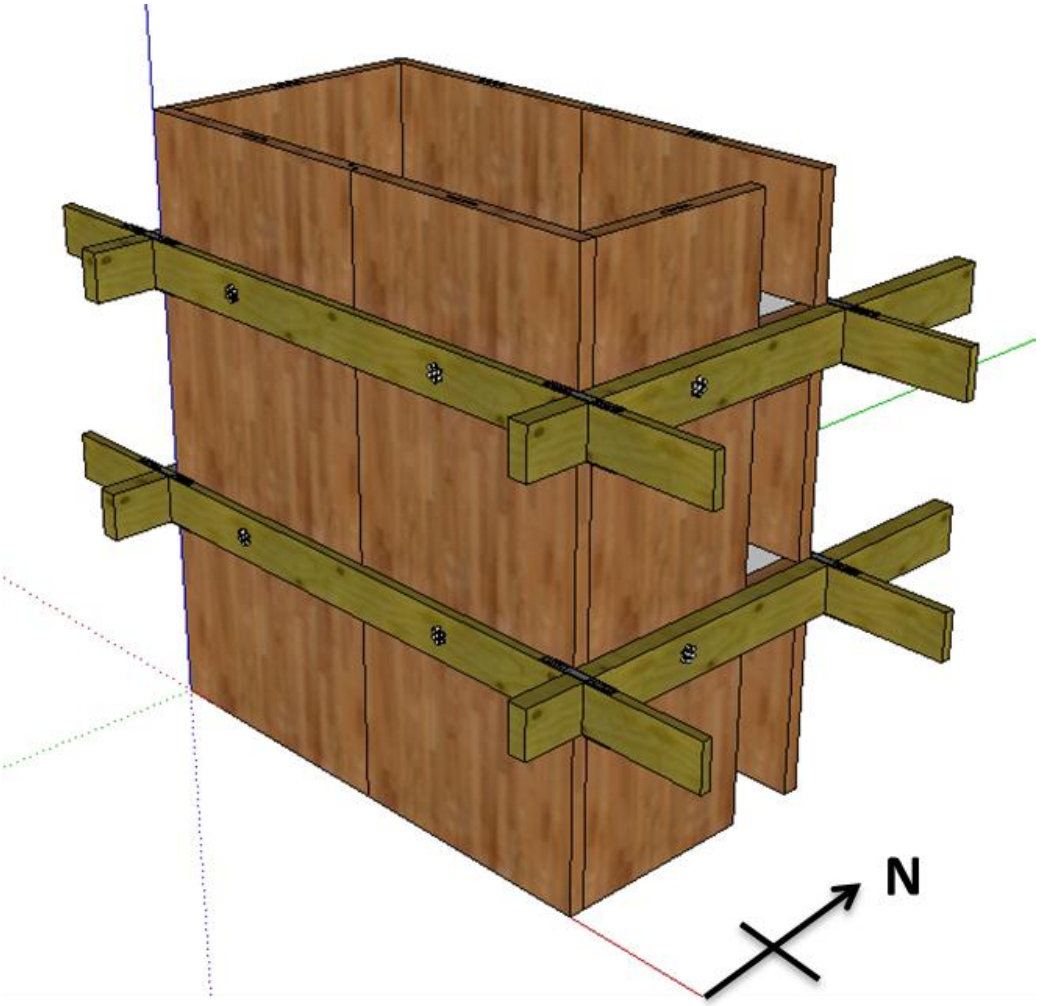

Figure 3-2: 3D rendering and general orientation of the test specimens

3.3 Material Properties

The following material properties, shown in Table 3-1, were used in the design of the post-tensioned CLT walls and components. The wall panels were constructed at XLam Ltd in Nelson, New Zealand. The panels were made up of standard Douglas Fir MSG8 planks.

The post-tensioning strand that was used in the experimental testing was 7-wire strand. For the coupled walls 12.7mm strand was used and 15.2mm strand was used for the single walls.

Standard steel flats were used to make the UFPs by spring manufacturer Bellamy and East Ltd.

Table 3-1: Material Properties of CLT panels and components

	Symbol	***Unit***
Cross Laminated Timber		
Modulus of Elasticity	E	8 GPa
Shear modulus	G	500 MPa
Bending strength	f_b	14 MPa
Tensile strength	f_t	6 MPa
Shear strength	f_s	3.8 MPa
Compressive strength	f_c	18 MPa
Density	ρ	5 kN/m^3
Post-tensioning Strand		
Modulus of Elasticity	E_{PT}	190 GPa
Yield strength	f_{Pty}	1560 MPa
Ultimate strength	f_{PTu}	1750 MPa
Nominal Area		
12.7 mm strand	A_{PT}	99 mm^2
15.2 mm strand	A_{PT}	143.3 mm^2
UFPs		
Modulus of Elasticity	E_s	200 GPa
Yield strength	f_{sy}	375 MPa
Steel Columns		
Modulus of Elasticity	E_s	200 GPa
Yield strength	f_{sy}	300 MPa

3.4 General Design Procedure

The numerical design of post-tensioned timber walls can be performed using the Moment-Rotation procedure proposed by Pampanin et al. 2001 with the addition of the Modified Monolithic Beam Analogy (MMBA) proposed by Palermo, 2004. The general steps within the iterative procedure are described below.

Step 1: Impose a rotation

For preliminary design, assume that the design rotation is equal to the imposed rotation neglecting the elastic deformation of the wall panels.

Step 2: Guess a neutral axis depth

The neutral axis depth c can be estimated at approximately 0.3 times the length of the wall for a first guess.

Step 3: Estimate the increased strain in the post-tensioned tendons

Using the guess of the neutral axis depth, the increase in strain in the un-bonded tendons due to the imposed rotation can be calculated. This strain can be calculated from the following:

$$\Delta\varepsilon_{pt} = \frac{n_{gap}\Delta_{pt}}{l_{ub}}$$

l_{ub} is the un-bonded length of the tendon.

Δ_{pt} is the elongation of the tendon due to the imposed rotation, given by

$$\Delta_{pt} = \vartheta(d - c)$$

c is the neutral axis depth.

d is the distance from the edge of the section to the position of the tendon

Step 4: Estimate the strain in the timber

Due to the use of an un-bonded post-tensioned tendon, strain compatibility cannot be used. Therefore a global strain compatibility relationship, referred to as the Modified Monolithic Beam Analogy (MMBA) (Palermo, 2004) is adopted. The MMBA is used to calculate the strain in the timber pre-yield. The strain is calculated in proportion to the decompression curvature and the neutral axis depth.

$$\varepsilon_t = c\left(3\frac{\theta_{imp}}{L_{cant}} + \phi_{dec}\right)$$

ε_t is the strain at the extreme fibre of the timber element

L_{cant} is taken as the effective height of the wall when represented as a single degree of freedom system.

ϕ_{dec} is the decompression curvature

$$\phi_{dec} = \frac{2}{E}\frac{1}{b_w h_w^2} T_{PT-initial}$$

E is the elastic modulus of the timber parallel to grain

b_w is the width of the wall

h_w is the height of the wall

$T_{PT\text{-}initial}$ is the initial post-tensioning force

The assumption of a triangular stress block is made as the strain in the timber is below its yield point.

Step 5: Determine section equilibrium

Using the estimated neutral axis, section equilibrium must be achieved. In this case the tension force (T_{PT}) in the post-tensioned tendon is equal to the compressive force (C_t) in the timber as shown in Figure 3-3. It should be noted that the equilibrium equation changes with the addition of energy dissipaters as shown in Section 3.4.1 and 3.4.2.

The compression force in the timber is given by

$$C_t = 0.5E_{con}\varepsilon_t c b_w$$

E_{con} is the effective connection elastic modulus. For this application E_{con} was approximated to be 0.55 of the mean parallel to grain elastic modulus.

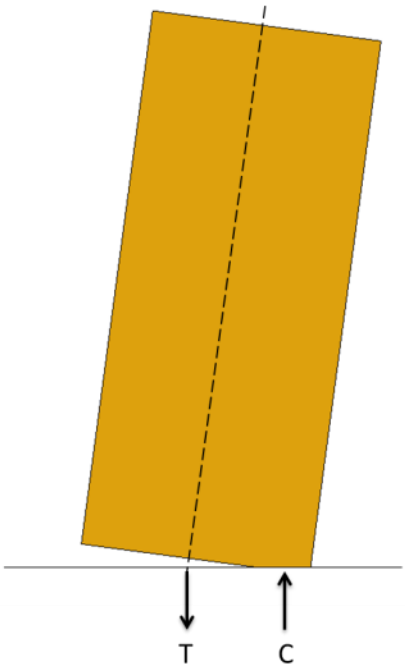

Figure 3-3: Force equilibrium of a post-tensioned wall with no energy dissipaters

The tension force in the tendon is the sum of the initial post-tension force and the additional elongation force due to the uplift of the wall.

$$T_{PT} = T_{PT,initial} + \Delta T_{PT}$$

The additional tendon force ΔT_{PT} is given by the following expression using the increase in strain from Step 3.

$$\Delta T_{PT} = \Delta \varepsilon_{pt} E_{PT} A_{PT}$$

E_{PT} is the elastic modulus of the post-tensioned strand

A_{PT} is the nominal cross-sectional area of the strand

It should be noted that the maximum tendon stress should be less than 90% of the yield stress

$$f_{PT} < 0.90 f_{PTy}$$

In this case where there are no energy dissipaters for equilibrium:

$$C_t = T_{PT}$$

Once the section equilibrium is calculated, the above procedure is iterated varying the neutral axis depth c until section equilibrium is achieved. Following this, the moment capacity can be calculated about the neutral axis.

A summary of the procedure described above is shown in Figure 3-4.

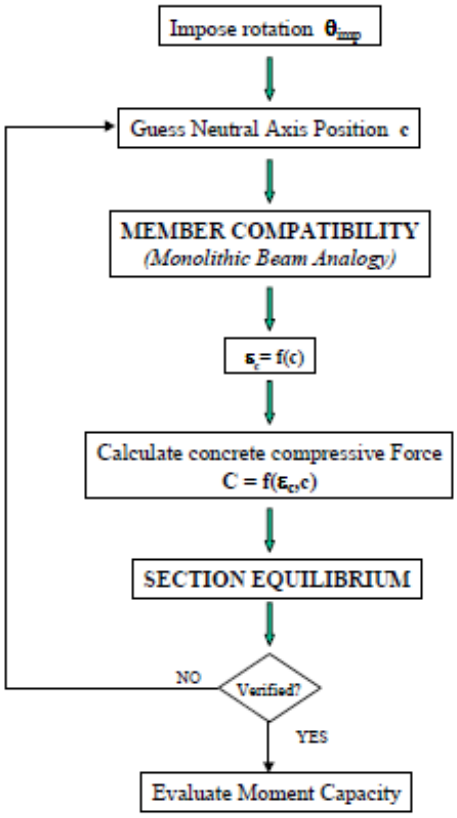

Figure 3-4: The moment rotation procedure for jointed ductile connections (Pampanin et al. 2001)

3.4.1 Modifications for Single Walls with Dissipation Devices

For the design of the single walls within the stairwell core, minor additions were made to the procedure described above. The calculations for the compression force in the timber and the tension force in the strand remain the same. The changes occur at the section equilibrium level with the inclusion of UFPs.

The UFPs are only activated where the uplift occurs in the wall (Figure 3-5). A small amount of relative movement occurs at the opposite end which is neglected for the design.

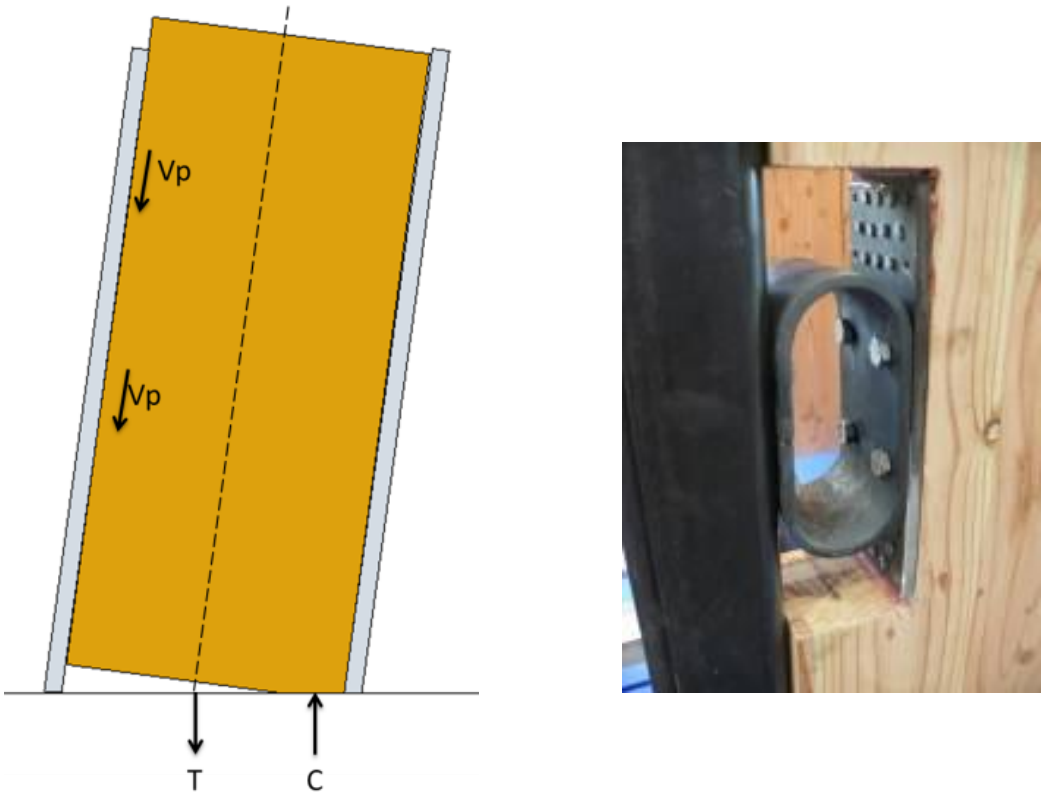

a) b)

Figure 3-5: a) Force equilibrium of a single post-tensioned wall with energy dissipaters, b) UFP between a CLT wall and column

The force equilibrium is given by

$$C_t - T_{PT} - 2V_p = 0$$

The neutral axis is varied until section equilibrium is achieved following the same procedure outlined in Section 3.4

3.4.2 Modifications for Coupled Walls without Corner Columns

The force equilibrium is the similar to that of the single wall above. Wall 1 and Wall 2 behave slightly differently as demonstrated in Figure x. The relative movement between the two walls activates the UFPs producing an upward force acting on Wall 1 and a downward force acting on Wall 2.

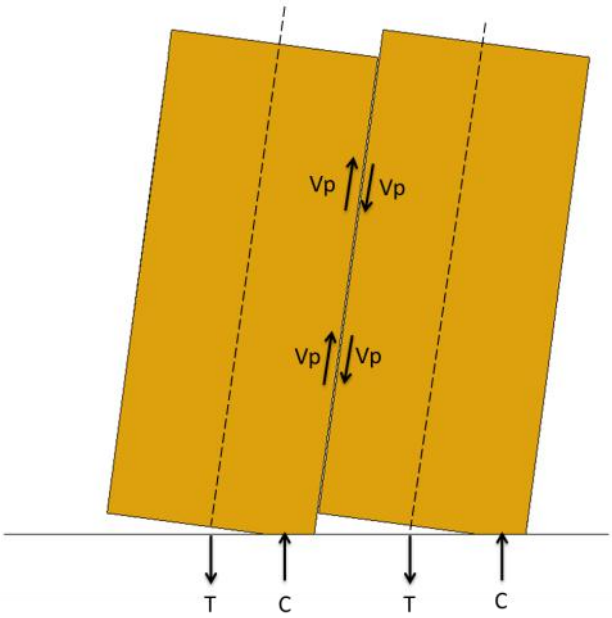

Figure 3-6: Force equilibrium of coupled post-tensioned walls with energy dissipaters situated at the coupling joint only

For equilibrium of Wall 1, the forces from the UFPs act in the same direction as the compression in the timber

$$C_t - T_{PT} + 2V_p = 0$$

For equilibrium of Wall 2, the UFP's act in the opposite direction to that of Wall 1

$$C_t - T_{PT} - 2V_p = 0$$

The same iterative procedure is performed for each of these walls yielding a different neutral axis depth for Wall 1 and Wall 2.

3.4.3 Modifications for Coupled Walls with Corner Columns

For the design of the coupled walls with corner columns, minor additions were made in the determination of the force equilibrium. The calculations for the compression force in the timber and the tension force in the strand remain the same.

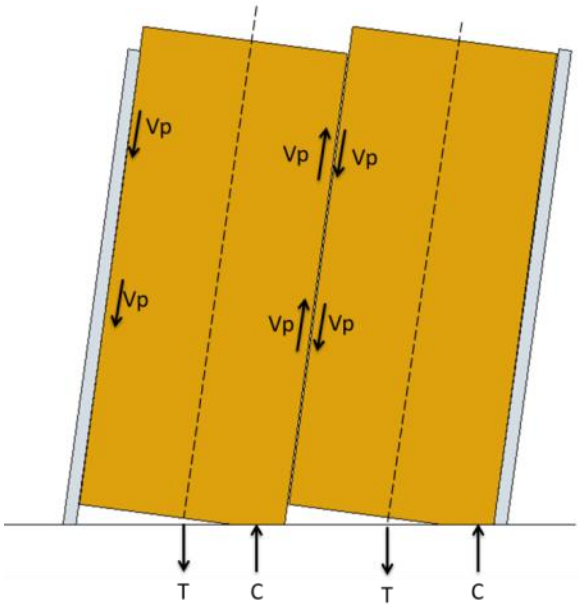

Figure 3-7: Force equilibrium of coupled post-tensioned walls with energy dissipaters situated at the coupling and the outside edge of the walls

Wall 1 and Wall 2 behave slightly differently as demonstrated in Figure 3-7. The relative movement between the two walls activates the UFPs producing an upward force acting on Wall 1 and a downward force acting on Wall 2. The uplift of Wall 1 (at the left hand Figure x) produces a relative movement between the wall and the column which is held down. This displacement produces a force from the UFPs acting downward on Wall 1. At the right hand end of Wall 2, there is no uplift of the wall. Therefore the UFP devices are not activated. A small amount of relative movement between the column and Wall 2 occurs however this is negligible in the design.

For equilibrium of Wall 1, the forces from the UFPs on each end of the wall cancel out

$$C_t - T_{PT} + 2V_p - 2V_p = 0$$

Therefore

$$C_t = T_{PT}$$

For equilibrium of Wall 2, the right hand side UFPs do not activate. Therefore the equation of equilibrium is

$$C_t - T_{PT} - 2V_p = 0$$

The same iterative procedure is performed for each of these walls yielding a different neutral axis depth for Wall 1 and Wall 2.

3.4.4 Design of UFP Devices

In the early 1970s, experimental testing of rolling of mild steel plates in the form of U-shaped Flexural Plates (UFPs) was carried out by Kelly et al. (1972). The curved steel plates are attached usually between two separated walls. As the walls rock during an earthquake a relative vertical displacement between the walls occurs. This relative displacement deforms the UFPs resulting in energy dissipation (Figure 3-8).

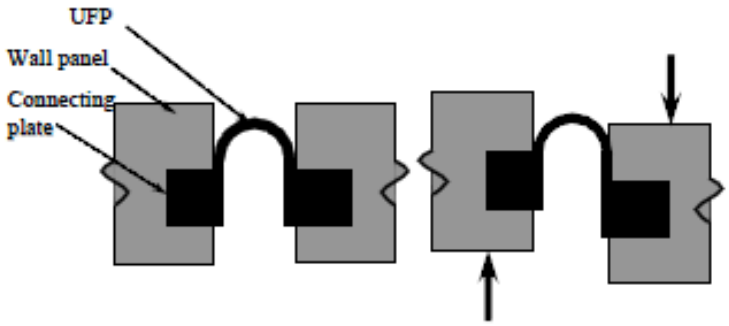

Figure 3-8: Working mechanism of UFPs between walls (Iqbal 2010)

The advantage of using UFP dissipaters is that the maximum strain within the steel remains constant during positive and negative displacements. The constant strain demand is related to the radius and thickness of the UFP. The maximum strain ε_{max} is limited by the stroke and cyclic fatigue determined through experimental testing by Kelly et al. (1972).

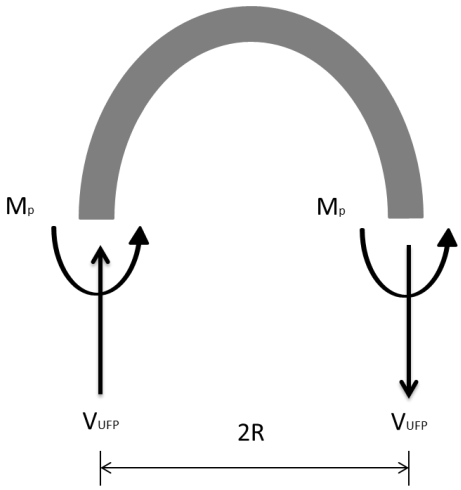

Figure 3-9: Plastic moment and coupling shear of a single UFP

The constant strain demand is defined as

$$\varepsilon_{max} = \frac{t_p}{2R}$$

For a single UFP plate the yield load is given by:

$$V_{UFP} = \frac{2M_p}{2R} = \frac{M_p}{R}$$

M_p is the plastic moment capacity of the steel plate given by

$$M_p = f_y \frac{b_p t_p^2}{4}$$

Therefore,

$$V_{UFP} = f_y \varepsilon_{max} \frac{b_p t_p}{2}$$

For UFP plates that are in pairs, as is used in this research, the coupling shear from a pair of UFP devices is

$$\mathbf{V_P = f_y \varepsilon_{max}\, b_p t_p}$$

The maximum load of a UFP device is likely to exceed that calculated using the equations above due to strain hardening of the steel (Kelly et al. 1972).

3.5 Design of Test Specimens

The design of the High Seismic and Low Seismic test specimens was constrained by strength limitations to the testing apparatus in the laboratory at the University of Canterbury. The primary constraint was the strength of the laboratory strong floor, which limited the shear force applied to the system to 200kN. The design of the coupled walls for the High Seismic specimen is shown below. The material properties from Section 3.3, and the moment rotation design procedure detailed in Section 3.4, were used in the design.

3.5.1 Design of Coupled Walls for the High Seismic specimen

The maximum shear force of 200kN was assumed to act at approximately 2.25m above the base of the wall. Therefore, the design moment of the coupled walls for the High Seismic specimen was 450kNm.

A re-centring ratio of λ = 1.5 was used. Assuming two UFPs per joint were to be used, a capacity of 30kN for each UFP was required.

$$V_P = f_y \varepsilon_{max}\, b_p t_p = 30kN$$

For $\varepsilon_{max} = 0.1$, and b_p = 100 mm:

$$t_p = \frac{V_p}{f_y b_p \varepsilon_{max}} = \frac{30kN}{375MPa\ x\ 100mm\ x\ 0.1} = 8mm$$

$$R = \frac{t_p}{2\varepsilon_{max}} = \frac{8mm}{2x0.1} = 40mm$$

Therefore, UFPs made from 8mm steel flat, bent to a radius of 40mm were used, with a capacity of 30kN each. These UFPs provide approximately 180kNm of moment capacity, and the remaining 270kNm is provided by the post-tensioning of the walls.

The two coupled walls, Wall 1 (left) and Wall 2 (right), behave slightly differently as shown in Figure 3-10. Therefore, the moment capacity of the coupled walls as a whole is not split evenly between the two walls.

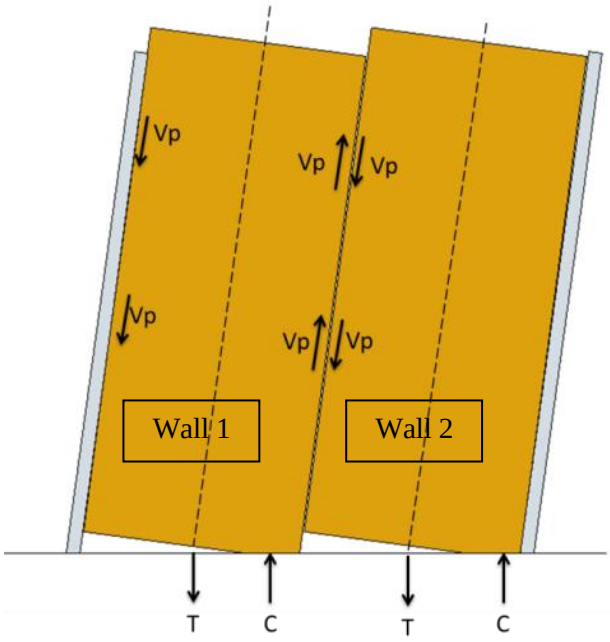

Figure 3-10: Force equilibrium of coupled post-tensioned walls with energy dissipaters situated at the coupling and the outside edge of the walls

For Wall 1:

For an imposed rotation, θ = 1.5%, the elastic contribution is θ_{el} = 0.15%, therefore the design rotation is θ_d = 1.35%.

For a neutral axis depth c = 380mm

For two 12.7mm post-tensioned tendons

$$\Delta_{pt} = \vartheta(d-c) = 1.35\% \cdot \begin{pmatrix} 750-379.8 \\ 850-379.8 \end{pmatrix} = \begin{pmatrix} 5.01 \\ 6.36 \end{pmatrix} mm$$

$$\Delta\varepsilon_{pt} = \frac{n_{gap}\Delta_{pt}}{l_{ub}} = \begin{pmatrix} 0.00133 \\ 0.00169 \end{pmatrix}$$

$$\Delta T_{PT} = \Delta\varepsilon_{pt} E_{PT} A_{PT} = \begin{pmatrix} 25.1 \\ 31.9 \end{pmatrix} kN$$

With an initial post-tensioning force of 100kN in each tendon:

$$T_{PT} = T_{PT,initial} + \Delta T_{PT} = \begin{pmatrix} 125.1 \\ 131.9 \end{pmatrix} kN$$

$$\phi_{dec} = \frac{2}{E}\frac{1}{b_w h_w^2} T_{PT-initial} = \frac{2}{8GPa}\frac{1}{0.1 \cdot 1.6^2} 100 = 7.81 \times 10^{-8}$$

$$\varepsilon_t = c\left(3\frac{\theta_{imp}}{L_{cant}} + \phi_{dec}\right) = 379\left(3\frac{1.35\%}{3.75m} + 7.81 \times 10^{-8}\right) = 0.0041 < 0.0042 \ \therefore Ok$$

$$C_t = 0.5 E_{con} \varepsilon_t c b_w = 257.2\ kN$$

Check Equilibrium:

$$\mathrm{C_t} - \mathrm{T_{PT}} - N = 257.2 - (125.1 + 131.9) = 0 \therefore Ok$$

Moment Capacity of Wall 1:

$$M_{w1} = T_{PT1}\left(d_1 - \frac{c}{3}\right) + T_{PT2}\left(d_2 - \frac{c}{3}\right) + 2V_{UFP} l = 271.2\ kNm$$

The moment contributions from the post-tensioning and UFPs/friction are:

$$M_{PT1} = T_{PT1}\left(d_1 - \frac{c}{3}\right) + T_{PT2}\left(d_2 - \frac{c}{3}\right) = 175.2 kNm$$

$$M_{s1} = 2V_{UFP}l = 96kNm$$

Therefore the re-centring ratio of Wall 1 is:

$$\lambda = \frac{M_{PT1}}{M_{s1}} = \frac{175.2}{96} = 1.82$$

For Wall 2:

The same design rotation of θ_d = 1.35% is used

For a neutral axis depth c = 475mm

For two 12.7mm post-tensioned tendons

$$\Delta_{pt} = \vartheta(d - c) = 1.35\% \cdot \begin{pmatrix} 750 - 475 \\ 850 - 475 \end{pmatrix} = \begin{pmatrix} 3.72 \\ 5.07 \end{pmatrix} mm$$

$$\Delta\varepsilon_{pt} = \frac{n_{gap}\Delta_{pt}}{l_{ub}} = \begin{pmatrix} 0.00099 \\ 0.00135 \end{pmatrix}$$

$$\Delta T_{PT} = \Delta\varepsilon_{pt}E_{PT}A_{PT} = \begin{pmatrix} 37.3 \\ 50.9 \end{pmatrix} kN$$

With an initial post-tensioning force of 100kN in each tendon:

$$T_{PT} = T_{PT,initial} + \Delta T_{PT} = \begin{pmatrix} 137.3 \\ 150.9 \end{pmatrix} kN$$

$$\phi_{dec} = \frac{2}{E}\frac{1}{b_w h_w^2}T_{PT-initial} = \frac{2}{8GPa}\frac{1}{0.1 \cdot 1.6^2}100 = 7.81 \times 10^{-8}$$

$$C_t = 0.5E_{con}\varepsilon_t c b_w = 348.7\ kN$$

Check Equilibrium:

$$\mathrm{C_t} - \mathrm{T_{PT}} - 2Vp = 349 - (137 + 151) - 2x30 = 0 \therefore Ok$$

Moment Capacity of Wall 1:

$$M_{w2} = T_{PT1}\left(d_1 - \frac{c}{3}\right) + T_{PT2}\left(d_2 - \frac{c}{3}\right) + 2V_{UFP}\left(l - \frac{c}{3}\right) = 274kNm$$

The moment contributions from the post-tensioning and UFPs/friction are:

$$M_{PT1} = T_{PT1}\left(d_1 - \frac{c}{3}\right) + T_{PT2}\left(d_2 - \frac{c}{3}\right) = 187.5kNm$$

$$M_{s1} = 2V_{UFP}l = 86.5kNm$$

Therefore the re-centring ratio of Wall 1 is:

$$\lambda = \frac{M_{PT1}}{M_{s1}} = \frac{187.5}{86.5} = 2.17$$

The total moment is given by the sum of the moment for each wall

$$M_{Total} = M_{w1} + M_{w2} = 271 + 274 = 545kNm$$

A summary of the design details of the coupled walls is shown in Table 3-2.

Table 3-2: Summary of design details of the coupled walls for the High Seismic option

Post-Tensioned Tendons	
No. tendons	2 bars
Diameter	12.7mm
Anchor spacing (either side of centre)	100 mm
Area of Strand, Apt	99 mm^2
Initial post-tension force per tendon	100 kN
UFP Devices	
Plate width	100mm
Thickness	8mm
Radius	40mm
Steel yield stress, fy	350MPa
Section Capacity	
Moment Capacity, Mn	545 kNm
Re-centring Ratio, λ	1.82

3.5.2 Design of Single Walls for the High Seismic specimen

The single walls for the High Seismic specimen were designed such that they had the same post-tensioning force, and same UFP properties. Therefore, a lower moment capacity than that of the coupled walls was achieved.

3.5.3 Design of the Low Seismic specimen

The Low Seismic specimen was designed to be equivalent to that of the High Seismic specimen. Therefore, the same post-tensioning force of 100kN per tendon with two tendons was used. The screw connection between the coupled wall panels was designed to give the same shear force as that produced by two UFPs. The design of the screws was performed following the procedure outlined in the Timber Design Guide (2008).

3.6 Details of Test Specimens

The CLT wall panels were constructed at the XLam factory in Nelson, New Zealand, from Douglas Fir timber. The panels were approximately half-scale, with each wall 3.75 m high and approximately 1.7 m wide. Each panel was 100mm thick consisting of five 20mm layers, three in the longitudinal direction and two in the transverse direction. A void 200 mm wide was left down the centre of each wall to allow for post-tensioning tendons. The East panel with the doorway openings was delivered with the openings pre-cut.

Stair and landing panels were also produced by XLam Ltd. These panels consisted of three 35mm layers (two in the longitudinal direction and one in the transverse direction) with an overall thickness of 105mm. The landing panels were 1.675m long and 0.7m wide, and the stair panels were 2.5m long and approximately 0.85m wide.

3.6.1 Low Seismic Details

The Low Seismic Specimen consisted of post-tensioned CLT walls connected by screws to form a stairwell core. The core was 3.4m long, 1.875m wide and 3.75m high. The geometry of the CLT panels used is detailed in Table 3-2. The six post-tensioned CLT panels were arranged as shown in Figure 3-11.

Table 3-2: Geometry and position of CLT walls for the Low Seismic Specimen

	Location	Height (mm)	Width (mm)	Thickness (mm)	Comments
Coupled Panels	North and South sides	3750	1740	100	80 mm lap joint along one edge of panel
Door Panel	East side	3750	1220 (1675)	100	Door opening 455x1100 mm
End Panel	West side	3750	1675	100	

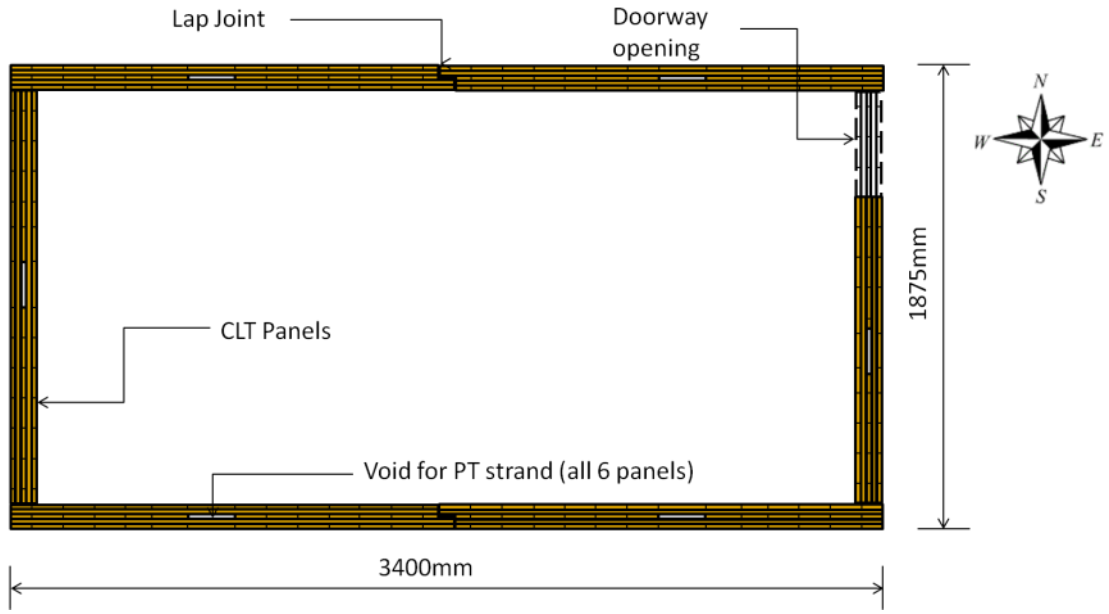

Figure 3-11: Plan view of the core showing orientation of the panels and features

The walls were connected to the foundation by post-tensioned tendons (Figure 3-12). For the coupled walls on the North and South sides of the core two 12.7mm strands were used in each wall. The single walls on the East and West sides contained a single 15.2mm strand. The post-tensioning force applied to each strand was varied between two levels. One that would simulate the gravity load on the structure called "Low Post-tensioning" and another much larger level simulating "High post-tensioning".

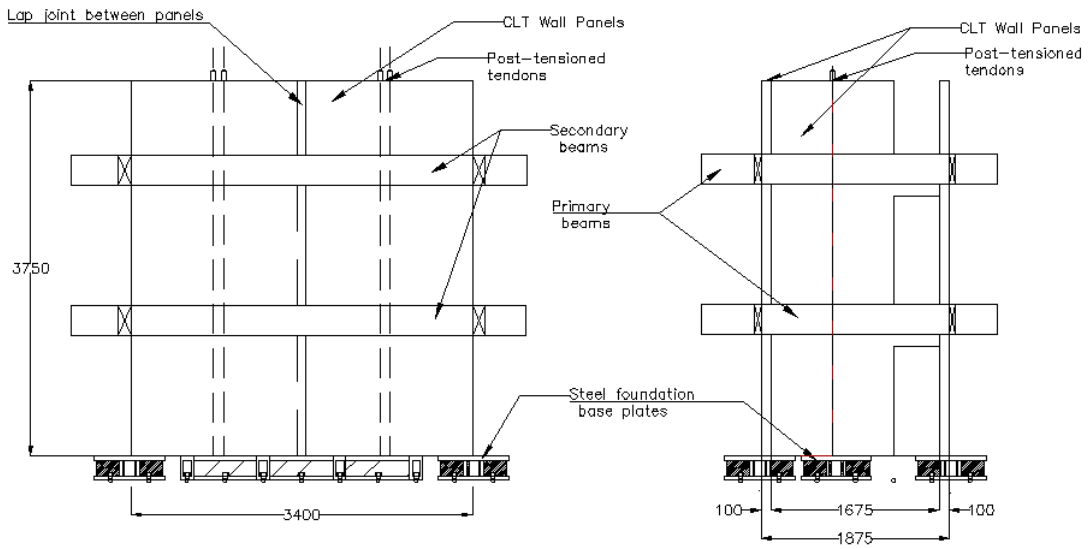

Figure 3-12: General details of the Low Seismic specimen; a) side elevation, b) end elevation

Two types of screw connections were used between the CLT panels (Figure 3-13). A halved lap joint connects the coupled walls with 6 mm diameter x 90 mm long SPAX screws. In the corners, a perpendicular screwed connection was used with 6 mm diameter x 200 mm long SPAX screws. Testing was performed with very few screws, three per joint, and a large number of screws, 20 per joint. The shear capacity of 20 screws was designed to provide approximately the same shear capacity as the two UFPs used in the High seismic option (Section 3.5.2).

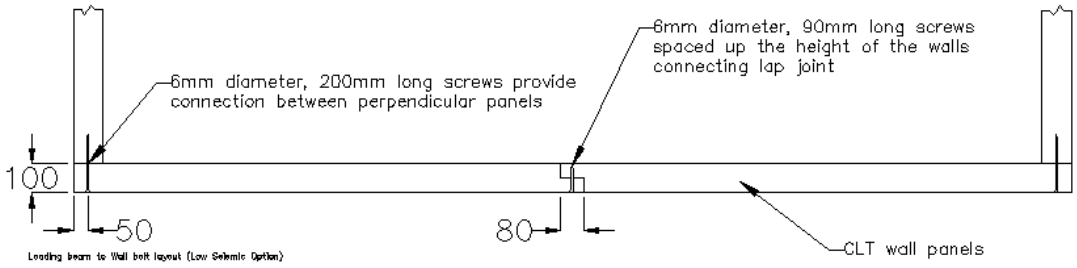

Figure 3-13: Screw connections at the step joint between coupled walls and at the end of the panels

Shear keys were provided at the base of the walls, in the form of angled brackets bolted to the foundation as shown in Figure 3-14. The angles were flexible enough to allow some rotation of the wall, whilst providing a shear connection.

Figure 3-14: Steel angle shear keys, bolted to the foundation, at the base of the walls

3.6.2 High Seismic Details

The High Seismic Specimen consisted of post-tensioned rocking CLT walls coupled with energy dissipating UFP devices. Steel SHS columns were situated in the corners of the core. The core was the same overall geometry of 3.4m long, 1.875m wide and 3.75m high as the Low Seismic option. The geometry of the CLT panels used is detailed in Table 3-3 and Figure 3-15. The walls were modified from the previous specimen to allow for the corner columns. Inserts were also cut into the edge of the panels to house the UFP devices.

Table 3-3: Geometry and position of CLT walls for the High Seismic Specimen

	Location	Height (mm)	Width (mm)	Thickness (mm)	Comments
Coupled Panels	North and South sides	3750	1600	100	
Door Panel	East side	3750	1220 (1675)	100	Door opening 455x1100 mm
End Panel	West side	3750	1675	100	

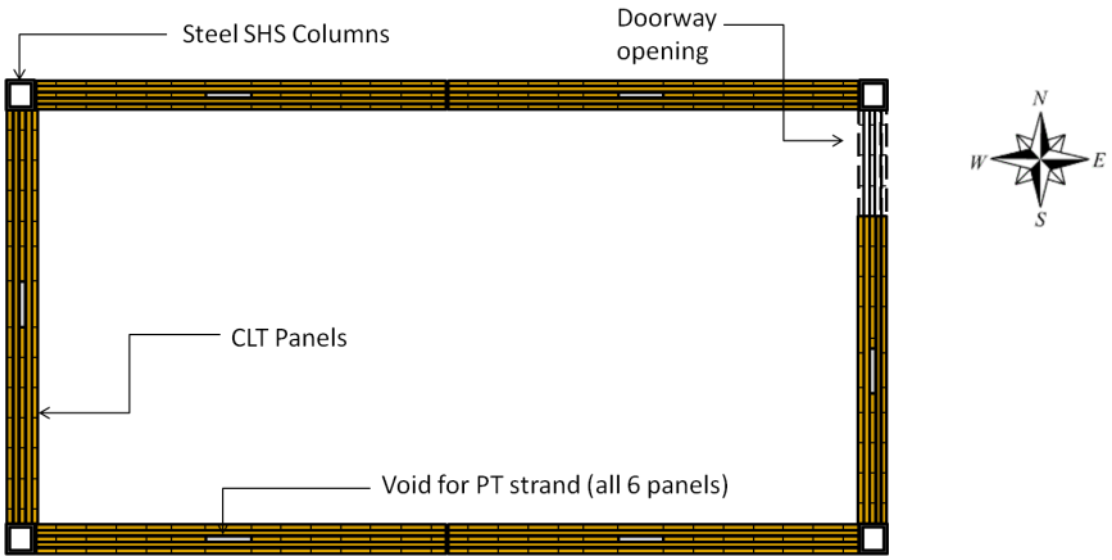

Figure 3-15: Plan view of the core showing orientation of the panels and features

The CLT walls were post-tensioned using 7-wire strand. The coupled walls on the North and South sides of the core have two 12.7mm in each wall. The single walls on the East and West sides contained a single 15.2mm strand. The post-tensioning force applied to each strand was varied between two levels. One that would simulate the gravity load on the structure called "Low Post-tensioning" and another much larger level simulating "High post-tensioning".

Steel corner columns were 100x100x10 in cross-section and 3.75m long. Each column was bolted to the foundation with a single 24mm (Grade 10.9) bolt. A washer was used at the base of the column to allow some rotation of the column to occur. The corner columns served to transfer the lateral forces from the loading beams into the post-tensioned walls. The wall panels were in contact with the corner columns and connected only through the UFP devices. The UFPs were assumed act only in the vertical direction and provide no horizontal resistance. The general details of the High Seismic specimen are shown in Figure 3-16.

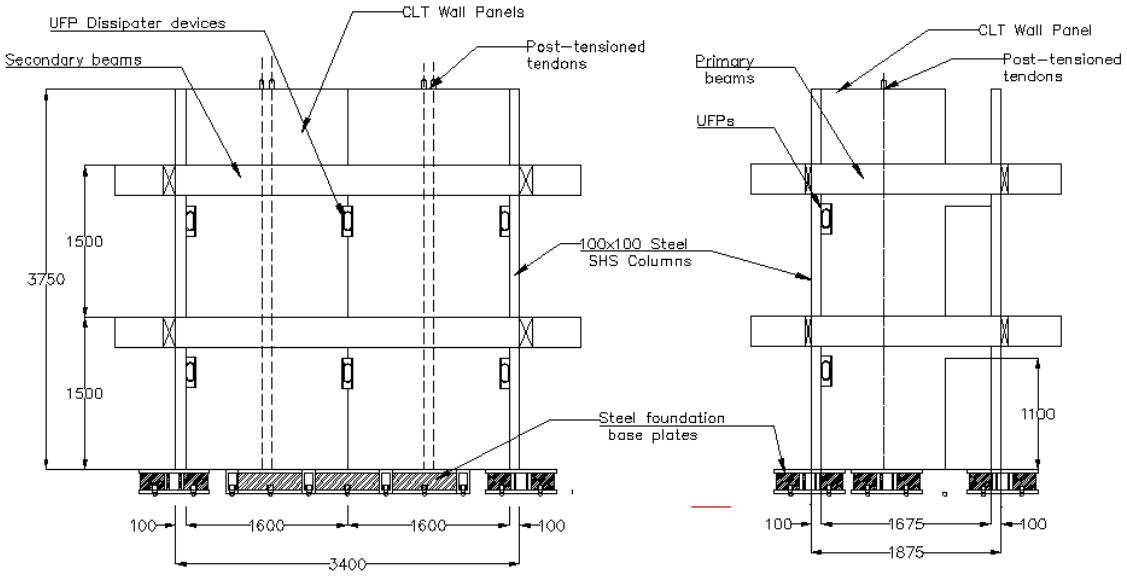

Figure 3-16: General details of the High Seismic specimen; a) side elevation, b) end elevation

The UFP dissipater devices were designed such that the overall system had a re-centring ratio of 1.5. This corresponded to a required capacity of 30kN per UFP. The UFPs were 100mm wide and 8mm thick with a radius of 40mm (Figure 3-17). Steel plates were attached to the edges of the CLT panels with timber rivets (Zarnani and Quenneville 2013). The steel plates had threaded holes in which the UFP device was bolted onto the riveted plates as shown in Figure 3-17. The riveted plates were also epoxied into position such that they had some bearing against the timber slot to increase the stiffness of the connection. The UFPs were able to be un-bolted and replaced.

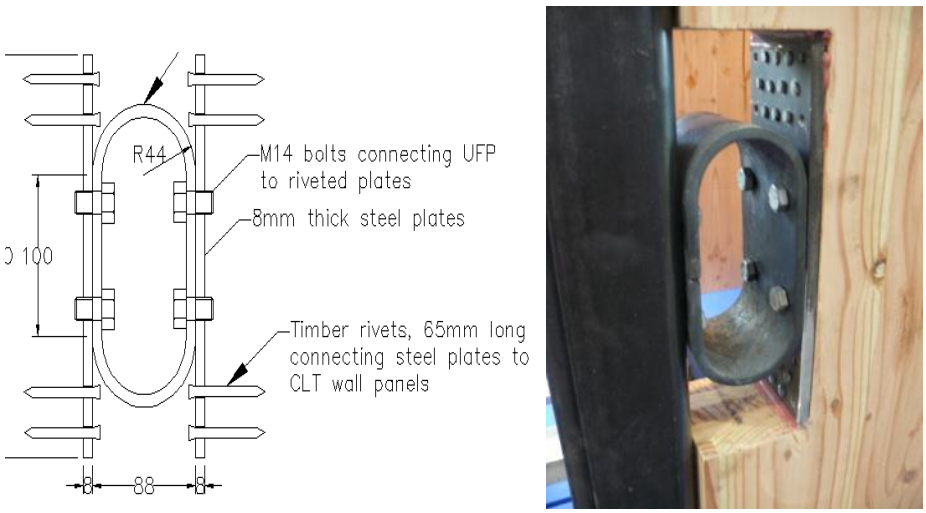

Figure 3-17: Details of the UFPs and connections

3.6.3 Stairs and Landings

Half-flight stair and landings made from CLT panels were included during testing of both the High seismic and Low seismic options. The panels consisted of three 35mm layers (2 in the longitudinal direction and 1 in the transverse direction) with an overall thickness of 105mm. The landing panels were 1.675m long and 700m wide, and the stair panels were 2.5m long and approximately 850mm wide.

The landings were seated on corbels screwed into the North and South walls so that the landings span in the N-S direction. The stair panels and landings were cut with a matching step joint and screwed to the landings at the top of the stair (Figure 3-18). The bottom of the stair panel rested on the lower landing such that it was allowed to slide as the wall panels rocked during testing.

Figure 3-18: Stair and landings; a) connection at the top of the stair, b) stair seated on the landing below

3.7 Loading beam connections

LVL beams used to transfer the applied load into the walls and represent the floor slab were connected to each specimen such that there were beams running in the long direction (E-W) and short direction (N-S) of the core at two levels. A general representation of the beam orientation is shown in Figure 3-19 and Figure 3-20. The beams running in the N-S direction simulate the primary beams in a structure such that they were approximating the main gravity frame within a structure. The primary beams were 126mmx300mm in cross-section and approximately 2.5m long. The secondary beams were used as the equivalent to drag beams which run perpendicular to the primary beams. These beams do not carry any gravity load and such were 63mmx300mm in cross-section and 3.4m long.

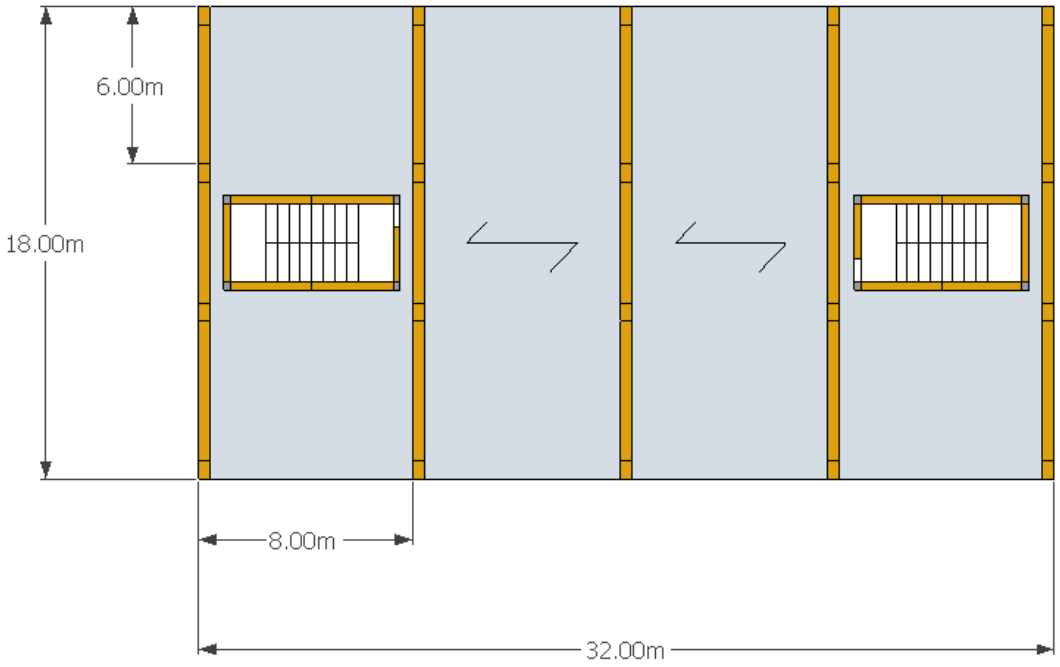

Figure 3-19: The plan representation of how a stairwell core could be utilised within a building and the orientation of the primary and secondary beams

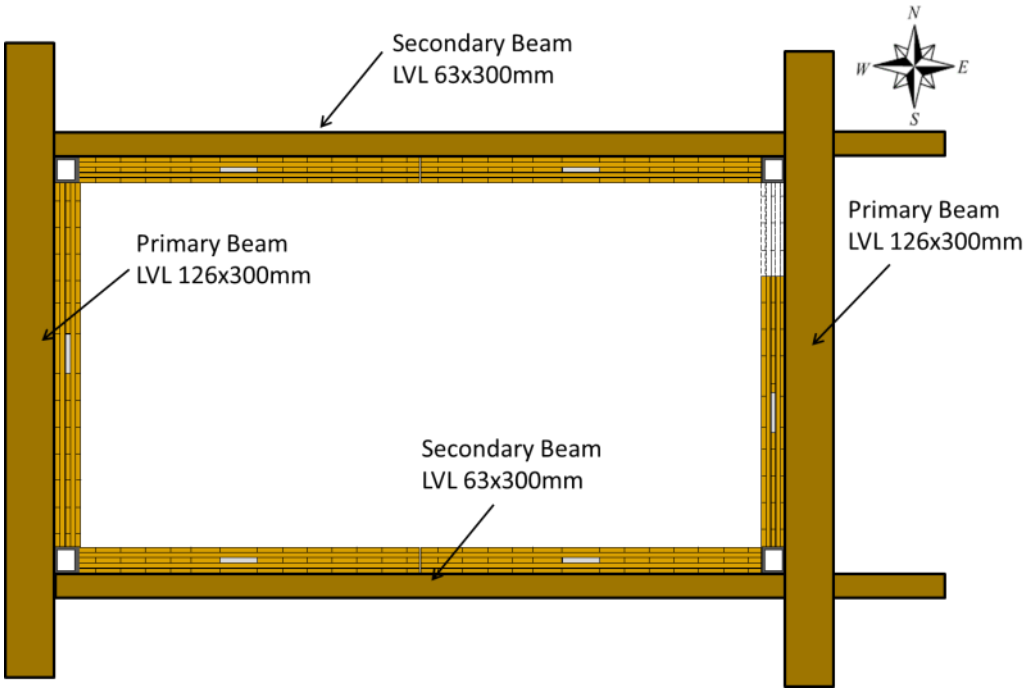

Figure 3-20: Layout of Primary and Secondary beams for the High Seismic and Low Seismic specimens

In the case of the Low seismic specimen the loading beams were connected directly into the walls as described further in Section 3.6.2. Whereas the loading beams in the High Seismic specimen were connected to the SHS corner columns and not directly into the Wall panels.

3.7.1 Primary beam – Secondary beam

The primary and secondary beams were orientated perpendicular to each other. The secondary beam was discontinuous and spanned 3.4m between the primary beams. Steel plates with timber rivets connect beam stubs to secondary beams (Figure 3-21a). The rivet connections were only activated in tension, in compression the load was transferred into the secondary beam by contact.

The rivets were used on the edge grain of the LVL beams. The achieved tensile capacity of the rivet connection on the end-grain was less than what was designed. Therefore to increase the tensile capacity of the connections reid-bar rods were added. Two 25mm bars on each side of the top level and two 12mm bars on each side of the bottom level were used (Figure 3-21b).

a) b)

Figure 3-21: Connection between the primary and secondary beams; a) riveted steel plates, b) reid-bar tie rods

3.7.2 Beam-wall (Low Seismic Only)

For the Low Seismic specimen the load is applied directly from the loading beams to each wall panel. Rings of bolts connect the beams to the walls. Each ring of bolts was intended to act as a pin transferring the lateral load while allowing some rotation of the connection to occur. Each ring of bolts was made up of seven M16 bolts as shown in Figure 3-22 and was located at approximately the centre of each wall. Due to the direct connection between the beams and the walls, when the walls rock the beams are uplifted. The expected behaviour of the loading beams is shown in Figure 3-22c.

a)  b) 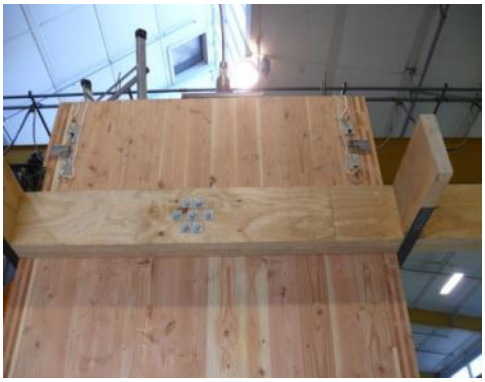

c) 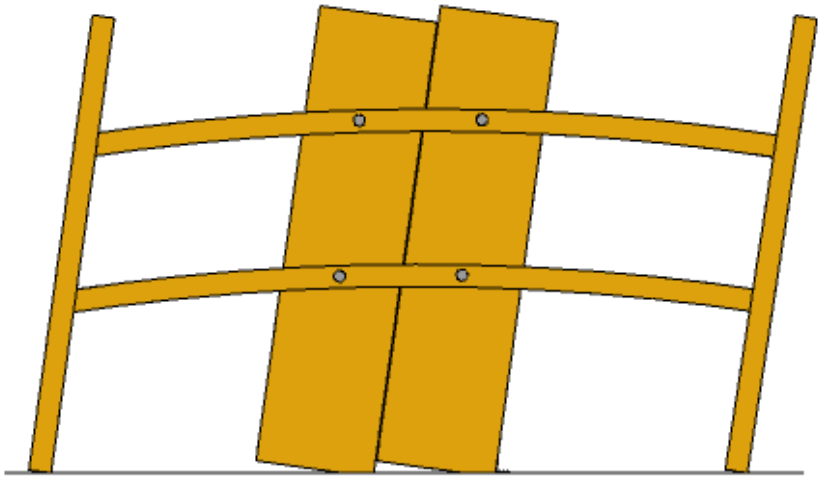

Figure 3-22: a) and b) Ring of bolts transferred the forces from the loading beams into the walls (Low Seismic only), c) expected behaviour of loading beams

3.7.3 Beam-Column (High Seismic Only)

The loading beams for the High Seismic specimen were connected into the SHS corner columns. A single 24mm diameter bolt protruded from the column. The force was transferred from the primary beam via a steel plate screwed to the inside of the beam (Figure 3-23a). The screwed plated was recessed into the beam and epoxy used around the edge of the plate to provide a bearing surface. This connection provided a perfect pin about which any rotation could occur freely (Figure 3-23b). The expected behaviour of the loading beams, with the pinned connection, is shown in Figure 3-23c.

a) 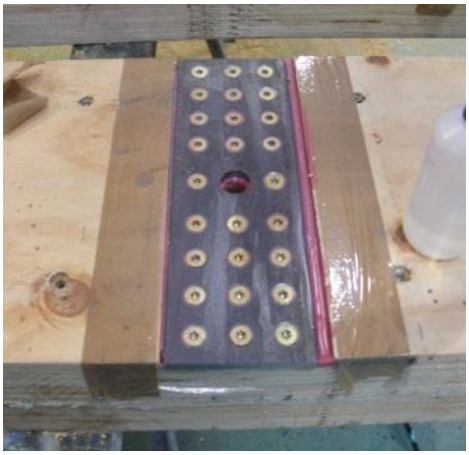 b) 

c) 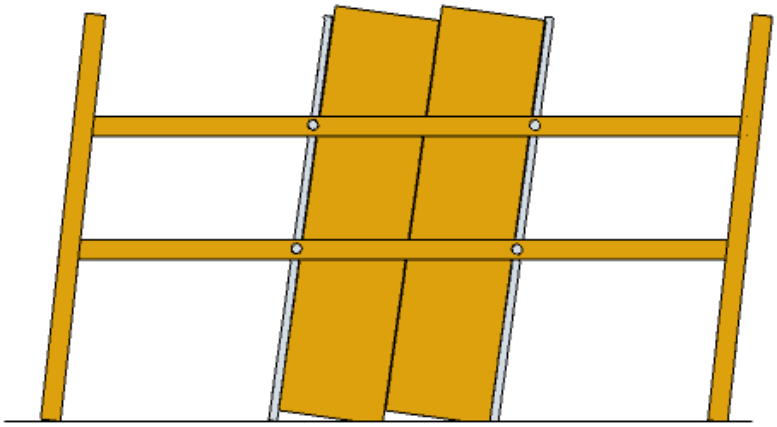

Figure 3-23: Connection between loading beams and steel columns for the high seismic specimen, a) screwed and epoxied steel plate onto the inside of the loading beam, b) bolt through the steel column during construction, c) expected behaviour of loading beams

3.8 Summary of Design of Test Specimens

To investigate the seismic performance of post-tensioned core-wall systems, two test specimens were designed; one aimed at a high seismicity region and another aimed at a low seismicity region. The High Seismic test specimen comprised of post-tensioned rocking CLT walls coupled with energy dissipating U-shaped Flexural Plates (UFPs). Steel SHS columns were situated in the corners of the core. The UFP devices were attached between wall panels and the steel SHS corner columns. The Low Seismic specimen had the same layout as the high seismicity specimen. However, in place of SHS corner columns and dissipater devices, horizontal screws were used to connect perpendicular panels.

The design of the test specimens were governed by the strength and geometrical requirements of the Structures Extension Laboratory.

4 CONSTRUCTION OF TEST SPECIMENS

This chapter discusses the construction of two ½ scale, two-storey post-tensioned CLT stairwell cores. A general representation of the core is shown in Figure 4-1. CLT panels were manufactured by XLam Ltd in Nelson. The LVL that was used for the loading beams was produced at Nelson Pine Ltd. Modifications to the CLT panels and LVL beams were made at the University of Canterbury. Steel-work required for the project was ordered off the shelf and components manufactured by the laboratory technicians. The timber screws that were used in the testing were supplied by SPAX. Timber rivets were provided by TimberConnect. Any other necessary fasteners and brackets were purchased off the shelf.

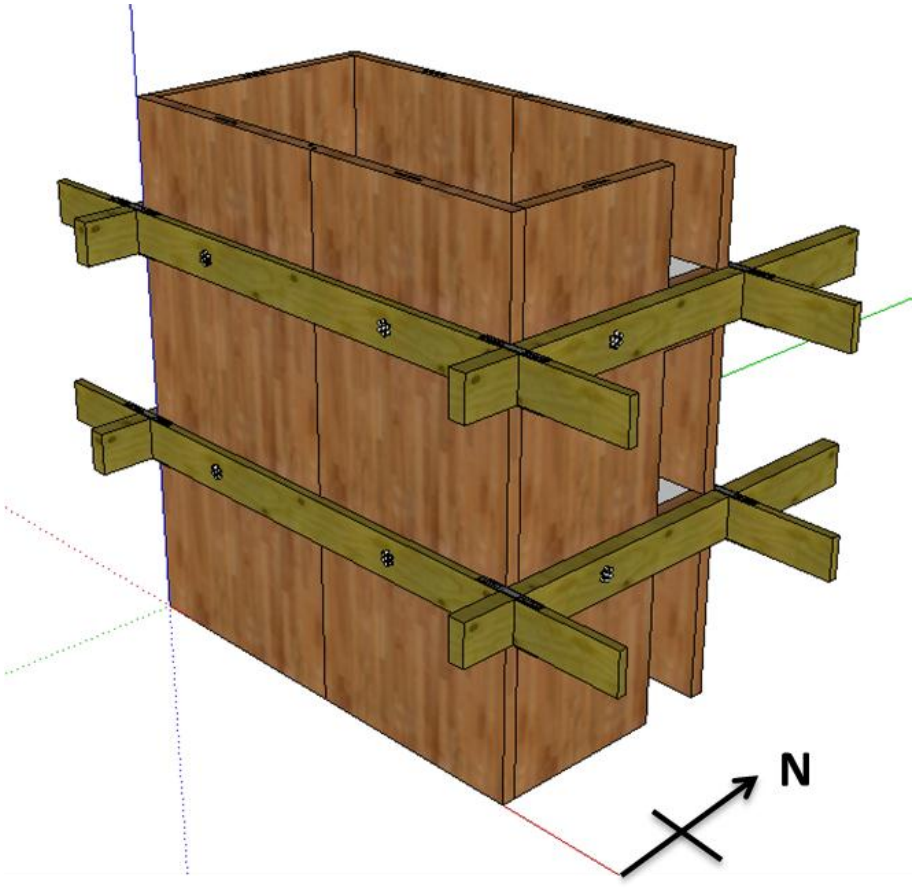

Figure 4-1: General representation of the test specimens

4.1 Loading beams

The LVL for the loading beams was ordered from Nelson Pine coming with a cross-section of 63x300mm. The secondary beams required a cross-section of 63x300mm and the primary beams were

126x300mm in cross-section. The primary beams were laminated together using screws to provide the clamping pressure while the glue sets. A one-component polyurethane adhesive was used.

Following screw-lamination, epoxy rods were inserted in one end of each beam shown in Figure 4-2a. End plates were bolted onto the end of the beams as shown in Figure 4-2b and 4-2c. The epoxy rods provided the tensile capacity of the connection between the beams and the loading rig (Figure 4-2d). The secondary beams did not have epoxy rods, but instead timber rivets. The 65mm timber rivets were hammered in, in a radial pattern.

For the Low Seismic specimen, holes were drilled through the primary and secondary beams for the rings of bolts, which formed the connection between the beams and walls (Figure 4-2e). The beams were clamped into position on the walls, and the holes drilled through each beam and into the wall to ensure that holes lined up perfectly.

The primary beams for the High Seismic specimen, were modified such that a steel plate was rebated into the inside of beam as can be seen in Figure 4-2f. The plate was screwed in place with 10mm diameter screws and epoxied. A single 24mm diameter hole was drilled through the steel plate and the beam such that a bolt could be inserted.

a) Drilling holes for epoxy rods

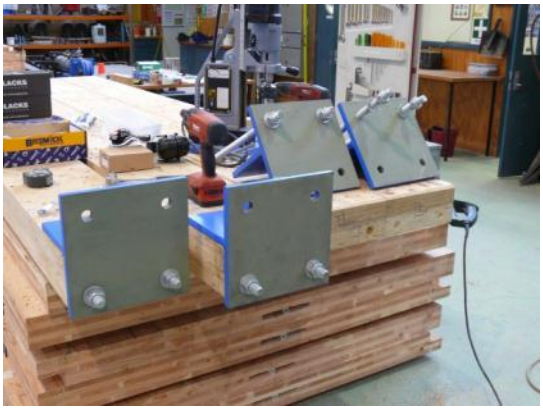

b) End plates anchored by epoxy rods

c) End plates to connect to loading rig

d) Spreader beam connected primary beams

e) Ring of bolts for Low Seismic specimen

f) Inset screwed plate- High Seismic specimen

Figure 4-2: Loading beam components for Low Seismic and High Seismic specimens

4.2 Stairs

Half-flight stairs and landings were included in both of the test specimens. CLT Stair and landing panels were ordered from XLam Ltd and modified in the laboratory. The landing panels were cut such that they had a ledge 50mm wide and 50mm deep running along the length of one of the sides (Figure 4-3a). The top of the stair panels were cut, such that they had a matching ledge (Figure 4-3b and 4-3c). The top of the stairs were screwed to the landings. The bottom of the stair panels were cut on an angle such that they had 100mm seating on the lower level (Figure 4-3d). The bottoms of the stairs were not connected to the landings, such that they were able to slide. The full flight stairs and landings are shown in Figure 4-3e.

a) Landing panel with 50mm ledge

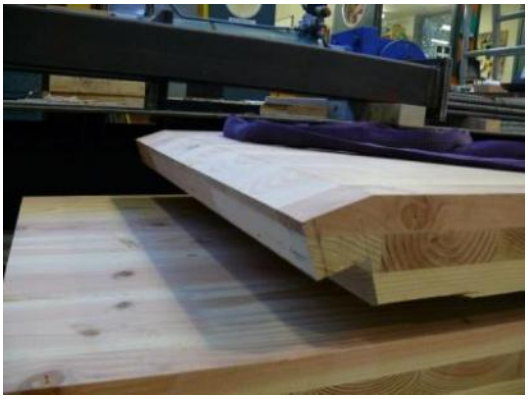

b) Top of stair panel with 50mm ledge

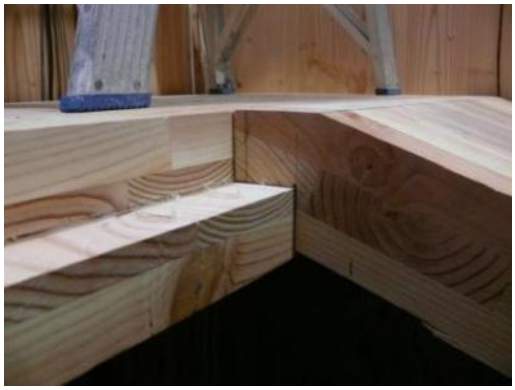

c) Top of stair joining with landing

d) Bottom of stair seated on landing

Full half-flight stairs and landings

Figure 4-3: Stairs and landings included in both Low Seismic and High Seismic tests

4.3 Low seismic General Construction

The construction of the Low seismic specimen was very simple. CLT wall panels were ordered from XLam. The panels were manufactured with a void down the centre of each panel and lap joints pre-cut in each of the coupled walls. During the manufacturing of the wall panels, a plastic tube was inserted in the void within the panel. This allowed the tendons to be easily inserted down the centre of each wall (Figure 4-4a).

The loading beams were bolted into position on each wall. The single walls were lifted into place first (Figure 4-4b). The coupled walls were fitted together on the ground and lifted into position as shown in Figure 4-4c. The partially completed core is shown in Figure 4-4d. The perpendicular panels were then screwed together with five screws up the height of the panels. Lastly, each wall was post-tensioned (Figure 4-5a). Steel angles were bolted to the foundation with M16 bolts, at the corners of the core to form shear keys as shown in Figure 4-5b. The completed Low Seismic specimen, with and without the loading apparatus, is shown in Figure 4-6.

a) Void with plastic tube to house tendons

b) East panel lifted into position

c) Coupled walls positioned together

d) Partially completed core

Figure 4-4: Construction of the Low Seismic specimen

a)  b) 

Figure 4-5: Construction of Low Seismic specimen, a) post-tensioning of walls, b) steel angle shear keys

a) 

b) 

Figure 4-6: Completed Low Seismic construction, a) without loading rig and b) with the loading rig in place

4.4 High Seismic

Construction of the High Seismic specimen was more complex than the construction of the Low Seismic specimen. The overall geometry of the core was the same, but, with the addition of steel corner columns and UFP devices. This required some modification of the components from the Low Seismic specimen. The High Seismic specimen was constructed using the same CLT panels as the Low Seismic specimen. However, the panels were modified to account for the corner columns such that the coupled wall panels were cut down to 1.6m in width with the lap joint removed. The single wall panels were the same geometry as the Low Seismic specimen and were not cut down. The UFPs were made to order, by spring manufacturer Bellamy and East Ltd. The fabrication of the corner columns and UFP rebates are described below in addition to the general erection procedure.

4.4.1 Corner Columns

Off the shelf 100x100 square hollow section steel columns were ordered from Steel&Tube. Four columns were cut to 3.75m in length. A 20mm base plate with a central 24mm hole was welded to the bottom of each column as shown in Figure 4-7a. A 'window' was cut out of the wall of each column such that a 24mm bolt and ratchet could be inserted as can be seen in Figure 4-7b. The single bolt through the base of the columns acted as a shear key for the walls.

A pattern of four 10mm threaded holes were drilled in the wall of each column on two sides in which to bolt the UFPs (Figure 4-7c).

Two 24mm bolts were inserted horizontal through the columns and tack-welded at the head (Figure 4-7d). These bolts were used connect the loading beams to the core and were spaced 1.5m apart.

a) Base of SHS columns with 24mm hole

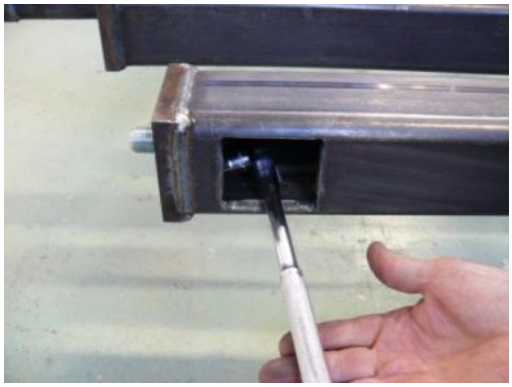

b) 'Window' at the base of SHS to tighten bolt

c) 10mm threaded holes to bolt UFPs to SHS

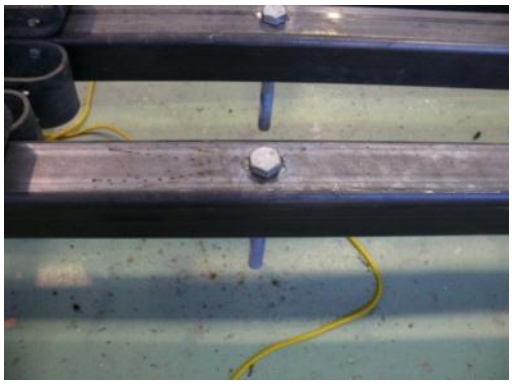

d) Bolts tack-welded to SHS to connect loading beams

Figure 4-7: SHS corner columns

4.4.2 UFP Rebates and Connections

Rebates, in which the UFPs were situated, were cut into the edge of the wall panels (Figure 4-8a). The rebates were required, such that the UFPs could be inserted, and the panels remain in contact with each other. The rebates were approximately 300mm long and 50mm deep on the coupled walls and 100mm deep where each wall was adjacent to a corner column. The rebates were manufactured by making a series of cuts with the Skill Saw and then knocking the pieces out with a hammer or cutting them with a smaller jigsaw (Figure 4-8b and c). The surface was sanded until it was smooth and level. The rebates were cut longer than the rivet plates that were to be inserted, to allow for tolerance. The rivet plates were positioned such that they lined up with the appropriate SHS column or wall as shown in Figure 4-8d. Epoxy was used to hold the plates in place, and to fill the gap between the end of the plate and the rebate (Figure 4-8e). Once the epoxy was dry, rivets were driven into the edge of each wall through the pre-drilled plate in a radial pattern with a club hammer.

a) Rebates marked for cutting

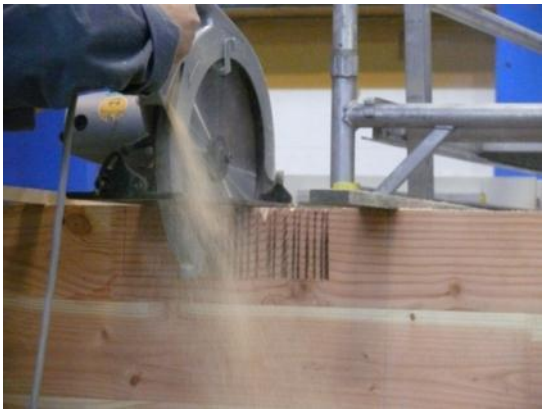

b) Cutting the rebate with the skill saw

c) Flattening the surface of the rebate

d) Positioning the rivet plates

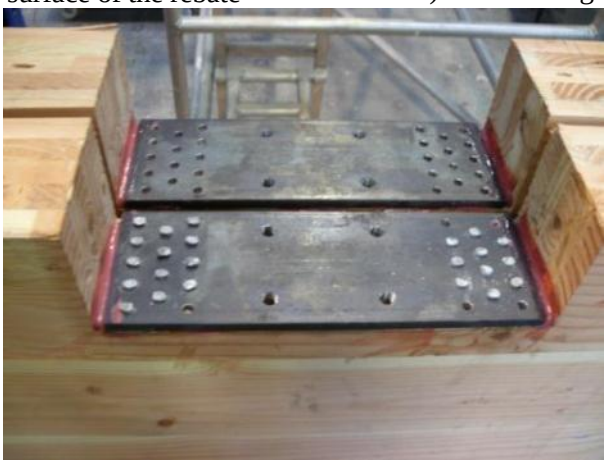

e) Plates epoxied into position and riveted

Figure 4-8: Construction of UFP rebates

4.4.3 General Erection

The general erection procedure for the High Seismic specimen was as follows. The corner columns on the West side of the core were installed first. The West wall was then inserted between the two columns (Figure 4-9a), with the UFPs holding the wall and columns together. The coupled walls were then erected off the West wall. The East side columns and single wall were erected last. Clamps were

required to compress the coupled walls together, such that the corner columns could be installed (Figure 4-9b). The primary loading beams were then placed on the bolts protruding from the corner columns (Figure 4-9c), with the secondary beams spanning perpendicular to the primary beams. Finally the walls were post-tensioned using a hand-held Hydraulic Jack. The completed High Seismic specimen is shown in Figure 4-10.

a) 

b) 

c) 

Figure 4-9: Construction of the High Seismic specimen, a) installation of the West wall, b) clamps needed to install bolt at the base of SHS, c) loading beams fitted onto column bolts

Figure 4-10: Completed construction of the High Seismic specimen

4.5 Summary of Construction

In general, the construction of the Low Seismic and High Seismic specimens was straight forward and simple. The prefabrication of the elements enabled a very rapid erection. The Low Seismic specimen was easier and faster to construct then the High Seismic option, due to the simple screwed connection between the panels. Tolerance was not an issue in the construction of the Low Seismic specimen. The High Seismic option however, was much more reliant on having tight tolerances. The corner columns were bolted to the foundation in specific positions, and the panels in between the columns had to be in contact. The issue with tolerance was more prevalent for the coupled walls than the single walls. In addition to the tolerance required for the corner columns, a tight tolerance was also required for the UFPs. The UFP devices were manufactured, in a way that they were not square and level. Therefore, it was difficult to match the UFPs up with the rivet plates and columns. This was partially mitigated by drilling over-sized oval holes for the bolts through the UFPs.

A significant amount of time relative to the rest of the build time was spent preparing rebates in the wall panels for the UFPs. In reality, the rebates would be cut in the factory and delivered to site which would reduce the build time and potential for error.

Due to the simplicity of the connections between panels and the insensitivity to tolerance, the Low Seismic specimen was much faster and easier to assemble.

5 TESTING PROCEDURE

Two, two-storey ½ scale stairwell cores were tested under a quasi-static cyclic loading regime. The first specimen was the Low Seismic specimen, consisting of post-tensioned CLT walls screwed together. The second specimen, the High Seismic specimen, comprised of post-tensioned CLT walls coupled with UFP devices. Numerous tests were performed on each specimen varying the post-tensioned force and connection details.

The purpose of testing these specimens was to:

- Investigate the behaviour of CLT walls when incorporated into the Pres-Lam system.
- Determine the response of post-tensioned walls orientated orthogonal to each other and not just in-plane.
- Observe the effect of the number of screws connecting adjacent panels.
- Observe the effect of the uplift of the CLT walls on the loading beams, which simulate the floor diaphragm, when the beams are connected directly into the walls and when they are connected to a steel column.
- Compare the differences in performance of a simple system with screwed connections and a more complex system with energy dissipation devices.
- Address practical issues with respect to the implementation of CLT core-wall systems.

5.1 Test Apparatus Setup

The Low Seismic and High Seismic specimens were tested, in a subassembly rig, in the Extension Laboratory at the University of Canterbury. For both specimens the same loading rig and test setup were used. Hydraulic actuators, acting horizontally, were used to apply load through the floor beams to the stairwell core. A single 1000kN ram was used to apply load in the East-West direction, which is labelled as the X direction, and two separate 300kN rams were used at the NE and NW corners to apply load to the single walls (Y direction) as shown in Figure 5-1. Rotary string potentiometers were used to control each ram. The rotary potentiometers were situated 50mm above the second level beam in the centre of the East wall for the 1000kN ram, and at the NE and NW corners and the two 300kN rams.

Figure 5-1: Orientation of loading apparatus

Spreader beams, were used to apply a two-point loading to the specimen in each of the Y direction rams, and a four-point loading in the X direction. Each ram was bolted to a vertical spreader beam at 2/3rds the height (1m from the bottom). This produced a triangular distribution of load, where 2/3rds of the load was applied to the top beam and 1/3rd of the load was applied to the lower beam. In the Y direction, each vertical spreader beam was connected directly to the loading beams. In the X direction two horizontal spreader beams were used in addition to the vertical spreader to apply the force to the core. A schematic of the test rig is shown in Figure 5-2.

A series of steel foundation bases were used to secure the test specimens to the strong floor in the Structures Extension Laboratory. In addition to securing the specimens to the strong floor, the steel bases allowed the walls of the specimens to be post-tensioned in a simple manner, with access below the bottom of the specimens, in which to anchor the post-tensioned tendons. These steel bases have been used for previous projects at the University of Canterbury. Six square base plates and two long bases were used in the arrangement illustrated in Figure 5-3. The square bases were 700mm wide and approximately 300mm high while the long bases were approximately 2400mm long, 700mm wide and 300mm high. Two additional bases plates were made to fill the large gaps on the East and West sides.

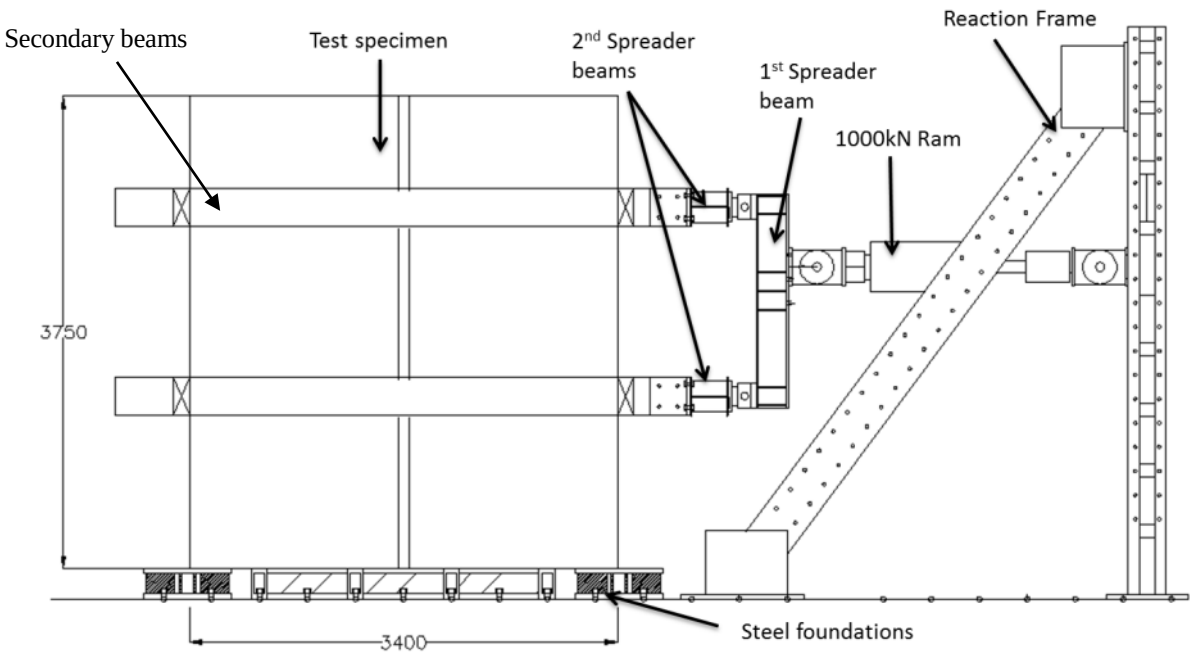

a) Loading in the X direction

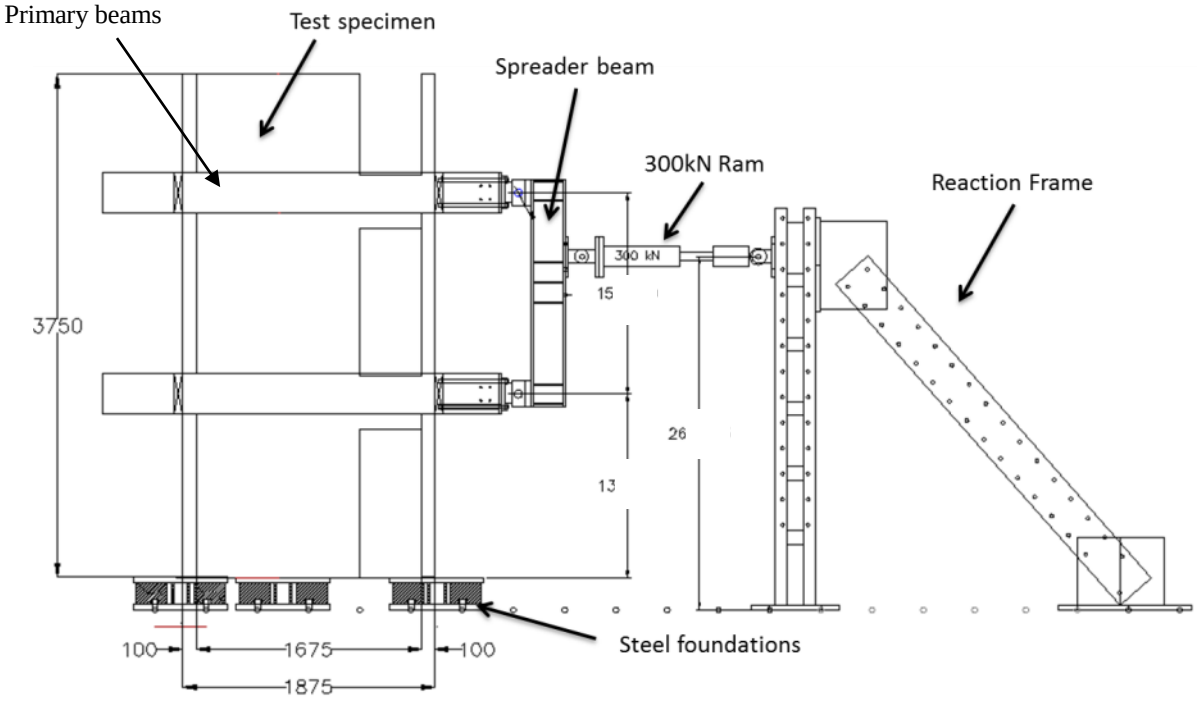

b) Loading in the Y direction

Figure 5-2: Test apparatus used for testing of the Low Seismic and High Seismic specimens

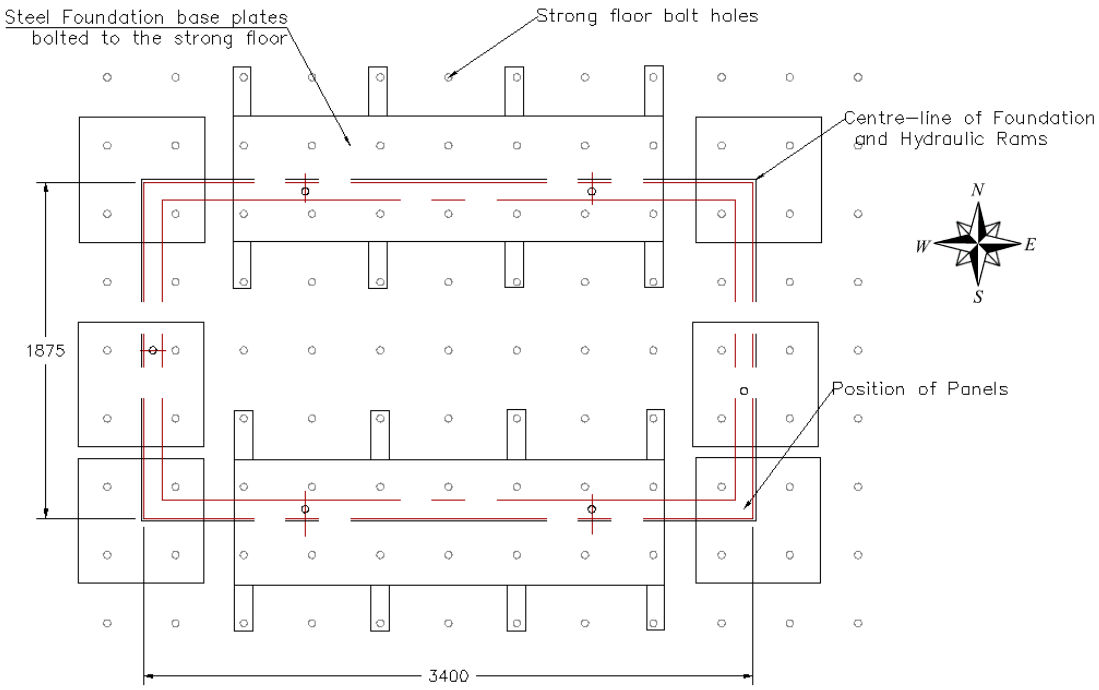

Figure 5-3: Layout of steel foundation base plates used in the testing of both specimens

5.2 Test Procedure

The extent of testing for the High Seismic and Low Seismic specimens is detailed in this section. The design parameters are described for each test as well as the loading protocol. A displacement controlled loading system was used, which applied increasing load until a specified displacement, at the second level beam, was achieved. The loading protocol for each test followed the American Concrete Institute's guidelines for Un-bonded Post-tensioned Precast Structural Walls (ACI ITG-5.1, 2007).

Figure 5-4: Test set-up and specimens for a) Low Seismic specimen and b) High Seismic specimen

5.2.1 Low Seismic

For the purposes of this investigation six tests were undertaken. Each test had three primary variables, the post-tensioned level, the number of screws per joint and the type of loading. A summary of the Low Seismic test schedule is shown in Table 5-1.

Table 5-1: Summary of the Test schedule for the Low Seismic specimen

Test	*Post-Tension Level*	*No. Screws per joint*	*Loading*	*Maximum Drift (%)*
1	Low (40kN/tendon)	3	Bi-directional	1.5
2	Low (40kN/tendon)	20	Bi-directional	0.5
3	High (100kN/tendon)	3	Bi-directional	1.5
4	High (100kN/tendon)	3	Clover	1.25
5	High (100kN/tendon)	20	Bi-directional	1.25
6	High (100kN/tendon)	20	Clover	1.05

5.2.1.1 Post-tension Force

Two different levels of Post-tensioned force were considered for the tests, a low post-tensioned level and a high post-tensioned level. The purpose of the low post-tensioned level was to simulate the likely gravity load acting on the core walls from approximately 100m^2 of floor area. The low post-tensioning level, equated to approximately 40kN in each of the two 12.7 mm tendons in the coupled walls, and 80kN in the single 15.2 mm tendons located in the East and West walls. Therefore, each wall has 80kN of axial load. This axial load is only an approximation of the likely gravity load. It is not an accurate representation, as the post-tensioning force increases due to the elongation of the tendons once gap opening occurs.

The high post-tensioned level represented the post-tensioning required to ensure re-centering of the system. The post-tensioned force, for the high post-tensioned tests, was set at approximately 100kN in each of the two 12.7 mm tendons and 150kN in the 15.2 mm tendon. The stress in the tendons from the initial post-tension force corresponded to $0.75f_y$ in the 12.7mm tendons, and $0.77f_y$ for the 15.2mm tendons. The maximum design stress in the tendons for all tests was limited to $0.9f_y$.

The post-tensioned force for Test 1 and Test 2, of the Low Seismic specimen, was set at the low post-tensioning level. The force in each tendon was set prior to the start of the first test. The tendons were not re-stressed in between each test, as the tendon force remained approximately constant. The post-tension force was then increased to the high post-tension level, for Test 3, Test 4, Test 5 and Test 6. As before, the force in each strand did not change significantly after each subsequent test, so the strands were not re-stressed after each test.

For practical reasons the low post-tensioning force tests were performed first. It was deemed much simpler to increase the post-tensioned force than lower it due to the anchorages of the tendons.

5.2.1.2 Screw Joints

Screws were used to connect the perpendicular wall panels and the coupled panels. At the corners of the stairwell, 6x200mm screws were used and 6x100mm screws were used in the lap-joints. Two different screw configurations were used in the testing, three screws per joint and 20 screws per joint. For Test 1, Test 3 and Test 4, three screws per joint spaced at approximately 950mm were used. This screw layout differed in the NE corner, where the doorway is situated, to three screws in each doorway lintel. The loading beams were covering the majority of the doorway lintels. Therefore, to avoid taking the loading beams on and off three screws spaced at approximately 100mm were inserted prior to the installation of the loading beams. The purpose of having only three screws per joint for these tests was to hold the panels together, whilst providing little resistance to the rocking of the panels.

Further tests, Test 2, Test 5 and Test 6, were performed with 20 screws per joint spaced at approximately 150mm. For these tests, the same types of screws as the previous tests were used. Following the completion of each test, the screws were removed and replaced with new screws for the next test. In most cases, unless a screw had broken during testing, the new screws were replaced back into the same holes as the previous screws. The purpose of using a large number of screws was to stiffen the joints between the panels, and create a core that didn't act as individual panels.

5.2.1.3 Loading Protocol

The Low Seismic subassembly was subjected to bi-directional quasi-static cyclic loading. For some tests the loading was applied in the X and Y directions separately, while two of the tests were subject to a clover-leaf protocol. The loading protocol for each test, shown in Figure 5-5, was in accordance with the American Concrete Institute (ACI) acceptance criteria for Un-bonded Post-tensioned Precast Structural Walls (ACI ITG-5.1, 2007). Test specimens were subject to three cycles at each drift level. For each test the initial drift level was set such that the specimen was still in the elastic range. Subsequent drift levels were then increased by a factor greater than 1.25 but less than 1.5. The maximum drift level was

modified for each test depending on the post-tension level and the number of screws. The largest maximum drift level of 1.5% was used in Test 1. Subsequent tests, where the post-tensioning force was increased were subject to lower peak drifts such that the applied load did not exceed the capacity of the loading beams. With the exception of Test 2, the peak drift in each test was between 1.05% and 1.5%. A low peak drift of only 0.5% was used in Test 2, so that there would be minimal damage to the screws and timber in the joints, as they would be used again for subsequent tests.

The load was applied in the X and Y directions independently for, Test 1, Test 2, Test 3 and Test 5. Bi-directional clover-leaf loading protocols were used for Test 4 and Test 6 as shown in Figure 5-6.

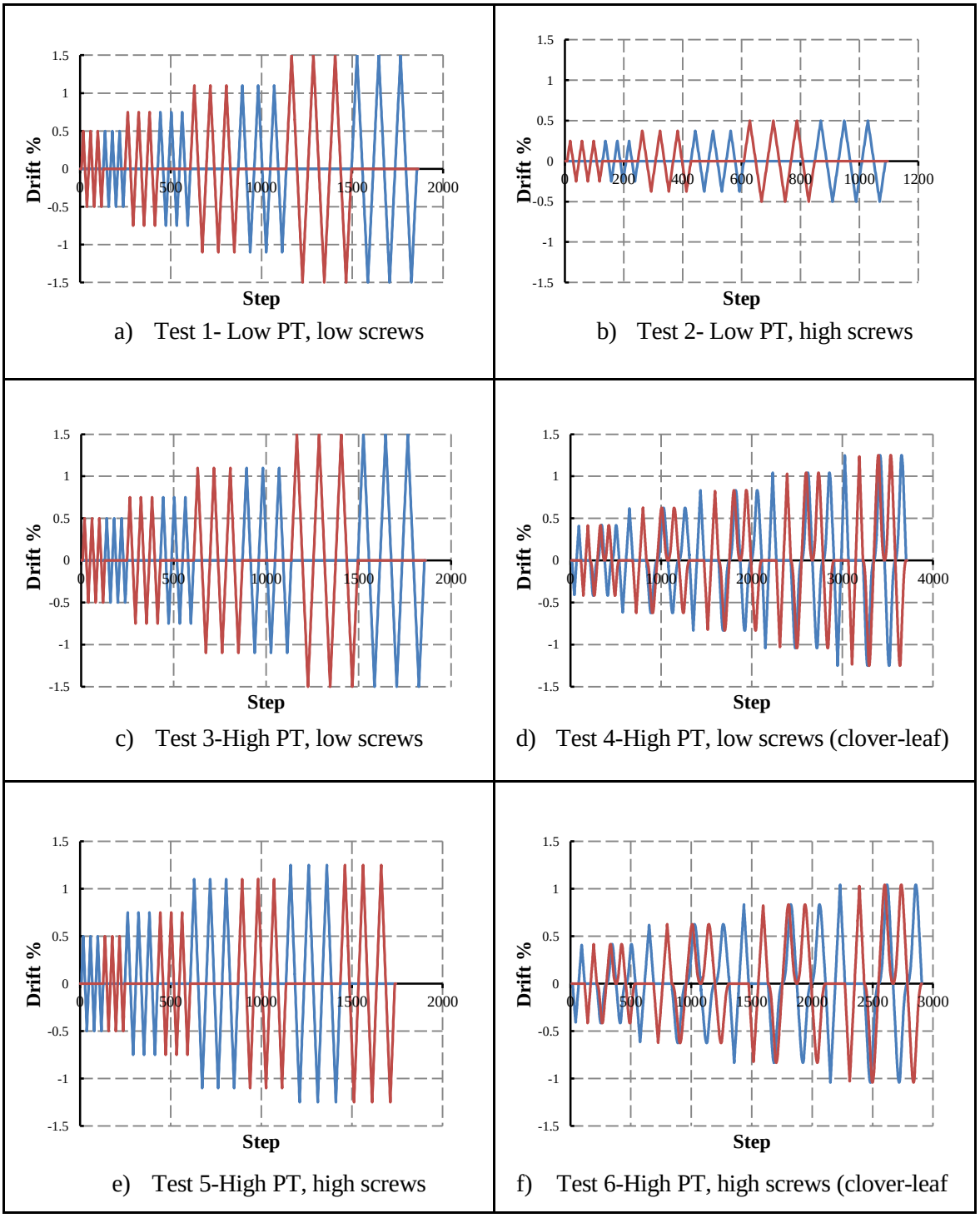

a) Test 1- Low PT, low screws

b) Test 2- Low PT, high screws

c) Test 3-High PT, low screws

d) Test 4-High PT, low screws (clover-leaf)

e) Test 5-High PT, high screws

f) Test 6-High PT, high screws (clover-leaf

Figure 5-5: Loading protocols for each of the Low Seismic tests. X direction displacement is shown in red and Y direction displacement shown in blue

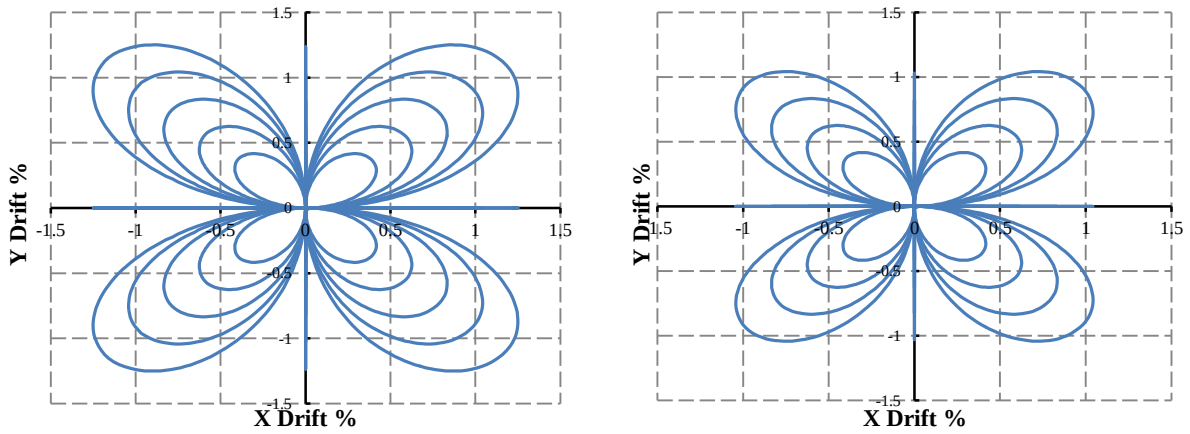

a) Test 4 –High PT, low screws, max 1.25% drift

b) Test 6 – High PT, high screws, max 1.05% drift

Figure 5-6: Bi-directional clover-leaf loading protocols for a) Test 4 and b) Test 6

5.2.2 High Seismic

For the purposes of this investigation seven tests were undertaken. In a similar fashion to the Low Seismic tests, each test had three primary variables, the post-tensioned level, the number of dissipaters and the type of loading. A summary of the High Seismic test schedule is shown below in Table 5-2. The following section describes each test in more detail.

Table 5-2: Summary of the Test schedule for the High Seismic specimen

Test	*Post-Tensioning*	*UFP's per joint*	*Loading*	*Maximum Drift (%)*
1	Low (40kN/tendon)	2	Bi-directional	1.5
2	Low (40kN/tendon)	2	Clover	1.05
3	High (100kN/tendon)	2	Bi-directional	1.0
4	High (100kN/tendon)	1	X only	1.25
5	High (100kN/tendon)	2	Y only	1.75
6	High (100kN/tendon)	0	Y only	3.5
7	High (100kN/tendon)	0	X only	3

5.2.2.1 Post-tension Force

Two different levels of Post-tensioned force were considered for the tests, a low post-tensioned level and a high post-tensioned level, the same as that of the Low Seismic specimen. The purpose of the low post-tensioned level was to simulate the likely gravity load acting on the core walls from approximately $100m^2$ of floor area. The low post-tensioning force equated to approximately 40kN in each of the two 12.7 mm strand, in the coupled walls, and 80kN in the 15.2 mm strand located in the East and West walls. Therefore, each wall had 80kN of axial load. This axial load is only an approximation of the likely gravity load. It is not an accurate representation as the post-tensioning force increases due to the elongation of the tendons once gap opening occurs.

The high post-tensioned level represented the post-tensioning required to ensure re-centering of the system. The post-tension force for the high post-tensioned tests was set at approximately 100kN in each of the two 12.7 mm strand and 150kN in the 15.2 mm strand. The stress in the tendons from the initial post-tension force corresponded to $0.75f_y$ in the 12.7mm strands and $0.77f_y$ for the 15.2mm strands. The maximum design stress in the tendons for all tests was limited to $0.9f_y$.

The post-tensioned force for Test 1 and Test 2 of the High Seismic specimen was set at the low post-tensioning level. The force in each tendon was set prior to the start of the first test. The tendons were not re-stressed in between each test, as the tendon force remained approximately constant. The post-tension force was then increased to the high post-tension level, for Test 3, Test 4, Test 5, Test 6 and Test 7. As before, the force in each strand did not change significantly after each subsequent test, so the tendons were not re-stressed after each test.

For practical reasons the low post-tensioning force tests were performed first. It was deemed much simpler to increase the post-tensioned force than lower it due to the anchorages of the tendons.

5.2.2.2 Dissipaters

Energy dissipating UFPs were used between the coupled walls and between the walls and corner columns. Initially, two UFPs per joint were installed. Tests were performed with and without UFPs.

The High Seismic specimen was tested with two UFPs per joint for Test 1, Test 2, Test 3 and Test 5. These tests had a relatively low level of peak drift (approximately 1.5%). The stiffness and strength of the High Seismic specimen, was much higher than expected. As a result, the peak displacement was limited such that the capacity of the loading apparatus, including the loading beams was not exceeded. The UFPs were not replaced after each test. In some cases, where required, the UFP bolts were tightened.

Following the above tests, one UFP per joint was removed from the coupled walls and the specimen tested again (Test 4). Little difference in the stiffness and strength was noticed. Further tests, Test 6 and Test 7, were performed where the UFP devices were removed altogether.

5.2.2.3 Loading Protocol

The High Seismic subassembly was subjected to bi-directional quasi-static cyclic loading. For some tests, the loading was applied in the X and Y directions separately while two of the tests were subject to a clover-leaf protocol. The loading protocol for each test, shown in Figure 5-7, was in accordance with the American Concrete Institute (ACI) acceptance criteria for Un-bonded Post-tensioned Precast Structural Walls (ACI ITG-5.1, 2007). Test specimens were subject to three cycles at each drift level. For each test the initial drift level was set such that the specimen was still in the elastic range. Subsequent drift levels were then increased by a factor greater than 1.25 but less than 1.5. The maximum drift level was modified for each test depending on the post-tension level and the number of UFP devices. In the initial tests, low peak drift levels were used such that no damage occurred in the specimen. The peak drift for subsequent tests were increased.

The load was applied in the X and Y directions independently for Test 1 and Test 3. Bi-directional clover-leaf loading protocols were used for Test 2 and Test 6 (Figure 5-6). Separate tests were performed for the X and Y directions with Test 4 and Test 7 loading in the X direction only and Test 5 and Test 6 loading in the Y direction only (Figure 5-8).

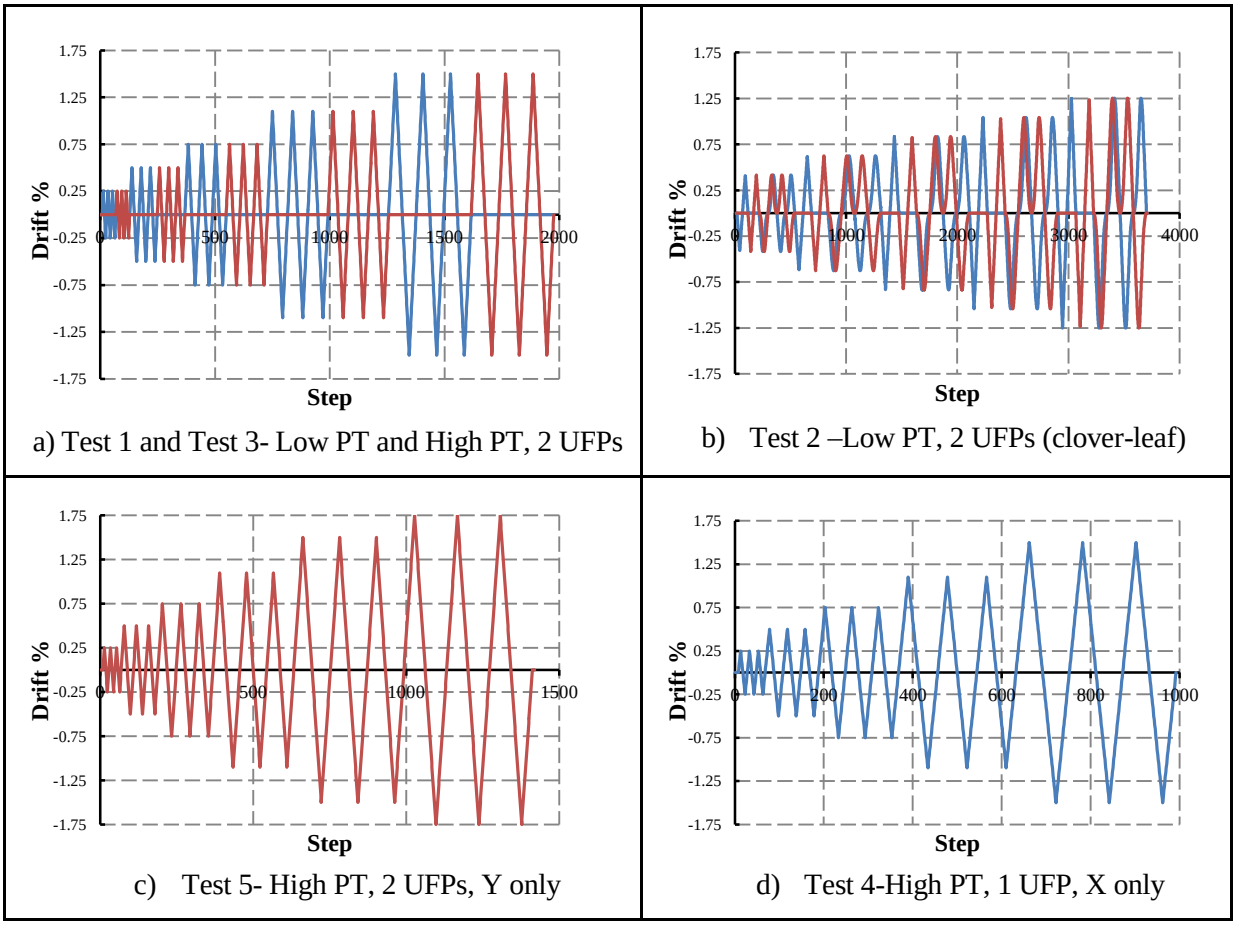

a) Test 1 and Test 3- Low PT and High PT, 2 UFPs

b) Test 2 –Low PT, 2 UFPs (clover-leaf)

c) Test 5- High PT, 2 UFPs, Y only

d) Test 4-High PT, 1 UFP, X only

Figure 5-7: Loading protocols for the low peak displacement tests of the High Seismic specimen, X displacement shown in blue, Y displacement shown in red.

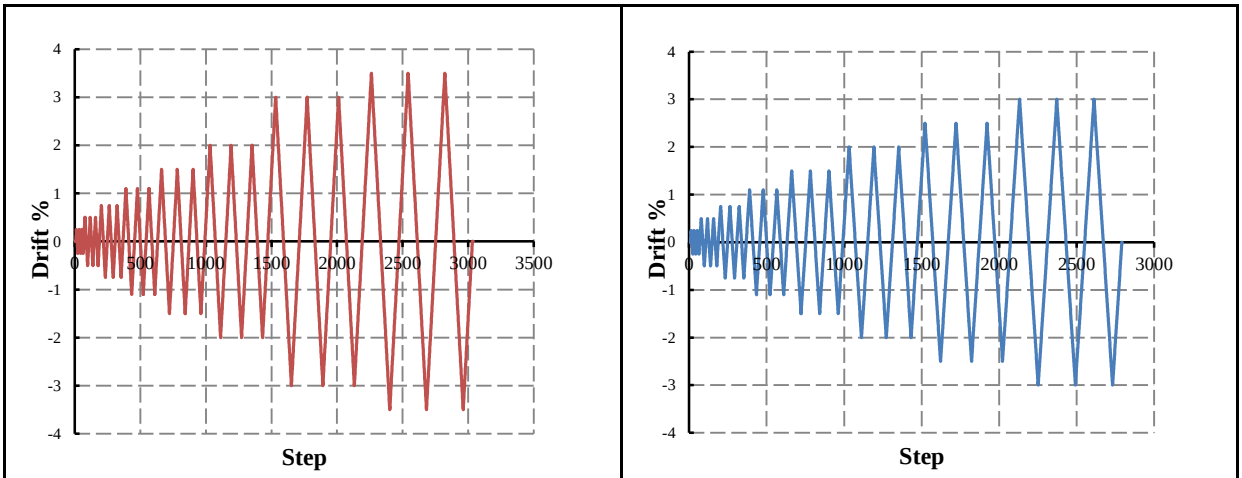

a) Test 4 –High PT, no UFPs, max 3.5% drift, Y only

b) Test 7 – High PT, no UFPs, max 3% drift, X only

Figure 5-8: Loading protocols for Test 6 and Test 7 of the High Seismic tests. X direction displacement is shown in red and Y direction displacement shown in blue

5.3 Instrumentation

The instrumentation used for the High Seismic and Low Seismic tests is described below. A full list of the instruments and the relevant data channels is provided in Appendix B.

5.3.1 Rotary Potentiometers

Eight rotary potentiometers were used for measuring the horizontal displacement of the each specimen. The rotary pots were positioned 50mm above the lower level beam and the upper level beam, at four places, measuring the lateral displacement of each single or coupled wall as shown in Figure 5-9. These were located in the NE corner (measuring Y direction); NW corner (measuring X and Y) and the SE corner (measuring X). Three additional rotary pots were used to control the three hydraulic actuators. The single 100kN ram, acting in the X direction, was controlled using a rotary pot located in the centre of the East wall, 50mm above the second level beam. The two 300kN rams, acting in the Y direction, were each controlled by a rotary pot positioned above the second level beam in line with the East wall and West wall.

Further rotary pots were used to measure the deflection of the lower beam on the N wall. They were anchored to the beam with the string fixed to the steel foundation as shown in Figure 5-10.

5.3.2 Spring Potentiometers

Spring potentiometers were used to measure uplift of the walls, and differential movement between panels. The layout of spring potentiometers is shown in Figure 5-10.

Three potentiometers situated at the base of the E, N and W walls were used to measure the uplift of each of the panels. The potentiometers were spaced evenly apart, with one in the centre of the wall and the two outer potentiometers positioned approximately 100mm from the edge of the wall.

On the E and W walls, spring potentiometers were used to measure the relative movement between the adjacent walls, for the Low Seismic specimen, and between the wall and corner columns, for the High Seismic specimen.

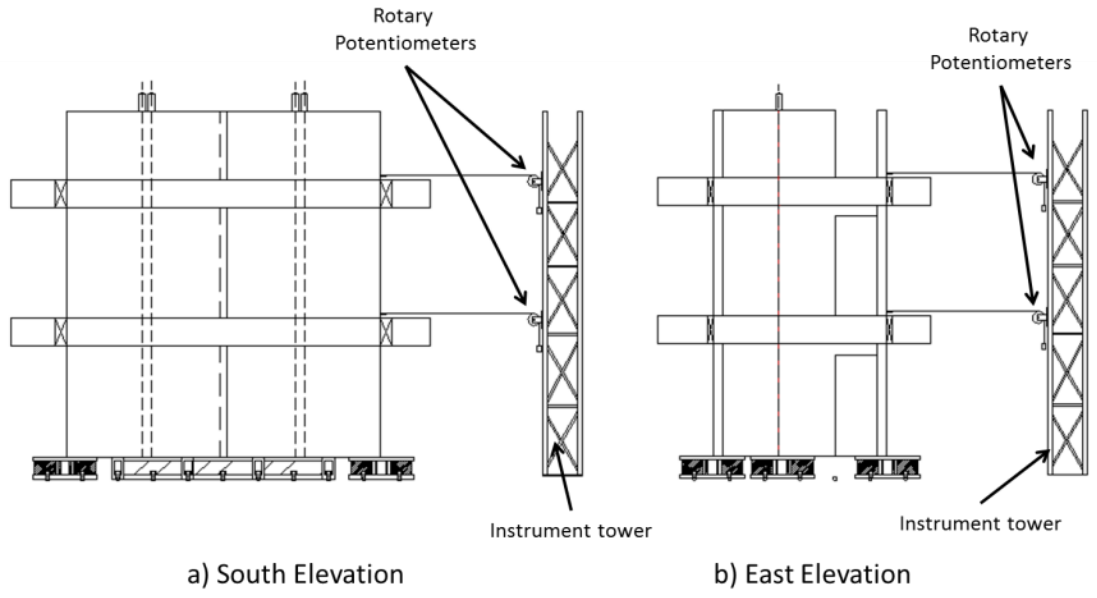

Figure 5-9: Location of Rotary potentiometers measuring lateral displacements of the walls; a) South elevation, b) East elevation

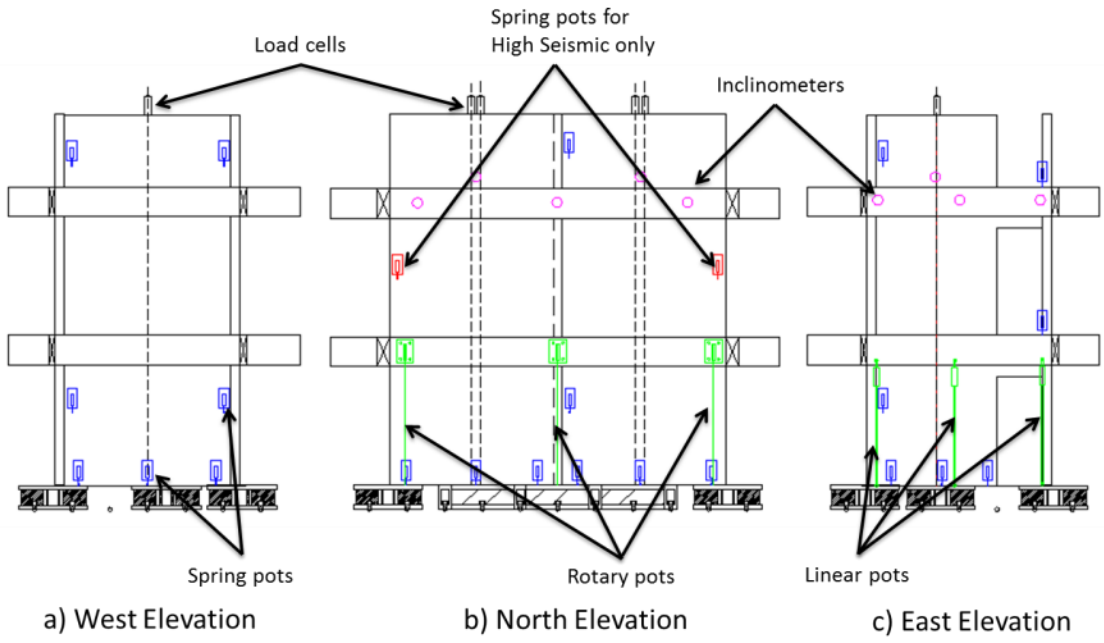

Figure 5-10: Position of spring potentiometers, inclinometers and additional rotary potentiometers used during testing

5.3.3 Inclinometers

Inclinometers were used to measure the rotation of second level beams and the rotation of the wall panels. The position of the inclinometers is shown in Figure 5-10. On the East wall, three inclinometers

were used to measure the rotation of the second storey beam, and one measuring the rotation of the wall. Five inclinometers were used to measure the rotation of the second storey beam on the North walls. One inclinometer on each of the coupled walls, measured the rotation of each of the walls.

5.3.4 Slip Spring Potentiometers

Spring potentiometers were installed at the base of the panels during testing as shown in Figure 5-11. The original orientation of the slip potentiometers (Figure 5-11a) did not accurately measure the slip of the panels. Prior to the commencement of Test 4 of the High Seismic specimen the slip potentiometers were repositioned as shown in Figure 5-11b. This allowed are more representative measurement of the movement at the base of the walls.

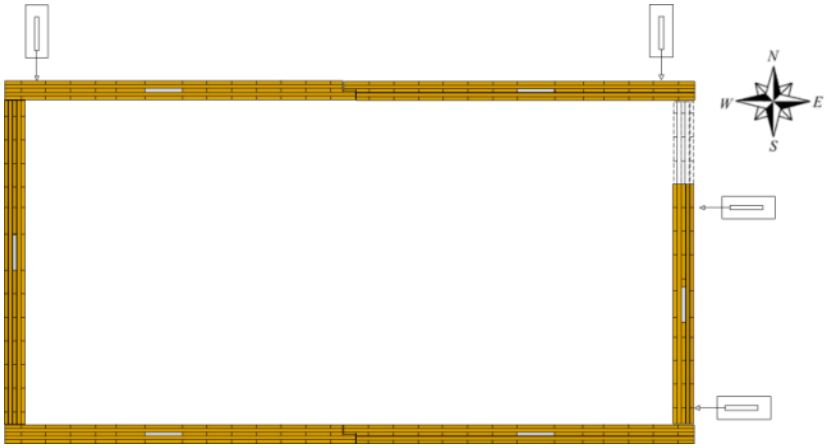

a) Original layout

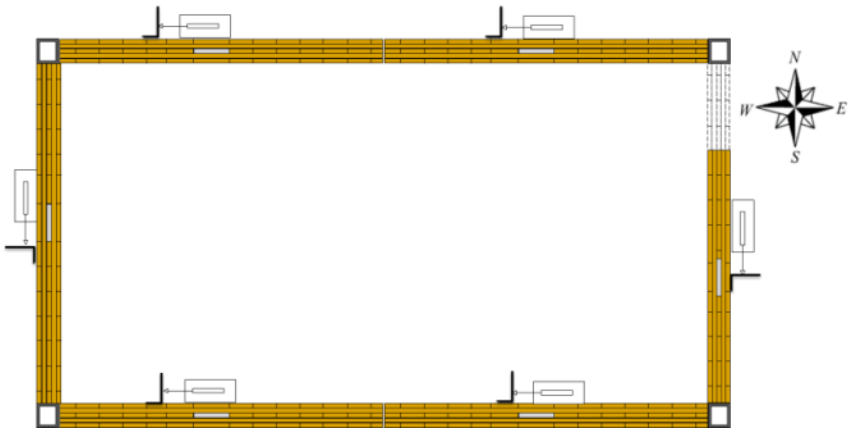

b) Modified layout

Figure 5-11: Layout of spring potentiometers measuring the slip movement at the base of the walls; a) original layout, b) modified layout

5.3.5 Load Cells

The load in the hydraulic actuators and the post-tensioned tendons was measured by load cells. The applied load in the X direction was measured with a 1000kN load cell, and the load in the two rams acting in the Y direction was each measured by a 300kN load cell.

A 150kN load cell was used to record the load in each of the 12.7mm post-tensioned tendons, located in the North and South walls. The load in the 15.2mm tendons in the East and West walls were each measured by a 300kN load cell.

The load cells for the hydraulic rams and post-tensioned tendons were calibrated in the Avery Testing Machine.

5.4 Summary of Testing Procedure

The Low Seismic and High Seismic stairwell cores were tested under a quasi-static cyclic loading regime. For each specimen, tests were performed in the X direction and Y direction separately, and combined in a clover-leaf protocol. The loading protocol for each test was in accordance with the American Concrete Institute acceptance criteria, for Un-bonded Post-tensioned Precast Structural Walls (ACI ITG-5.1, 2007).

For the Low Seismic specimen, six tests were undertaken. Each test had three primary variables, the post-tensioned level, the number of screws per joint and the type of loading. For the High Seismic specimen, seven tests were undertaken. In a similar fashion to the Low Seismic tests, each test had three primary variables, the post-tensioned level, the number of dissipaters and the type of loading.

Rotary potentiometers, spring potentiometers, inclinometers and load cells were used to measure displacements, rotations and the tendon force in the walls.

6 TEST RESULTS OF LOW AND HIGH SEISMIC SPECIMENS

This section details the test results of the Low Seismic and High Seismic specimens. The main results considered, are the global hysteretic response, the behaviour of the post-tensioned tendons, the hysteretic behaviour of selected joints and the observed damage.

6.1 Global Behaviour

The global hysteretic response of the Low Seismic and High Seismic specimens are plotted in terms of the applied force against the displacement at the top of the second level beam for each wall direction. A general representation of the test specimens is shown in Figure 6-1

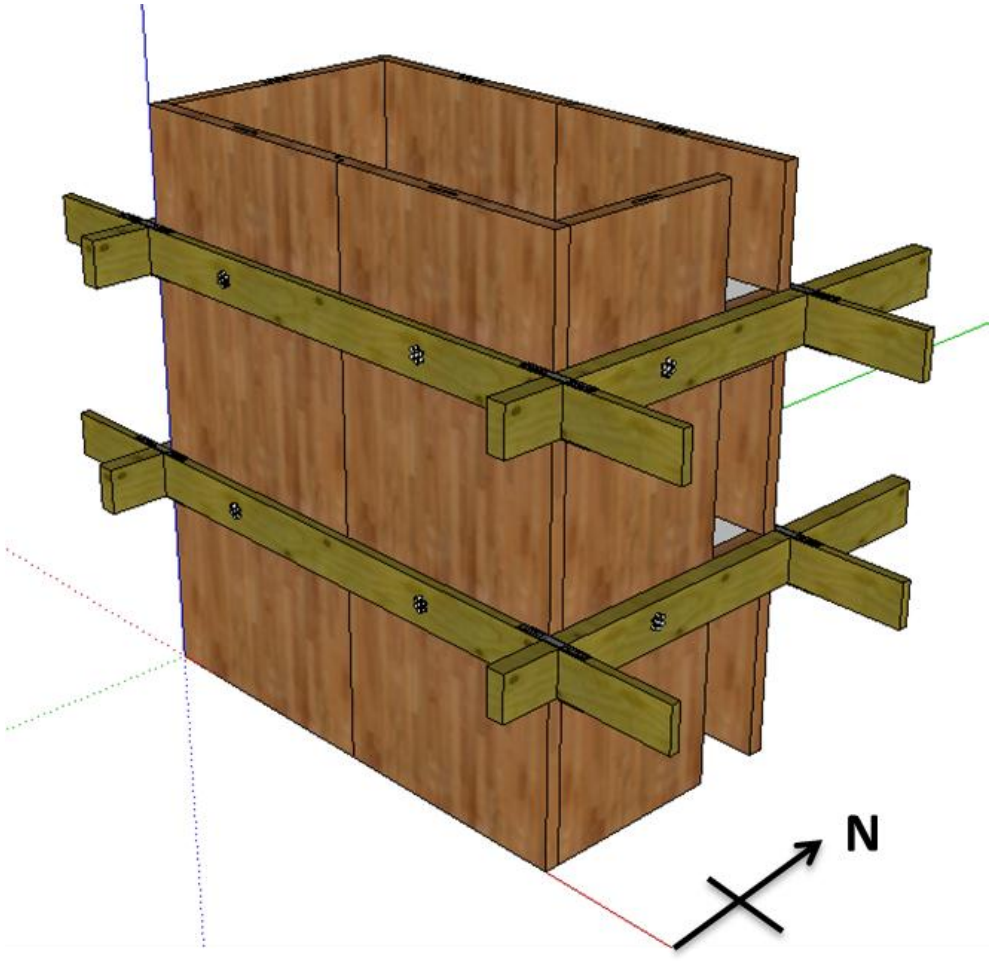

Figure 6-1: General representation of the test specimens

6.1.1 Low Seismic Results

Global hysteretic behaviour for the north coupled walls and the west single wall from Test 1, Test 2, Test 3 and Test 5 for are shown in Figure 6-2. A summary of the Test schedule for the Low Seismic specimen is shown in Table 6-1.Test 1 had a low post-tensioned force and a low number of screws. Test 2 had the same low post-tension force, but with a large number of screws. Test 3 and Test 5, had a low number of screws and a high number of screws respectively. Both had a high post-tension level. All of the tests showed stable hysteretic response, with minimal stiffness and strength degradation. Small losses in stiffness were observed in some tests at high drift levels. These losses were primarily due to loosening of the screwed connections. Re-centring behaviour was observed for all of the test configurations. A greater level of re-centring was seen for the Low screw configurations.

Table 6-1: Summary of Test schedule for the Low Seismic Specimen

Test	*Post-Tension Level*	*No. Screws per joint*	*Loading*	*Maximum Drift (%)*
1	Low (40kN/tendon)	3	Bi-directional	1.5
2	Low (40kN/tendon)	20	Bi-directional	0.5
3	High (100kN/tendon)	3	Bi-directional	1.5
4	High (100kN/tendon)	3	Clover	1.25
5	High (100kN/tendon)	20	Bi-directional	1.25
6	High (100kN/tendon)	20	Clover	1.05

Slip that occurred at the base of the coupled walls in each test, primarily due to the movement of the foundation base plates, could be observed in the hysteretic behaviour of the coupled walls. This had the effect, to artificially portray a large residual deformation in the data which was not physically observed. Where possible, the 'slip' in the data was removed, and the adjusted hysteresis is shown in Figure 6-2.

For each test the coupled walls behaved noticeably different from that of the single walls. The West single wall, for test configurations with a low number of screws (Figure 6-2b and f), displayed the hysteretic response of a wall with post-tensioning only. This behaviour is characterised by a bi-linear elastic response with no energy dissipation. Under small displacement cycles the wall behaved elastically with no gap opening. Once sufficient displacement was imposed, gap opening occurred. The bi-linear shape of the response was produced by a geometrical non-linearity, whereby there was a sudden re-positioning of the neutral axis, as gap opening occurred. The effect that increasing the post-

tensioning force had, was to delay the occurrence of gap opening. Full re-centring behaviour was observed for these test configurations. For test configurations with a large number of screws (Figure 6-2d and h), more energy dissipation was observed in the hysteretic behaviour. The area enclosed by the force-displacement relationship, equates to the amount of energy that is dissipated. For the tests with a high number of screws, slightly 'fatter' hysteretic loops than the low screw tests were observed.

For all of the tests, significantly more energy dissipation was observed in the hysteretic behaviour of the coupled walls than the single walls. For the coupled walls, approximately 15% hysteretic damping was observed, and up to 12% for the single walls (Figure 6-2h). Even for the tests with a low number of screws, a large amount of energy dissipation was observed. Whilst some of the energy dissipation was provided by the deformation of screws, the majority was produced by friction between adjacent wall panels, predominantly at the lap-joint. For the high screws tests (Figure 6-2c and g), the effect of having a large number of screws, was to restrict the relative movement between the coupled panels, more so than increase the energy dissipation. With a low number of screws, the panels were able to 'rock' freely, relative to one another. The large number of screws locked the panels together, significantly reducing the uplift of the panels, in comparison to the low screw configurations. Although the uplift was reduced, a greater strength and stiffness was observed for the high screw configurations. However, this produced large horizontal forces at the toe of the wall resulting in inelastic crushing of the timber. The North and South coupled walls behaved almost identically, as can be seen by comparing Figure 6-2 and 6-3.

For each test, the screw configuration was different for the East and West single walls. As a result, differing hysteretic behaviour was observed for the East and West walls as can be seen in Figure 6-4. The East wall contained doorway openings, as a result, the number of screws that could be inserted between that panels and the adjacent panel were limited. Therefore there were more screws on one side of the East wall than the West wall, for the low screw configurations. This produced a 'fatter' hysteresis loop, with more energy dissipation, than the West wall due to the additional deformation of screws. The length of the East wall was less than that of the West wall, due to the doorway opening. This resulted in a smaller lever-arm to the post-tensioning, and therefore, a lower capacity.

In addition to the test results in Figure 6-2, Figure 6-3 and Figure 6-4, bi-directional clover-leaf tests were performed for high post-tensioned force, with low and high screw configurations. Observations from these tests are discussed in Section 6.1.3. The hysteretic behaviour of the clover-leaf tests are shown in Appendix D.

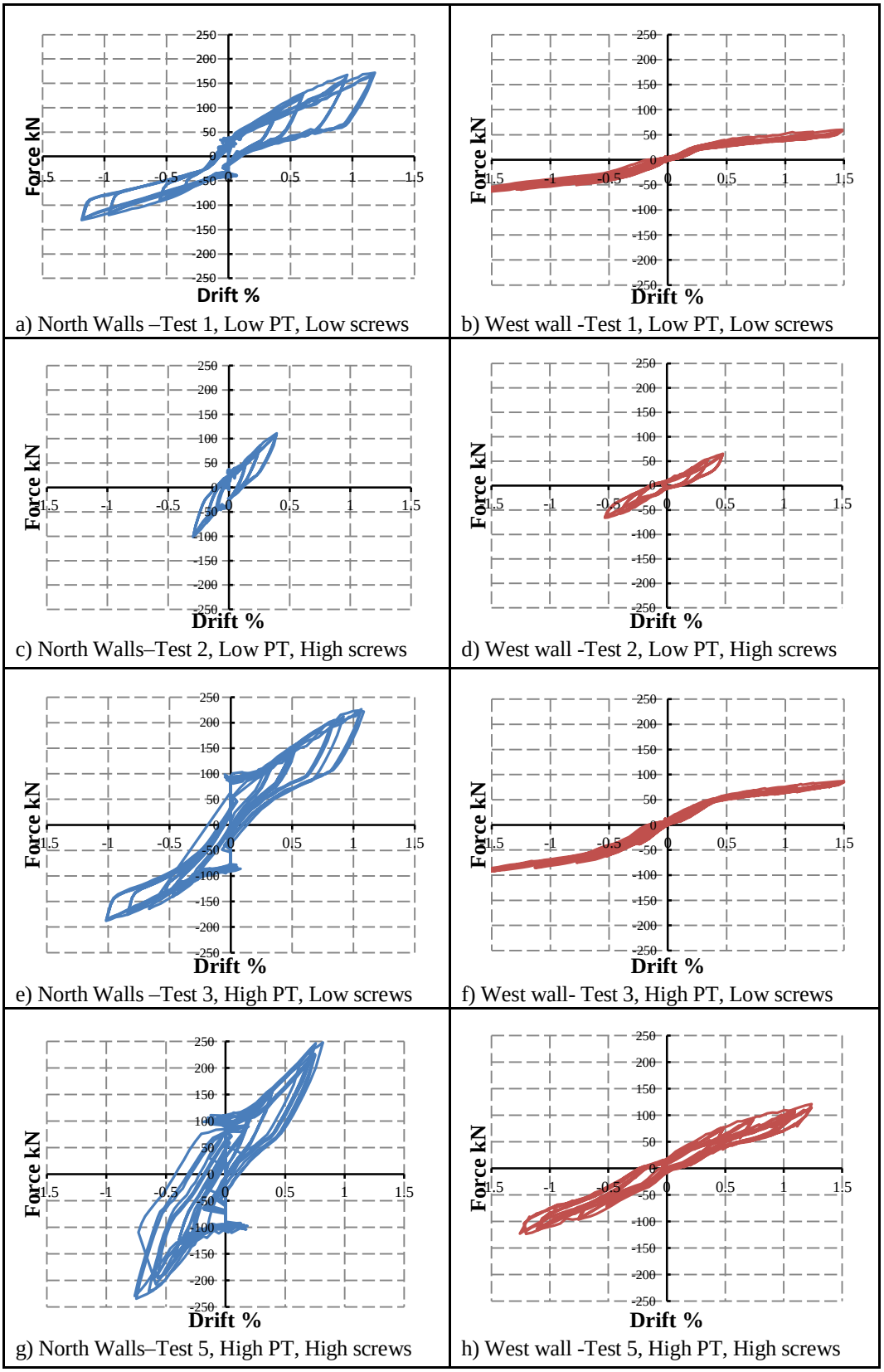

a) North Walls –Test 1, Low PT, Low screws

b) West wall -Test 1, Low PT, Low screws

c) North Walls–Test 2, Low PT, High screws

d) West wall -Test 2, Low PT, High screws

e) North Walls –Test 3, High PT, Low screws

f) West wall- Test 3, High PT, Low screws

g) North Walls–Test 5, High PT, High screws

h) West wall -Test 5, High PT, High screws

Figure 6-2: Global hysteretic response of the North coupled walls (blue) and the West wall (red) for the Low Seismic specimen

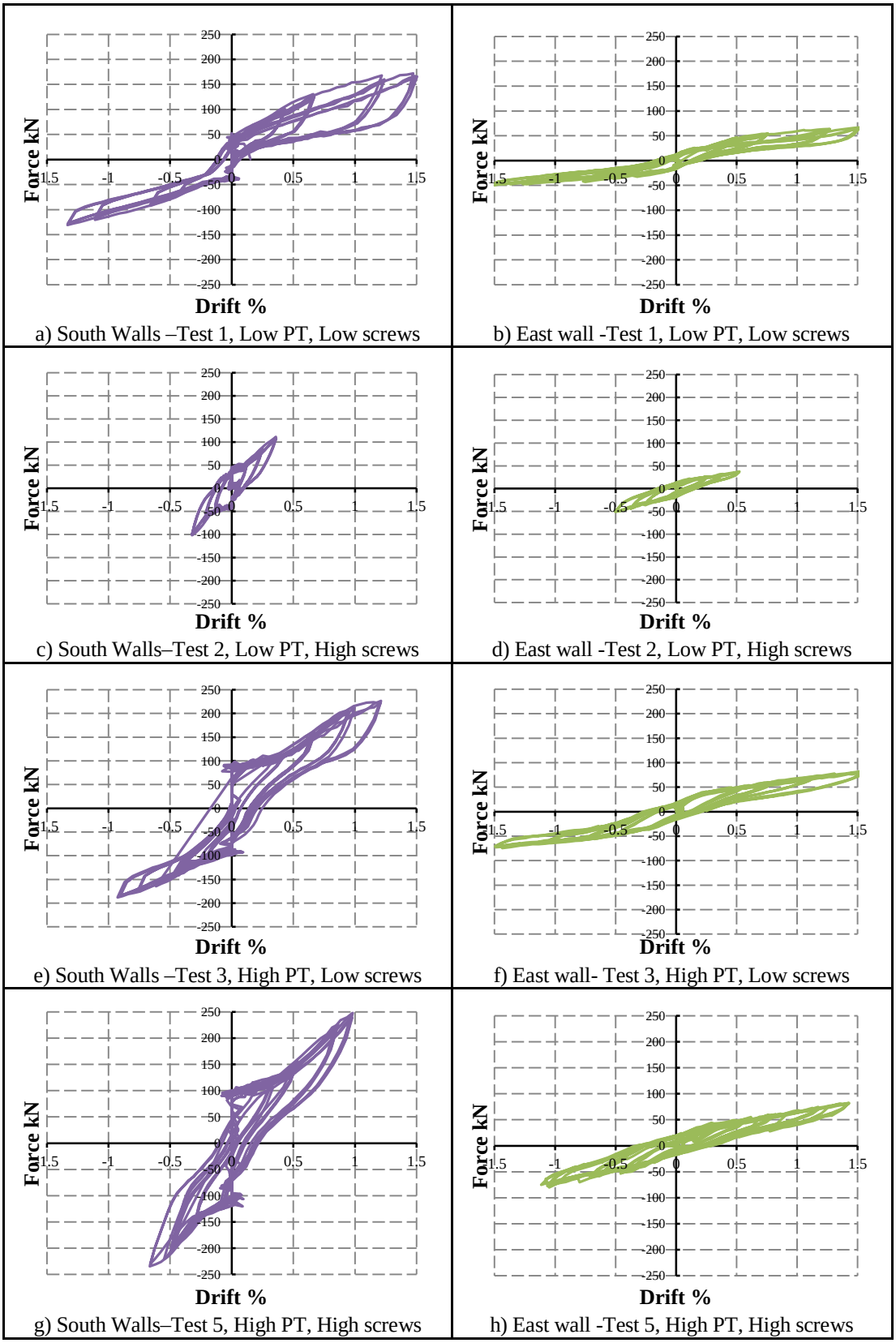

a) South Walls –Test 1, Low PT, Low screws

b) East wall -Test 1, Low PT, Low screws

c) South Walls–Test 2, Low PT, High screws

d) East wall -Test 2, Low PT, High screws

e) South Walls –Test 3, High PT, Low screws

f) East wall- Test 3, High PT, Low screws

g) South Walls–Test 5, High PT, High screws

h) East wall -Test 5, High PT, High screws

Figure 6-3: Global hysteretic response of the South coupled walls (purple) and the East wall (green) for the Low Seismic specimen

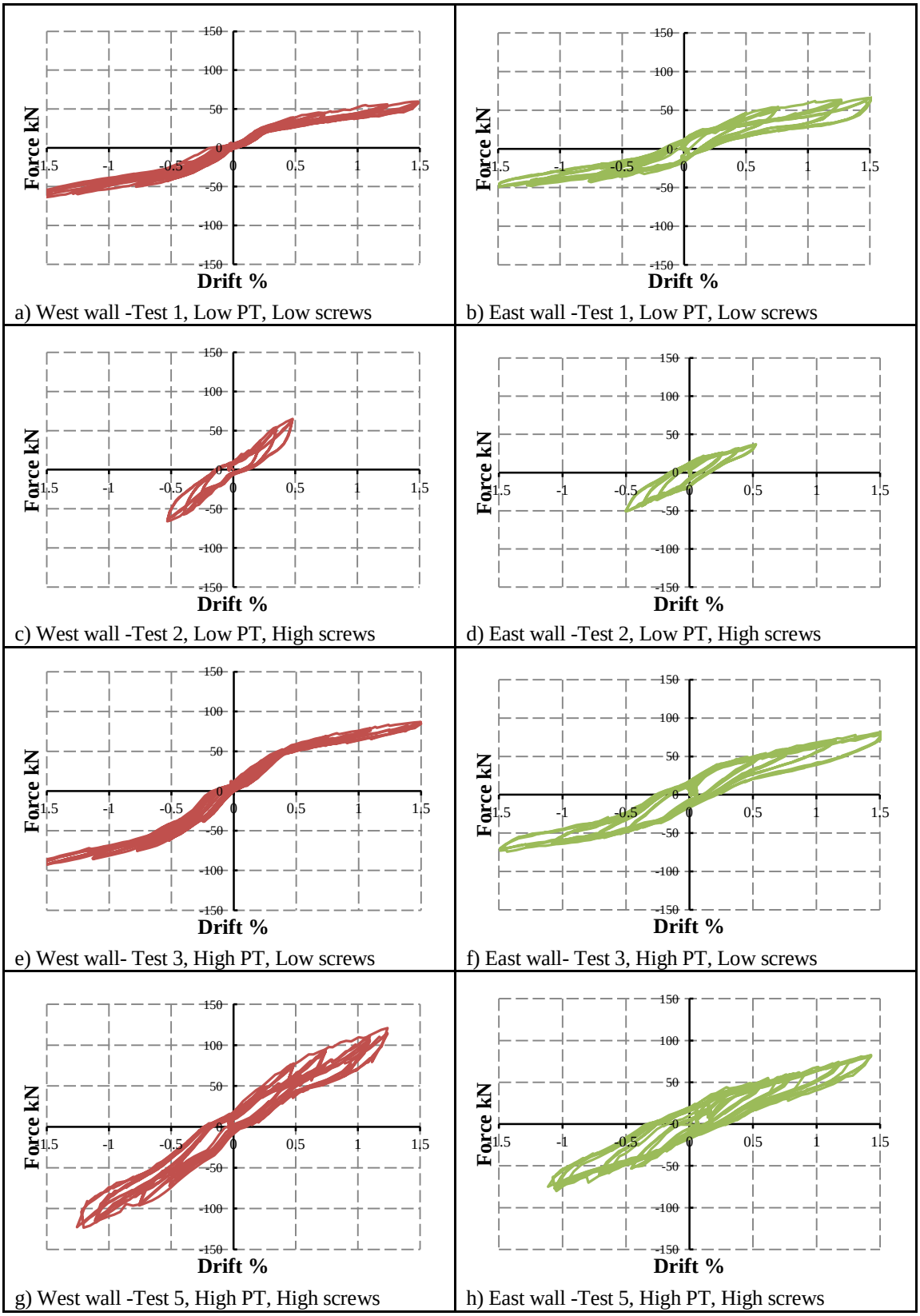

a) West wall -Test 1, Low PT, Low screws

b) East wall -Test 1, Low PT, Low screws

c) West wall -Test 2, Low PT, High screws

d) East wall -Test 2, Low PT, High screws

e) West wall- Test 3, High PT, Low screws

f) East wall- Test 3, High PT, Low screws

g) West wall -Test 5, High PT, High screws

h) East wall -Test 5, High PT, High screws

Figure 6-4: Global hysteretic response of the West wall (red) and the East wall (green) for the Low Seismic specimen

6.1.2 High Seismic Results

The global hysteretic behaviour for the North coupled walls and the West single wall from Test 1, Test 3, Test 4 and Test 5 are shown in Figure 6-5. A summary of the test schedule for the High Seismic specimen is shown in Table 6-2. Test 1, had a low post-tensioned force and two UFP devices. Test 3, had a high post-tension force and the same UFP devices as Test 1. Test 4, had a high post-tension level, with one UFP removed on the coupled walls. Test 5, had the same configuration as Test 3, but was taken to a larger displacement. Similarly to the Low Seismic tests, stable hysteretic behaviour, with minimal stiffness and strength degradation was observed. Each of the test configurations displayed re-centring properties.

Table 6-2: Summary of test schedule for the High Seismic specimen

Test	*Post-Tensioning*	*UFP's per joint*	*Loading*	*Maximum Drift (%)*
1	Low (40kN/tendon)	2	Bi-directional	1.5
2	Low (40kN/tendon)	2	Clover	1.05
3	High (100kN/tendon)	2	Bi-directional	1.0
4	High (100kN/tendon)	1	X only	1.25
5	High (100kN/tendon)	2	Y only	1.75
6	High (100kN/tendon)	0	Y only	3.5
7	High (100kN/tendon)	0	X only	3

For each test, the hysteretic behaviour of the coupled walls was significantly different to that of the single walls. For the coupled walls, approximately 13% hysteretic damping was observed, and up to 10% for the single walls. Similarly to that of the Low Seismic specimen, the response of the coupled walls was influenced significantly by friction between adjacent panels. For small displacement cycles the walls deflected elastically. Gap opening occurred at approximately 0.2% drift and 0.35% drift, for the low post-tensioned and high post-tensioned configurations respectively. Following gap opening, a relative movement occurred between adjacent panels and between the wall panels and corner columns. This produced an additional friction force, which effectively increased the stiffness and strength of the system. The friction generated within the system was a function of the applied load. The greater the applied load, the greater the friction generated. Therefore, an approximately linear backbone curve to the hysteretic response was observed, instead of the anticipated bi-linear response. This was especially

prevalent in the behaviour of the coupled walls. This type of behaviour may not be ideal in a real building. In some cases, it is not desirable to have such stiff and strong elements. Particularly, for example, if a stairwell core attracted more load than the capacity of the tie beams or connections. Furthermore, very stiff elements may cause large accelerations within a structure, causing damage to secondary, non-structural elements. However, although the system was very stiff, good energy dissipation was achieved. In addition, a large proportion of the energy was dissipated by friction between the walls, which resulted in no observed damage.

A similar increase in stiffness occurred in the single walls however to a lesser extent, due to less friction being generated, between the panels and the steel columns, in comparison to that of panel to panel. The East single wall displayed a similar, approximately linear, backbone curve to that of the coupled walls. The West single wall displayed more of a bi-linear response but with a relatively high post-gap stiffness.

The UFP devices did not have a significant influence on the hysteretic behaviour of the coupled walls. From Test 3 (Figure 6-5c), to Test 4 (Figure 6-5e) one UFP per joint was removed from the coupled walls. It can be seen that this had little effect on the strength and stiffness. The energy dissipation contribution to the hysteresis was heavily influenced by friction between the coupled wall panels. Therefore, the effect of removing half of the UFPs was insignificant.

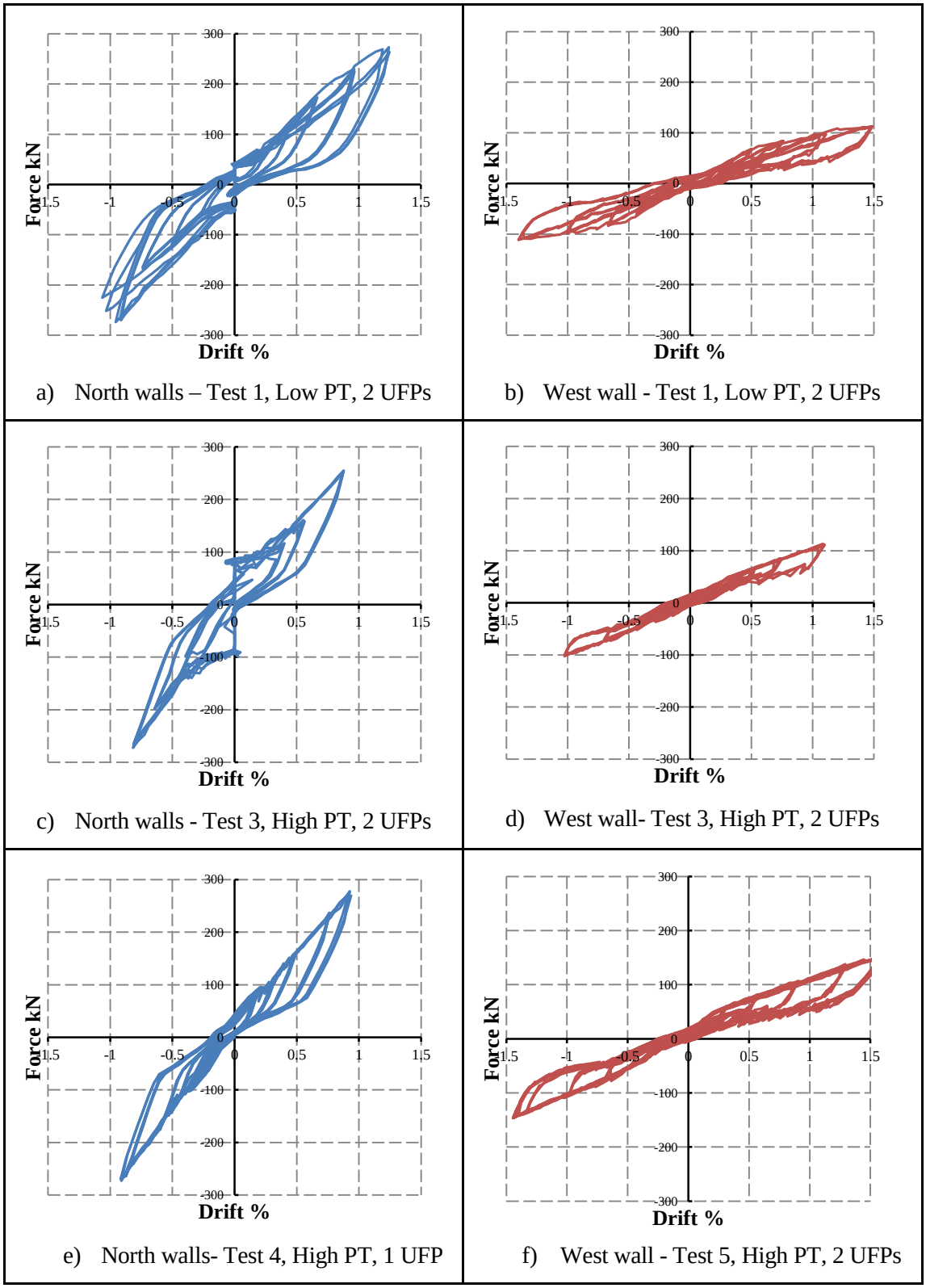

a) North walls – Test 1, Low PT, 2 UFPs

b) West wall - Test 1, Low PT, 2 UFPs

c) North walls - Test 3, High PT, 2 UFPs

d) West wall- Test 3, High PT, 2 UFPs

e) North walls- Test 4, High PT, 1 UFP

f) West wall - Test 5, High PT, 2 UFPs

Figure 6-5: Global hysteretic response of the North coupled walls (blue) and the West wall (red) for the High Seismic specimen

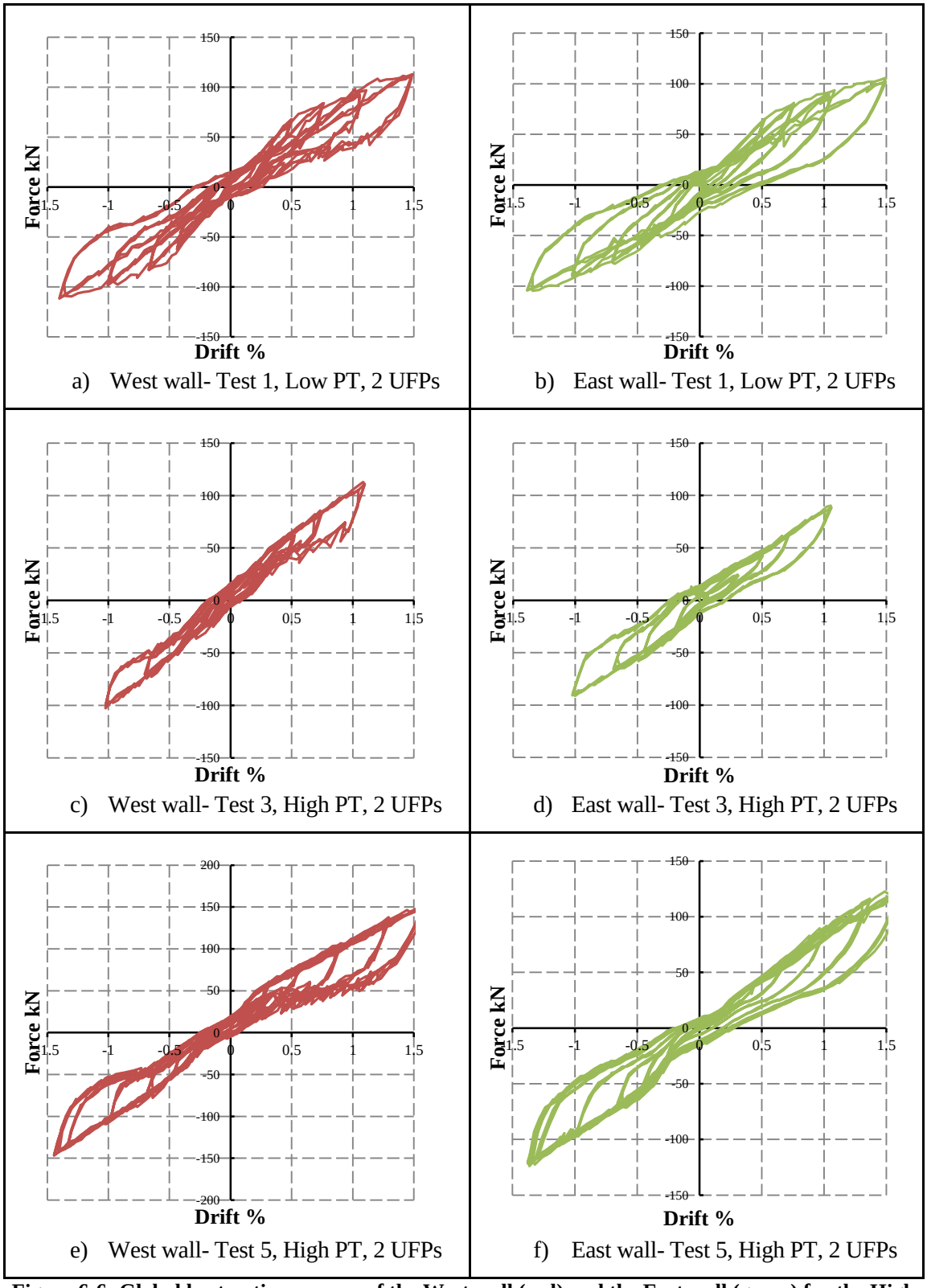

a) West wall- Test 1, Low PT, 2 UFPs

b) East wall- Test 1, Low PT, 2 UFPs

c) West wall- Test 3, High PT, 2 UFPs

d) East wall- Test 3, High PT, 2 UFPs

e) West wall- Test 5, High PT, 2 UFPs

f) East wall- Test 5, High PT, 2 UFPs

Figure 6-6: Global hysteretic response of the West wall (red) and the East wall (green) for the High Seismic specimen

The East and West walls behaved in a similar manner, with respect to strength and stiffness. In general the capacity was the same for each wall, despite the doorway opening on the East wall. The UFPs positioned above the doorways, were designed such that they were smaller, and provided a lower vertical force than that of the other UFPs. Although these UFPs were smaller, the increased lever arm from the neutral axis, due to the doorway, produced an approximately equivalent response to that of the West wall.

The effect of friction between adjacent elements was much less pronounced in the response of the single walls than that of the coupled walls. It can be seen from Figure 6-6 that the unload line is much more curved than that of the coupled walls, especially for the East wall. The sharp almost vertical drop off in force seen in the un-loading response of the coupled walls is indicative of a significant friction influence. Whereas the more rounded un-loading response of the single walls, suggests a reduced contribution of friction and a greater contribution from yielding of the UFPs. This reduction in friction was due to there being a lower friction coefficient between timber and steel, in comparison with timber-timber.

Further tests were performed, where the energy dissipating UFP devices were removed from the coupled walls (Figure 6-7) and the single walls (Figure 6-8). A reduction in stiffness and strength for both the coupled walls and single walls was observed. Due to this reduction, larger displacements were able to be reached without exceeding the capacity of the loading apparatus. The specimen was taken to a maximum of more than 2.5% drift in the coupled wall direction and over 3% drift in the single wall direction. For all walls, especially the coupled walls, a significant amount of energy dissipation was achieved, even with the removal of all of the dissipating devices. Approximately 15.5% hysteretic damping was observed for the coupled walls, and on average 9% for the single walls. The single walls displayed the more conventional hybrid hysteretic behaviour, consisting of a bi-linear backbone curve, with energy dissipation and re-centring properties. The West wall had a higher capacity than the East wall, due to the greater lever-arm generated from the longer length of the West wall. The response of the West wall was much more jagged than that of the other walls. This was due to the construction of the specimen, whereby the West wall fitted very tightly between the SHS corner columns, resulting in greater static friction between the wall and the columns. For both single walls, no stiffness or strength degradation occurred. Some stiffness degradation was observed in the response of the coupled walls, however. Up until approximately 1% drift, there was a linear backbone curve and no loss of stiffness, consistent with the previous test configurations. At larger drift cycles the slope of the backbone curve reduced, producing a more rounded hysteresis. In addition to this, stiffness degradation occurred past 1% drift; however, the hysteresis remained stable. The degradation was due to the onset of minor crushing at the toe of each wall.

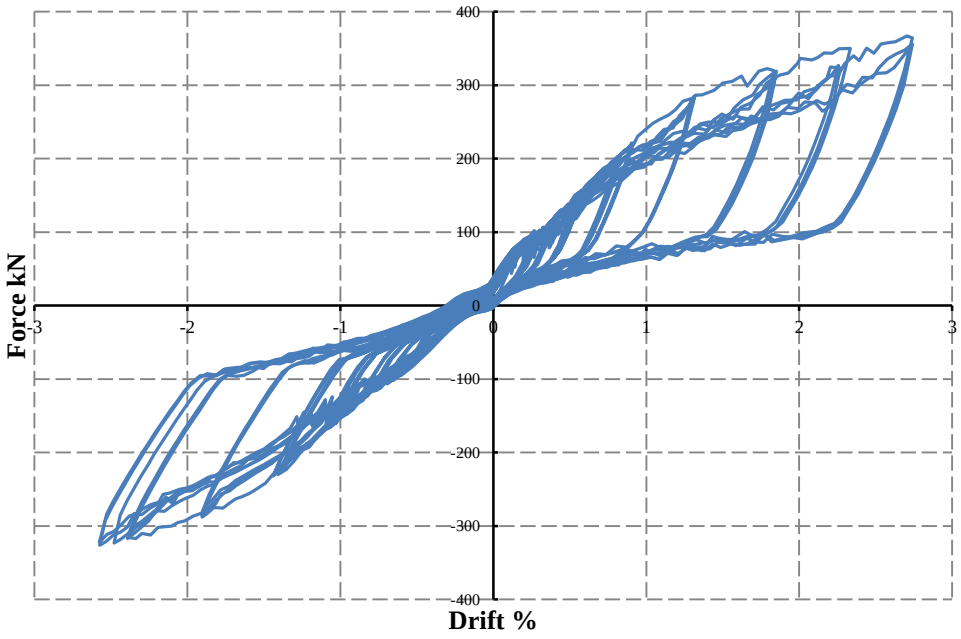

Figure 6-7: Hysteretic behaviour of the North coupled walls from Test 6 with High PT and no UFPs

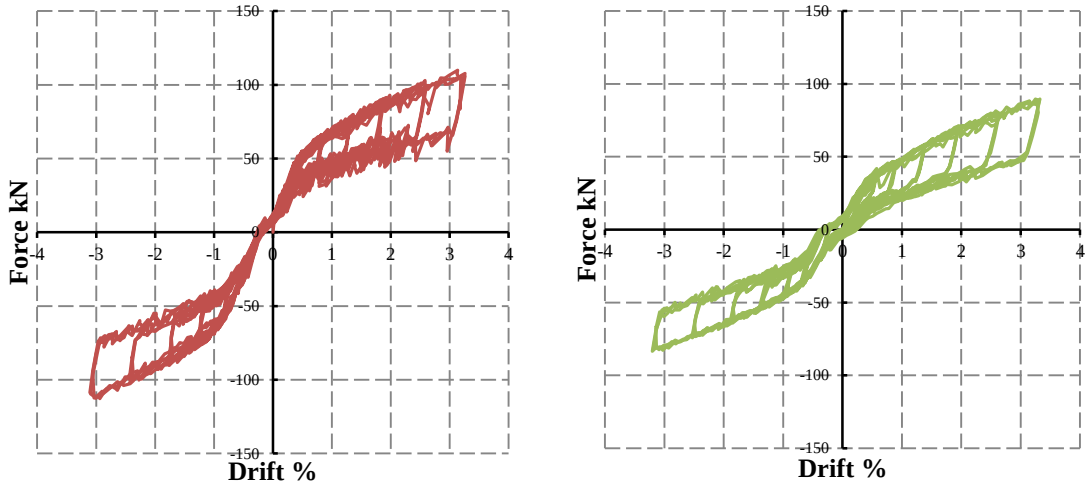

a) b)

Figure 6-8: Hysteretic behaviour from Test 7 with High PT and no UFPs for, a) West wall, b) East wall

6.1.3 Test Observations from Clover-leaf Tests

Additional tests to those detailed above were performed on the Low Seismic and High Seismic specimens. These tests differed from the others, in that the specimens were subjected to a bi-directional clover-leaf loading protocol as shown in Figure 6-9.

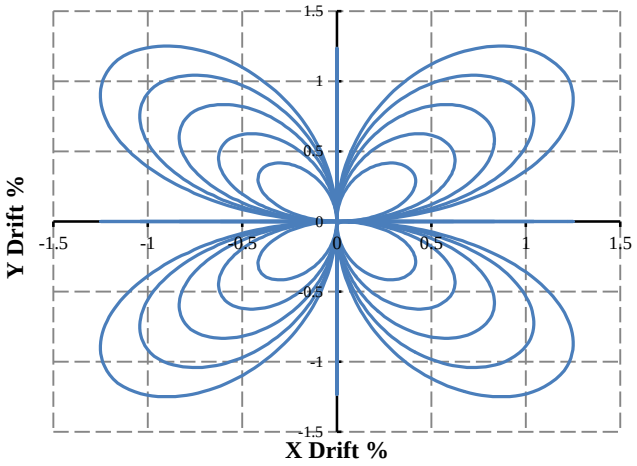

Figure 6-9: Bi-directional clover-leaf loading protocol used for testing of the Low Seismic and High Seismic specimens

Clover-leaf protocols were used to test the Low Seismic specimen, with a high post-tension force, and low (Test 4) and high (Test 6) screws configurations. The performance of the specimen, for each of these configurations was very similar to the corresponding tests, where the loading was applied in each direction separately. Test 4, the low screw configuration, behaved the same as Test 3 (Figure 6-2e and f) with respect to the individual panels. Similarly in Test 6, the high screw configuration, the behaviour was comparable to that of Test 5 (Figure 6-2g and h) with limited uplift. The main difference between the clover-leaf Tests and the previous tests was that the stairs and landings were subject to out-of-plane forces. The landing panels in particular were required to twist as the core was pushed diagonally. Although much more noise was produced during these tests, no damage was observed to the stairs or landings. The screwed connections, between the landings and the corbels on which they were seated, were flexible enough to allow the twisting movement induced in the core.

For the High Seismic specimen a further test with a clover-leaf loading protocol was performed. The test configuration consisted of, a low post-tensioned force and all of the UFPs inserted; the same as that of Test 1. Once again, the behaviour of Test 2 was very similar to that of Test1 (Figure 6-5a and b). Similarly to the Low Seismic specimen, the stairs and landings were subject to twisting displacements. Likewise, no damage was observed.

6.2 Post-tensioned Strand Behaviour

The tendon forces from various test configurations, for the Low Seismic and High Seismic specimens, are detailed in the following section. The combined tendon force for each wall, is plotted against the corresponding lateral displacement.

6.2.1 Low Seismic Post-tensioning

The behaviour of the post-tensioning strand for the coupled and single walls from Test 1, Test 2, Test 3 and Test 5 for are shown in Figure 6-10. The tension force, in each tendon; remained constant at low drift cycles, until 'gap opening' occurred. The gap opening caused the tendons to elongate, thus, increasing the tension force in the tendon. The largest increase of tension force, in the tendons, was produced by the low screw configurations. The low screw configurations, allowed the wall panels to rock relatively freely. Due to this, greater uplift of the panels was observed for the low screw test configurations (Figure 6-10a, b, e and f). The increase in tension force was greater for the single walls, in particular the West wall. The West wall, is the longest wall at 1.675m, therefore, the greatest amount of uplift was generated resulting in a larger tension force within the tendons.

The test configurations with a high number of screws, (Test 2, Figure 6-10c and d, and Test 5, Figure 6-10g and h) displayed much less of an increase in the tension force of the tendons. This was especially noticeable for the coupled walls. The large number of screws in the joints restricted the rocking behaviour of the panels significantly. Therefore the uplift of the panels, and hence elongation of the tendons, was much less than that of the low screw configuration. Comparing Figure 6-10a and 6-10g, the effect of this can be clearly seen, where the tension force in the strands from Test 5 remain approximately constant. Minor gap opening occurred, with the majority of the displacement of the specimen, being lateral translation rather than rotation of the wall.

At the conclusion of each test, the tension force in the tendons was approximately the same as the beginning, with negligible losses. This indicates that there was no local crushing of the timber or deflection of the post-tensioned tendon anchor plates at the top of each wall.

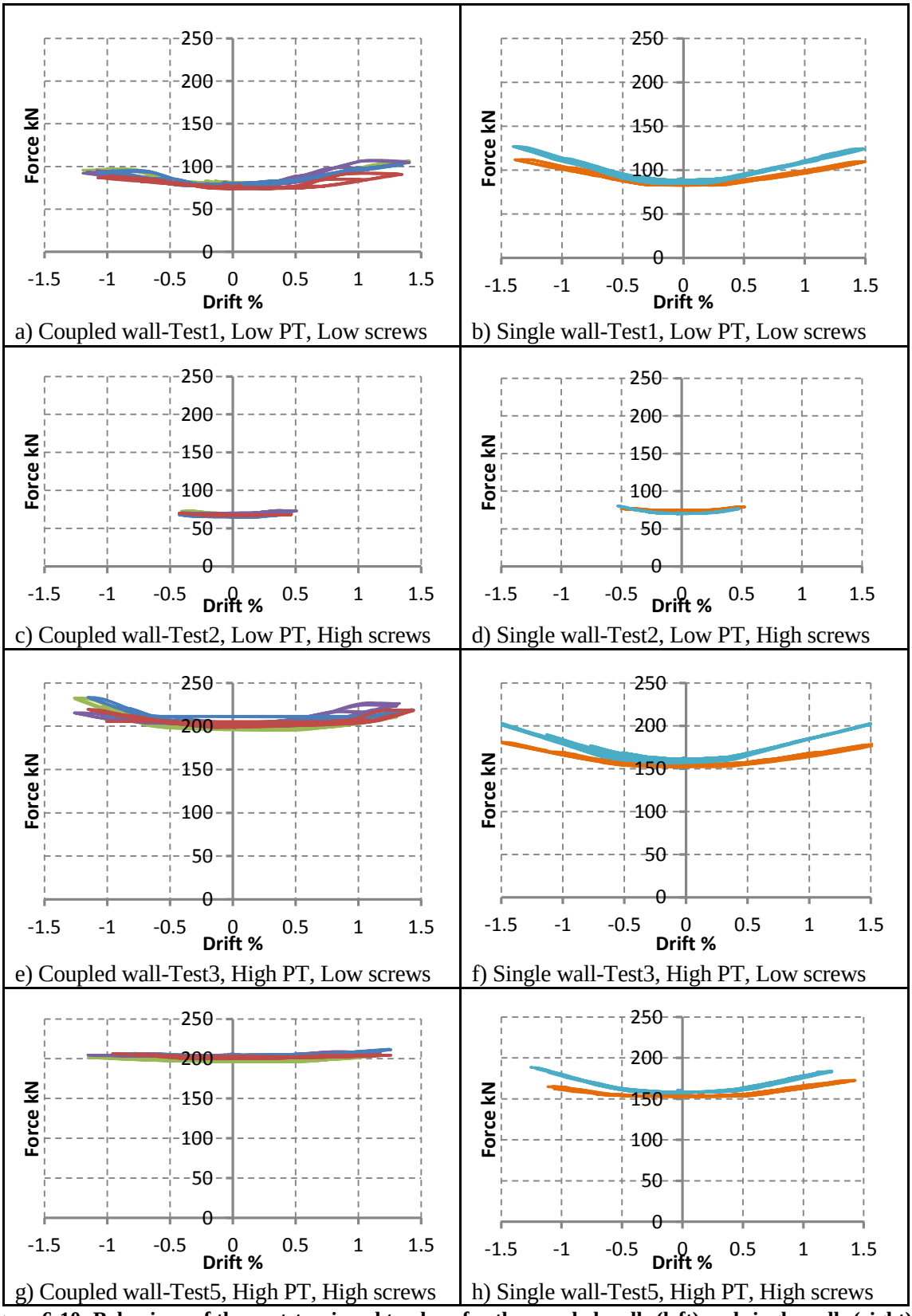

a) Coupled wall-Test1, Low PT, Low screws

b) Single wall-Test1, Low PT, Low screws

c) Coupled wall-Test2, Low PT, High screws

d) Single wall-Test2, Low PT, High screws

e) Coupled wall-Test3, High PT, Low screws

f) Single wall-Test3, High PT, Low screws

g) Coupled wall-Test5, High PT, High screws

h) Single wall-Test5, High PT, High screws

Figure 6-10: Behaviour of the post-tensioned tendons for the coupled walls (left) and single walls (right) of the Low Seismic specimen

6.2.2 High Seismic Post-tensioning

The post-tensioning force for each wall's tendons, from Test 1, Test 3, Test 4 and Test 5, for the High Seismic specimen is shown in Figure 6-11. As described previously, gap opening at the base of the wall panels causes the tendons to elongate, thus increasing the tension force in the tendon.

The largest increase in tension force, in the tendons, was produced by the single walls, in particular the West wall. The West wall is the longest wall at 1.675m. Therefore the greatest amount of uplift is generated resulting in a larger tension force within the tendon.

The behaviour of the tendons in the coupled walls was less pronounced. The greatest increase in post-tensioning force was displayed in Test 1 (Figure 6-11a and 6-11b). Test 1 had a low post-tension force, which meant that gap opening occurred at a lower drift. Therefore a greater uplift was generated and hence a greater increase in the post-tensioning force. Increasing the post-tension force, did not influence the behaviour of the tendons (Figure 6-11b and 6-11c). The removal of one of the UFPs per joint on the coupled walls appeared to have little effect on the behaviour of the tendons (Figure 6-11e).

At the conclusion of each test, the tension force, in the tendons, was approximately the same as the beginning, with negligible losses. This indicates that there was no local crushing of the timber or deflection of the anchor plates at the top of each wall.

Further tests were performed, where the energy dissipating UFP devices were removed from the coupled walls (Figure 6-12a), and the single walls (Figure 6-12b). The specimen was also pushed to a much larger displacement, of approximately 3% in the coupled walls direction, and 3.5% for the single walls. Once again, a larger increase in tension force was observed in the single wall tendons than those of the coupled walls. For the coupled walls, there was very little loss of the tension force within the tendons following the test. Whereas, some loss of post-tensioning force, in each of the single walls, was observed. The tendon in the West wall had a yield force of approximately 213kN, which was exceeded at approximately 2.5% drift. No damage was observed as a result of the tendon yielding, and full re-centring of the system was still achieved. Local crushing of the timber around the anchorage plate did not contributing to this loss.

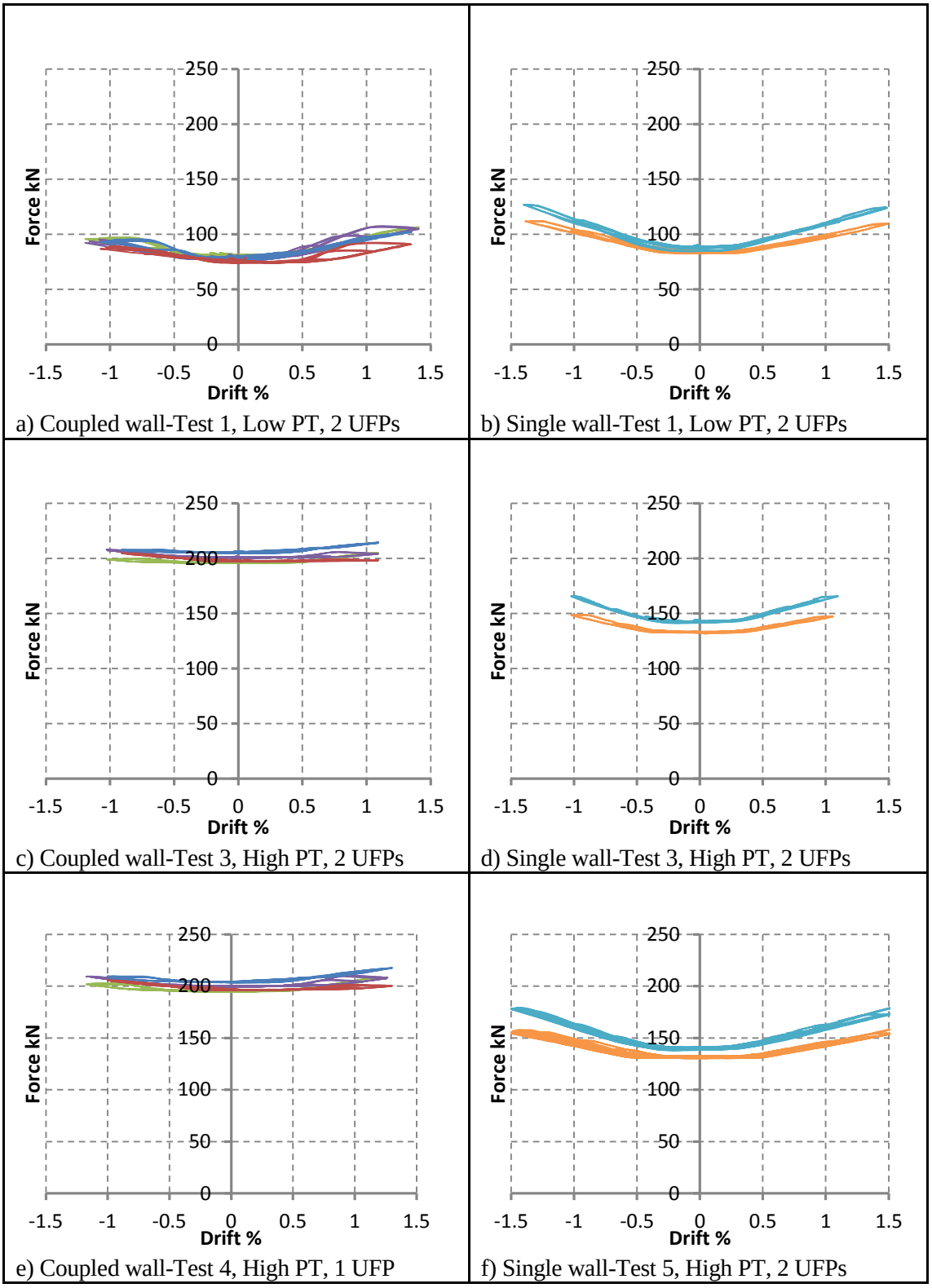

a) Coupled wall-Test 1, Low PT, 2 UFPs

b) Single wall-Test 1, Low PT, 2 UFPs

c) Coupled wall-Test 3, High PT, 2 UFPs

d) Single wall-Test 3, High PT, 2 UFPs

e) Coupled wall-Test 4, High PT, 1 UFP

f) Single wall-Test 5, High PT, 2 UFPs

Figure 6-11: Behaviour of the post-tensioned tendons for the coupled walls (left) and single walls (right) of the High Seismic specimen

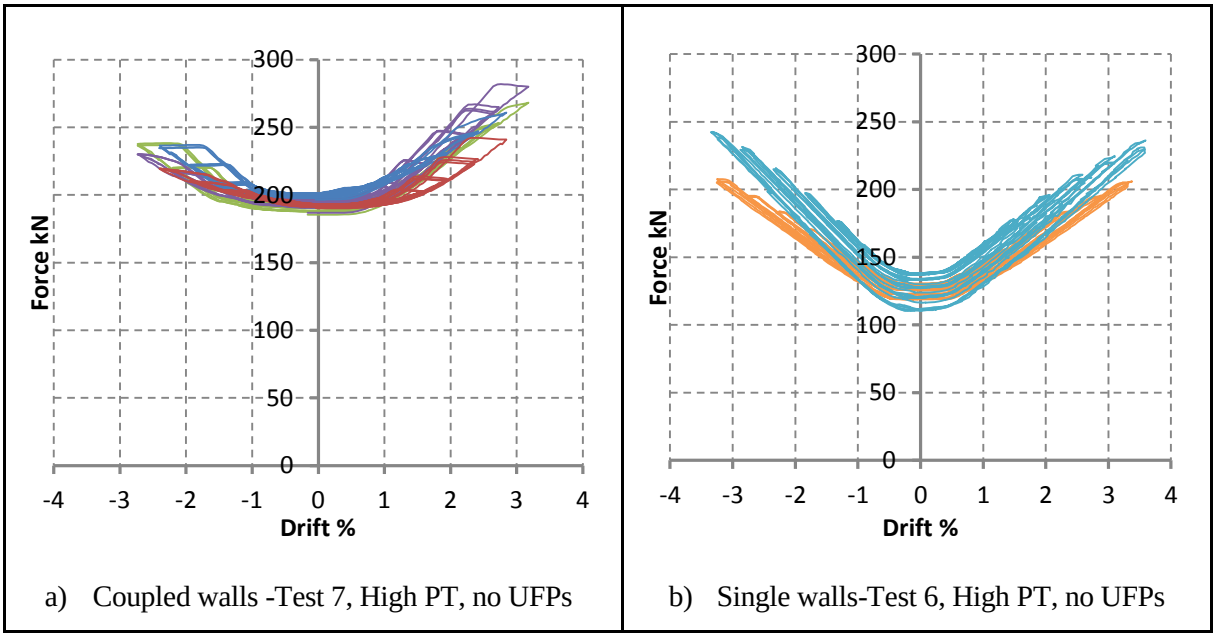

a) Coupled walls -Test 7, High PT, no UFPs

b) Single walls-Test 6, High PT, no UFPs

Figure 6-12: Behaviour of the post-tensioned tendons for the coupled walls (a) and single walls (b) of the High Seismic specimen with UFPs removed

6.3 Uplift of Panels

The uplift of the wall panels was measured at three points along the base of the wall. The amount of uplift varied for each test, depending on the configuration. For the Low Seismic tests, the number of screws in particular had a significant effect on the uplift of the panels. The post-tension force also influenced the uplift. For the High Seismic tests, the effect of the dissipater devices and the post-tension force on the uplift was less significant.

The force-displacement relationships measured at the base of selected walls are shown for the Low Seismic specimen and the High Seismic specimen. The uplift behaviour is shown, for one of the North coupled walls, and the West wall. The positions of the spring potentiometers, that were used to measure the uplift for both test specimens, are shown in Figure 6-13 and Figure 6-16. They are located in approximately the same position for both specimens, at 150mm from the edge of the wall.

6.3.1 Low Seismic

The hysteretic response from the uplift of the wall panels is shown in Figure 6-15 below. The uplift behaviour is shown for the base of one end of the West wall, and one end of the North coupled walls, as shown in Figure 6-13.

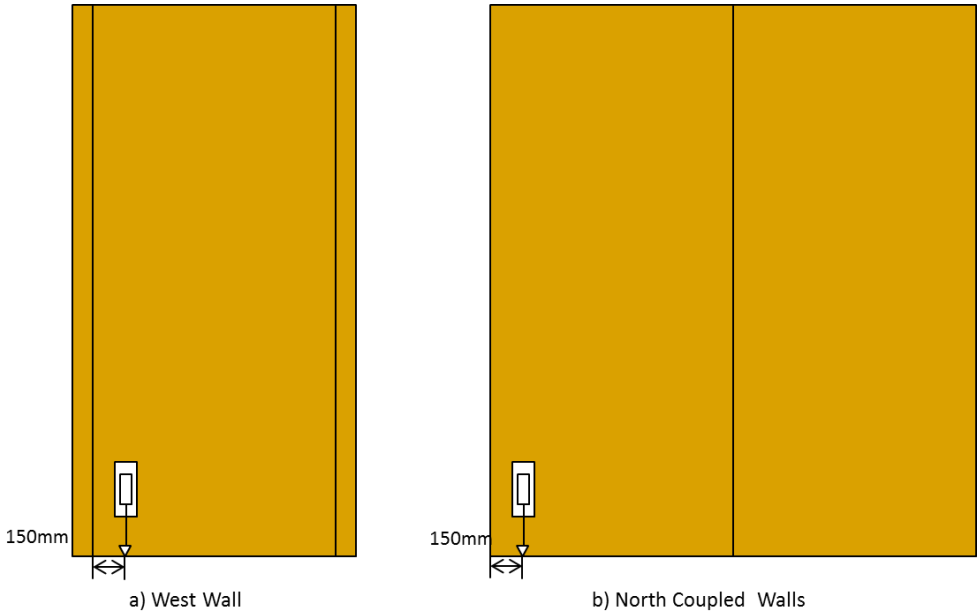

Figure 6-13: Location of spring potentiometers for the results shown in Figure 6-x

The amount of uplift generated by the rocking of the post-tensioned panels is significantly influenced by the number of screws per joint. For the test configurations with a low number of screws, Test 1 and Test 3, a much larger amount of uplift was observed for similar drift levels (Figure 6-14a). For the configurations with a high number of screws per joint, Test 2 and Test 5, the uplift was significantly reduced (Figure 6-14b). The uplift from Test 2 is much less than those of the other tests, primarily due a much lower drift level.

a) Test 1- low screws 1.25%

b) Test 5 – high screws 1.25%

Figure 6-14: Comparison between the uplift of the coupled wall panels at 1.25% for (a) low screw test and (b) a test with a large number of screws

For the couple walls, the amount of energy dissipation, signified by the area beneath the Force-Displacement curve, is greater for the low screw test configurations. This is primarily due to the increased displacement at the coupling join between the two panels, for the low screw tests. As the panels were allowed to rock more freely, greater friction dissipation was generated than that of the restricted, high screw configurations (Figure 6-15a, e). The energy dissipation, which comes from the deformation of the screws, was minimal. For the high screw configurations, the extra screws had the effect to increase the stiffness rather than increase the energy dissipation (Figure 6-15g). The energy dissipation from the deformation of the screws was minimal, this time due to the restricted amount of uplift. The screws were not subjected to as large shear displacements, as that of the low screw tests, and therefore, were not able to develop as much plastic deformation. The majority of the energy dissipation was generated by friction at the coupling joint, consistent with the low screw configurations.

In general the uplift of the single walls was much greater than the coupled walls as can be seen in Figure 6-15(b, d, f, and h). For the coupled walls, for both the high and low screw configurations, an amount of lateral movement was generated by direct sliding of the panels. Therefore, the amount of uplift generated was reduced. This was especially significant for the high screw configurations, and in particular Test 5 (Figure 6-15g). Due to the large number of screws connecting the coupled panels together, the uplift was restricted. Therefore, the contribution of rocking behaviour to the lateral displacement was also limited. As a result, a larger contribution of direct shear translation occurred, which was resisted by shear keys at the toe of the walls. This caused significant crushing of the timber against the shear key, in addition to deformation of the shear key itself (further discussed in Section 6.5). This behaviour was in contrast to that of the single walls, whereby very little sliding occurred, with most of the lateral displacement, as a result of rocking behaviour.

The energy dissipation for the single walls was very minimal. For the low screw configurations (Figure 6-15b and 6-15f) it can be seen that the behaviour is effectively bi-linear elastic. There are too few screws for the energy dissipation from them to be seen in the behaviour, and the single wall does not have the coupling joint to generate friction damping. The high screw configurations, in particular Test 5 (Figure6-15h), generated some energy dissipation. However, this was only on the first cycle, following that, stiffness degradation occurred. For all of the tests, full re-centring behaviour was observed.

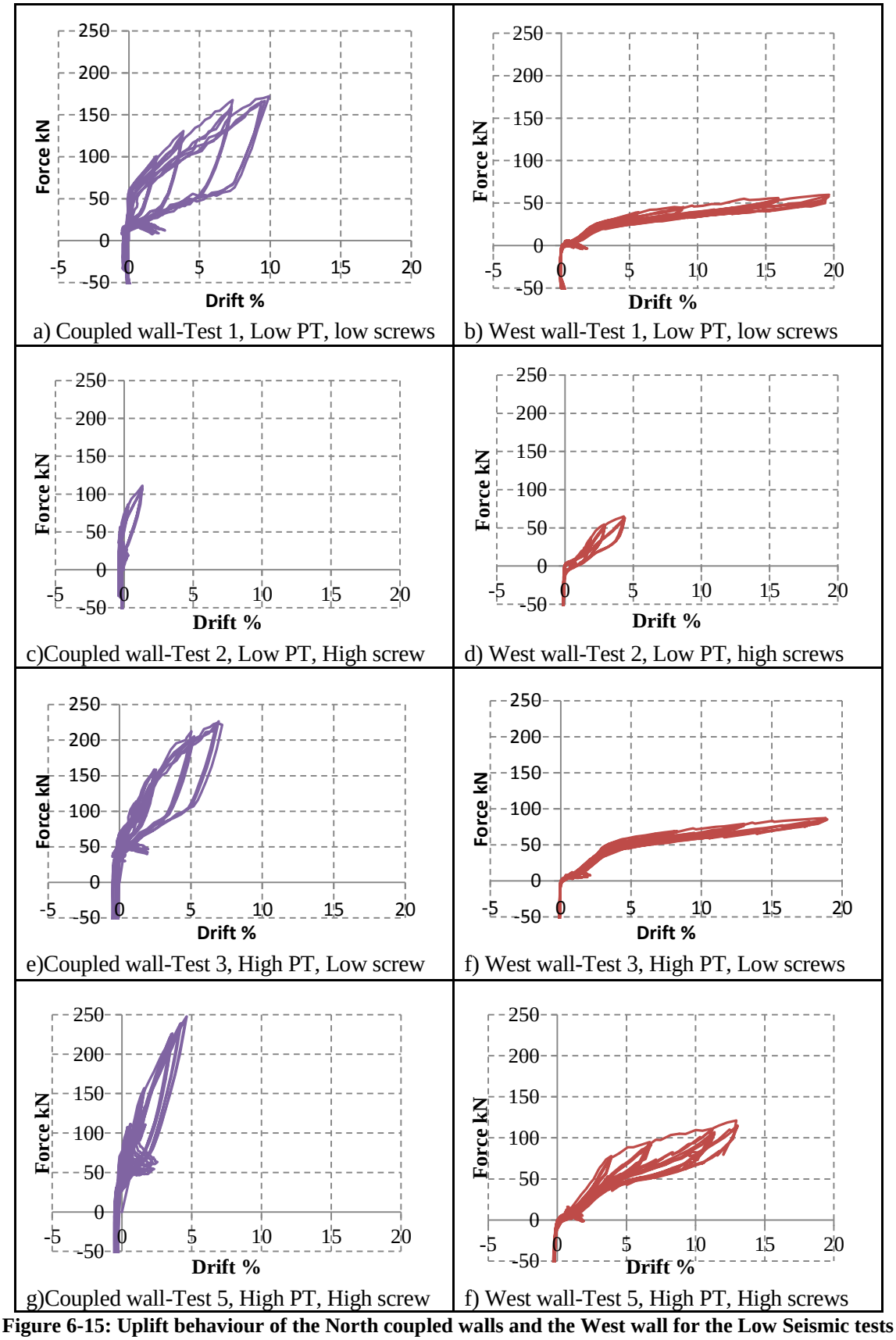

a) Coupled wall-Test 1, Low PT, low screws

b) West wall-Test 1, Low PT, low screws

c)Coupled wall-Test 2, Low PT, High screw

d) West wall-Test 2, Low PT, high screws

e)Coupled wall-Test 3, High PT, Low screw

f) West wall-Test 3, High PT, Low screws

g)Coupled wall-Test 5, High PT, High screw

f) West wall-Test 5, High PT, High screws

Figure 6-15: Uplift behaviour of the North coupled walls and the West wall for the Low Seismic tests

6.3.2 High Seismic

The hysteretic response from the uplift of the wall panels for the High Seismic tests are shown in Figure 6-17. The uplift behaviour is shown for the base of one end of the West wall, and one end of the North coupled walls, at the positions shown in Figure 6-16.

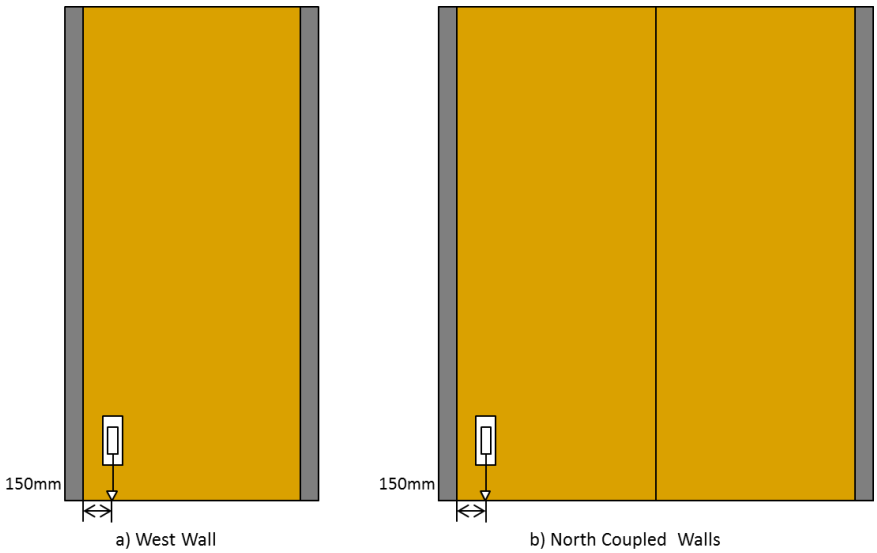

Figure 6-16: The positions of spring potentiometers measuring uplift which is discussed in this section

The amount of uplift, generated by the rocking of the post-tensioned panels, was influenced by the number of dissipaters, and the post-tension force. The effect the number of dissipaters had; was much less significant for the High Seismic tests, than the number of screws for the Low Seismic tests. However, reductions in the amount of uplift can be observed for Test 4, with high post-tension force and two UFPs per joint (Figure 6-17e). For Test 1 (Figure 6-17a and b) the maximum uplift of the coupled walls and single wall are approximately 8mm and 17mm respectively. The maximum uplift from Test 3 was approximately 4.5mm and 11mm for the coupled walls (Figure 6-17c) and the single wall (Figure 6-17d) respectively. Whilst some of the reduction in uplift is due to a reduced input drift, the majority is due to the increase in post-tension force, from 80kN to 200kN for each of the coupled walls, and 80kN to 150kN in the single walls. Following Test 3, one of the UFPs per joint was removed from the coupled walls. This had the effect to increase the amount of uplift compared to the previous level, as can be seen in Figure 6-17e. The amount of uplift did not have a significant effect on the amount of energy dissipation achieved. Neither did the number of dissipaters. It can be seen from Figure 6-17e that Test 4, which had only one UFP per joint, achieved a very similar level of dissipation to Test 1 and Test 3, with two UFPs per joint. This was due to a significant contribution of friction to the energy dissipation.

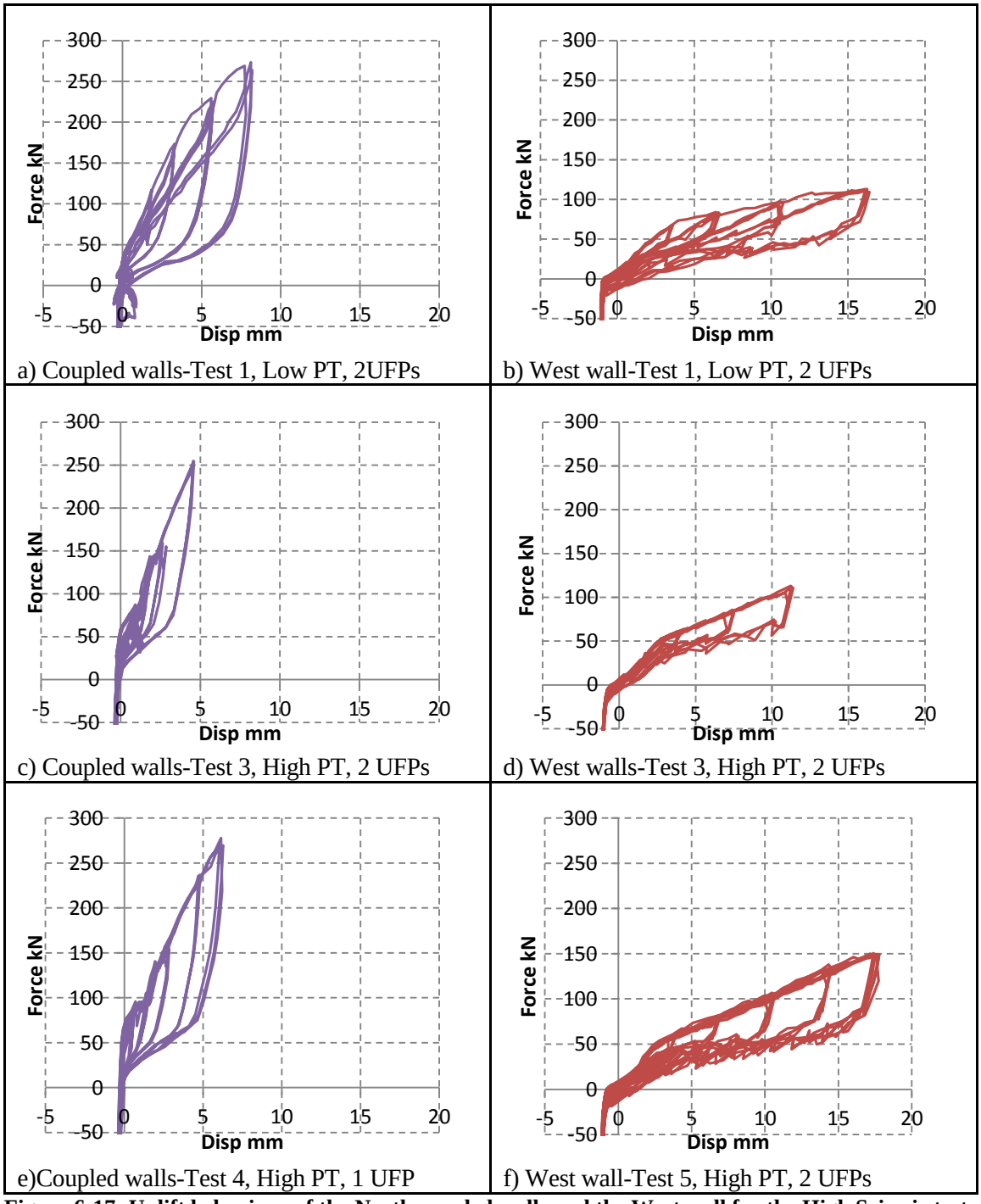

a) Coupled walls-Test 1, Low PT, 2UFPs

b) West wall-Test 1, Low PT, 2 UFPs

c) Coupled walls-Test 3, High PT, 2 UFPs

d) West walls-Test 3, High PT, 2 UFPs

e)Coupled walls-Test 4, High PT, 1 UFP

f) West wall-Test 5, High PT, 2 UFPs

Figure 6-17: Uplift behaviour of the North coupled walls and the West wall for the High Seismic tests

Further tests were performed with all of the UFPs removed. The coupled walls (Figure 6-18a) were taken to 3% drift, and the single walls (Figure 6-18b) were pushed to 3.5% drift. Significant amounts of energy dissipation were achieved, even without the dissipation devices, especially for the coupled walls. The hysteretic uplift behaviour was consistent with friction dissipation, which is identifiable by the almost vertical initial return stiffness displayed for both the coupled and single walls.

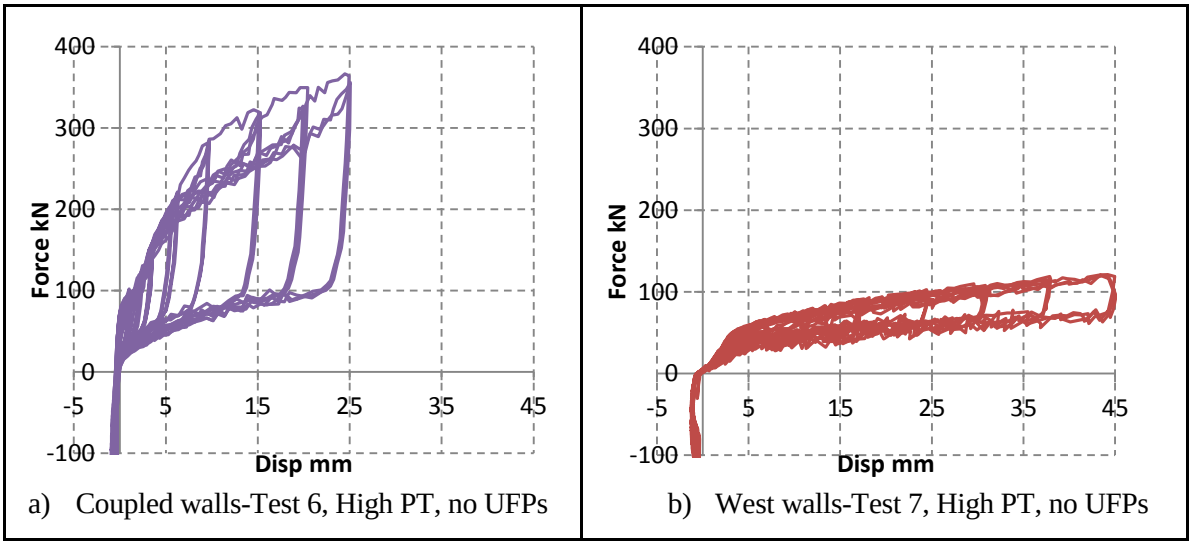

a) Coupled walls-Test 6, High PT, no UFPs

b) West walls-Test 7, High PT, no UFPs

Figure 6-18: Uplift behaviour of, a) the North walls and b) the West wall with UFPs removed

In general the uplift of the single walls was much greater than the coupled walls as can be seen in Figure 6-17 and 6-18. For the coupled walls, as was the case for the Low Seismic specimen, an amount of lateral movement was provided by direct sliding of the panels. Therefore the amount of uplift generated was reduced. This effect for the High Seismic tests was much less pronounced than that of the Low Seismic tests, due to the presence of the corner columns. For all of the tests, full re-centring behaviour was observed.

6.4 Loading Beams Behaviour

Beams representing the floor slab were connected to the stairwell core, such that there were two beams, running in the long direction and short direction of the core. The behaviour of the loading beams was representative of the likely displacements that a floor diaphragm would be subject to. The behaviour of the loading beams was recorded with respect to vertical displacement and rotation of the beams, relative to that of the walls. The loading beams were not varied during each set of tests. Therefore, the behaviour of the loading beams for the Low Seismic and the High Seismic specimens is shown for one test, from each specimen.

6.4.1 Low Seismic beams

The loading beams for the Low Seismic specimen were connected to each wall, by a ring of bolts acting as pins, at approximately the centre of each wall. This allowed the lateral loads to be transferred directly from the beams into the walls. While the ring of bolts transferred the lateral loads they were subject to vertical displacements, due to the uplift of the rocking walls as shown in Figure 6-19. The uplift of the

beams was approximately half of that of the corresponding wall panel, as the ‘pin’ was located at approximately the centre of each wall.

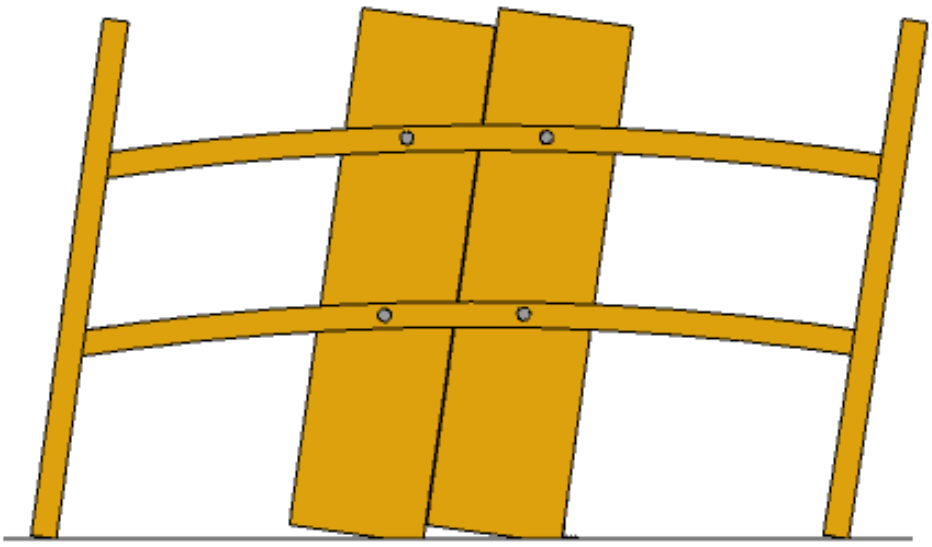

Figure 6-19: Representation of the uplift of the loading beams, as a result of the walls rocking during the Low Seismic Tests

A single positive and negative displacement cycle, from Test 1 is shown in Figure 6-20. The rotation of the wall is plotted against the rotation of the loading beam for the North coupled walls. The corresponding deflection of the loading beams, on the North coupled walls and the East single wall, are shown in Figure 6-21. The 16 points shown on Figure 6-20 signify the lines 1 to 16 in Figure 6-21. Loading in the positive direction, pushing on the walls, until the peak horizontal displacement occurred, the vertical displacement of the loading beams increased (Figure 6-21a). The displacement then decreased as the loading was reduced, from the peak positive displacement towards zero (Figure 6-21b). The same behaviour was then observed for the negative cycle, whereby the vertical displacement of the beams increased up to the peak (Figure 6-21c) and then decreased back towards zero (Figure 6-21d). The displaced shape of the loading beams on the North walls was different for the positive and negative cycles. This was due to the way in which the load was applied in the coupled wall direction. For positive displacement cycles where the beams were pushed, the angle of the hydraulic ram pushed slightly upwards. This produced a greater vertical displacement in the (left) end of the beam which was closest to the ram. For the negative cycles where the ram was pulling, the same behaviour was not observed. As a result, the uplift at the left end of the North wall beams was not as large and the displaced shape differed. The same situation created a relatively large apparent uplift in the East wall beam. For loading in this direction, the vertical displacement was expected to be minimal like that of the

negative cycle. This vertical displacement was caused by the influence of the North wall beams on the East wall beams, in addition to the out of plane rotation of the East wall. The combination of these two factors produced the unexpected vertical displacement of the East wall beams. It is noted that this behaviour only occurred when 'pushing' and not 'pulling'.

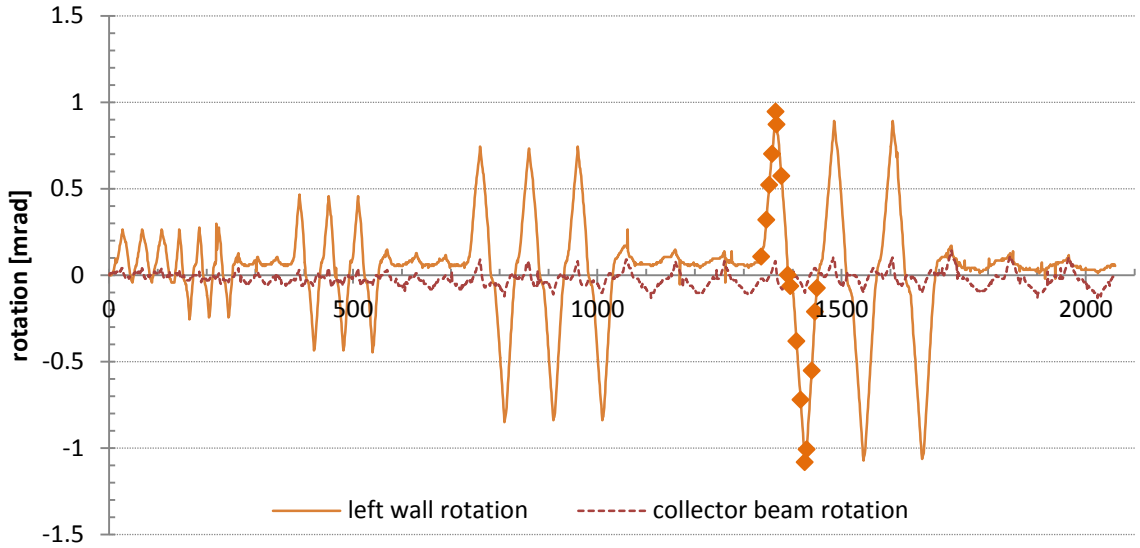

Figure 6-20: Rotation of North walls displaying 16 points on one displacement cycle which correspond to Figure 6-21

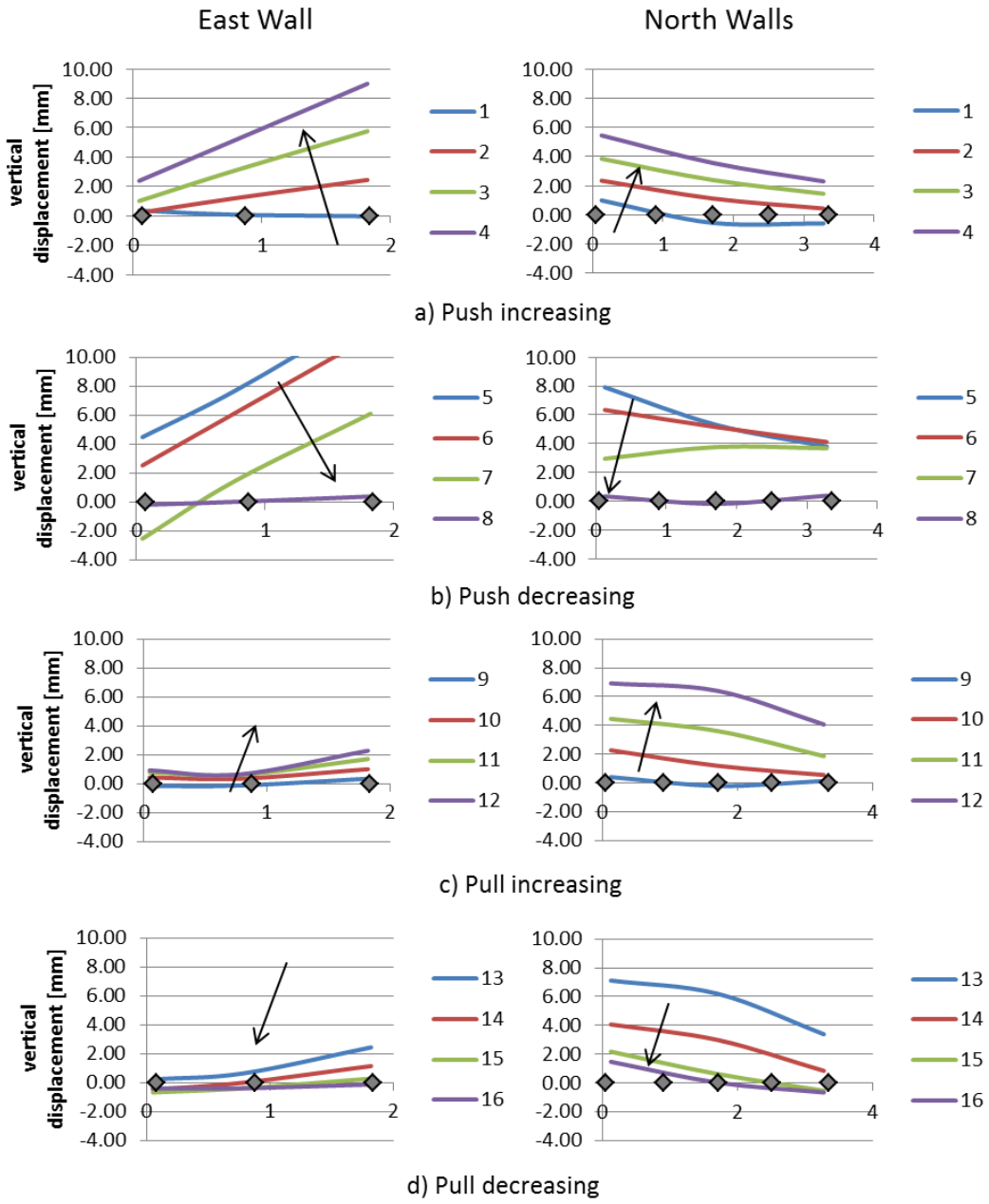

Figure 6-21: Vertical displacement of North wall and East wall loading beams for the displacement cycle shown in Figure 6-20

6.4.2 High Seismic

The loading beams for the High Seismic specimen were connected to the corner columns, such that there were two beams running in the long direction, and two in the short direction of the core. The beams transferred the lateral load into the columns. The wall panels were in contact with the columns, such that the load was able to be transferred into the walls by friction. The objective of applying the load through the columns, and into the walls, was to minimise deformations of the floor slab. When the walls were subject to lateral loading, one end of each wall uplifts. By eliminating a direct connection between the loading beams and the wall panels the beams were separated from the vertical displacement associated with the rocking walls. A representation of the behaviour of the loading beams during the High Seismic tests is shown in Figure 6-22.

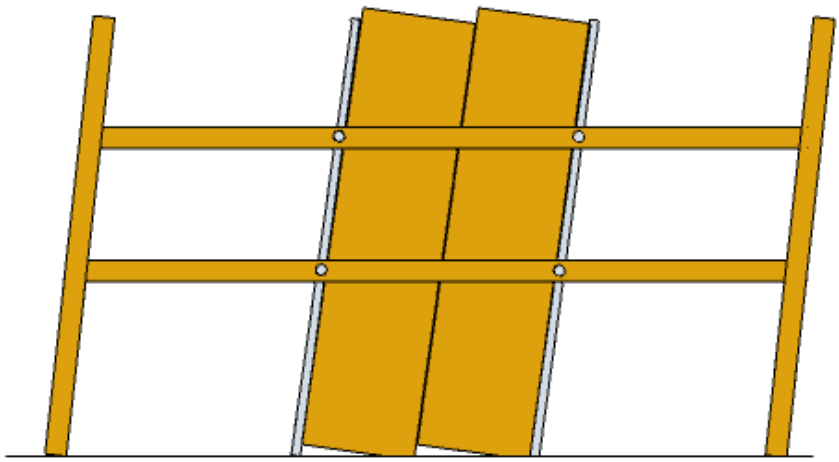

Figure 6-22: Representation of the behaviour of the loading beams, as a result of the walls rocking during the High Seismic Tests

A single positive and negative displacement cycle from High Seismic Test 1 is shown in Figure 6-23. The rotation of the wall is plotted against the rotation of the loading beam for the North coupled walls. The corresponding deflection of the loading beams, on the North coupled walls and the East single wall, are shown in Figure 6-24. The 16 points shown on Figure 6-23, signify the lines 1 to 16 in Figure 6-24. Loading in the positive direction (pushing on the walls) up until the peak horizontal displacement, the vertical displacement of the loading beams increased (Figure 6-24a). The displacement then decreased as the loading was reduced from the peak positive horizontal displacement towards zero (Figure 6-24b). The vertical displacement of the loading beams was minimal, especially during the negative cycle when the ram was pulling. The larger vertical displacement of the left end of the North wall beams; was due to the way in which the load was applied similar to that of the Low Seismic specimen. For positive displacement cycles, where the beams were pushed, the angle of the hydraulic ram pushed slightly

upwards. This produced a greater vertical displacement in the left end of the beam which was closest to the ram.

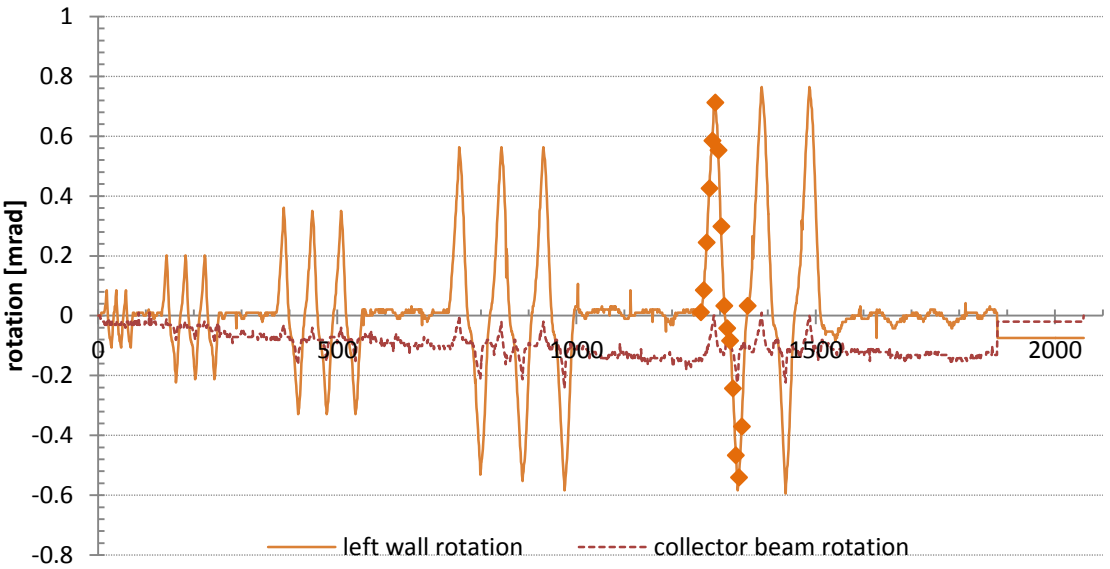

Figure 6-23: Rotation of North walls from Test 1 of the High Seismic tests displaying 16 points on one displacement cycle which correspond to Figure 6-24

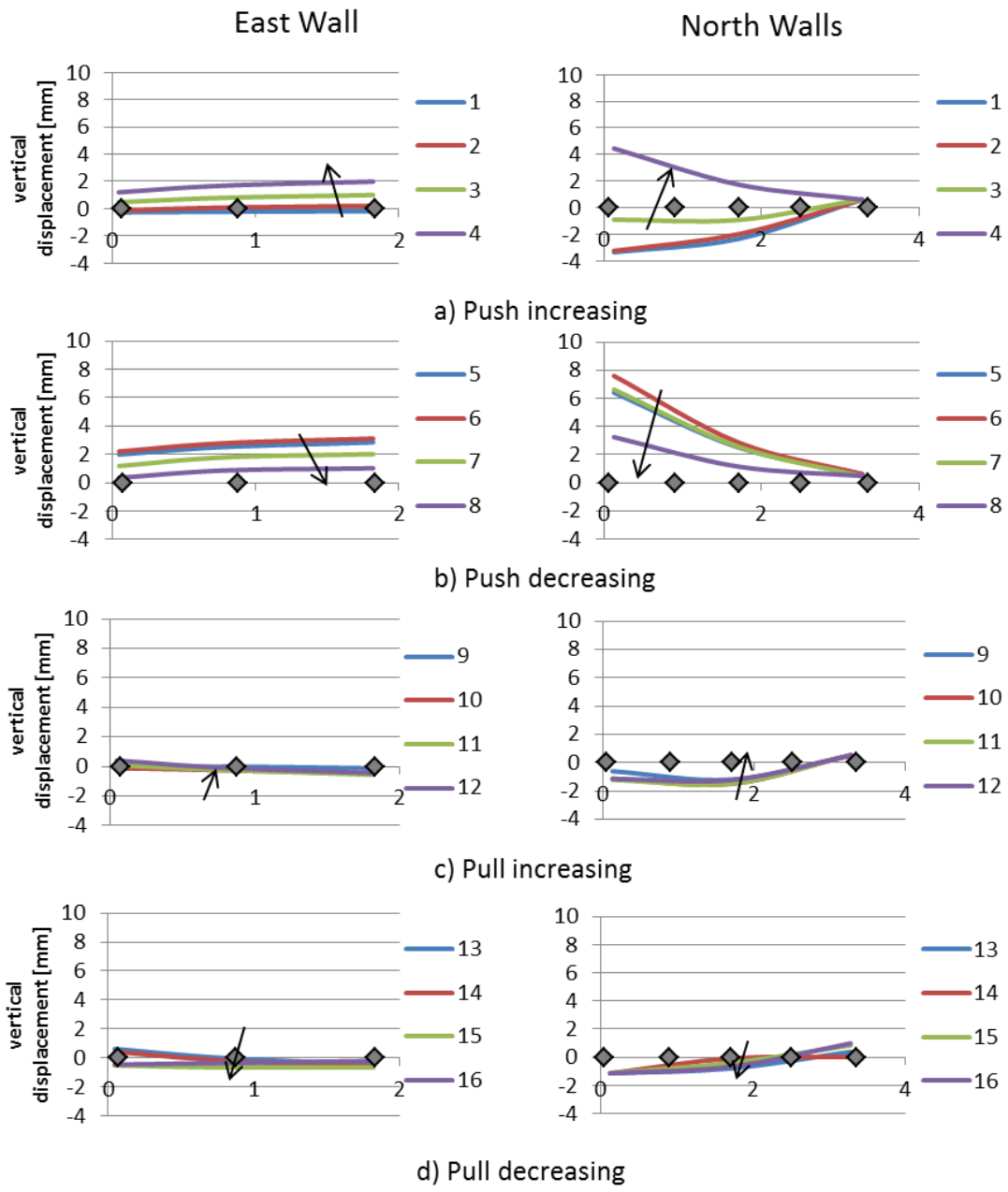

Figure 6-24: Vertical displacement of North wall and East wall loading beams from Test 1 of the High Seismic tests for the displacement cycle shown in Figure 6-23

In general, the vertical displacement of the loading beams during the High Seismic tests was very minimal, due to the use of the corner columns. The corner columns were very effective in isolating the loading beams from the vertical uplift of the walls. This effect was especially prevalent in the single walls, on the East and West sides of the core. It can be seen from Figure 6-24 that the maximum vertical displacement of the East wall beam is 2mm. This uplift is negligible when designing the floor diaphragm to account for any vertical movement. Figure 6-25 shows the West wall at 3.5% drift. At this

drift level, an uplift at the outside edge of the wall of approximately 50mm occurred. For a system where the beams are connected directly into the rocking walls this would have resulted in uplift of the beam of at least 25mm. However, as the beams are not connected directly into the walls, they remain approximately horizontal while the walls rotate. This ensured that the floor system, which would have been seated on the beams, would have been protected. There are still small vertical displacements of the beams; however, any type of floor system, including timber and concrete, would easily be able to accommodate this small uplift. This research contributed to on-going investigations into the behaviour of floor diaphragms for rocking systems (Moroder, 2013 and ongoing)

Figure 6-25: Loading beams isolated from the rotation and uplift of the post-tensioned wall at 3.5% drift

6.5 Damage

For the High Seismic and Low Seismic tests, minimal damage was observed. The majority of damage was associated with the deformation of screws or UFPs. In addition to this, at large displacement drift levels, some crushing of the timber at the toe of the walls was observed. No damage was observed to the stair or landing panels for both tests. Damage that occurred to the wall panels and components for the Low Seismic and High Seismic tests are described in this section.

Some failures of the loading apparatus occurred including a bolt shear failure of one beam stub and failure of a rivet connection. However, this did not affect the behaviour of the specimen as a whole.

6.5.1 Low Seismic Damage

For the Low Seismic specimen, the damage from all tests was minimal. The damage primarily corresponded to the deformation of the screws between adjacent panels. Horizontal screws were used to connect perpendicular panels. A small number of screws connected the panels with a semi-rigid connection, such that when the walls rocked, there was relative movement between the wall panels. The relative movement caused deformation in the screws, which acted as ductile fuses and resulted in some, but very little, energy dissipation.

For the tests with a low number of screws, larger relative displacements between the wall panels were observed. This resulted in large displacements that the screws had to accommodate. Two types of screw connections were used between the panels. A halved lap joint connected the coupled walls with 6 mm diameter x 90 mm long SPAX screws. In the corners, 6 mm diameter x 200 mm long SPAX screws connected the perpendicular panels. The long screws in the corners were able to withstand the large relative displacement between the panels, and deform in a ductile manner. The profile of the screws formed a double plastic hinge, at the interface of the two panels, as can be seen in Figure 6-26a and Figure 6-26c. Some of the screws were pulled into the timber as shown in Figure 6-26b. The short screws at the lap joint of the coupled walls had the same displacement demand but with a much shorter length in which to develop the plastic mechanism. This resulted in the shear failure of all of the lap joint screws. The shear failure of these screws occurred at approximately 1% drift. Although the screws at the lap joint failed, the coupled walls were still held together by the loading beams.

For the tests with a high number of screws, the relative displacement between the panels was much less than the low screw tests. As a result, less deformation of the screws occurred. The long screws did not form a double plastic hinge mechanism. Many of the screws were just slightly bent. The short screws also had less deformation, although some of the screws still had shear failures. This was only occurred to approximately 1/3 of the screws, compared to all of the screws for the low screw tests (Figure 6-26d). The remaining short screws were slightly bent in a similar manner to the long screws. The remnants of the screws that failed in shear following the completion of all the tests, is shown in Figure 6-26e.

a)

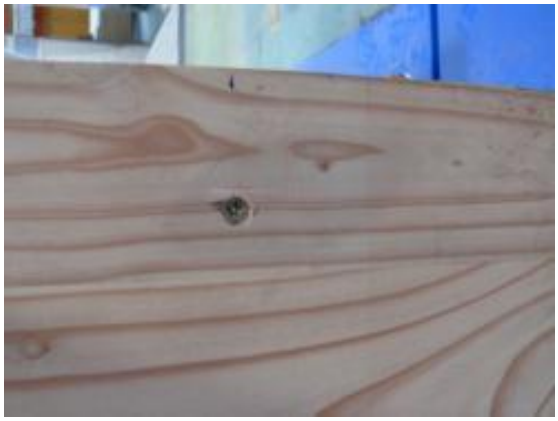

b)

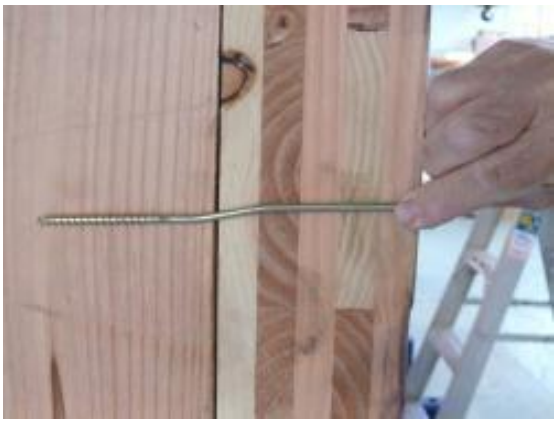

c)

d)

e)

Figure 6-26: Deformations to components from the Low Seismic tests showing; a) deformation of long and short screws from a low screw test, b) Screw pulled into timber during testing, c) deformation of corner screw with double plastic hinge, d) deformation of short screws from Test 5 (a high screw test) and e) remains of the short screws that had been sheared off during testing

In addition to damage to the screws, some crushing in the timber at the base of the walls, and deformation of the shear keys was observed. Crushing of the timber was only observed at large drifts levels. For the majority of the tests, the crushing was insignificant. However, the amount of crushing was much greater for Test 5 and Test 6. These tests consisted of a high post-tensioned force and a large number of screws configuration. As discussed previously, the large number of screws, that connected the coupled panels together, restricted the uplift of the panels. Therefore the contribution of rocking behaviour to the lateral displacement was also limited. As a result, a larger contribution to the lateral displacement went into direct shear movement, which was resisted by the shear keys at the toe of the walls. This caused significant crushing of the timber in the panel against the shear key, in addition to deformation of the shear key itself as seen in Figure 6-27. The transverse layers within the CLT panels provided the panel's additional perpendicular to grain stiffness. Had the panel not had any transverse layers, the crushing may have been greater.

a) Left end of North walls b) Right end of North walls

Figure 6-27: Crushing of timber at the toe of the coupled walls and deformation of the shear keys from Low Seismic Test 5

In general minimal damage was observed for the Low Seismic specimen. The damage was mainly concentrated in the deformation of the screws connecting adjacent panels. The crushing at the toe of some panels could be minimised by ensuring that the screws connecting the panels are spaced widely, such that the panels are not restricted from forming a rocking mechanism. Furthermore, it is recommended that highly ductile screws be used. Long slender screws, in which a double plastic hinge was formed, gave the most desirable performance.

6.5.2 High Seismic

For the High Seismic specimen, like the Low Seismic specimen, the damage from all the tests was minimal. The damage was limited to the plastic deformation of the energy dissipating UFP devices. As the walls rocked, a relative movement was produced between coupled walls, and between the walls and the corner columns. This produced deformation, and hence energy dissipation from the UFPs.

Throughout the tests on the High Seismic specimen, the UFPs were not changed. They were subject to many cycles, up to a maximum of 1.75% drift (Figure 6-28). Figure 6-28a shows a UFP between coupled walls at maximum drift, and Figure 6-28b shows a UFP between a wall and column at the same drift level as Figure 6-28a. Following the commencement of these tests the UFPs were unbolted with and simply removed. If necessary, replacement UFPs could have easily been substituted, however, this was not deemed necessary.

a)  b) 

Figure 6-28: Deformation of UFPs during testing at 1.5% drift for a) coupled wall UFP and b) wall-column UFP

For design level drifts at around 1.5% drift, there was little to no damage to the CLT panels. Some very minor crushing was observed where the base of each corner column was bearing against the adjacent wall (Figure 6-29a and 6-29c). This damage was insignificant and did not affect the performance of the system. For the last two tests, Test 6 and Test 7, where the UFPs were removed, the system was pushed to 3% and 3.5% for the coupled walls and the single walls respectively. These drift levels represented a displacement, greater than what may be expected for a maximum credible earthquake. At these very

large drift levels, more significant crushing at the base of the walls was observed as shown in Figure 6-29. On the West wall a small section of the outer layer buckled outwards when in compression as can be seen in Figure 6-29b. The outer layer consisted of a small strip approximately 20mm wide. The panels were manufactured such that they were glued on the face of each board and not edge glued. Therefore the small strip was vulnerable to being wedged off. Furthermore, a defect was located near the base of the strip which acted as leverage for the strip to buckle outwards.

a)  b) 

c) 

Figure 6-29: Crushing of timber at the toe of the coupled walls (a) and (c), buckling of small strip on West wall (b) following tests to 3.5% drift

In general minimal damage was observed for the High Seismic specimen. The damage was concentrated to the deformation of replaceable energy dissipating UFP devices. Some crushing of the timber at the toe of each wall occurred, at drift levels greater than the design level. The crushing could

be reduced, by ensuring stiffer and stronger material be positioned at the locations of large strains in the timber. Such locations would include the toe of the walls and below the anchorage of the post-tensioning.

6.6 Summary of Results

The global hysteretic response of the Low Seismic and High Seismic specimens, behaviour of the post-tensioned strand, and uplift behaviour at selected positions were shown. The observed damage from the two specimens was discussed. In general, good seismic behaviour for both the High Seismic and Low Seismic specimens with energy dissipation and full re-centring was observed.

6.6.1 Low Seismic specimen:

- The low screw configurations produced the best seismic behaviour with respect to displacement capacity of the system.
- The high screw configurations restricted the amount of uplift, and produced a lateral sliding displacement mechanism, with some rocking, that led to more significant crushing at the base of the walls than the low screw configurations.
- The high screw configurations gave increased stiffness and strength, but reduced displacement capacity. These configurations would be better suited to an elastic design procedure.
- For both low and high screw configurations, very little energy dissipation was provided by the deformation of the screws. For all low seismic tests, a large amount of energy dissipation was generated from friction at the vertical joint between the two coupled wall panels in the same plane, and less from the joints between panels at the corners of the stairwell.
- Particular attention must be paid to preventing horizontal sliding of the panels by providing appropriate shear keys at the foundation.

6.6.2 High Seismic specimen:

- Through all tests, good hysteretic response was observed, whereby excellent energy dissipation and re-centring was achieved.
- The energy dissipation contribution to the total hysteretic behaviour of the system was significantly influenced by friction. Friction occurred when a relative movement was created between adjacent elements. The friction component of the energy dissipation was greatest for the coupled walls. For tests where all of the UFPs were removed, there was a significant amount of energy dissipation from friction alone.

- The steel corner columns were very effective in isolating the floor system from the uplift of the rocking walls. Minimal vertical displacement of the loading beams was observed during testing. The corner columns were also very effective in acting as a shear key.

7 ANALYTICAL MODELLING

This chapter outlines analytical modelling of a post-tensioned stairwell core. The core was modelled as individual single and coupled wall sub-assemblies, acting independently of one another. Predictions were compared with experimental test results, and modifications were made to the analytical model to better predict the observed behaviour.

7.1 Lumped Plasticity Model

A lumped plasticity approach was adopted for the modelling of the single and coupled wall sub-assemblies. This type of model concentrates the main inelastic demand at the base, where the controlled rocking occurs. The seismic response of post-tensioned rocking systems can be well described using one-dimensional wall elements, representing the members, and rotational springs, to model the concentrated inelastic behaviour at the base of the walls. The accuracy of this type of model has been verified in many previous investigations (Pampanin et al. 2001, Spieth et al. 2004, Palermo et al. 2005).

The hysteretic behaviour of a post-tensioned connection is characterised by a flag-shaped hysteresis. This combines a re-centring contribution from the post-tensioning, and a dissipation contribution from yielding steel dissipaters. The full flag-shape hysteresis can be modelled using two inelastic rotational springs in parallel, a bi-linear re-centring spring, and an elasto-plastic steel yielding spring as shown in Figure 7-1.

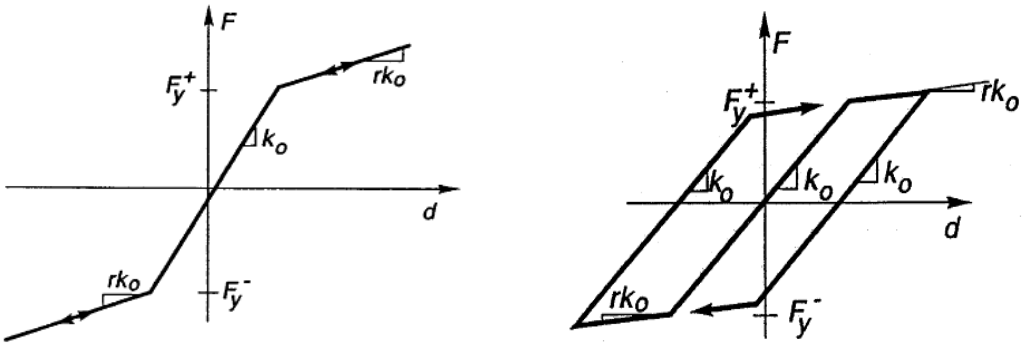

Figure 7-1: Hysteretic properties of a) bi-linear elastic rotational spring to represent the post-tension and b) bi-linear elasto-plastic spring representing the UFP devices

7.2 Numerical Predictions

Predictions were made using a lumped plasticity model and the finite element, non-linear dynamic computer program, RUAUMOKO (Carr 2008), for the Low Seismic and High Seismic specimens. Estimations of the bi-linear elastic spring, representing the post-tensioning and bi-linear elasto-plastic springs representing UFPs were made using the design procedure demonstrated in Chapter 3. The analysis was performed using a cyclic load displacement history, which cycled up to a maximum of 2% drift, as shown in Figure 7-2.

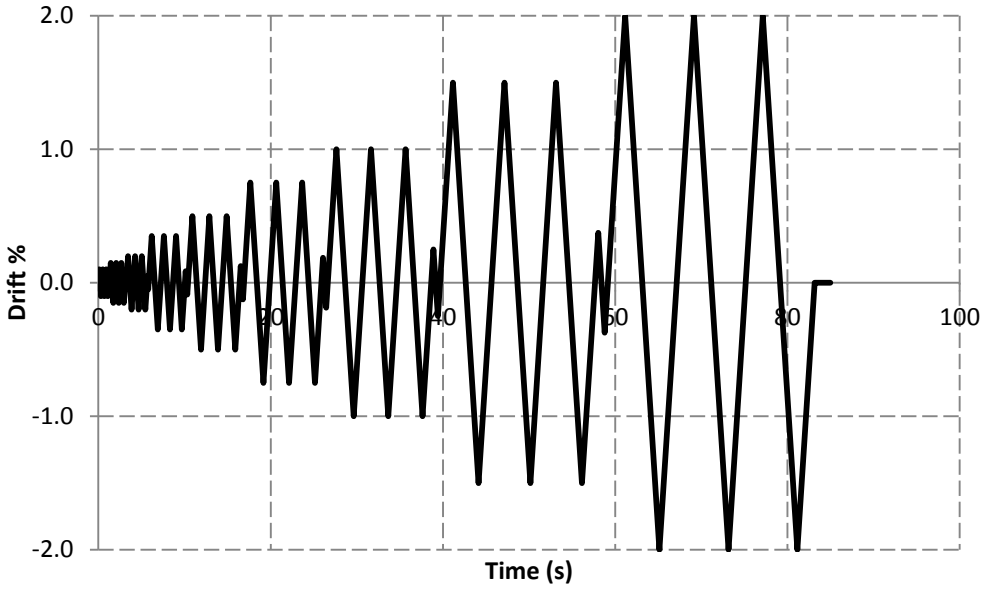

Figure 7-2: Imposed cyclic load displacement history used for the preliminary analytical models

7.2.1 Low Seismic

General representations of the models, for the Low Seismic sub-assemblies are shown in Figure 7-3. The analytical models were setup for the single walls on the East and West sides of the specimen (Figure 7-3a), as well as the North coupled walls (Figure 7-3b). The focus of the analysis for the Low Seismic specimen was to model the results of Test 3. The characteristics of Test 3 consisted of a high post-tensioning force and a low number of screws. Therefore, the single walls were assumed to behave similarly to that of a wall with post-tensioning only and no energy dissipation. To represent this, a simple model was established with a rotational spring at the base, for the post-tensioning, and an elastic element on top, for the wall, as shown in Figure 7-3a. The North walls were assumed to behave as coupled walls with weak coupling elements, representing the screws. A single bi-linear elastic spring was used at the base of each wall to represent the post-tensioning. Rigid links were used to connect the coupler springs, representing the screwed lap joint, to the wall elements as shown in Figure 7-3b. For

simplicity in the initial model, the coupling springs were described by a bi-linear elasto-plastic hysteresis rule.

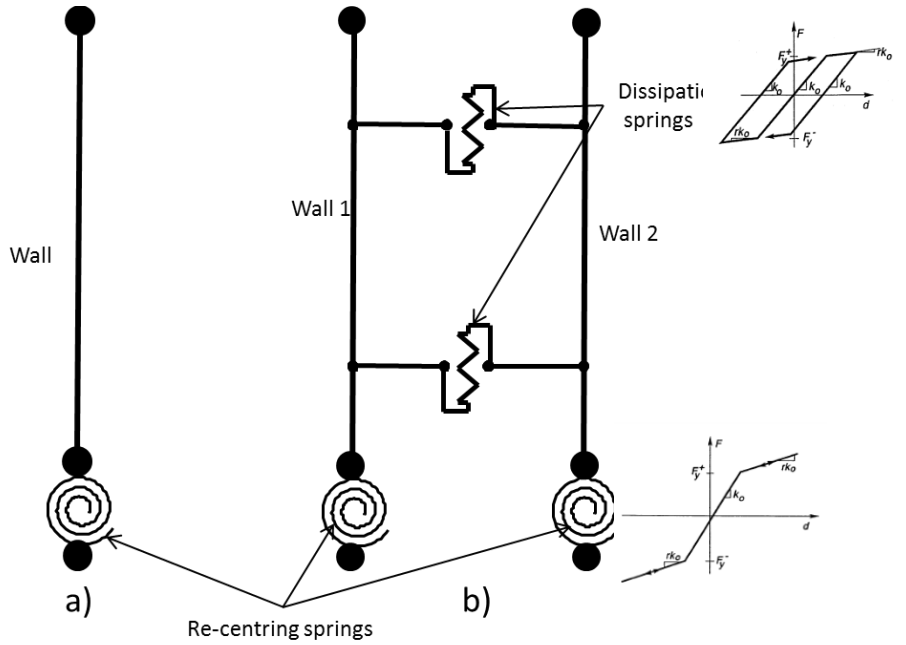

Figure 7-3: Representations of the Low Seismic preliminary models for, a) the east and west walls, and b) the coupled walls

For the Low Seismic specimen, bi-linear backbone curves were used as an initial approximation, with the yield moment and stiffness of the spring, derived from the design. For the preliminary prediction of the single walls, a bi-linear elastic spring with a yield moment of 120kNm and an initial stiffness of 40000kNm/rad was used. For the prediction of the coupled walls, a bi-linear spring was used at the base of each wall with the same properties as that of the single wall, with a yield moment of 120kNm and rotational stiffness of 40000kNm/rad. For the coupling elements, a yield force of 10kN was adopted and an initial stiffness of 15000kN/m was used as an initial approximation.

Displacement controlled analyses, of the single and coupled wall models, were run in Ruaumoko2D. The results of the preliminary predictions for the Low Seismic specimen in comparison with the experimental results are shown in Figure 7-4.

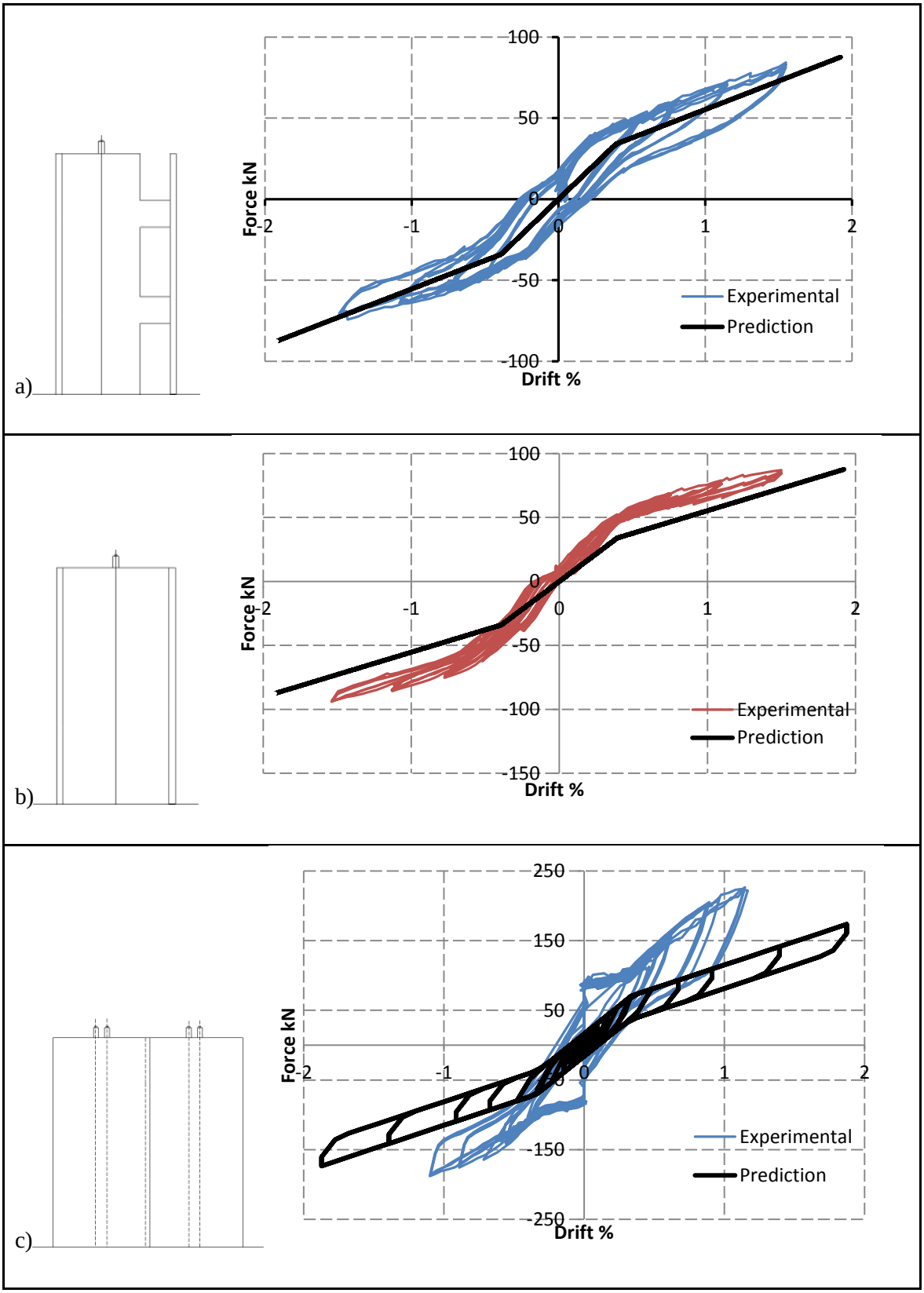

Figure 7-4: Preliminary analytical predictions compared with the experimental results of the Low Seismic specimen for a) the East wall, b) the West wall and c) the North coupled walls

The preliminary predictions for the East wall, West wall and North coupled walls, under-estimated the strength and stiffness, in comparison to the experimental results, with the exception of the East wall as shown in Figure 7-4. The capacity of the East wall (Figure 7-4a) was lower than the West wall (Figure 7-4b) due to the narrower width of the East wall. The smaller width generates less of a lever arm, resulting in a reduced moment capacity. The preliminary model did not account for this effect. Furthermore, the preliminary model did not take into account the small amount of energy dissipation that was observed during testing. For the coupled walls, the preliminary model underestimated the initial and post-yield stiffness of the system, in addition to the amount of energy dissipation, as shown in Figure 7-4c.

7.2.2 High Seismic

General representations of the models representing the High Seismic sub-assemblies are shown in Figure 7-5. The focus of the analysis for the High Seismic specimen was to model the results of Test 5, with a high post-tensioned force and two UFPs per joint. The wall panels and steel corner columns were represented by elastic elements. A single bi-linear elastic spring was used at the base of each wall, to represent the post-tensioning. Rigid links were used to connect the coupler springs, representing the UFPs, to the wall elements. The UFPs were described by a bi-linear elasto-plastic hysteresis rule from RUAUMOKO (Carr, 2008).

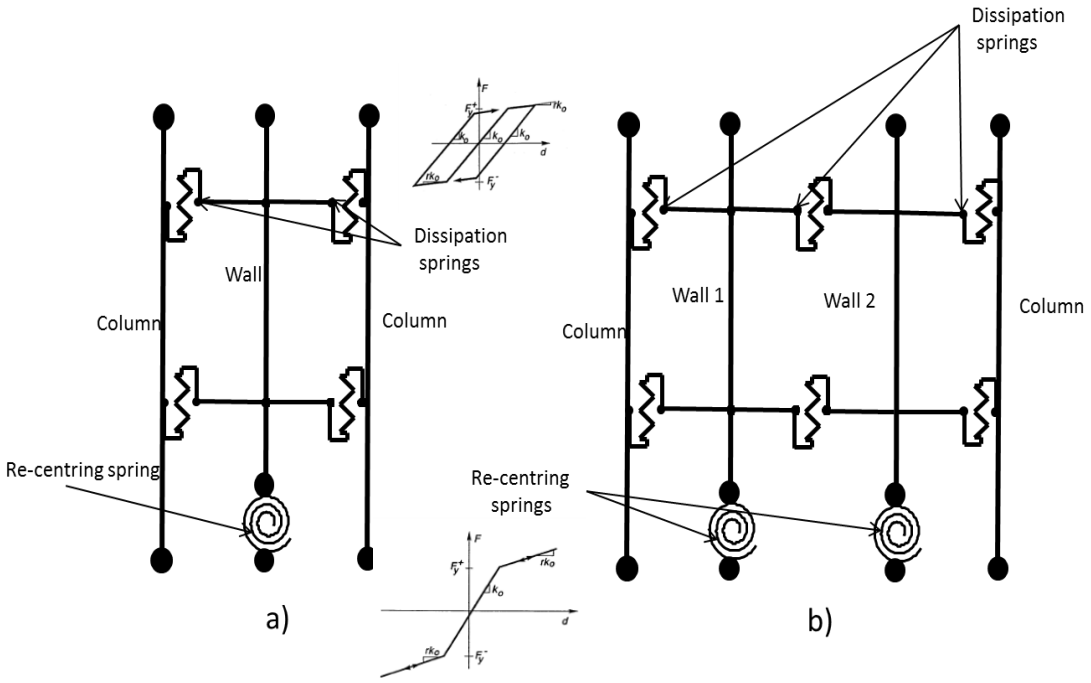

Figure 7-5: Representations of the High Seismic preliminary models for, a) the east and west walls, and b) the coupled walls

The yield moment and stiffness of the rotational spring, representing the post-tensioning, and the properties of the elasto-plastic springs, representing the UFP devices, were derived from the design. For the preliminary prediction of the single walls, a bi-linear elastic spring with a yield moment of 120kNm and an initial stiffness of 40000kNm/rad was used. Four UFP springs were used, two on each side, with a yield force of 30kN and initial stiffness of 17000kN/m.

For the coupled walls, bi-linear elastic springs with a yield moment of 200kNm and an initial stiffness of 100,000kNm/rad were used at the base of each wall, for the preliminary prediction. Elasto-plastic springs were used between the coupled walls, and between the walls and corner columns. A yield force of 30kN and an initial stiffness of 17000kN/m were used for the properties of the springs representing the UFPs, the same as that for the single walls.

A displacement controlled analysis was run in Ruaumoko. The results of the preliminary predictions for the High Seismic specimen, in comparison with the experimental results, are shown in Figure 7-6.

The preliminary predictions for the east wall, west wall and north coupled walls underestimated the ultimate capacity of each wall. In general, the estimation of the initial stiffness was approximately equivalent to the experimental results. However, the predicted behaviour and the observed behaviour differed greatly following the non-linearity. The bi-linear stiffness of the experimental tests was much greater than that of the predictions. For the coupled walls in particular, the experimental behaviour displayed what was essentially a linear backbone curve without a non-linearity, as shown in Figure 7-6c. However, similar behaviour was also observed in the coupled wall results as shown in Figure 7-6a and 7-6b.

The dissipation springs representing the UFP devices in the model, produced a constant amount of dissipation throughout each displacement cycle. This behaviour was inconsistent with what was observed experimentally. For each of the walls, the amount of energy dissipation increased at each drift level producing greater amounts of energy dissipation at larger drift cycles. Therefore, elasto-plastic springs do not represent the observed behaviour, with respect to the amount of energy dissipation.

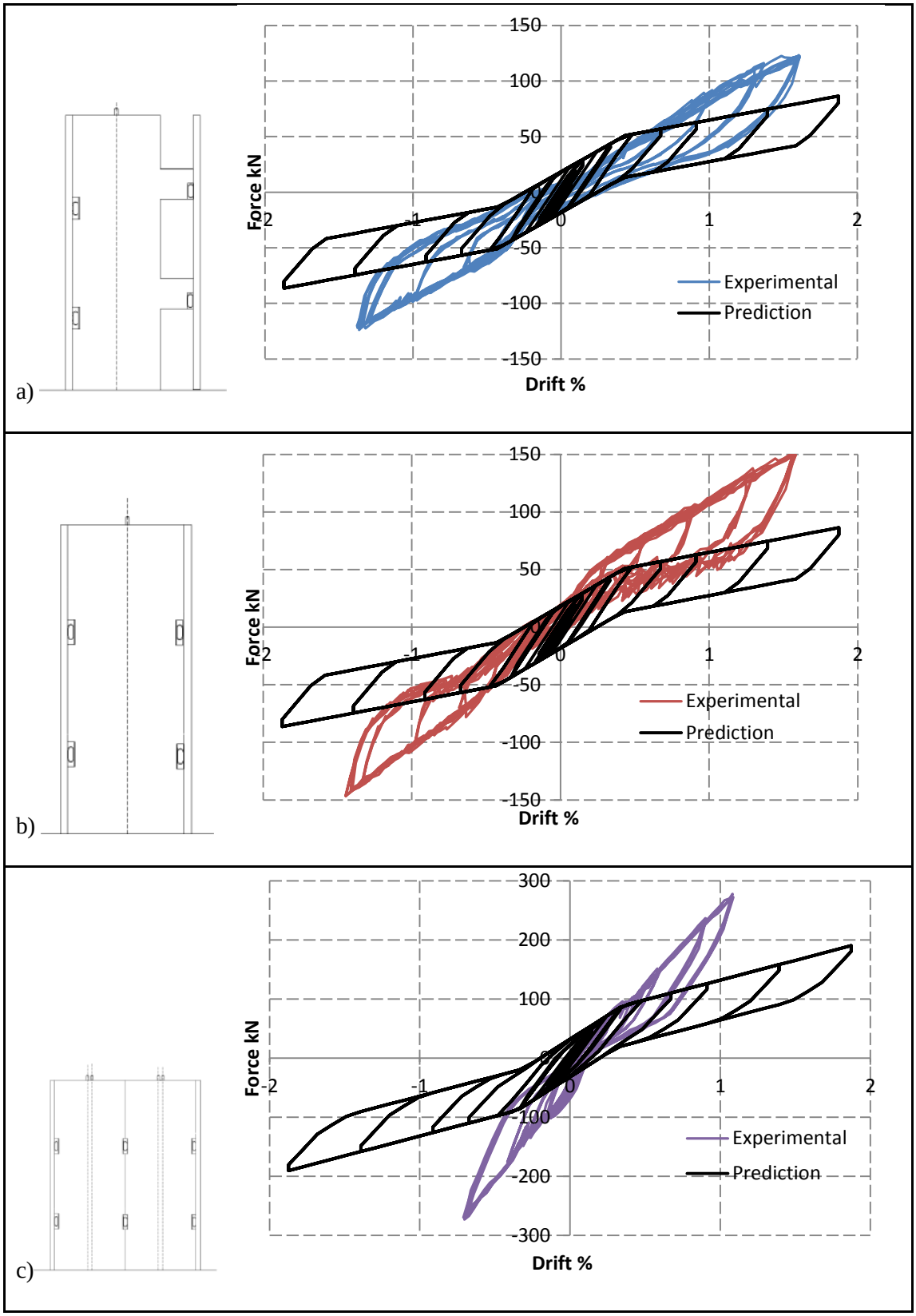

Figure 7-6: Preliminary analytical predictions compared with the experimental results of the High Seismic specimen for a) the East wall, b) the West wall and c) the North coupled walls

7.3 Refined Analytical Model

The focus of the refinements to the analytical models, were made based on calibration with the experimental results of the High Seismic specimen. The experimental results demonstrated that a significant contribution to the hysteretic behaviour of the system; was provided by friction. Therefore an additional energy dissipation spring was positioned in parallel with each UFP spring as shown in Figure 7-7.

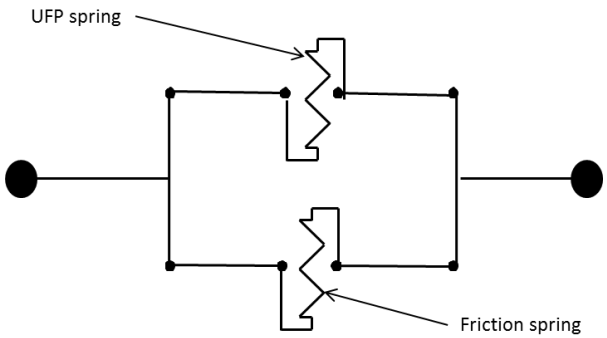

Figure 7-7: Refinements to the analytical model made with UFP and friction springs in parallel

The additional friction dissipation occurred mainly at the joint between the coupled walls, and to a lesser extent between the walls and the corner columns. The friction was only generated once gap opening had occurred, and there was a relative movement between adjacent elements. Therefore for low drift cycles, prior to gap opening, no friction was generated. Due to this a typical bi-linear in-elastic spring would not suffice. A bi-linear flag-shaped hysteresis rule was selected to represent the friction (Figure 7-8b). This spring, coupled with an elasto-plastic spring (Figure7-8a), best represented the observed behaviour of the friction and UFP devices within the system. Bi-linear elastic springs at the base of each wall, were still used to represent the behaviour of the post-tensioning strands.

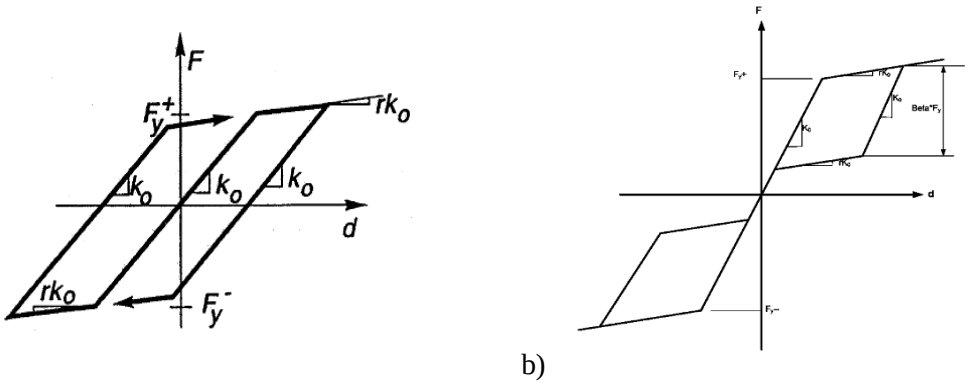

a) b)

Figure 7-8: Hysteretic properties of a) the bi-linear elasto-plastic springs representing the UFP devices and b) the flag-shaped hysteretic behaviour representing the friction in the system

The refined models in comparison with the experimental results of the High Seismic specimen, with and without UFP devices, are shown in Figure 7-9 and Figure 7-10 respectively. The analytical models for the east wall, west wall and north coupled walls for each of the tests is shown. The calibration of the flag shaped 'friction' springs was done such that the yield force of the springs represented the forces caused by friction in the joint between elements. The friction springs were lumped with the UFP springs for simplicity.

The spring properties of the analytical model representing the system with UFP devices were:

- For the east wall, a bi-linear elastic post-tensioning spring with a yield moment of 120kNm and an initial stiffness of 40000kNm/rad was used. The bi-linear inelastic UFP springs had a yield force of 30kN and an initial stiffness of 12000kN/m. The friction flag-shaped springs were calibrated with a yield force of 50kN, an initial stiffness of 10000kN/m and a beta factor of 0.6.
- For the west wall, a bi-linear elastic post-tensioning spring with a yield moment of 120kNm and an initial stiffness of 40000kNm/rad was used. The bi-linear inelastic UFP springs had a yield force of 30kN and an initial stiffness of 12000kN/m. the friction flag-shaped springs were calibrated with a yield force of 50kN, an initial stiffness of 10000kN/m and a beta factor of 0.6.
- For the coupled walls, bi-linear elastic springs with a yield moment of 200kNm and an initial stiffness of 100000kNm/rad were used at the base of each wall. A yield force of 30kN and an initial stiffness of 12000kN/m were used for UFP springs. The friction flag-shaped springs were calibrated with a yield force of 50kN, an initial stiffness of 10000kN/m and a beta factor of 0.6.

The spring properties of the analytical model representing the system with friction only and no UFP devices were:

- For the east wall, a bi-linear elastic post-tensioning spring with a yield moment of 120kNm and an initial stiffness of 40000kNm/rad was used. The friction flag-shaped springs were calibrated with a yield force of 50kN, an initial stiffness of 10000kN/m and a beta factor of 0.6.
- For the west wall, a bi-linear elastic post-tensioning spring with a yield moment of 120kNm and an initial stiffness of 40000kNm/rad was used. The friction flag-shaped springs were calibrated with a yield force of 50kN, an initial stiffness of 10000kN/m and a beta factor of 0.6.
- For the coupled walls, bi-linear elastic springs with a yield moment of 200kNm and an initial stiffness of 100000kNm/rad were used at the base of each wall. The friction flag-shaped springs were calibrated with a yield force of 50kN, an initial stiffness of 10000kN/m and a beta factor of 0.6.

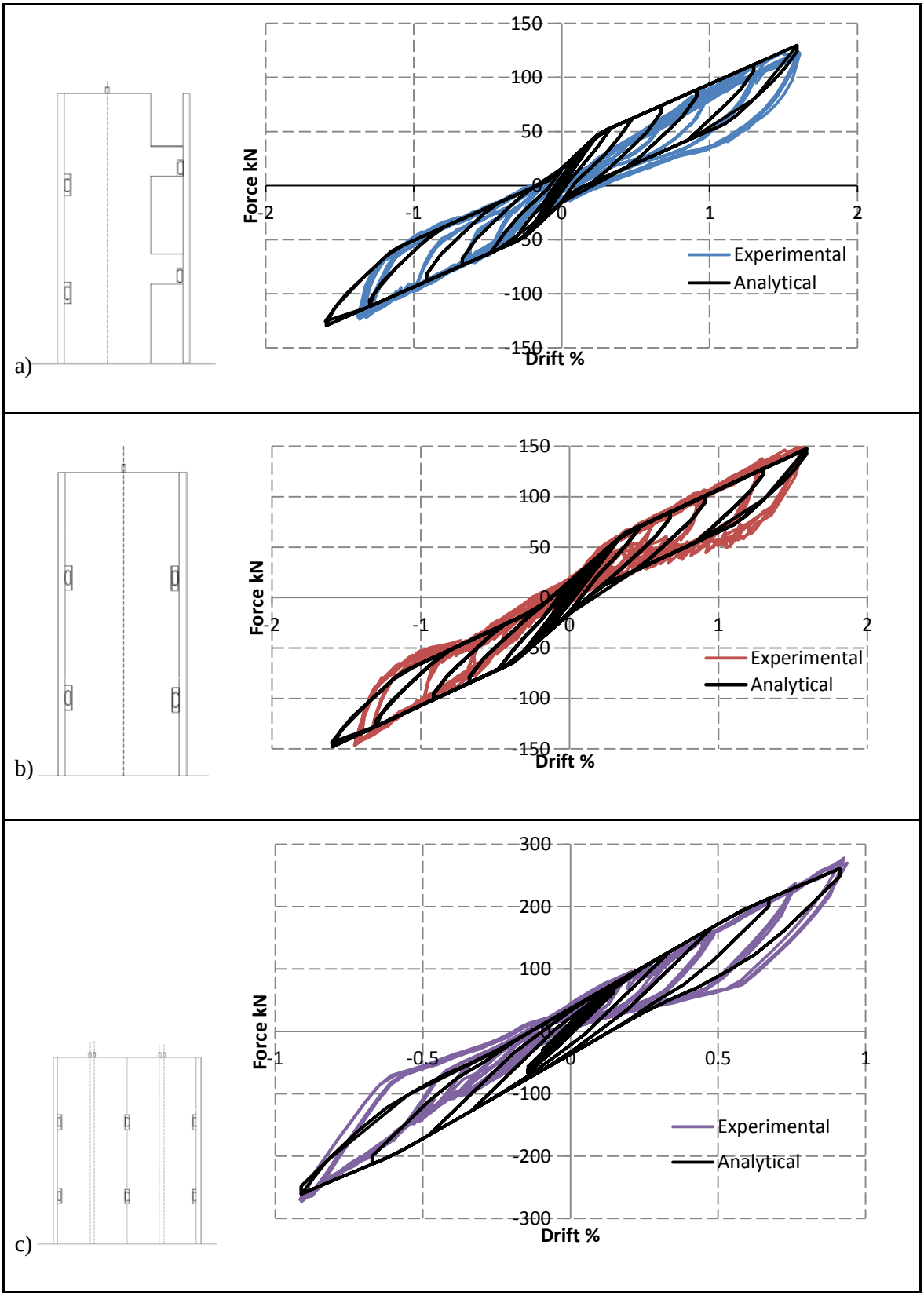

Figure 7-9: Refined analytical model compared with the experimental results of the High Seismic specimen with UFP devices for a) the East wall, b) the West wall and c) the North coupled walls

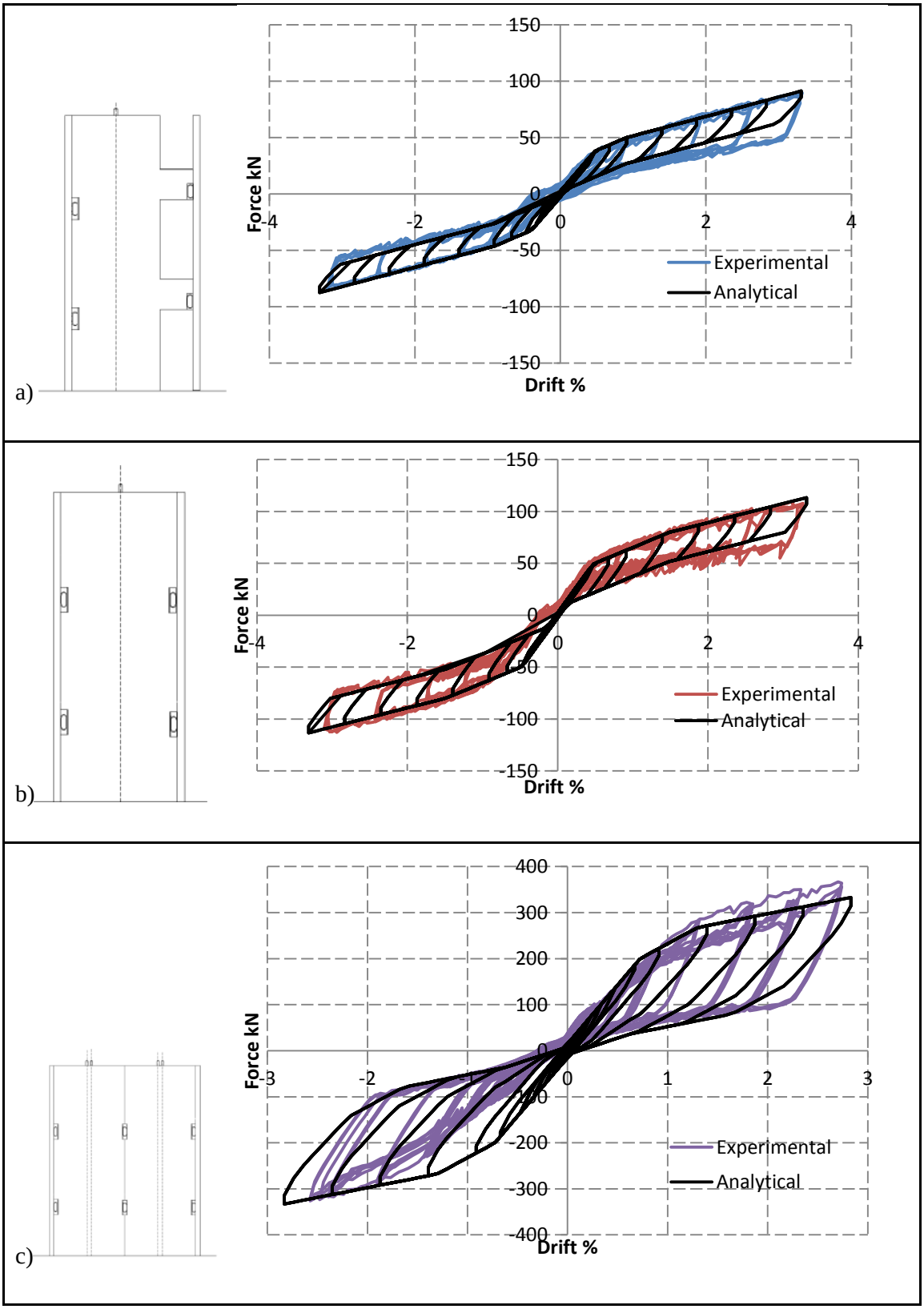

Figure 7-10: Refined analytical model compared with the experimental results of the High Seismic specimen with no UFP devices for a) the East wall, b) the West wall and c) the North coupled walls

In general, the refined analytical models fitted the experimental behaviour very well. However, in some cases, the linear back bone, with energy dissipation and full re-centring behaviour, was not fully captured, as shown in Figure 7-9a and 7-9c. The behaviour of the single and coupled walls, when the UFPs were removed, was captured very well by the refined model, as shown in Figure 7-10.

7.4 Summary of Analytical modelling

Predictions were made using a lumped plasticity model and the finite element, non-linear dynamic computer program RUAUMOKO (Carr 2008), for the Low Seismic and High Seismic specimens. Refinements to the preliminary analytical models were made and compared with the experimental results of the High Seismic specimen, with and without UFP devices.

- In general, the preliminary predictions underestimated the ultimate capacity that was observed during experimental testing.
- Refinements were made to the analytical models with the addition of a flag-shaped spring to represent the friction in the system, positioned in parallel with the UFP springs.
- The accuracy of the refined model was much better than the preliminary model, in particularly for the east and west walls.
- In some cases, for the models with UFPs, the initial stiffness of the analytical model was slightly overestimated.
- The refined model produced accurate results for a very simple lumped plasticity model.

Further research is required to validate the refinements of the analytical models, specifically, with regards to the friction component of the response.

8 CASE STUDY BUILDING

This chapter presents a full case study of the seismic design of a core-wall system, forming the lateral load resisting system, for a five storey timber building. The evaluation of seismic loading and design base shear is carried out with reference to the current New Zealand seismic loading standards (AS/NZS 1170.0:2002; NZS 1170.5:2004), following a displacement-based design approach.

8.1 General Description

The case study building was adapted from PART 2 of the STIC design guide (STIC, 2013), and consists of a five storey building with four suspended floors and a light weight portal frame roof. The building has an approximate plan of 32m in the longitudinal direction, and 18m in the transverse direction, with a floor area of approximately 600m^2 per floor.

The building is assumed to be located in the Christchurch Central Business District on soil type D. The proposal is for the building to be constructed with post-tensioned, pre-fabricated, CLT wall panels as the seismic system, and a separate timber gravity system. The gravity system is not considered in this case study.

8.2 Building Structural System

The structural system for resisting lateral loads acting on the structure consists of five post-tensioned frames in one direction, and four sets of coupled walls around the stairwell cores acting in the other direction. The three bay frames in the transverse direction, resist seismic and gravity loads. An additional four single walls, positioned around the stairwell cores, act in the transverse direction in conjunction with the three bay frames. The lateral loads in the longitudinal direction are resisted by four sets of post-tensioned CLT coupled walls. The floor slabs consist of timber-concrete composite units that span 8 metres in the longitudinal direction. Two plan views are shown in Figure 8-1. Figure 8-1a shows the proposed layout as described above whereas Figure 8-1b shows a structural layout with four additional pairs of coupled walls. These two plans represent the structural layouts of the high seismic option (8a) and the low seismic option (8b). Side and end elevations of the proposed structure are shown in Figure 8-2.

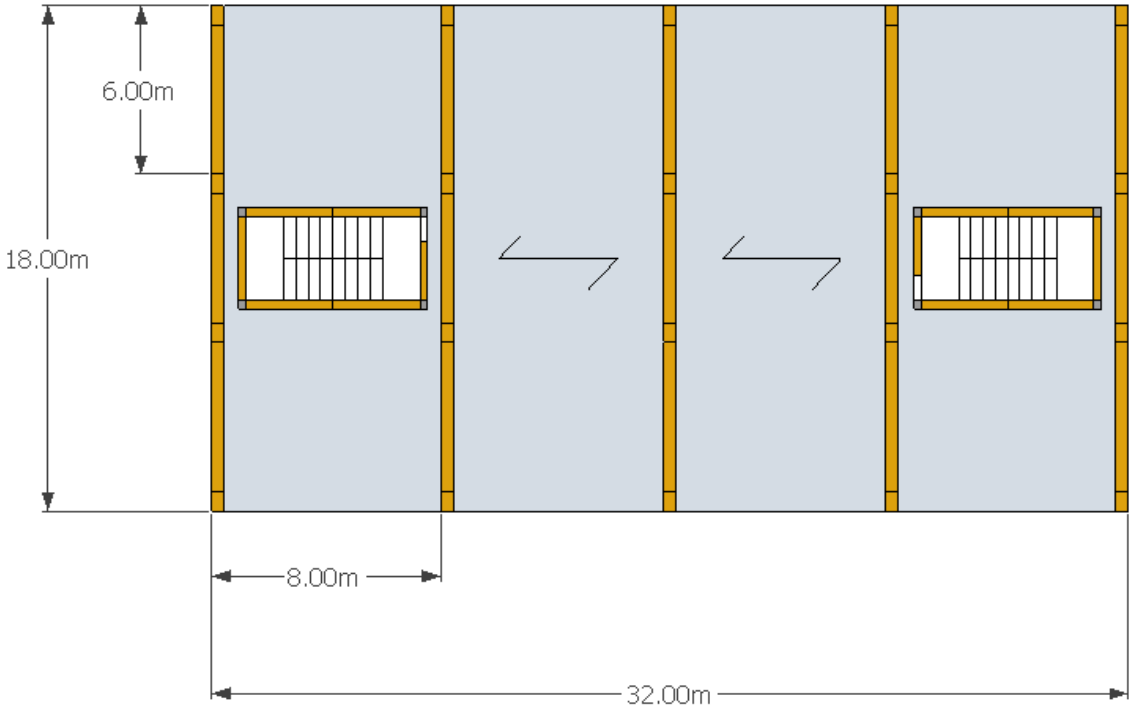

a) High Seismic plan view

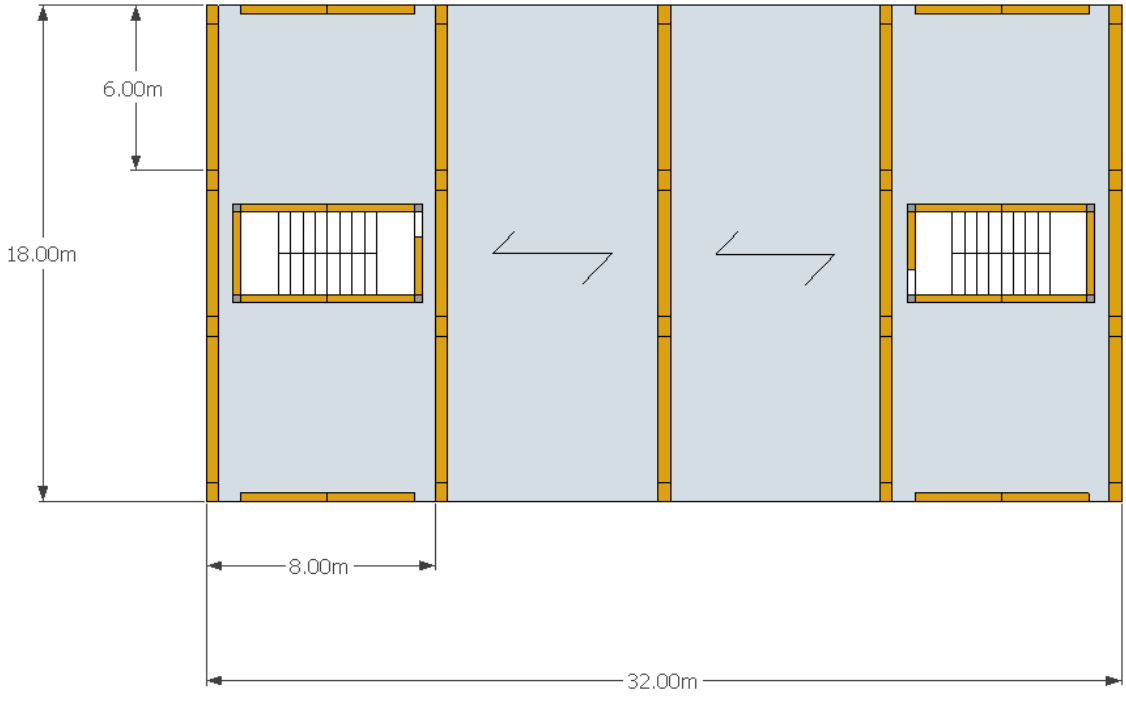

b) Low Seismic plan view

Figure 8-1: The plan layout of the four storey case study building with a) two stairwell cores forming the lateral load resisting system for the high seismic option and b) two stairwell cores and four pairs of additional coupled walls for the Low Seismic option.

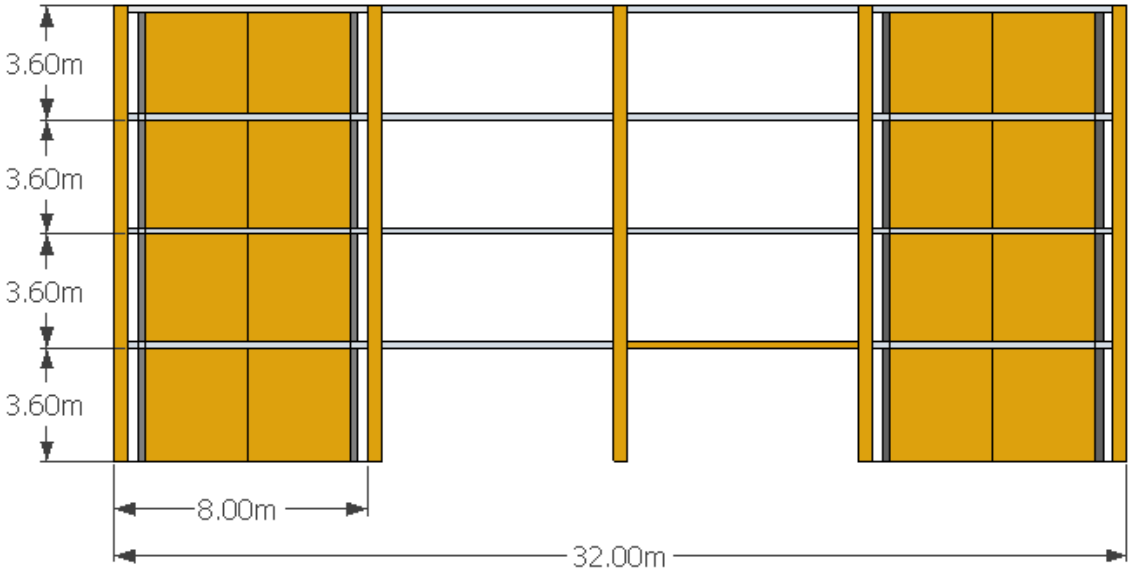

a) Side elevation

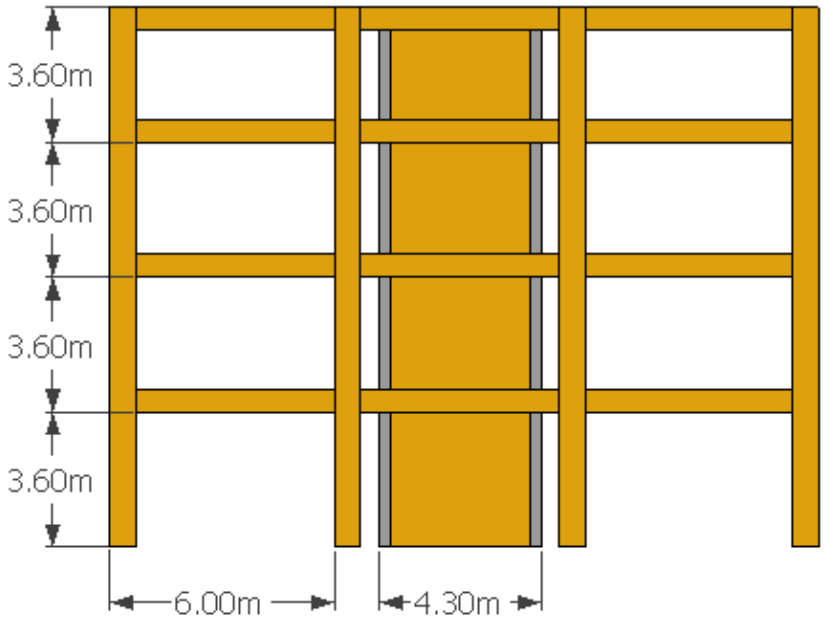

b) End elevation

Figure 8-2: Structural layout of the four storey case study building with two stairwell cores forming the lateral load resisting system; a) side elevation, b) end elevation

Two alternatives are presented for the lateral load resisting system of the case study building, a high seismic option and a low seismic option. For the purposes of this case study, only the design of the post-tensioned CLT core walls will be considered. Design of post-tensioned timber frames is detailed in Part 2 of STIC design guide (STIC, 2013).

8.2.1 High Seismic Option

The High Seismic option consists of post-tensioned rocking CLT walls, coupled with energy dissipating U-shaped Flexural Plates (UFPs). Steel SHS columns are situated in the corners of the core. The UFP devices are attached between wall panels and the steel SHS corner columns, as shown in Figure 8-3. The drag beams that supply the load to the walls are connected to the corner columns. The columns transfer the forces into the walls. The purpose of these columns is to separate the drag beams and hence the floor diaphragm from the rocking walls. The rocking walls have significant uplift at the design drift level, whereas the uplift associated with the columns is negligible. Therefore, by connecting the drag beams to the columns instead of directly into the walls, the uplift of the beams, and hence floors, is minimised. The columns which are bolted to the foundation also serve as a shear key for the wall panels.

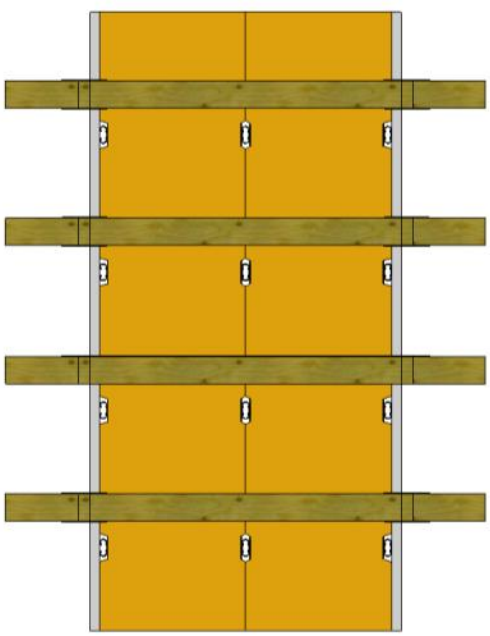

a) Side elevation

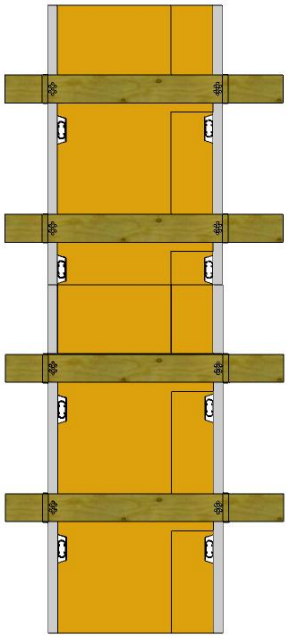

b) End elevation

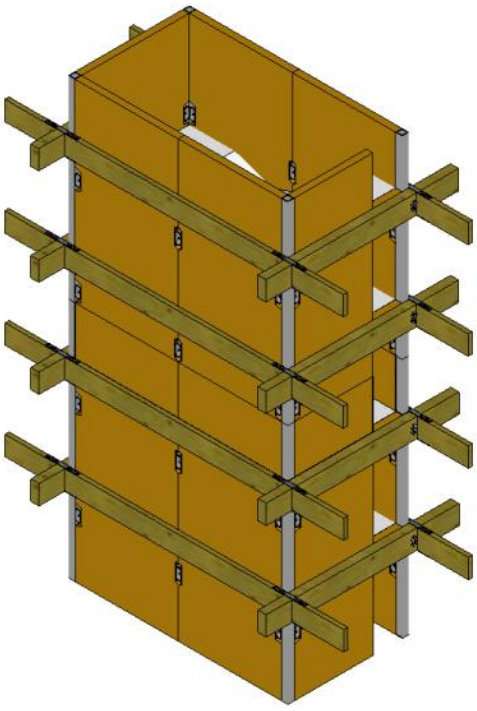

c) Isometric elevation

Figure 8-3: Lateral load resisting system for the High Seismic option consisting of post-tensioned CLT walls coupled with UFP devices; a) Side elevation, b) End elevation, c) Isometric elevation

8.2.2 Low Seismic Option

The Low Seismic option has the same layout as the high seismicity specimen (Figure 8-4). However, in the place of SHS corner columns and dissipater devices, horizontal screws were used to connect perpendicular panels. For this option, a low number of screws would be used to connect adjacent panels. It is intended that the screws connect the panels with a semi-rigid connection, such that when the walls rock, there is a relative movement between the wall panels. The relative movement causes deformation in the screws, which act as ductile fuses, and result in some energy dissipation. Although some energy dissipation can be achieved from screws, it is very minimal and was neglected in the design of the walls. The primary role of these screws is to hold panels together.

Furthermore, four pairs of additional walls are required in the longitudinal direction, to account for the lower capacity and higher design forces for the low seismic option, in comparison to the high seismic option. The screwed connections are assumed to act to clamp the walls in-plane but not contribute to the moment capacity. The consequences of this are described in Section 8.5.2.

In this case the drag beams are connected directly into the walls. Therefore as the wall panels 'rock' during seismic loading, the beams and hence the floors, would be uplifted, which would need to be considered in the design of the floor diaphragm.

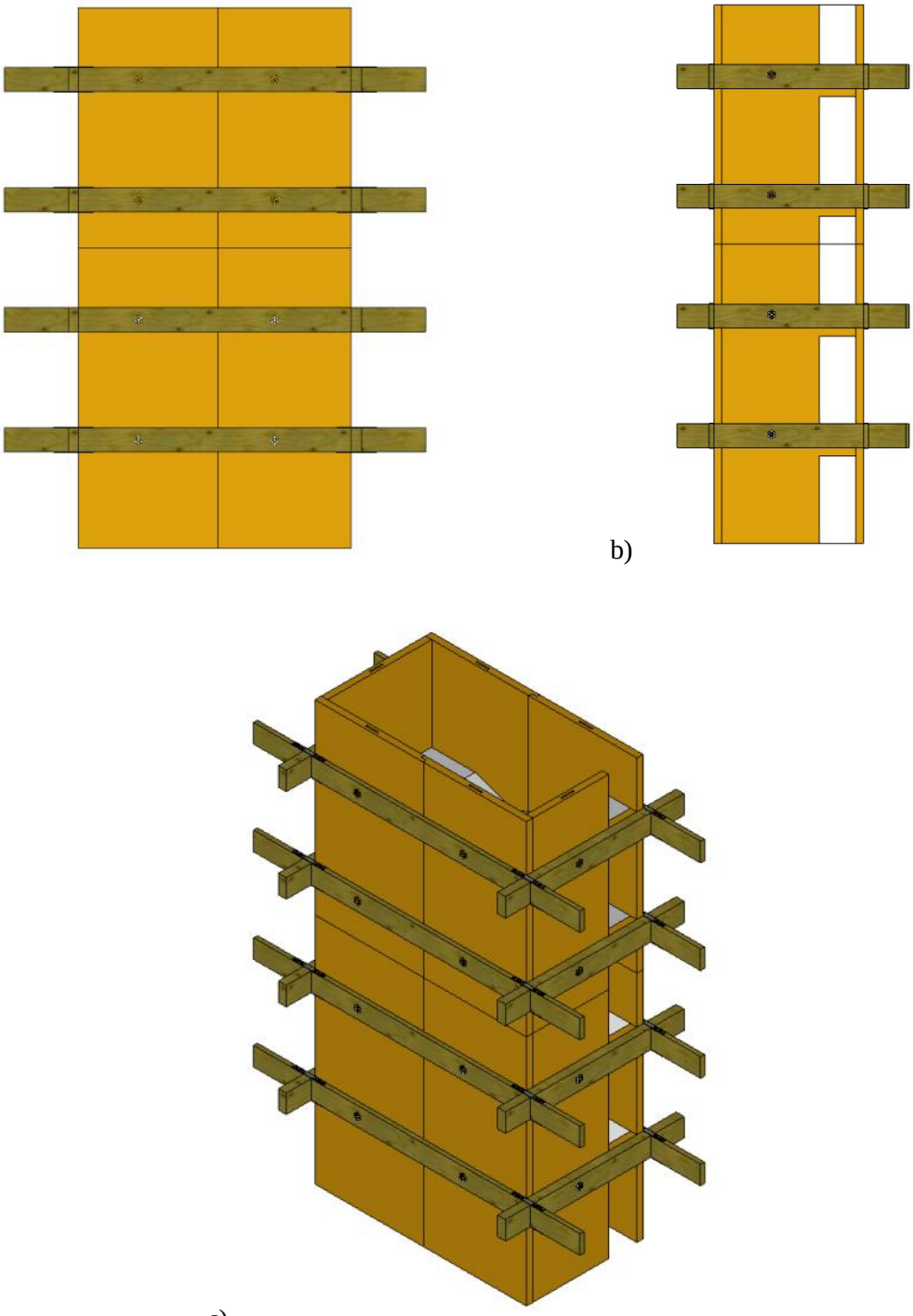

Figure 8-4: Lateral load resisting system for the Low Seismic option consisting of post-tensioned CLT walls coupled with screws; a) Side elevation, b) End elevation, c) Isometric elevation

8.3 Material Properties

The following material properties, shown in Table 8-1, were used in the design of the post-tensioned CLT walls and components. It is assumed that the general properties of the CLT panels are that of the input material of MSG15 sawn timber.

The post-tensioning rods used in the design were 60mm diameter MacAlloy bar.

Table 8-1: Material properties used in the design of the High Seismic and Low Seismic options

Type	*Symbol*	*Unit*
Cross Laminated Timber		
Modulus of Elasticity	E	15 GPa
Shear modulus	G	667 MPa
Bending strength	f_b	28 MPa
Tensile strength	f_t	14 MPa
Shear strength	f_s	3.8 MPa
Compressive strength	f_c	25 MPa
Density	ρ	5 kN/m^3
Post-tensioning MacAlloy bar		
Modulus of Elasticity	E_{PT}	170 GPa
Yield strength	f_{Pty}	835 MPa
Ultimate strength	f_{PTu}	1030 MPa
Diameter	D	60 mm
Area	A	2827.4 mm^2
UFPs		
Modulus of Elasticity	E_s	200 GPa
Yield strength	f_{sy}	375 MPa
Steel Columns		
Modulus of Elasticity	E_s	200 GPa
Yield strength	f_{sy}	300 MPa

8.4 Seismic Mass

The seismic mass at each level of the case study building according to NZS1170.1 (2002) used in design, is shown in Table 8-2. For each of the lateral force resisting systems, the seismic weights are the same.

Floor Area: $A_{floor} = [(8 \cdot 4 + 0.441)(6 \cdot 3 + 0.7)] = 600m^2$

Floor Weights:

- Concrete $W_{conc} = 0.090m \cdot \frac{24kN}{m^3} = 2.16kPa$
- Plywood $W_{ply} = 0.021m \cdot \frac{6kN}{m^3} = 0.13kPa$
- Joists $W_{joists} = 0.09m \cdot 0.4m \cdot \frac{1m}{0.6m}\frac{6kN}{m^3} = 0.36kPa$
- Superimposed Dead Load $W_{SDL} = 0.80kPa$
- Total Weight $W_{floor} = 3.45kPa$
- Floor Weight $G_{floor} = 3.45kPa \cdot 600m^2 = 2071kN/floor$

Seismic Live Loads (NZS1170.1:2002):

- Level 1-3 (Office for General Use) $Q_{floor} = 3kPa$
- Level 4 (Penthouse for Residential Use) $Q_{floor} = 1.5kPa$
- Live Load Reduction Factor $\psi_E = 0.3$
- Level 1-3 Live Load $\psi_E Q_{floor,1-3} = 0.3 \cdot 600m^2 \cdot 3kPa = 540kN$
- Level 4 Live Load $\psi_E Q_{floor,4} = 0.3 \cdot 600m^2 \cdot 1.5kPa = 270kN$

Adding column, beam and wall self-weights:

$$W_{LVL} = 6kN/m^3$$

$$G_{structure} = 352kN/floor$$

Allowing for weight of façade:

$$W_{facade} = 0.3kPa$$

$$G_{facade} = 110kN/floor$$

Weight of the penthouse roof structure:

$$W_{penthouse} = 0.6kPa$$

$$G_{facade} = 361kN/floor$$

Seismic weight at L1-3 (ignoring floor penetrations):

$$W_{t,i} = \sum G_i + \psi_E Q_i$$

$$W_{t,i} = 2071kN + 540kN + 352kN + 110kN = 3074kN$$

$$W_{t,i} = \frac{3046kN}{600m^2} = 5.0kPa$$

Seismic weight at L4 assuming weight of penthouse structure is lumped at level 4:

$$W_{t,i} = 2071kN + 270kN + 236kN + 110kN + 361kN = 3048kN$$

$$W_{t,i} = \frac{3030kN}{600m^2} = 5.0kPa$$

Note: the weight of the superstructure has been reduced at level 4 to account for the reduced length of columns and walls at this level.

Assuming rigid diaphragm behaviour, the total seismic weight of the building can be equally distributed amongst the lateral load resisting systems in each direction.

The seismic weight acting on each frame and pair of coupled walls is thus 1/5 and 1/4 of the total seismic weight, respectively. A summary of the seismic weight distribution up the height of the structure is given in Table 8-2.

Table 8-2: Summary of Seismic Weights

Level	$W_{i,\,total}$ *(kN)*	M_i *(t)*
4	3048	311
3	3074	313
2	3074	313
1	3074	313
Total	12269	1251

8.5 Lateral Force Design

Evaluation of base shear and internal actions, using a Displacement-based Design approach, were determined for the High Seismic and Low Seismic options. A comparison of the results for the three solutions is shown.

The procedure for determining the lateral design forces, using the DBD method, for the proposed building is outlined below for the High Seismic option. The design forces were determined for the Low Seismic options following the same procedure.

The New Zealand Design Spectrum for the Christchurch region (PGA=0.30g), for a deep or soft soil (Category D), used in the design, is shown in Figure 8-5. The spectral displacement S_d, which was calculated off of the acceleration spectrum, is also shown. It should be noted that a structural performance factor, Sp = 1.0 was taken instead of 0.7 as suggested in the code. This factor was set to 1 as it would represent the actual behaviour of the structural skeleton without any additional (difficult to define) damping or over strength coming from a number of other sources, such as non-structural elements and soil or foundations.

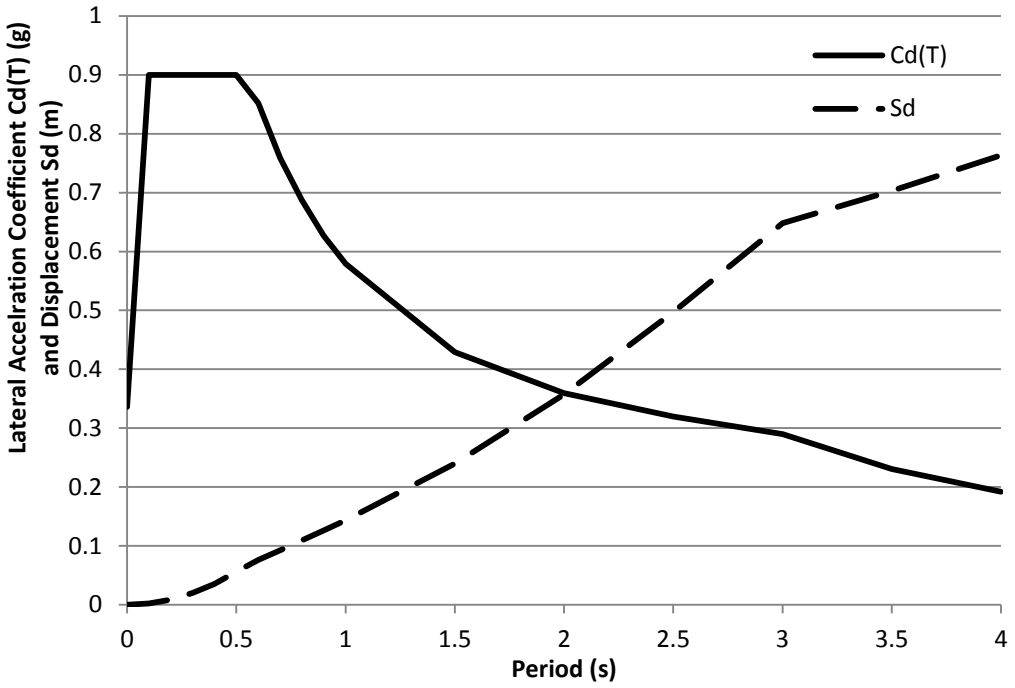

Figure 8-5: Design spectrum: Acceleration spectrum and displacement spectrum (Note: an Sp factor of 1 was used)

8.1.1 High Seismic

Step 1: Set the target displacement and determine the displacement, effective mass and effective height of a SDOF representation.

The target drift is set at θ = 1.5%. Due to the low number of storeys (less than 5) it is appropriate to assume a linear displaced shape of the structure. From this assumption, the displacement at each level is determined by: $\Delta_i = \vartheta \times H_i$

Table 8-3: Summary of factors used to calculate the effective displacement, effective mass and the effective height

Storey i	Height Hi (m)	Mass mi (tonnes)	Weight wi (KN)	Δi (m)	mi*Δi	mi*Δi^2	mi*Δi*Hi
4	14.4	311	3050.91	0.216	67.18	14.51	967.33
3	10.8	313	3070.53	0.162	50.71	8.21	547.62
2	7.2	313	3070.53	0.108	33.80	3.650832	243.39
1	3.6	313	3070.53	0.054	16.90	0.912708	60.85
Sum			**12262.5**		168.59	27.30	1819.19

The equivalent peak design displacement Δ_d, effective mass m_e and effective height H_e for a single degree of freedom system were determined using the equations below.

$$\Delta_d = \frac{\Sigma(m_i\Delta_i^2)}{\Sigma(m_i\Delta_i)} = \frac{27.30}{168.59} = 0.162m$$

$$m_e = \frac{\Sigma(m_i\Delta_i)}{\Delta_d} = \frac{224.8}{0.216} = 1042\ tonnes$$

$$H_e = \frac{\Sigma(m_i\Delta_i H_i)}{\Sigma(m_i\Delta_i)} = \frac{2425.6}{224.8} = 10.8m$$

Step 2: Calculate the equivalent viscous damping and reduced displacement spectrum

The design spectrum is reduced by the reduction factor, R, which is a function of the structural damping:

$$R = \left(\frac{7}{2+\xi}\right)^{\alpha}$$

Where ξ is the system damping ratio of the structure, taken as a combination of the elastic damping ξ_{el} and the hysteretic damping ξ_{hyst}, and α is equal to 0.5 and 0.25 for far-field and near field seismic spectra respectively. The hysteretic damping is calculated as a function of the re-centring ratio, β, and defined as ratio between the re-centring contribution M_{pt} and the total moment M_{con} (taken as 0.6), the ductility of the structure (assumed to be 2) and the post-yield stiffness ratio (r taken as 0.1) (STIC, 2013):

$$\xi_{\text{hyst}} = \frac{(2-2\beta)(\mu-1)}{\mu\pi\big(1+\text{r}(\mu-1)\big)} = \frac{(2-2\times 0.6)(2-1)}{2\pi\big(1+0.1(2-1)\big)} = 12\%$$

The above equation is based on the assumption of the combination of a non-linear elastic and elasto-plastic system in parallel.

In reality a timber system is significantly softer than this assumption would suggest and therefore it is recommended that 65% of the above value be used (STIC, 2013).

The elastic damping contribution must also be adjusted by the factor $\mu^{-0.43}$ giving (STIC, 2013):

$$\xi = \mu^{-0.43}\xi_{\text{el}} + 0.65\xi_{\text{hyst}} = 2^{-0.43}\cdot 5\% + 0.65\cdot 12\% = 3.71\% + 7.8\% = 11.5\%$$

This level of hysteretic damping is consistent with what was observed during testing of approximately 12%.

The spectral reduction factor η is applied to 5% elastic design displacement spectrum to account for an equivalent viscous damping of the system. It is assumed that the source of the ground shaking may be a near field event and so $\alpha_{sf} = 0.25$. Where R is

$$R = \left(\frac{7}{2+\xi_{eq}}\right)^{\alpha_{sf}} = \left(\frac{7}{2+11.5}\right)^{0.25} = 0.848$$

Step 3: Determine the effective period from the reduced design displacement spectrum

The displacement spectrum is calculated from the acceleration spectrum using

$$S_d = \frac{T^2}{4\pi^2}S_a$$

Using this reduction factor, the design displacement spectrum (Figure 8-6) was determined. From this the effective period of the SDOF system is read off the chart, for Sd = 0.162m, to be

$$T_e = 1.24s$$

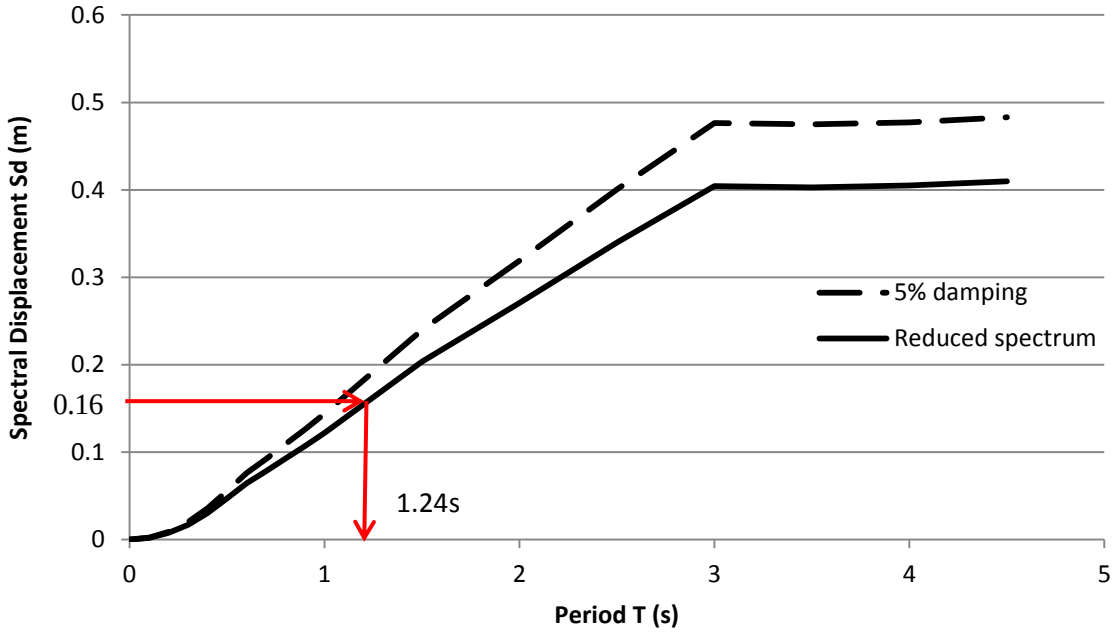

Figure 8-6: Reduced spectral displacement to interpolate the effective period of the equivalent SDOF system

Step 4: Calculate the equivalent stiffness and determine the base shear

The equivalent linear stiffness is the secant stiffness to the peak displacement response which was calculated to be

$$K_e = \frac{4\pi^2 m_e}{T^2} = \frac{4\pi^2 \times 1042t}{1.59s^2} = 16237\frac{kN}{m}$$

The design base shear on the structure is then

$$V_b = K_e \Delta_d = 16237 \times 0.216 = 3504\ kN$$

Step 5: Distribute the base shear up the structure

In the same manner as that of FBD, the design base shear is distributed to each floor in proportion to the floor mass and the overall floor height such that 90% is distributed amongst the floors with the

remaining 10% added to the top floor. The below Equation was used in the calculation of the floor forces shown.

$$F_i = F_t + 0.9V_b(m_i\Delta_i)/\sum_{i=1}^{n}(m_i\Delta_i)$$

Where: $F_t = 0.1V_b$ when i = n (at the roof)
= 0 when i ≠ n (all floors excluding the roof)

For the High Seismic option, the distributed base shears are shown in Table 8-4.

Table 8-4: Summary of forces at each floor and total base shear for the High Seismic option

Storey i	mi*Δi	Fi (kN)
4	89.6	1607
3	67.6	949
2	45.1	632
1	22.5	316
Sum	**224.8**	**3504**

8.5.1 Low Seismic

The method outlined above was repeated for the Low Seismic solutions. The only modification was that the value of damping was recalculated. The Low Seismic solution is assumed to behave as a post-tensioned only solution. Therefore the contribution of the post-tensioning to the total moment is equal to 1. This results in a hysteretic damping of 0%. The hysteretic damping is likely to be much greater than 0%, however, as it is primarily generated by friction it is unable to be used in the determination of the system damping. The only contribution to damping is the elastic damping of 3.7% calculated above ($\mu^{-0.43}\xi_{el}$) . Due to the very low damping, the design displacement spectrum is increased by R

$$R = \left(\frac{7}{2+\xi_{eq}}\right)^{\alpha_{sf}} = \left(\frac{7}{2+3.7}\right)^{0.25} = 1.05$$

Using this factor, the design displacement spectrum was determined. From this the effective period of the SDOF system is read off the chart to be

$$T_e = 1.32s$$

The equivalent linear stiffness is the secant stiffness to the peak displacement response which was calculated to be

$$K_e = \frac{4\pi^2 m_e}{T^2} = \frac{4\pi^2 \times 1042t}{1.59s^2} = 23653.5\frac{kN}{m}$$

The design base shear on the structure is then

$$V_b = K_e \Delta_d = 16237 \times 0.216 = 5105\ kN$$

The distributed base shear for the Low Seismic option is shown in Table 8-5.

Table 8-5: Summary of forces at each floor and total base shear for the Low Seismic option

Storey i	mi*Δi	Fi (kN)
4	89.6	2341
3	67.6	1382
2	45.1	921
1	22.5	461
Sum	**224.8**	**5105**

8.5.2 Comparison between HS and LS

A comparison of the results of the DBD for the High Seismic and the Low Seismic options, is shown in Table 8-6. The base shear for the High Seismic option is considerably less than that of the Low Seismic. This is due to the very different values of damping that were assumed, 11.5% for the High Seismic and 3.7% for the Low Seismic option. Such a low level of damping in general is not desirable. The actual damping for the Low Seismic option could be in practice greater than 3.7% due to friction between panels and the deformation of screws. However, these sources of damping are not reliable. This low value was adopted to be conservative as no specific energy dissipation devices are included in the Low Seismic option.

Table 8-6: Comparison between HS and LS base shears

	High Seismic	Low Seismic
Effective Period T_e (s)	1.59	1.32
Effective Stiffness K_e (kN/m)	16237	23654
Base Shear V_b (kN)	3504	5105

8.6 Internal Actions

The calculation of internal actions of a wall is relatively straight forward. The design moment at the base of the wall, is calculated from the sum of base shear V_b and the effective height H_e. The total moment demand for a High Seismic solution and a Low Seismic solution are shown in Table 8-7 below.

Table 8-7: Summary of the base action for the High Seismic and Low Seismic options from the DBD

	High Seismic	Low Seismic
Effective Height H_e (m)	10.8	10.8
Base Shear V_b (kN)	3504	5105
Moment Demand (kNm)	37843	55134

In the longitudinal direction of the building, for the High Seismic option, four pairs of coupled walls are used to resist the lateral loads. For the Low Seismic solutions the demand is much higher and the walls with only post-tensioning and no mild steel contribution have a much lower capacity than that of the High Seismic solution. Therefore eight pairs of coupled walls are used. Using ϕ=0.85, the design moment and base shear at the base of each of the coupled walls for the High Seismic solution and the Low Seismic solution are shown in Table 8-8.

Table 8-8: Summary of the internal actions of coupled walls for the High Seismic and Low Seismic Options

	High Seismic	Low Seismic
No. of coupled walls	4	8
φ	0.85	0.85
Base Shear V_b (kN)	1031	748
Design Moment M* (kNm)	11130	8336

The single walls acting in the transverse direction are, for simplicity, assumed to resist half of the base shear and moment of the coupled walls. In a dual system with frames and walls acting together the walls are much stiffer than the frames. Therefore the ratio is likely to be greater than 50:50, and more like 70:30 or 60:40 Walls: Frames (Priestley et al. 2007). Post-tensioned frames which are used for the gravity system are assumed to be designed to resist the remainder of the seismic forces that aren't accounted for by the walls (Table 8-9).

Table 8-9: Summary of internal actions for the single walls for the High and Low Seismic Options

	High Seismic	**Low Seismic**
No. of single walls	4	4
φ	0.85	0.85
Base Shear per wall (kN)	515.5	750
Design Moment per wall (kNm)	5565	8108

8.7 Design Procedure

The design process of the single and coupled walls, which make up the High Seismic and Low Seismic solutions, is demonstrated in Figure 8-7. The numerical design of the post-tensioned timber walls was performed using the Moment-Rotation procedure proposed by Pampanin et al. 2001 with the addition of the Modified Monolithic Beam Analogy (MMBA) proposed by Palermo, 2004. The general steps within the iterative procedure are described below.

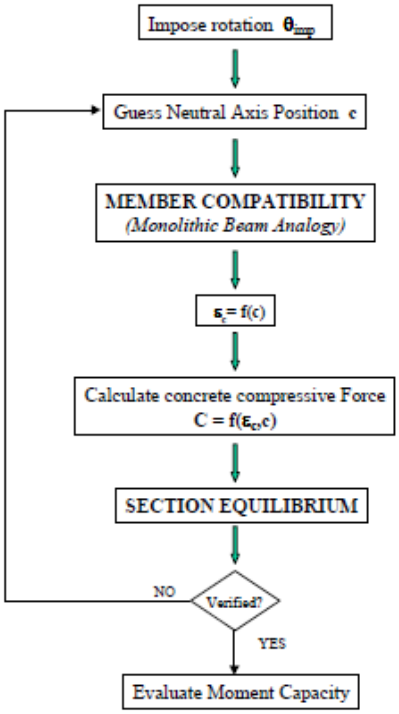

Figure 8-7: The moment rotation procedure for jointed ductile connections (Pampanin et al. 2001)

8.8 High Seismic Design

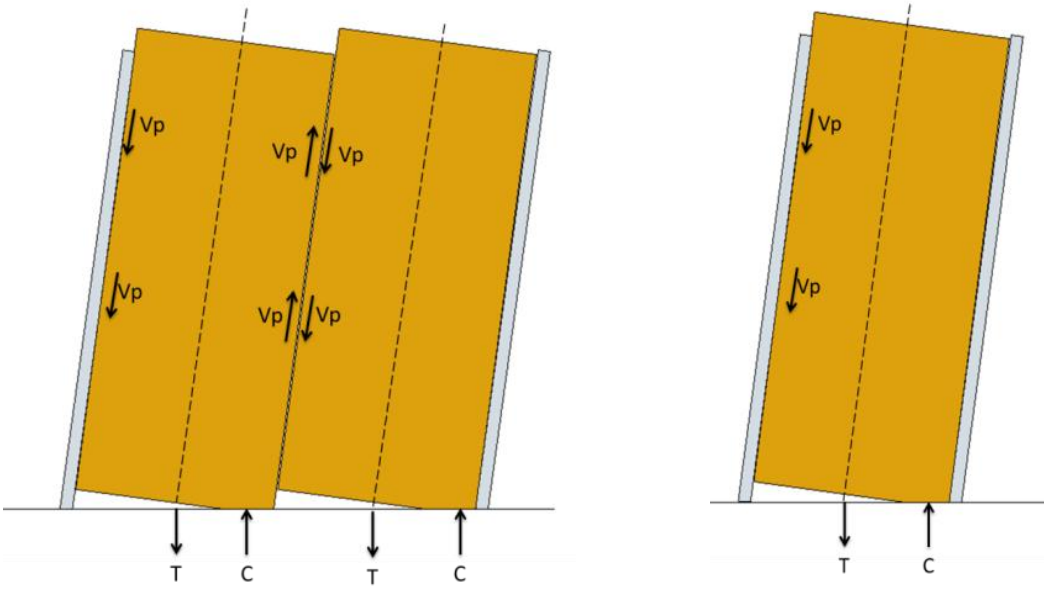

a) b)

Figure 8-8: Free body diagram of a) the coupled walls and b) the single walls for the High Seismic option

8.8.1 Preliminary Design of Coupled Walls

For the coupled walls, each of the two walls is assumed to carry the same moment. A re-centring ratio $\lambda = 1.5$ (or β=0.4) mild steel is assumed. Therefore the post-tensioning contribution will be 60% of total required base moment.

$$\phi M_{pt} = \phi(T_{pt} + N) j_d = \phi(T_{pt} + N)\left(d - \frac{c}{3}\right)$$

N= Axial force from gravity loads. This is ignored for the preliminary design.

First, assuming *c/h = 0.40* and assuming a triangular (linear) stress distribution;

$$j_d = 0.5h - c/3 = 0.37h$$

Rearranging and solving for the post-tensioned force at the target drift,

$$T_{pt} = \frac{0.6 \cdot 14118kNm}{0.37 \cdot 3.3m} = 4718kN$$

The maximum suggested stress limit on post-tensioning bars is:

$$f_{pt} \leq 0.7 f_{py}$$

For a 60mm post-tensioning bar this would result into a maximum allowable force of:

$$T_{pt} = 70\% A_{pt} f_{py} = 0.7 \cdot 2827mm^2 \cdot 835MPa = 1653kN$$

Therefore, three 60mm bars would be sufficient.

The tendon elongation can now be evaluated as:

$$\Delta_{pt} = \theta_{imp}(0.5h - c) = 0.015rad \cdot (0.5 \cdot 3.3m - 0.40 \cdot 3.6m) = 4.8mm$$

The tendon force due to gap opening is calculated knowing the additional tendon strain, where the un-bonded length of the tendon, in this example is as follows,

$$L_{ub} = 14.4m$$

$$\Delta T_{pt} = n_{pt} E_{pt} A_{pt} \frac{n_{gap} \cdot \Delta_{pt}}{l_{ub}} = 2 \cdot 170GPa \cdot 2827mm^2 \frac{1 \cdot 4.8mm}{14.4m} = 481kN$$

Therefore, the initial post-tensioned force is given by the difference between the required force at the target drift and the additional tendon force due to elongation.

$$T_{pt,initial} = 4718kN - 481kN = 4238kN$$

The initial total post-tension force corresponds to about 1410kN/bar.

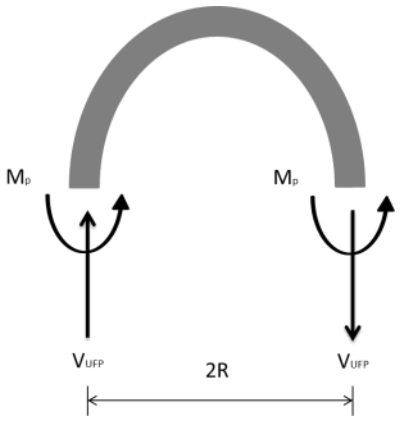

Figure 8-9: Plastic moment and coupling shear forces of a single UFP

For the design of the UFP devices it is assumed that they carry 40% of total moment. A significant contribution at the coupled joint is provided by friction. Using an equilibrium approach the moment contribution of the UFP devices is

$$OTM * 0.4 = nV_p\left(2l - \frac{c}{3}\right) + Fl$$

Where: n is the number of UFPs

Vp is the required capacity of the UFPs

F is the friction force with a coefficient of friction of approximately 0.4 for wood to wood.

Considering 8 pairs of UFP plates, the capacity of each shall be:

$$V_p = \frac{0.4OTM - Fl}{n(2l - c/3)} = \frac{0.4 \times 14118 - (0.4 \times 1265) \times 3.3}{8(2 \times 3.3 - (0.4 \times 3.3)/3)} = 92.8\ kN$$

The coupling elements are mild steel U-shaped Flexural Plates (UFPs), which can be design according to Kelly et al. 1974 as follows (See Chapter 3).

$$V_{UFP,pair} = f_{sy}\frac{bt^2}{D} = 350MPa \cdot \frac{300mm \cdot 10^2 mm^2}{50mm} = 105\ kN$$

Where f_{sy} = steel yield stress

b = plate width

t = plates thickness

D = diameter of UFP device

8.8.2 Detailed Design of Coupled Walls

The final iteration of the general design procedure for the High Seismic option is described below.

8.8.2.1 Wall 1

Step 1: Impose the design rotation

As stated previously the target drift is 2%. The connection rotation at the base of the wall is evaluated subtracting the wall's elastic contributions to the drift which are function of the force distribution along the building height.

The contribution of bending to the total displacement is given by

$$\Delta_{bend} = \frac{M_{dec} l^2}{3EI}$$

Where: M_{dec} is the decompression moment, determined from

T_{PTi} is the initial post-tensioning force

A_t is the cross-sectional area of the wall

N is the self-weight of the wall

$$M_{dec} = 2\left(\frac{T_{PTi} + N}{A_t}\right)Z = 2\left(\frac{3 \times 950 + 69}{0.96}\right)0.512 = \ 2954kNm$$

Therefore the deflection due to bending is:

$$\Delta_{bend} = \frac{M_{dec} l^2}{3EI} = \ \frac{2954 \times 3.3^2}{3 \times 15000 \times 0.8192} = 0.0166m$$

The shear contribution to the displacement is given by:

$$\Delta_{shear} = \frac{0.5OTM}{kGA_t} = \frac{0.5 \times 14118}{\frac{2}{3} \times 667000 \times 0.96} = 0.0165m$$

Where: OTM is the demand moment

k is the stiffness reduction factor (2/3)

G is the shear modulus of the timber

The total elastic contribution to the displacement is given by

$$\Delta_{el} = \Delta_{bend} + \Delta_{shear} = 0.0166 + 0.0165 = 0.0332m$$

Therefore the elastic rotation is

$$\theta_{el} = \frac{\Delta_{el}}{l} = \frac{0.0332}{14.4} = 0.230\%$$

The imposed rotation at the base of the wall is then reduced by 0.23% from 1.5% to 1.27%

Step 2: Guess a neutral axis depth

For preliminary design the neutral axis depth c can be estimated at approximately 0.4 times the length of the wall for a first guess (for CLT).

After an iterative procedure to obtain equilibrium the neutral axis depth was determined to be c = 994.7mm

Step 3: Determine the increased strain and force in the post-tensioned tendons

Using the neutral axis depth, the elongation of the Mac Alloy bar due to the imposed rotation is calculated to be:

$$\Delta_{pt} = \vartheta(d - c) = 1.34\% \times \begin{pmatrix} 1.485 - 0.995 \\ 1.65 - 0.995 \\ 1.815 - 0.995 \end{pmatrix} = \begin{pmatrix} 6.58 \\ 8.80 \\ 11.01 \end{pmatrix} mm$$

The increase in strain in each bar due to the imposed rotation is then:

$$\Delta\varepsilon_{pt} = \frac{n_{gap}\Delta_{pt}}{l_{ub}} = \begin{pmatrix} 0.000457 \\ 0.000611 \\ 0.000765 \end{pmatrix}$$

The additional tendon force ΔT_{PT} is given by the following expression using the increase in strain from Step 3.

$$\Delta T_{PT} = \Delta\varepsilon_{pt} E_{PT} A_{PT} = \begin{pmatrix} 192.9 \\ 266.9 \\ 341.0 \end{pmatrix} kN$$

The tension force in the tendon is the sum of the initial post-tension force and the additional elongation force due to the uplift of the wall.

$$T_{PT} = T_{PT,initial} + \Delta T_{PT} = 950 + \begin{pmatrix} 192.9 \\ 266.9 \\ 341.0 \end{pmatrix} = \begin{pmatrix} 1092.9 \\ 1166.9 \\ 1241.0 \end{pmatrix} = 3501kN$$

It should be noted that the maximum tendon stress should be less than 90% of the yield stress

$$f_{PT} = \begin{pmatrix} 386.5 \\ 412.7 \\ 438.9 \end{pmatrix} kPa < 0.90 f_{PTy}$$

Step 4: Estimate the strain in the timber

Due to the use of an un-bonded post-tensioned tendon, strain compatibility cannot be used. Therefore a global strain compatibility relationship, referred to as the Modified Monolithic Beam Analogy (MMBA) (Palermo, 2004) is adopted. The MMBA is used to calculate the strain in the timber pre-yield. The strain is calculated in proportion to the decompression curvature and the neutral axis depth.

The decompression curvature is:

$$\phi_{dec} = \frac{2}{E}\frac{1}{b_w h_w^2} T_{PT-initial} = \frac{2}{15GPa}\frac{1}{0.3 \times 3.3^2} 3 \times 950 = 1.16 \times 10^{-07}$$

The strain at the extreme fibre of the timber element is:

$$\varepsilon_t = c\left(3\frac{\theta_{imp}}{L_{cant}} + \phi_{dec}\right) = 0.995\left(3\frac{1.34\%}{14.4} + 1.16 \times 10^{-07}\right) = 0.00289$$

Step 5: Determine section equilibrium

Using the estimated neutral axis, section equilibrium must be achieved. In this case the tension force (T_{PT}) in the post-tensioned tendon is equal to the compressive force (C_t) in the timber as shown in Figure 8-11. It should be noted that the equilibrium equation changes with the addition of energy dissipaters.

The compression force in the timber is given by

$$C_t = 0.5E_{con}\varepsilon_t c b_w = 0.5 \times 0.7 \times 15GPa \times 0.00289 \times 0.995m \times 0.3m = 2724.2\ kN$$

E_{con} is the effective connection elastic modulus. For this application E_{con} was approximated to be 0.7 of the mean parallel to grain elastic modulus.

The equilibrium of Wall 1 is shown in Figure 8-10. The shear forces from the UFP devices are represented as Vp. The friction force F, is the product of the coefficient of friction between to wood layers and the total lateral force (base shear).

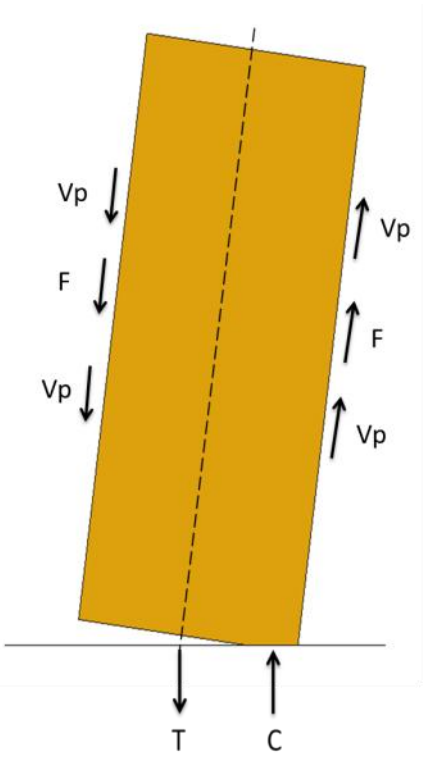

Figure 8-10: Force equilibrium of a Wall 1 with UFP dissipaters

Check equilibrium:

$$C_t - T_{PT} - \sum V_{UFP} - \sum F = 2724.2 - 3501 - 8 \times 105 + 8 \times 105 - 0.4 \times 1265 + 0.4 \times 1265 = 0 \ \therefore Ok$$

The moment for wall 1 is then evaluated:

$$M_{w1} = T_{PT1}\left(d_1 - \frac{c}{3}\right) + T_{PT2}\left(d_2 - \frac{c}{3}\right) + T_{PT3}\left(d_3 - \frac{c}{3}\right) + 8V_{UFP}l + F \times \frac{c}{3} = 7598\ kNm$$

The moment contributions from the post-tensioning and UFPs/friction are:

$$M_{PT1} = T_{PT1}\left(d_1 - \frac{c}{3}\right) + T_{PT2}\left(d_2 - \frac{c}{3}\right) + T_{PT3}\left(d_3 - \frac{c}{3}\right) = 4648kNm$$

$$M_{s1} = 8V_{UFP}l + F \times \frac{c}{3} = 2950 \text{ kNm}$$

Therefore the re-centring ratio of Wall 1 is:

$$\lambda = \frac{M_{PT1}}{M_{s1}} = \frac{46486}{2950} = 1.58$$

8.8.2.2 Wall 2

The design procedure for Wall 2 is the same as that for Wall 1. The values for Wall 2 are reported below. The internal actions of Wall 2 are represented in Figure 8-11.

$$\Delta_{pt} = \vartheta(d - c) = \begin{pmatrix} 2.11 \\ 4.33 \\ 6.54 \end{pmatrix} mm$$

$$\Delta\varepsilon_{pt} = \frac{n_{gap}\Delta_{pt}}{l_{ub}} = \begin{pmatrix} 0.00015 \\ 0.00030 \\ 0.00045 \end{pmatrix}$$

$$\Delta T_{PT} = \Delta\varepsilon_{pt}E_{PT}A_{PT} = \begin{pmatrix} 80.2 \\ 154.2 \\ 228.3 \end{pmatrix} kN$$

$$T_{PT} = T_{PT,initial} + \Delta T_{PT} = \begin{pmatrix} 980.2 \\ 1054.2 \\ 1128.3 \end{pmatrix} = 3162.7\ kN$$

$$\phi_{dec} = \frac{2}{E}\frac{1}{b_w h_w^2}T_{PT-initial} = 3.88 \times 10^{-08}$$

$$\varepsilon_t = c\left(3\frac{\theta_{imp}}{L_{cant}} + \phi_{dec}\right) = 0.003765$$

$$C_t = 0.5E_{con}\varepsilon_t c b_w = 4723.9\ kN$$

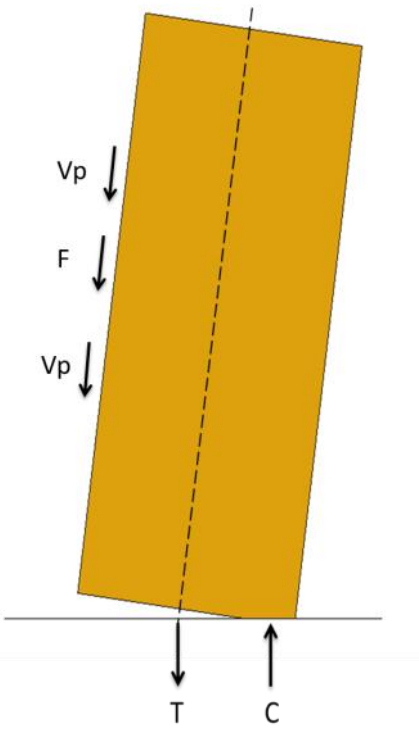

Figure 8-11: Force equilibrium of a Wall 2 with UFP dissipaters

Check equilibrium:

$$C_t - T_{PT} - \sum V_{UFP} - \sum F = 4724 - 3162.7 - 8 \times 105 - 0.4 \times 1265 = 0 \ \therefore Ok \qquad (8\text{-}1)$$

The moment for wall 1 is then evaluated:

$$M_{w2} = T_{PT1}\left(d_1 - \frac{c}{3}\right) + T_{PT2}\left(d_2 - \frac{c}{3}\right) + +T_{PT3}\left(d_3 - \frac{c}{3}\right) + 8V_{UFP}\left(l - \frac{c}{3}\right) + F\left(l - \frac{c}{3}\right) = 6493kNm$$

The moment contributions from the post-tensioning and UFPs/friction are:

$$M_{PT2} = T_{PT1}\left(d_1 - \frac{c}{3}\right) + T_{PT2}\left(d_2 - \frac{c}{3}\right) + T_{PT3}\left(d_3 - \frac{c}{3}\right) = \ 3938kNm$$

$$M_{s2} = 8V_{UFP}l + F \times \frac{c}{3} = 2406kNm$$

Therefore the re-centring ratio of Wall 1 is:

$$\lambda = \frac{M_{PT1}}{M_{s1}} = \frac{3938}{2406} = 1.64$$

8.8.2.3 Total Moment

The total moment is given by the sum of the moment for each wall

$$M_{Total} = M_{w1} + M_{w2} = 7598 + 6344 = 13942kNm \quad \therefore Ok$$

8.8.3 Summary of Coupled Walls

A summary of the design details of the coupled walls is shown in Table 8-10.

Table 8-10: Summary of design details of the coupled walls for the High Seismic option

Post-Tensioned Bars	
No. MacAlloy bar	3 bars
Diameter	60mm
Anchor spacing (either side of centre0	165 mm
Area of Strand, Apt	2827 mm^2
Initial post-tension force per bar	900 kN
UFP Devices	
Plate width	300mm
Thickness	10mm
Radius	50mm
Steel yield stress, fy	350MPa
Section Capacity	
Moment Demand, M*	11130 kNm
Nominal Capacity, M_n	13942 kNm
Factored Capacity, ϕM_n	11851 kNm
Re-centring Ratio, λ	1.61

8.8.4 Design of Single Walls

The design of the single walls follows exactly the same procedure as that of the coupled walls above. A force equilibrium diagram is shown in Figure 8-12. The single walls were designed to half of the

moment of the coupled walls. Therefore, the post-tensioning and UFP devices are the same as that for the coupled walls. A summary of the design of the single walls is shown in Table 8-11.

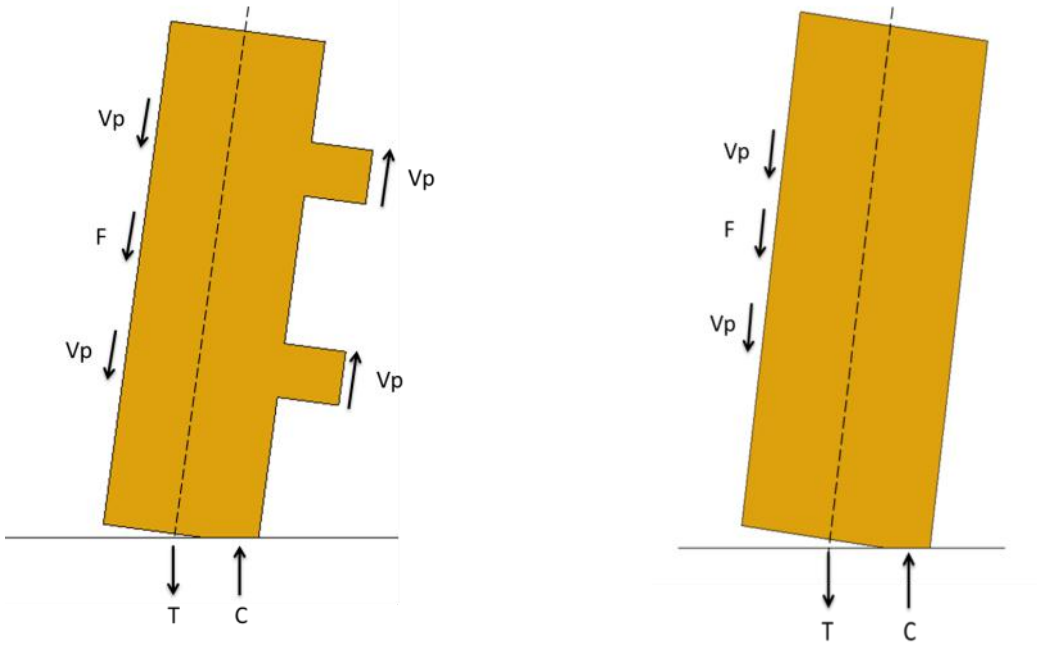

Figure 8-12: Free body diagram of a) a single wall with doorway openings and b) a single wall without doorway for the High Seismic option

Table 8-11: Summary of the design details of the single walls for the High Seismic option

Post-Tensioned Bars	***Wa1l with Opening***	***Wall without Opening***
No. MacAlloy bar	3 bars	3 bars
Diameter	60mm	60mm
Anchor spacing (either side of centre0	165 mm	165 mm
Area of Strand, Apt	2827 mm^2	2827 mm^2
Initial post-tension force per bar	1200 kN	1000 kN
UFP Devices		
Plate width	300mm	300mm
Thickness	10mm	10mm
Radius	50mm	50mm
Steel yield stress, fy	350MPa	350MPa
Section Capacity		
Moment Demand, M*	5565 kNm	5565 kNm
Nominal Capacity, M_n	3760 kNm	7132 kNm
Factored Capacity, ϕM_n	3384 kNm	6062 kNm
Re-centring Ratio, λ	1.18	1.57

8.8.5 Design Recommendations for Corner Columns

The corner columns do not contribute to the moment capacity of the system. However, the columns are required to resist the force of the UFP devices, and to act as a shear key. Furthermore, the columns must transfer the lateral load into the post-tensioned wall panels. The design of the corner columns is primarily governed by geometry and the connection to the floor slab. It is suggested that a steel SHS section the same width as that of the walls be used.

The columns should have a pinned connection at the base, to allow the columns to rock with the wall panels. This can be achieved by post-tensioning the columns, or bolting them to the foundation with a

single bolt. If a single bolt is used, it is recommended that a washer be used under the column to allow rotation to occur more readily. The 'pin' at the base of the column should be designed such that it is capable of resisting the full base shear into the wall. The shear capacity of the wall due to the post-tensioning should be ignored in the design of the shear key.

8.8.6 Design Recommendations for Anchorage Plates

The design of the anchorage plates is of significant importance in avoiding crushing of the wood under the plate and maintaining the post-tensioning force within the MacAlloy bars or tendons. Design recommendations for anchorage plates are given below.

- Ensure that there is a sufficient area of timber below the anchorage plate to take the full compression load of the post-tensioning, up to the ultimate drift level, without yielding of the timber
- It is recommended that the transverse layers in the timber, not be included in the compression area below the plate, with only the longitudinal layers used
- Anchorage plates must be sufficiently stiff, such that the compression load is spread evenly along the plate ensuring there is not a high concentration of load in the timber, at the centre of the anchorage. This can be achieved by a very thick steel plate or a steel channel.

8.9 Low Seismic Design

8.9.1 Preliminary Design of Walls

For the coupled walls, each of the two walls was assumed to carry the same moment. The re-centring ratio is for a post-tension only solution where β=1. Therefore the post-tensioning contribution will be 100% of total required base moment.

From the DBD, with a very low damping ratio, the design moment is

$$M_{pt} = \frac{8336/2}{0.85} = 4904kNm$$

$$\phi M_{pt} = \phi(T_{pt} + N)j_d = \phi(T_{pt} + N)\left(d - \frac{c}{3}\right)$$

N= Axial force from gravity loads. This is ignored for the preliminary design.

First, assuming *c/h = 0.40* and assuming a triangular (linear) stress distribution;

$$j_d = 0.5h - c/3 = 0.37h$$

Rearranging and solving for the post-tensioned force at the target drift,

$$T_{pt} = \frac{1 \cdot 4904kNm}{0.4 \cdot 3.3m} = 3715kN$$

The maximum suggested stress limit on post-tensioning bars is:

$$f_{pt} \leq 0.7 f_{py}$$

For a 60mm post-tensioning bar this would result into a maximum allowable force of:

$$T_{pt} = 70\% A_{pt} f_{py} = 0.7 \cdot 2827mm^2 \cdot 835MPa = 1653kN$$

Therefore, three 60mm bars would be sufficient.

The tendon elongation can now be evaluated as:

$$\Delta_{pt} = \theta_{imp}(0.5h - c) = 0.015rad \cdot (0.5 \cdot 3.3m - 0.30 \cdot 3.3m) = 4.95mm$$

The tendon force due to gap opening is calculated knowing the additional tendon strain, where the un-bonded length of the tendon, in this example is as follows,

$$L_{ub} = 14.4m$$

$$\Delta T_{pt} = n_{pt} E_{pt} A_{pt} \frac{n_{gap} \cdot \Delta_{pt}}{l_{ub}} = 3 \cdot 170GPa \cdot 2827mm^2 \frac{1 \cdot 4.95mm}{14.4m} = 496kN$$

Therefore, the initial post-tensioned force is given by the difference between the required force at the target drift and the additional tendon force due to elongation.

$$T_{pt,initial} = 3715kN - 496kN = 3219kN$$

This corresponds to about 1073kN/bar.

8.9.2 Detailed Design

As stated previously the target drift is 1.5%. The connection rotation at the base of the wall is evaluated subtracting the wall's elastic contributions to the drift which are function of the force distribution along the building height.

The decompression moment is:

$$M_{dec} = 2\left(\frac{T_{PTi} + N}{A_t}\right) Z = 2\left(\frac{3 \times 1000 + 71}{0.99}\right) 0.5445 = 3378.4$$

Therefore the deflection due to bending is:

$$\Delta_{bend} = \frac{M_{dec} l^2}{3EI} = \frac{3378.4 \cdot 3.3^2}{3 \cdot 15GPa \cdot 0.8984} = 0.0173m$$

The shear contribution to the displacement is given by:

$$\Delta_{shear} = \frac{0.5OTM}{kGA_t} = \frac{0.5 \cdot 4904}{\frac{2}{3} \cdot 666.7 \cdot 0.99} = 0.0105m$$

The total elastic contribution to the displacement is given by

$$\Delta_{el} = \Delta_{bend} + \Delta_{shear} = 0.0173 + 0.0105 = 0.0278m$$

Therefore the elastic rotation is

$$\theta_{el} = \frac{\Delta_{el}}{l} = \frac{0.0278}{14.4} = 0.193\%$$

The imposed rotation at the base of the wall is then reduced by 0.193% from 1.5% to 1.31%

8.9.2.1 Wall 1

Following the same procedure as the High Seismic option the design of Wall 1 is shown below.

For a neutral axis depth of c = 1133mm

$$\Delta_{pt} = \vartheta(d - c) = 1.31\% \cdot \begin{pmatrix} 1.485 - 1.13 \\ 1.65 - 1.13 \\ 1.815 - 1.13 \end{pmatrix} = \begin{pmatrix} 4.6 \\ 6.76 \\ 8.91 \end{pmatrix}$$

$$\Delta\varepsilon_{pt} = \frac{n_{gap}\Delta_{pt}}{l_{ub}} = \begin{pmatrix} 0.000320 \\ 0.000469 \\ 0.000619 \end{pmatrix}$$

$$\Delta T_{PT} = \Delta\varepsilon_{pt} E_{PT} A_{PT} = \begin{pmatrix} 153.6 \\ 225.6 \\ 297.6 \end{pmatrix}$$

$$T_{PT} = T_{PT,initial} + \Delta T_{PT} = \begin{pmatrix} 1153.6 \\ 1225.6 \\ 1297.6 \end{pmatrix}$$

$$\phi_{dec} = \frac{2}{E}\frac{1}{b_w h_w^2} T_{PT-initial} = \frac{2}{15GPa}\frac{1}{0.3 \cdot 3.3^2} 1000 = 1.224 \times 10^{-7}$$

$$\varepsilon_t = c\left(3\frac{\theta_{imp}}{L_{cant}} + \phi_{dec}\right) = 1133\left(3\frac{1.31\%}{14.4m} + 1.224 \times 10^{-7}\right) = 0.00322 < 0.0042 \ \therefore Ok$$

$$C_t = 0.5 E_{con} \varepsilon_t c b_w = 0.5 \cdot 10500 \cdot 0.00322 \cdot 1133 \cdot 300 = 3448.9\, kN$$

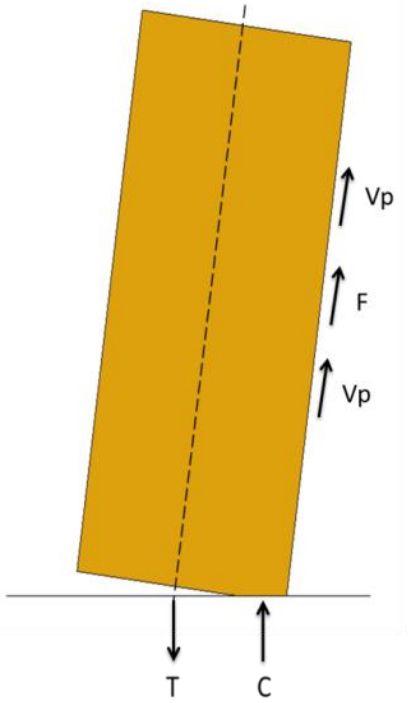

Figure 8-13: Force equilibrium of a Wall 1 for the Low Seismic option

The shear forces from the screws Vp as shown in Figure 8-13 are minimal and can be ignored. The friction force is the product of the coefficient of friction between to wood layers and the total lateral force (base shear). It should be noted that some contribution of friction has been included here as it was deemed to be too conservative to ignore it from the DBD procedure as well as the capacity of the system. The value of the friction coefficient used below is a preliminary estimate based on experimental testing. Further research is required to better define this term.

Check equilibrium:

$$C_t - T_{PT} - \sum V_p - \sum F = 3448.9 - 3676.8 + 0 + 0.4 \cdot 784 = 0 \ \therefore Ok \qquad (8\text{-}2)$$

The moment for wall 1 is then evaluated:

$$M_{w1} = T_{PT1}\left(d_1 - \frac{c}{3}\right) + T_{PT2}\left(d_2 - \frac{c}{3}\right) + T_{PT2}\left(d_2 - \frac{c}{3}\right) + +F\left(l - \frac{c}{3}\right) = 5448.5\ kNm$$

The moment contributions from the post-tensioning and UFPs/friction are:

$$M_{PT2} = T_{PT1}\left(d_1 - \frac{c}{3}\right) + T_{PT2}\left(d_2 - \frac{c}{3}\right) + T_{PT2}\left(d_2 - \frac{c}{3}\right) = 4781kNm$$

$$M_{s2} = F\left(l - \frac{c}{3}\right) = 667kNm$$

Therefore the re-centring ratio of Wall 1 is:

$$\lambda = \frac{5448.5}{667} = 7.2$$

8.9.2.2 Wall 2

The design of Wall 2 is shown briefly below.

For a neutral axis depth of c =1226mm

$$\Delta_{pt} = \vartheta(d - c) = \begin{pmatrix} 3.383 \\ 5.538 \\ 7.694 \end{pmatrix} mm$$

$$\Delta\varepsilon_{pt} = \frac{n_{gap}\Delta_{pt}}{l_{ub}} = \begin{pmatrix} 0.000235 \\ 0.000385 \\ 0.000531 \end{pmatrix}$$

$$\Delta T_{PT} = \Delta\varepsilon_{pt} E_{PT} A_{PT} = \begin{pmatrix} 112.9 \\ 184.9 \\ 256.8 \end{pmatrix}$$

$$T_{PT} = T_{PT,initial} + \Delta T_{PT} = \begin{pmatrix} 1112.9 \\ 1184.9 \\ 1256.8 \end{pmatrix} = 3554.6kN$$

$$\phi_{dec} = \frac{2}{E}\frac{1}{b_w h_w^2} T_{PT-initial} = 4.08 \times 10^{-8}$$

$$\varepsilon_t = c\left(3\frac{\theta_{imp}}{L_{cant}} + \phi_{dec}\right) = 0.003388 < 0.0042\ \therefore Ok$$

$$C_t = 0.5 E_{con}\varepsilon_t c b_w = 3925.1kN$$

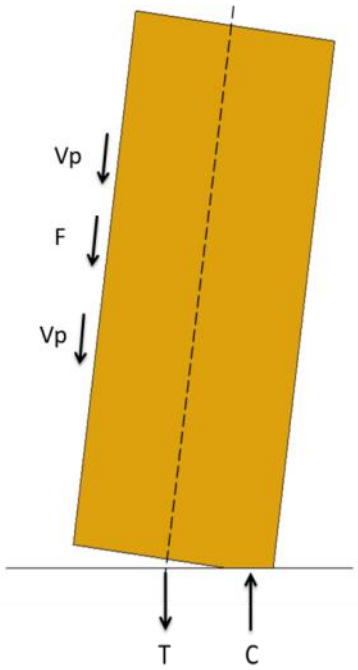

Figure 8-14: Force equilibrium of a Wall 2 for the Low Seismic option

Check equilibrium:

$$C_t - T_{PT} - \sum V_{UFP} - \sum F = 3925.1 - 3554.6 - 0 - 0.4 \cdot 784 = 0 \ \ \therefore Ok$$

The moment for wall 1 is then evaluated:

$$M_{w2} = T_{PT1}\left(d_1 - \frac{c}{3}\right) + T_{PT2}\left(d_2 - \frac{c}{3}\right) + T_{PT3}\left(d_3 - \frac{c}{3}\right) + F\left(l - \frac{c}{3}\right) = 4998.5\ kNm$$

The moment contributions from the post-tensioning and UFPs/friction are:

$$M_{PT2} = T_{PT1}\left(d_1 - \frac{c}{3}\right) + T_{PT2}\left(d_2 - \frac{c}{3}\right) + T_{PT3}\left(d_3 - \frac{c}{3}\right) = \ 4512.8\ kNm$$

$$M_{s2} = F\left(l - \frac{c}{3}\right) = 485.7\ kNm$$

Therefore the re-centring ratio of Wall 1 is:

$$\lambda = \frac{M_{PT1}}{M_{s1}} = \frac{4512.8}{485.7} = 9.29$$

8.9.2.3 Total Moment

The total moment is given by the sum of the moment for each wall

$$M_{Total} = M_{w1} + M_{w2} = 5448.5 \ + 4998.5 = 10447 \ kNm$$

Table 8-12: Summary of the design details of the coupled walls for the Low Seismic option

Post-Tensioned Bars	
No. MacAlloy bar	3 bars
Diameter	60mm
Anchor spacing (either side of centre0	165 mm
Area of Strand, Apt	2827 mm^2
Initial post-tension force per bar	1000kN
Friction	
Wood-Wood coefficient	0.4
Baseshear	784kN
Friction force	313.6kN
Section Capacity	
Moment Demand, M*	8336 kNm
Nominal Capacity, M_n	10447 kNm
Factored Capacity, ϕM_n	8880 kNm
Re-centring Ratio, λ	8.2

8.9.3 Design of Single Walls

The design of the single walls follows exactly the same procedure as that of the coupled walls. The force equilibrium diagrams of the single walls are shown in Figure 8-15. The single walls were designed to half of the moment of the coupled walls. Therefore the post-tensioning and UFP devices are the same as that for the coupled walls. A summary of the design of the single walls is shown in Table 8-13.

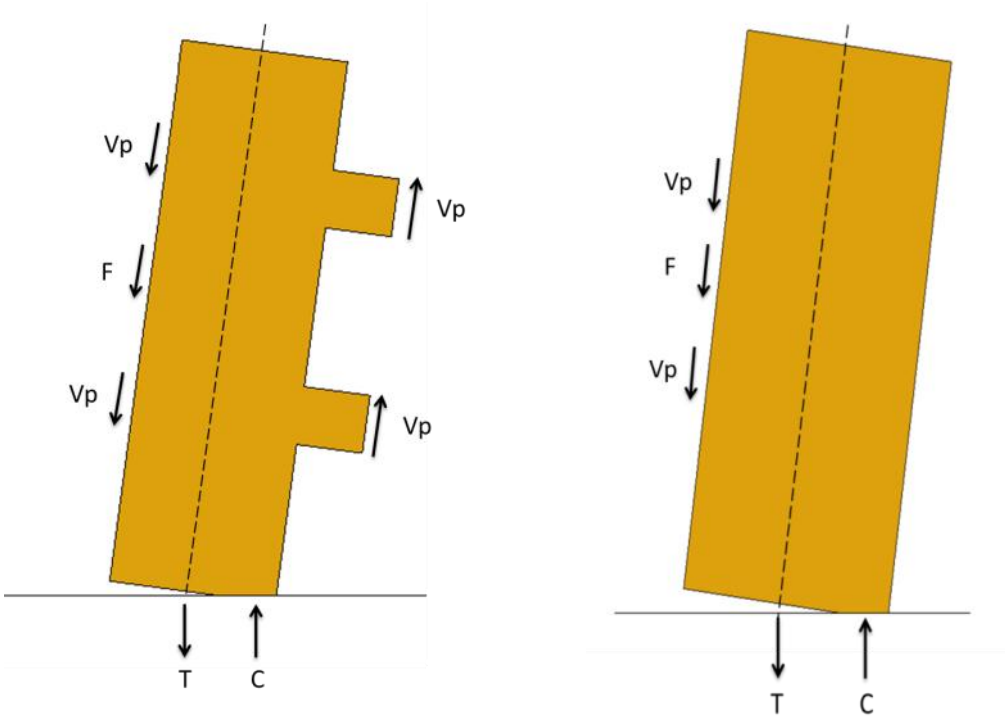

a) b)

Figure 8-15: Free body diagram of a) a single wall with doorway openings and b) a single wall without doorway for the High Seismic option

Table 8-13: Summary of the design details of the single walls for the Low Seismic option

Post-Tensioned Bars	***Wall with opening***	***Wall without opening***
No. MacAlloy bar	3 bars	3 bars
Diameter	60mm	60mm
Anchor spacing (either side of centre0	165 mm	165 mm
Area of Strand, Apt	2827 mm^2	2827 mm^2
Initial post-tension force per bar	1600 kN	1000 kN
Friction		
Wood-Wood coefficient	0.4	0.4
Base shear	784kN	784kN
Friction force	313.6kN	313.6kN
Section Capacity		
Moment Demand, M*	4168kNm	4168 kNm
Nominal Capacity, M_n	3111.4 kNm	4998.5 kNm
Factored Capacity, ϕM_n	2800 kNm	4249 kNm
Re-centring Ratio, λ	5.1	9.3

8.9.4 Design Recommendations for Shear Keys

The inclusion of shear keys at the base of the walls is crucial to prevent lateral sliding. Capacity design principles shall be applied, such that the shear keys are designed to resist the entire base shear for each wall. The friction at the base of the walls, due to the post-tensioning force, should be neglected in the design of the shear keys. Steel angles or channels bolted or welded to the foundation form adequate shear keys whilst allowing some rotation as shown in Figure 8-16.

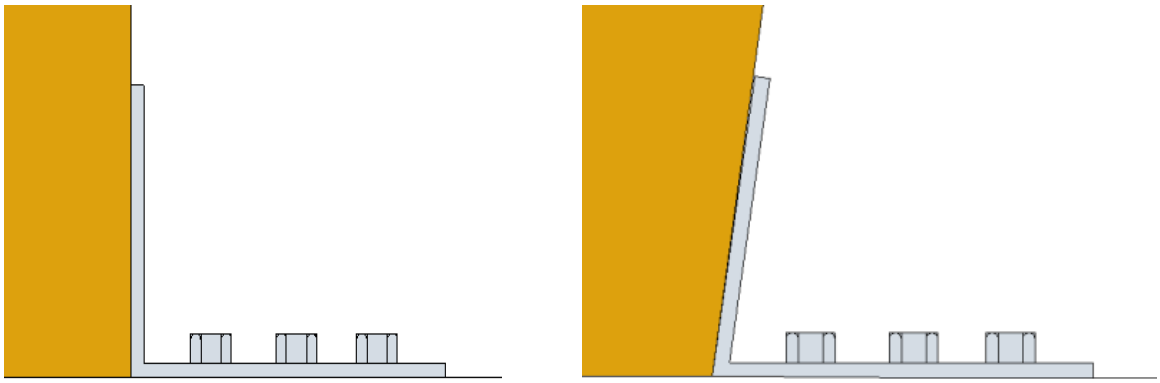

a) b)

Figure 8-16: Steel angle shear key when a) walls are stationary and b) a close up view during rocking

8.1.2 Design Recommendations for Anchorage Plates

The design of the Anchorage Plates is of significant importance in avoiding crushing of timber below the plate and maintaining the post-tensioning force within the MacAlloy bars or tendons. Design recommendations for Anchorage Plates are given below.

- Ensure that there is a sufficient area of timber below the Anchorage Plate to take the full compression load of the post-tensioning, up to the ultimate drift level, without yielding of the timber
- It is recommended that the transverse layers in the timber not be included in the compression area below the plate, with only the longitudinal layers used
- Anchorage Plates must be sufficiently stiff, such that the compression load is spread evenly such that there is not a high load concentration in the timber, at the centre of the anchorage. This can be achieved by a very thick steel plate or a steel channel.

8.10 Modelling

Numerical modelling of the Low Seismic and High Seismic wall systems based on a lumped plasticity approach, using the software Ruaumoko2D, was undertaken. This type of model concentrates the main inelastic demand at the base, where the controlled rocking occurs. The seismic response of post-tensioned rocking systems can be well described using one-dimensional wall elements representing the members, and rotational springs to model the concentrated inelastic behaviour at the base of the walls. The accuracy of this type of model has been verified in many previous investigations (Pampanin et al. 2001, Spieth et al. 2004, Palermo et al. 2005). The general representation of the analytical model used for the Low Seismic and High Seismic specimens is shown in Figure 8-17. The models incorporate the bi-linear elastic behaviour of the post-tensioning with a rotational spring at the base of each wall. Additional springs situated up the height of the wall, between the outside boundary elements and rigid links connected to the centre of the wall, represent the UFP devices and friction dissipation.

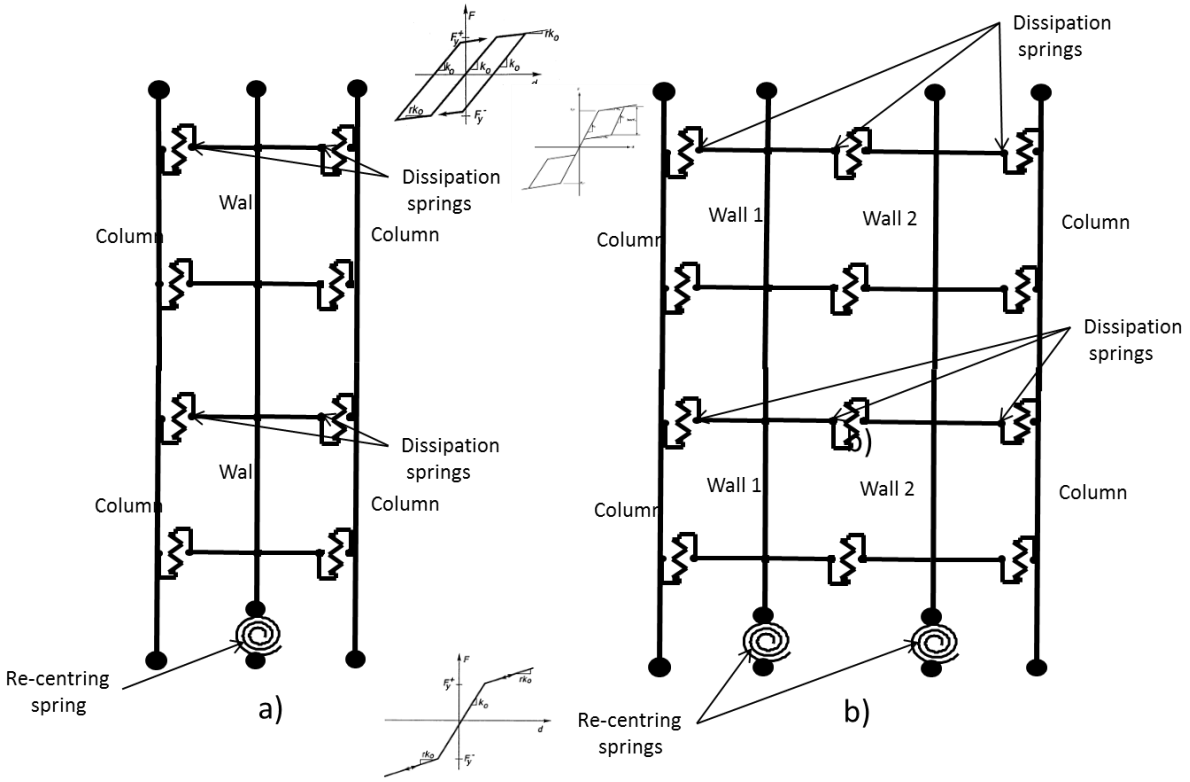

Figure 8-17: General representation of the lumped plasticity model used in Ruaumoko2D

The four storey single walls and coupled walls, for each specimen, were analysed under a cyclic displacement controlled analysis. The displacement input went past the design level of 1.5% drift to 2% drift (Figure 8-18).

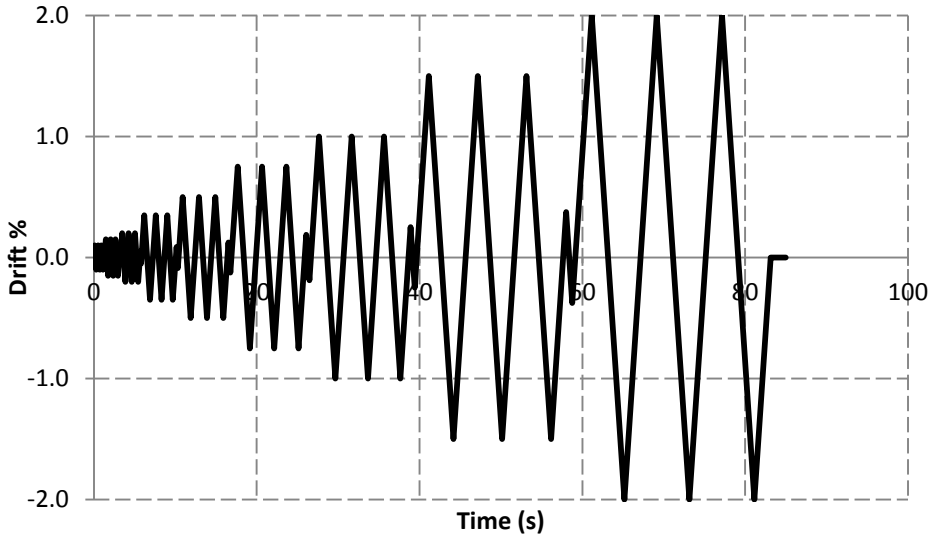

Figure 8-18: Displacement input for the Ruaumoko models

The results of the analyses on the system and subassemblies are described in the following for the High Seismic and Low Seismic options.

8.10.1 High Seismic Option

General representations of the models representing the High Seismic sub-assemblies are shown in Figure 8-17. The wall panels and steel corner columns were represented by elastic elements. Three bi-linear elastic springs were used at the base of each wall to represent each post-tensioning bar. Rigid links were used to connect the coupler springs, representing the UFPs, to the wall elements. The UFPs were described by a bi-linear elasto-plastic hysteresis rule from RUAUMOKO (Carr, 2008). Additional dissipation elements were also used to represent friction between adjacent panels.

The hysteretic behaviour of the post-tensioning, UFP and friction elements, are shown in Figure 8-19. Results of the numerical modeling of the single and coupled walls for the High Seismic option are shown in Figure 8-20.

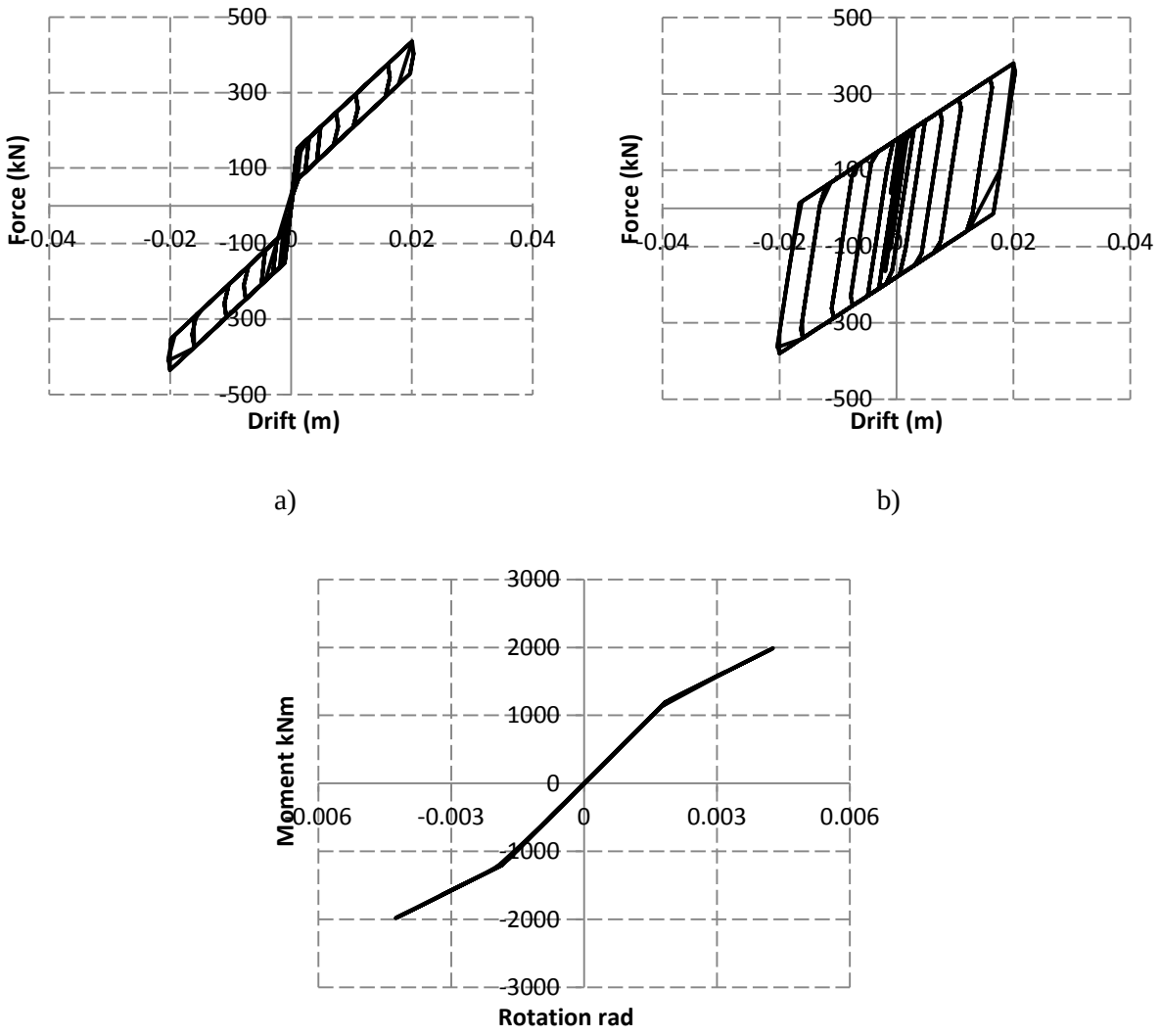

Figure 8-19: The hysteretic behaviour of the a) assumed friction contribution, b) UFP and c) post-tensioning elements for the High Seismic Option

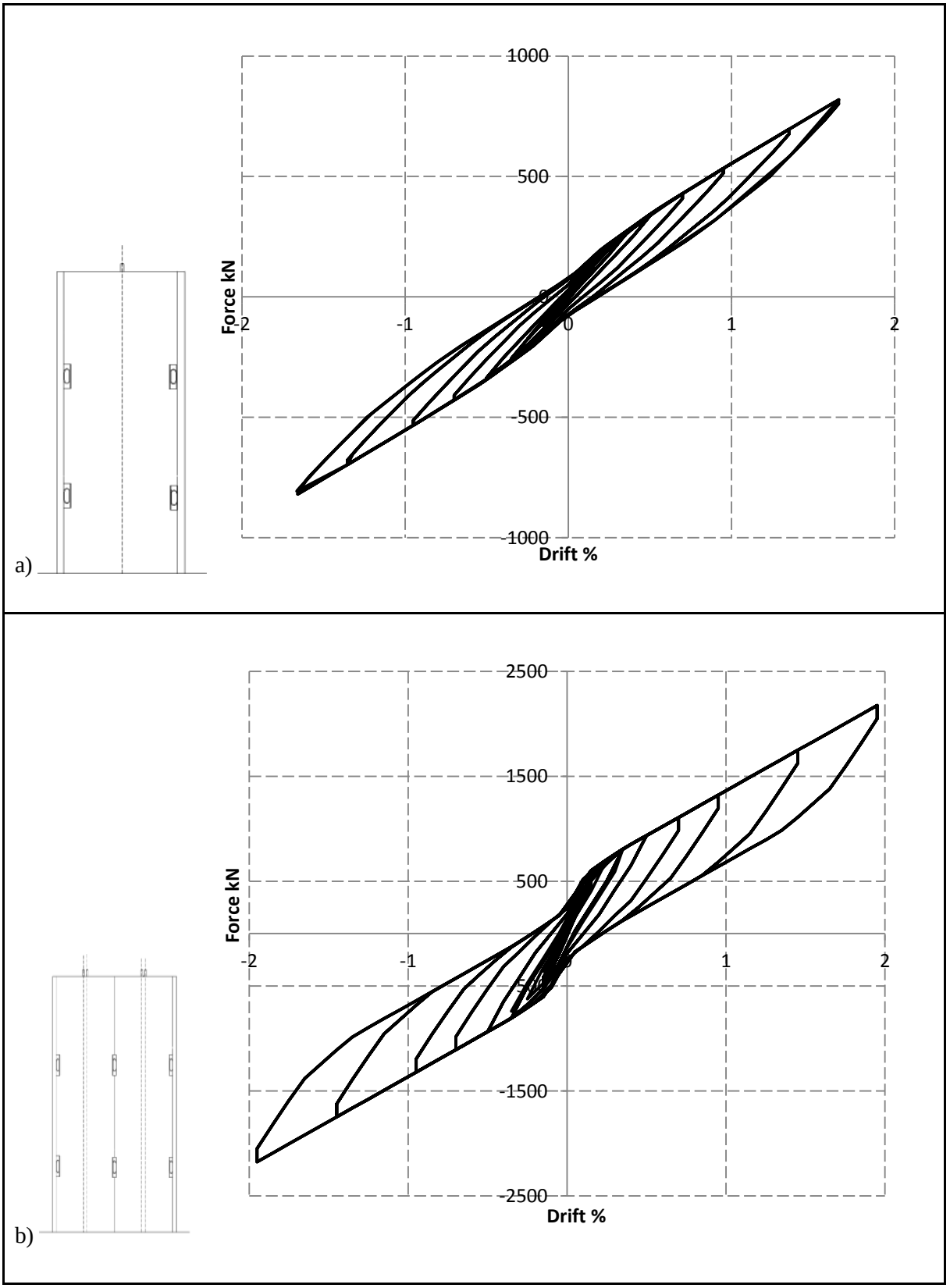

Figure 8-20: Numerical models of a) single walls and b) coupled walls of the High Seismic option

8.10.2 Low Seismic Option

A similar model to that of the High Seismic option was used to represent the Low Seismic option. The wall panels were represented by elastic elements and three bi-linear elastic springs were used at the base of each wall, to represent each post-tensioning bar. Rigid links were used to connect the coupler springs, representing screws and friction, between adjacent panels.

Results of the numerical modelling of the single and coupled walls for the Low Seismic option are shown in Figure 8-21.

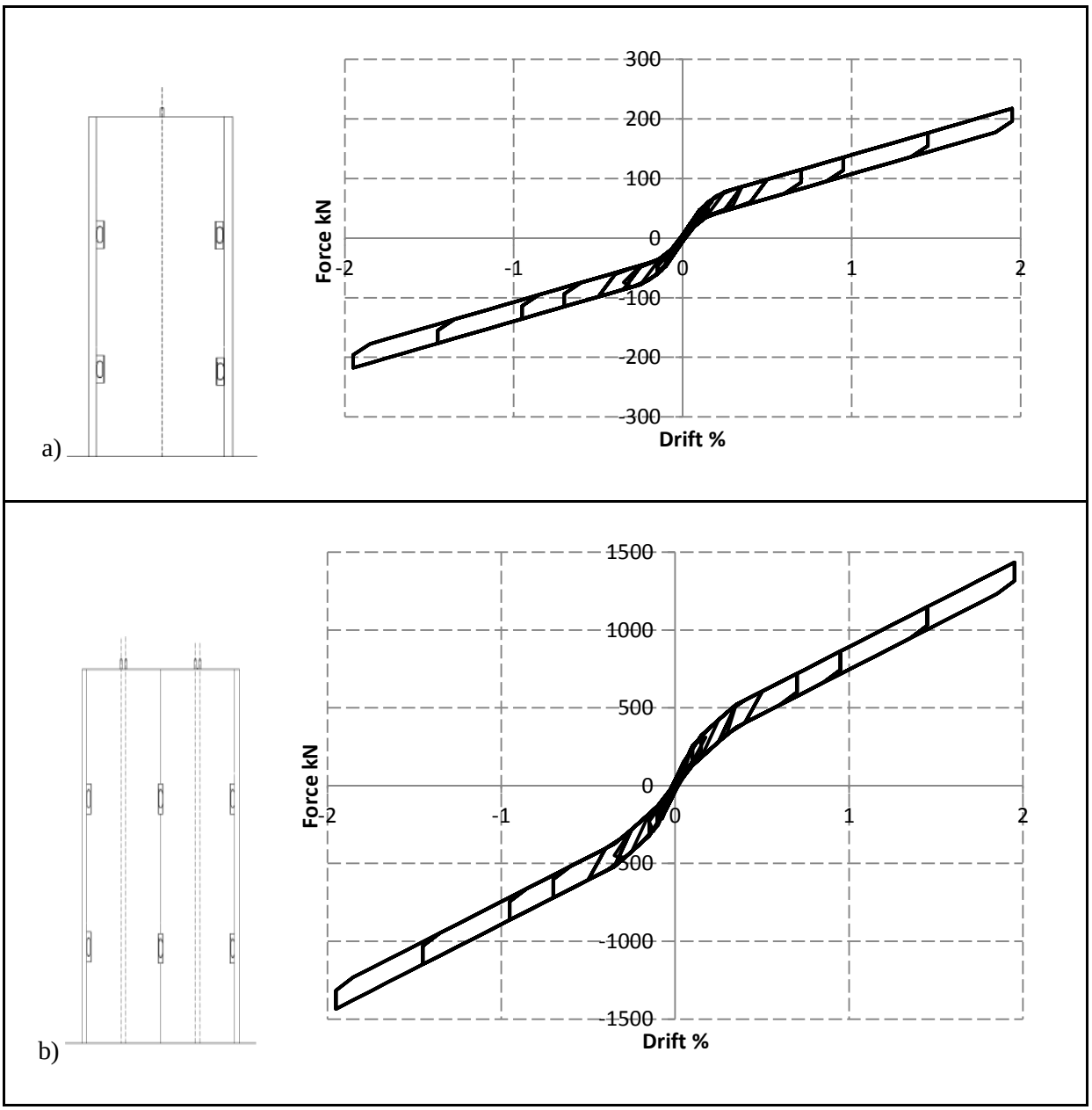

Figure 8-21: Numerical models of a) single walls and b) coupled walls of the Low Seismic option

8.11 Summary of Case Study Building Design

This chapter presented a full case study of the seismic design of a core-wall system, forming the lateral load resisting system of a five storey timber building. The evaluation of seismic loading and design base shear was carried out with reference to the current New Zealand seismic loading standards (NZS 1170.0:2002; NZS 1170.5:2004), following a displacement-based design approach.

- The base shear for the High Seismic option, from the DBD, was considerably less than that of the Low Seismic option. This was due to the very different values of damping that were assumed, 11.5% for the High Seismic and 3.7% for the Low Seismic option. Such a low level of damping is not desirable. The actual damping for the Low Seismic option is likely to be greater than 3.7%, due to friction between panels. Hysteretic damping of around 6% for the single walls, and upwards of 10% for coupled walls was observed from the experimental results. However, due to code requirements, friction is unable to be relied upon and hence cannot be counted towards the system damping. This low value was adopted to be conservative as no specific energy dissipation devices are included in the Low Seismic option.
- The lateral load resisting system of the High Seismic option consisted of five post-tensioned frames in one direction and four sets of coupled walls around the stairwell cores acting in the other direction. The lateral loads in the longitudinal direction were resisted by four sets of post-tensioned CLT coupled walls.
- Due to the much greater design loads for the Low Seismic option, four additional sets of coupled walls were required in the longitudinal direction to reduce the moment demand for each wall.
- Section analyses were performed for the High Seismic and Low Seismic options. Re-centring ratios of 1.5 were targeted for the High Seismic option. The re-centring capacity of the Low Seismic option was very large, due to the minimal moment contribution of friction and screws.
- Numerical modeling of single and coupled wall sub-assemblies was performed for the High Seismic and the Low Seismic options. Lumped plasticity models were used with the analysis program Ruaumoko2D. Force displacement hysteretic behaviour was obtained at a system level to verify the design.

9 CONCLUSIONS

9.1 Summary

The research presented in this thesis develops options for architects and engineers to utilise timber walls for around stairwells and lift shafts. Post-tensioned cross-laminated timber (CLT) wall panels were investigated as a potential solution for low and high seismicity regions. As part of this research, particular attention was paid to practical issues in implementing timber core walls as opposed to obtaining a seismically optimal solution.

The seismic performance of post-tensioned core-wall systems was investigated using two test specimens: one aimed at a high seismicity region and another aimed at a low seismicity region. Each specimen was a two storey, half scale stairwell core. A literature review on CLT and Pres-Lam systems, along with a number of stairwell and lift-shaft layouts, were investigated in Chapter 2. The design of each specimen was detailed in Chapter 3 and the construction of the test specimens was described in Chapter 4. The High Seismic test specimen comprised of post-tensioned rocking CLT walls coupled with energy dissipating U-shaped Flexural Plates (UFPs). Steel SHS columns were situated in the corners of the core. The UFP devices were attached between wall panels and the steel SHS columns. The Low Seismic specimen had the same layout as the high seismicity specimen. However, in the place of SHS corner columns and dissipater devices, horizontal screws were used to connect perpendicular panels.

The experimental program consisted of quasi-static bi-directional cyclic tests on the two half scale, two-storey stairwells. Different scenarios, described in Chapter 5, were investigated for each of the test specimens. The results of these tests were discussed in Chapter 6.

In Chapter 7, the results of simple analytical modelling of the High Seismic and Low Seismic specimens were discussed. The analytical models were used for predictions of the test results. The models were then refined to better fit the observed experimental behaviour.

Chapter 8 presented a full case study of the seismic design of a core-wall system forming the lateral load resisting system of a five storey timber building. The case-study building was adapted from Part 2 of the STIC design guide (STIC, 2013). The evaluation of seismic loading and design base shear was carried out with reference to the current New Zealand seismic loading standards (NZS 1170.0:2002; NZS 1170.5:2004), following a displacement-based design approach.

9.2 Conclusions

Experimental testing was performed on two half scale, two-storey stairwell cores. Key points from the results of the Low Seismic and High Seismic tests are shown below.

For the Low Seismic Tests:

- The construction of the Low Seismic specimens was simple and rapid, enabled by the prefabrication of elements and simple screw connections between panels. Tight tolerances were not a concern in the construction of the Low Seismic specimen.
- The low screw configurations allowed the wall panels to rock separately, with some friction at the vertical sliding joints between the panels. These configurations would be suitable for seismic design with a suitable damping factor to allow for the friction. Damage caused to screws can be replaced by adding another screw near the position of the old screw. The energy dissipation contribution of the low number of screws was negligible.
- The high screw configurations restricted the uplift of the panels, and hence the elongation of the tendons, and produced a lateral sliding displacement mechanism at the base of the walls, with some rocking of the walls. This led to more significant crushing at the base of the walls than the low screw configurations, due to the larger horizontal actions.
- The high screw configurations gave increased stiffness and strength but reduced displacement capacity. These configurations would be better suited to an elastic design procedure for regions governed by wind rather than earthquake loading where little to no rocking is desirable.
- For both low and high screw configurations, minimal energy dissipation was provided by the deformation of the screws. For the low screw configuration there were not enough screws to provide significant energy dissipation. For the high screw configuration, minimal uplift and hence minimal deformation in the screws occurred, which again produced minimal energy dissipation. For the pairs of coupled walls, a large amount of energy dissipation was generated from friction at the vertical coupling joint between the two panels.
- The connection of the floor transfer beams to the wall panels required some vertical uplift during rocking of the walls. Selected details allowed this to occur with no observed damage.

For the High Seismic Tests:

- In general the construction of the High Seismic specimen was rapid. However, a high degree of accuracy was required due to tight tolerances in connections between the corner columns and the foundation, the panels, the columns, and the coupled wall connections.

- The UFP devices were manufactured in a way that they were not square and level. This, therefore, made it difficult to match the UFPs up with the rivet plates and columns. This was partially mitigated by drilling over-sized oval holes for the bolts, through the UFPs.
- Good hysteretic response was observed with excellent energy dissipation and re-centring in all tests.
- The energy dissipation contribution to the total hysteretic behaviour was significantly influenced by friction. Friction occurred when a relative movement was created between adjacent elements. The friction component of the energy dissipation was greatest at the vertical joint between the pairs of coupled walls. For tests where all of the UFPs were removed, there was a significant amount of energy dissipation from friction alone.
- The steel corner columns were very effective in isolating the floor system from the uplift of the rocking walls, and minimal vertical displacement of the loading beams was observed during testing.
- The steel corner columns were very effective in acting as a shear key at the foundation connection.

9.3 Recommended Future Research

Whilst some practical issues in implementing CLT core-walls for multi-storey buildings have been investigated in this thesis, there is a significant amount of further research needed. Aspects of this are outlined below.

- This research is the first instance in which CLT panels have been used as part of a Pres-Lam (Pre-stressed Laminated timber) system. To better predict the behaviour of the system, further tests on the material properties of CLT panels should be investigated.
- A significant amount of friction between adjacent elements was observed during testing. The amount of friction is difficult to predict accurately. Testing with a reduced friction surface on joints between adjacent elements is recommended, to reduce the uncertainty surrounding the friction component.
- Large scale shake table tests should be carried out to assess the effects of dynamic friction on the overall damping of CLT core wall systems. The friction has the potential to reduce the seismic response and the need for specific energy dissipation devices, provided that the amount of friction can be accurately predicted.
- Full scale shake table tests will also allow investigation of the higher mode effects which may be important for tall and flexible timber structure.

9.4 Recommendations for Building Designers

- For buildings located in low seismic areas (such as Auckland, or Australia), the "low seismic" option can result in the most cost-effective design, using post-tensioned walls connected together with screws and designed to be elastic. In this case, the post-tensioning is not specifically needed for the rocking mechanism of the walls, but it is provided as a simple and robust method of connecting (with moment capacity) the core walls to the foundations. This solution should be designed such that minimal rocking occurs.
- For buildings in high seismic regions (such as Wellington), the "high seismic" option is the most suitable solution, using post-tensioned walls and steel corner posts, with UFPs at the vertical joints. The beneficial influence of friction on the response of the system can be accounted for with an increase in the level of damping in the calculation of lateral forces. Although care must be taken in specifying what level of damping is reliable.
- For intermediate seismic areas (such as Christchurch), either the "high seismic" option can be used or a modified "low seismic" option could be considered, using post-tensioned walls connected together with a small number of screws to allow relative movement between the panels. The beneficial influence of friction can be accounted for with an increase in the level of damping in the calculations, and some additional dissipation devices such as epoxied steel rods or other dissipaters can be provided if necessary.
- For all seismic zones, particular attention must be paid to preventing horizontal sliding of the panels by providing appropriate shear keys at the foundation.

9.5 Closure

Multi-storey timber structures are becoming increasingly desirable for architects and building owners due to their aesthetic and environmental benefits. In addition, there is increasing public pressure to have low damage structural systems with minimal business interruption after a moderate to severe seismic event. Post-tensioned timber systems, in this case incorporating CLT panels, are a viable solution. Furthermore, these systems can provide large open spaces for multi-storey buildings which are desirable for the New Zealand and overseas commercial building market.

Construction and design guidance presented in this thesis provides structural engineers and architects with options to utilise CLT walls for around stairwells and lift shafts of multi-storey timber buildings.

REFERENCES

ACI ITG-5.1, 2007, Acceptance Criteria for Special Unbonded Post-Tensioned Precast Structural Walls Based on Validation Testing and Commentary, ACI Innovation Task Group 5.

Applied Technology Council (2006) "Next-Generation Performance Based Seismic Design Guidelines", Program Plan for New and Existing Buildings Prepared for the Federal Emergency Management Agency, FEMA 445.

AS/NZS1170.0 (2002) "Structural Design Actions, Part 0: General Principles", Standards Australia/Standards New Zealand, Sydney.

AS/NZS1170.1 (2002) "Structural Design Actions, Part 1: Permanent, imposed and other actions", Standards Australia/Standards New Zealand, Sydney.

Buchanan A. H. (2008) "Timber Design Guide" New Zealand Timber Industry Federation, Wellington, New Zealand.

Carr, A.J. (2008), "RUAUMOKO Program for Inelastic Dynamic Analysis – Users Manual", Department of Civil Engineering, University of Canterbury, Christchurch, New Zealand.

Ceccotti, A. (2008) "New Technologies for Construction of Medium-Rise Buildings in Seismic Regions: The XLAM Case", Structural Engineering International, Science and Technology pg 156-165.

Ceccotti, A., Follesa, M. (2006) "Seismic Behaviour of Multi-Storey XLam Buildings", Proceedings of International Workshop on Earthquake Engineering on Timber Structures, Coimbra, Portugal.

Ceccotti A., Lauriola M., Pinna M., Sandhaas C., (2006) "SOFIE Project – Cyclic Tests on Cross-Laminated Wooden Panels", Proceedings of the 9th World conference on timber engineering, August 6-August 10, Portland, Oregon, USA.

Conley, J., Sritharan, S. and Priestley, M.J.N., (2002) "Precast Seismic Structural Systems PRESSS-3: The Five-Storey Precast Test Building Vol.3-1: Wall Direction Response. Structural Systems Research Report, University of California, San Diego.

Deam, B. (1997) "Seismic Design and Behaviour of Multi-storey Plywood sheathed timber framed Shearwalls", Research Report No 97/3, Department of Civil Engineering, University of

Canterbury.

FPInnovations (2011) CLT Handbook: Cross-Laminated Timber Canadian Edition, special publication SP528E

FPInnovations (2013) CLT Handbook: Cross-Laminated Timber US Edition, special publication SP529E

Follesa, M., Brunetti, M., Cornacchini, R., and Grasso, S. (2010). "Mechanical In-plane Joints Between Cross Laminated Timber Panels." 11th World Conference on Timber Engineering, Trentino, Italy

Gavric, I., Fragiacomo, M. and Ceccotti, A. (2012) "Strength and Deformation Characteristics of Typical X-Lam Connections", World Conference on Timber Engineering, Auckland, New Zealand.

Hare, J., Oliver, S. and Galloway, B. (2012) "Performance Objectives for Low Damage Seismic Design of Buildings", NZSEE Conference, Christchurch, New Zealand.

Henry, R. (2011) "Self-centering Precast Concrete Walls for Buildings in Regions with Low to High Seismicity", Doctor of Philosophy Thesis, Department of Civil and Environmental Engineering, University of Auckland, New Zealand.

Iqbal, A. (2010) "Seismic Response and Design of Sub-assemblies for Multi-Storey Prestressed Timber Buildings", Doctor of Philosophy Thesis, Department of Civil and Natural Resources Engineering, University of Canterbury, Christchurch, New Zealand.

Iqbal, A., Pampanin, S., Palermo, A. and Buchanan, A. H. (2010) "Seismic Performance of Full-scale Post-Tensioned Timber Beam-Column Joints", Proceedings of the 11th WCTE conference, Trentino, Italy.

Kelly, J. M., Skinner, R. I. and Heine, A. J. (1972) "Mechanisms of energy absorption in special devices for use in earthquake resistant structures" Bulletin of NZSEE, 5(3), 63-68

mgb ARCHITECTURE + DESIGN, Equilibrium Consulting, LMDG Ltd and BTY Group (2012) The Case for Tall Wood Buildings- How mass timber offers a safe, economical and environmentally friendly alternative for tall building structures.

Moroder, D., Sarti, F., Palermo, A., Pampanin, S. and Buchanan A.H. (2014) “Experimental Investigation of Wall-to-Floor Connections in Post-Tensioned Timber Buildings”, NZSEE Conference, Auckland, New Zealand.

Moroder, D., Buchanan, A.H. and Pampanin, S. (2013) “Preventing Seismic Damage to Floors in Post-Tensioned Timber Frame Buildings”, NZSEE Conference, Wellington, New Zealand.

Muller, A. (2010) “Structural Design for Energy Efficient Multi-storey Timber Houses-State of the Art in Europe” Proceedings of the International Convention of Society of Wood Science and Technology and United Nations Economic Commission for Europe, Geneva, Switzerland.

Newcombe, M.P., Pampanin, S., and Buchanan, A.H. (2010) “Design, Fabrication and assembly of a Two-storey Post-Tensioned Timber Building”, Proceedings of the 11th WCTE conference, Trentino, Italy.

Newcombe, M.P., Carradine, D., Pampanin, S., Buchanan, A.H., Deam, B.L., van Beerschoten, W.A., and Fragiacomo, M. (2009) “In-Plane Experimental Testing of Timber-Concrete Composite Floor Diaphragms”, Annual NZSEE Conference, Christchurch, New Zealand.

Newcombe, M.P., Pampanin, S., Buchanan, A.H., and Palermo, A. (2008) “Seismic Design and Numerical Validation of Post-tensioned Timber Frames”, 14th WCEE, Beijing, China.

NZS1170.5 (2004) “Structural Design Actions, Part 5: Earthquake Actions”, Standards New Zealand, Wellington.

Palermo, A. (2004) “Use of Controlled Rocking in the Seismic Design of Bridges”. 13th World Conference on Earthquake Engineering, Vancouver, B.C., Canada

Palermo, A., Pampanin, S., Buchanan, A.H., and Newcombe, M.P. (2005) “Seismic Design of Multi-storey Buildings Using Laminated Veneer Lumber”, NZSEE annual conference, Wairakei, New Zealand.

Pampanin, S., Priestley, M. J. N., & Sritharan, S. (2001). Analytical Modelling of the Seismic Behaviour of Precast Concrete Frames Designed with Ductile Connections. Journal of Earthquake Engineering, 5(3), 329-367.

Pampanin, S., Christopoulos, C., and Priestley, M. J. N. (2002). "Residual Deformations in the Performance-Based Seismic Assessment of Frame Structures." ROSE-2002/02, ROSE School,

Pavia.

Popovski, M., Schneider, J. and Schweinsteiger, M. (2010) “Lateral Load Resistance of Cross-Laminated Wood Panels” Proceedings of the 11th World Conference on Timber Engineering, Riva del Garda, Trentino, Italy.

Popovski, M. and Karacabeyli, E. (2011) “Seismic Performance of Cross-Laminated Wood Panels” 44th CIB-W18, Alghero, Italy.

Priestley M.J.N., Calvi, M.C., and Kowalsky, M.J. (2007) Displacement-Based Seismic Design of Structures IUSS Press, Pavia, Italy

Priestley, M.J.N. (1996) “The PRESSS Program – Current Status and Proposed Plans for Phase III”, PCI Journal 41:2, 22-40.

Priestley, M.J.N. (1997) “Displacement Based Seismic Assessment of Reinforced Concrete Buildings”, Journal of Earthquake Engineering, 1:1, 157-192.

Priestley, M.J.N., Sritharan, S., Conley, J.R. and Pampanin, S. (1999) “Preliminary Results and Conclusions from the PRESSS Five-storey Pre-cast Concrete Test Building”, PCI Journal 44:6, 42-67.

Quenneville, P. and Morris, P. (2007) “Japan Kobe Earthquake Shake Table Simulation: Earthquake Performance of Multi-storey Cross Laminated Timber Buildings”, Issue 4, Volume 15, NZ Timber Design.

Sarti, F., Smith, T.J., Palermo, A., Pampanin, S. and Carradine, D.M. (2013) “Experimental and analytical study of replaceable Buckling-Restrained Fuse-type (BRF) mild steel dissipaters”, NZSEE Conference, Wellington, New Zealand.

Sarti, F., Palermo, A. and Pampanin, S. (2014) “Quasi static cyclic tests of 2/3 scale post-tensioned timber wall and column-wall-column (CWC) systems”, NZSEE Conference, Auckland , New Zealand.

SEAOC Vision 2000 Committee (1995)” Performance-Based Seismic Engineering”, Report prepared by the Structural Engineering Association of California, Sacremento, U.S.A.

Smith, T. J. (2006) “LVL Rocking Shear walls: With External Dissipater Attachment”, 3rd Professional Year Project Report, University of Canterbury, Christchurch, New Zealand.

Smith, T. J. (2008) “Feasibility of Multi Storey Post-Tensioned Timber Buildings: Detailing, Cost and Construction”, Master of Engineering Thesis, Department of Civil and Natural Resources Engineering, University of Canterbury, Christchurch, New Zealand.

Smith, T. J., Carradine, D., Pampanin, S., Ditommaso, R. and Ponzo, F. C. (2012) “Seismic Performance of a post-tensioned LVL building subjected to the Canterbury earthquake sequence”, Proceedings of the Annual NZSEE Conference, Christchurch, New Zealand.

Speith, H.A.,Carr A.J., Pampanin, S., Murahidy, A.G. and Mander, J.B. (2004) “Modelling of Pre-cast Pre-stressed Concrete Frame Structures with Rocking Beam-Column Connections”, Research Report 2004-01, ISSN 0110-3326, Department of Civil Engineering, University of Canterbury.

Standards New Zealand (1999) “NZS3604 Timber Framed Buildings”, SNZ, Wellington, New Zealand

STIC 2013. Design Guide for Expan Frames and Walls, Structural Timber Innovation Company Ltd, Christchurch, New Zealand.

Zarnani, P. and Quenneville, P. (2013) “Timber Rivet Connection Design Guide”, Department of Civil and Environmental Engineering, University of Auckland, New Zealand.

APPENDIX A: CONSTRUCTION PHOTOS

This Appendix shows the construction of two ½ scale, two-storey post-tensioned CLT stairwell cores, for the Low Seismic and High Seismic tests.

A.1 Loading Beams

a) 

b) 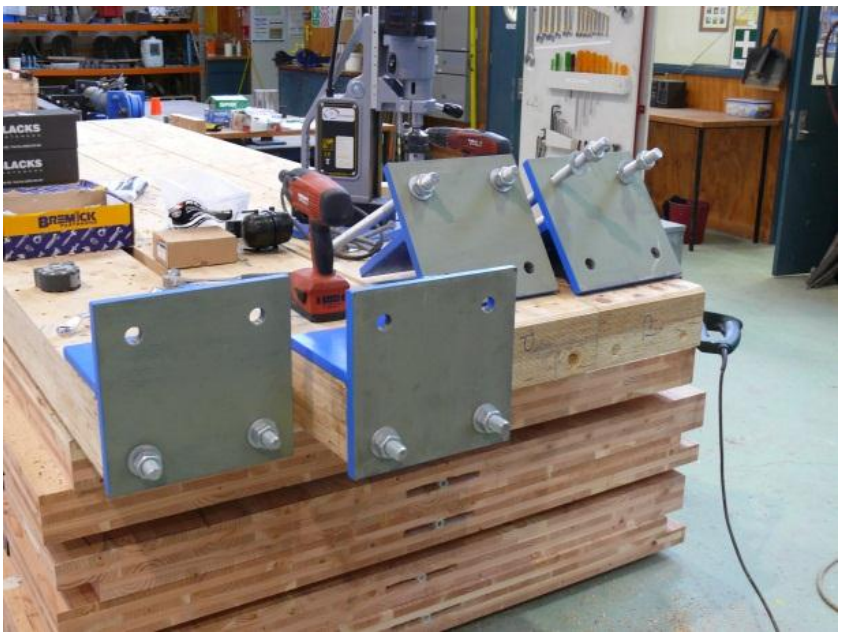

Figure A-1: Loading beam construction, a) Drilling holes for epoxy rods, b) End plates bolted onto epoxy rods

a)

b)

Figure A-2: Loading beam construction, a) End plates to connect to loading rid, b) Spreader beam bolted onto end plates

a)

b)

Figure A-3: Loading beam construction, a) Ring of bolts for Low Seismic specimen, b) Inset screwed plate for High Seismic specimen

a)

b)

Figure A-4: Loading beam connections, routing out insert (a) for steel screw plates (b)

Figure A-5: Loading beam components, screwed inset plate for High Seismic specimens

A.2 Stairs and Landings

a)

b)

Figure A-6: Stair and landing panels with 50mm edge for a) landing panel, b) stair panel

a)

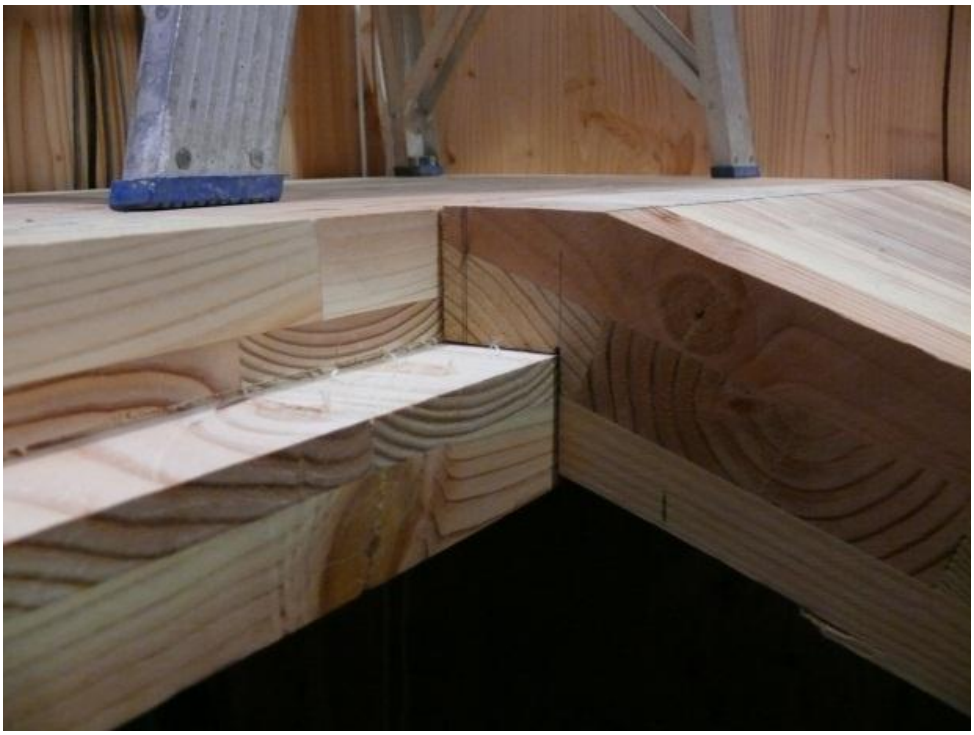

b)

Figure A-7: Stair panels, a) stair being lifted into place, b) top of stair joint with landing

Figure A-8: Bottom of stair seated on landing

Figure A-9: Full half-flight stairs and landings

A.3 Low seismic General Construction

a)

b)

Figure A-10: a) Void with plastic tube to house tendon within panel, b) East panel lifted into position

a)

b)

Figure A-11: a) Coupled walls positioned together, b) partially completed core

Figure A-12: Post-tensioning of walls

a)

b)

Figure A-13: Completed Low Seismic construction (a) without loading rigid and (b) with the loading rig in place

A.4 High seismic Construction

a)

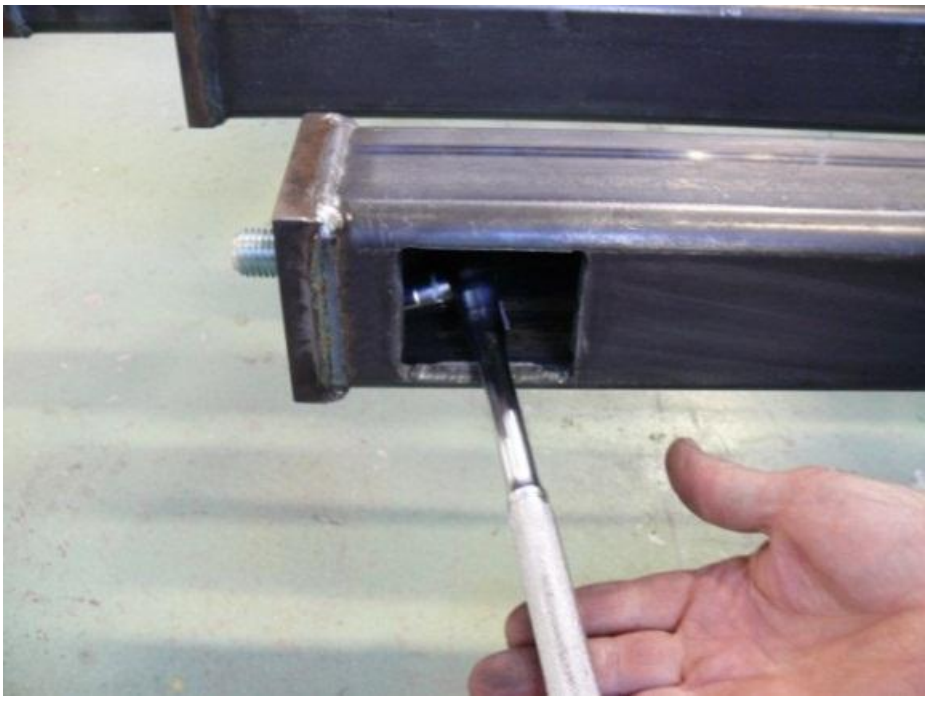

b)

Figure A-14: Corner columns, a) base of SHS with 24mm hole, b) 'window' at base of SHS to tighten bolt

a)

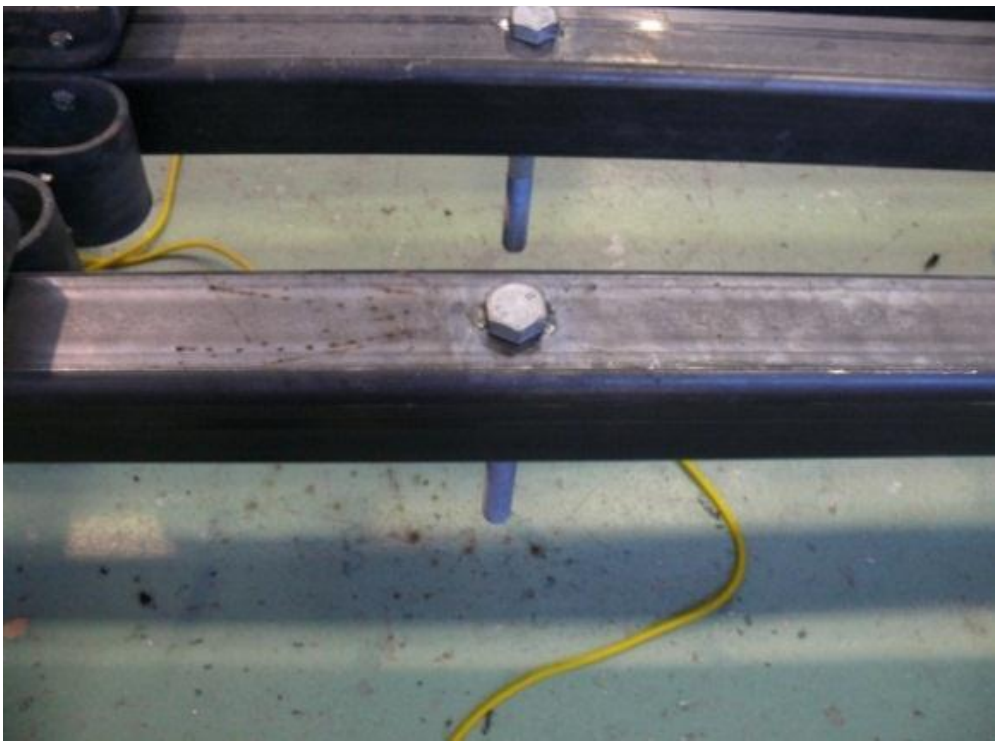

b)

Figure A-15: Corner column connections, a) 10mm threaded holes to bolt UFPs, b) bolts tack-welded to SHS to connect loading beam

a)

b)

Figure A-16: a) UFP bolted to SHS column, b) UFPs bolted at two levels along the columns

A.5 UFP Rebates and Connections

a)

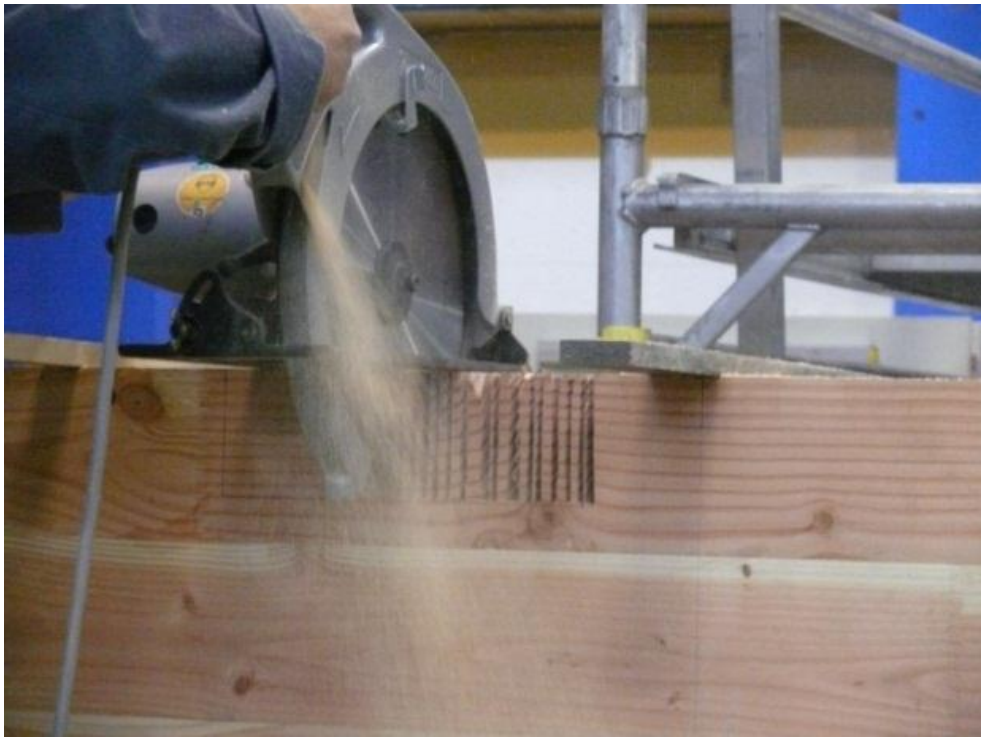

b)

Figure A-17: Rebates in panels for the UFPs; a) rebates marked out, b) cutting rebate with skill saw

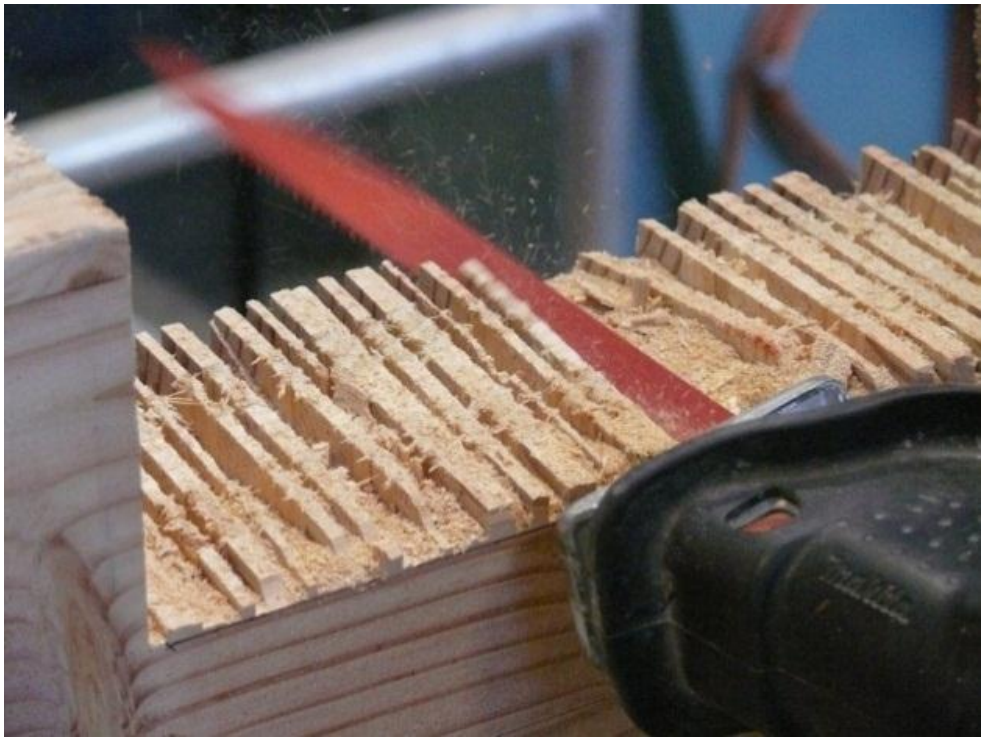

a)

b)

Figure A-18: Rebates in panels for the UFPs; a) flattening the surface of the rebate, b) finished sanded rebate

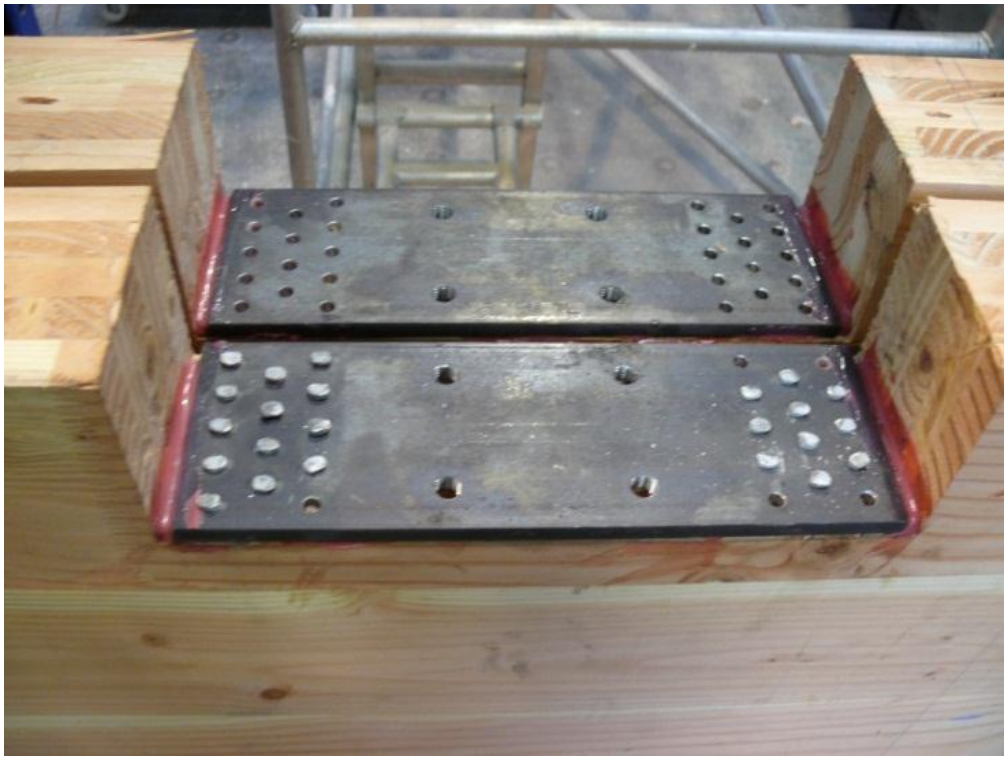

a)

b)

Figure A-19: Construction of UFP rebates; a) plates epoxied into position and riveted, b) lining up UFP plates on column

a)

b)

Figure A-20: a) Notches to allow for bolt head protruding from the columns, b) fitting column and panel together

A.6 High Seismic General Erection

Figure A-21: installation of East wall and SHS columns

Figure A-22: South East corner of the core with UFPs bolted in place

Figure A-23: Tight tolerance for construction, clamps required to install bolt at the base of the SHS column

a)

b)

Figure A-24: Completed construction of the High Seismic specimen

APPENDIX B: INSTRUMENTATION

Table B-1: Instrumentation log used for the High Seismic and Low Seismic test specimens

#	name	Type	Address	Notes	Device #	Box	Channel	Reset value	Calibration Factor
	A	Load cell (1000kN)	1000-347-4-I	Control	A chan	Control 8	1		0.50761
	B	Load cell (300 kN)	300-250-2.5 A	Control	A chan	Control 3	1		0.20562
	C	Load cell (300 kN)	300-250-2.5 B	Control	A chan	Control 2	1		0.183936
1	t1	Load cell (1000kN)		Logger	B chan	9	1	-2069	0.102965
2	x1	Load cell (300 kN)		Logger	B chan	10	1	4546	0.033471
3	x2	Load cell (300 kN)		Logger	B chan	10	2	1502	0.0350303
4	w1	Load cell (150 kN)		12.7 strand		12	1	144	-0.015843
5	w2	Load cell (150 kN)		12.7 strand		12	2	3461	-0.015839
6	y3	Load cell (150 kN)		12.7 strand		14	1	453	-0.015686
7	y4	Load cell (150 kN)		12.7 strand		14	2	250	-0.015827
8	z5	Load cell (150 kN)		12.7 strand		15	1	-2908	-0.015621
9	z6	Load cell (150 kN)		12.7 strand		15	2	254	-0.015608
10	v7	Load cell (150 kN)		12.7 strand		16	1	4117	-0.015781
11	v8	Load cell (150 kN)		12.7 strand		16	2	1989	0.015847
12	u9	Load cell (500 kN)		15.2 strand		18	1	74	0.054348
13	u10	Load cell (500 kN)		15.2 strand		18	2	1078	0.054645
14	k1	Rotary pot		North side	16	27	1		-0.0242
15	k2	Rotary pot		North side	9	27	2		-0.0249
16	k3	Rotary pot		North side	15	27	3		-0.0242
17	k4	Rotary pot		North side	12	27	4		-0.0243
18	k5	Rotary pot		North side	18	27	5		-0.0242
19	k6	Rotary pot		North side	14	27	6		-0.0242
20	k7	Rotary pot		North side	17	27	7		-0.0243
21	k8								
22	m1	Rotary pot		East	8	13	1		-0.0243

23	m2	Rotary pot		East	20	13	2		-0.0243
24	m3	Rotary pot		East	19	13	3		-0.0242
25	m4	Rotary pot		East	3	13	4		-0.0296
26	m5								
27	r1	Inclinometer				r	1		-0.1017
28	r2	Inclinometer				r	2		-0.1012
29	r3	Inclinometer				r	3		-0.1005
30	r4	Inclinometer				r	4		-0.1021
31	r5	Inclinometer				r	5		-0.1041
32	r6	Inclinometer				r	6		-0.1062
33	r7	Inclinometer				r	7		-0.102
34	r8	Inclinometer				r	8		-0.1151
35	r9	Inclinometer				r	9		-0.1136
36	r10	Inclinometer				r	10		0.0869
37	r11	Inclinometer				r	11		0.0897
38	r12	Inclinometer				r	12		0.0901
39	r13								
40	a1	Spring pot		East		22			
41	a2	Spring pot		East		22			
42	a3	Spring pot		East		22			
43	a4	Spring pot		East		22			
44	a5	Spring pot		East		22			
45	a6	Spring pot		East		22			
46	a7	Spring pot		East		22			
47	a8	Spring pot		East		22			
48	a9	Spring pot		East		22			
49	a10								
50	b1	Spring Pot		North		23			
51	b2	Spring Pot		North		23			
52	b3	Spring Pot		North		23			
53	b4	Spring Pot		North		23			
54	b5	Spring Pot		North		23			
55	b6	Spring Pot		North		23			
56	b7	Spring Pot		North		23			
57	b8	Spring Pot		North		23			
58	b9								
59	c1	Spring pot		West		24			
60	c2	Spring pot		West		24			
61	c3	Spring pot		West		24			
62	c4	Spring pot		West		24			
63	c5	Spring pot		West		24			
64	c6	Spring pot		West		24			
65	c7	Spring pot		West		24			
66	c8	Spring pot		West		24			
67	c9	Spring pot		West		24			
68	c10	Spring pot		West		24			
69	c11	Spring pot		West		24			
70	c12								
71	J1	Trigger							
72	m5	beam pots N		North		13			-0.0034
73	m6	beam pots N		North		13			-0.0034
74	m7	beam pots N		North		13			-0.0034
75		slip pots		East (door)					
76		slip pots		East					
77		slip pots		North					
78		slip pots		North					

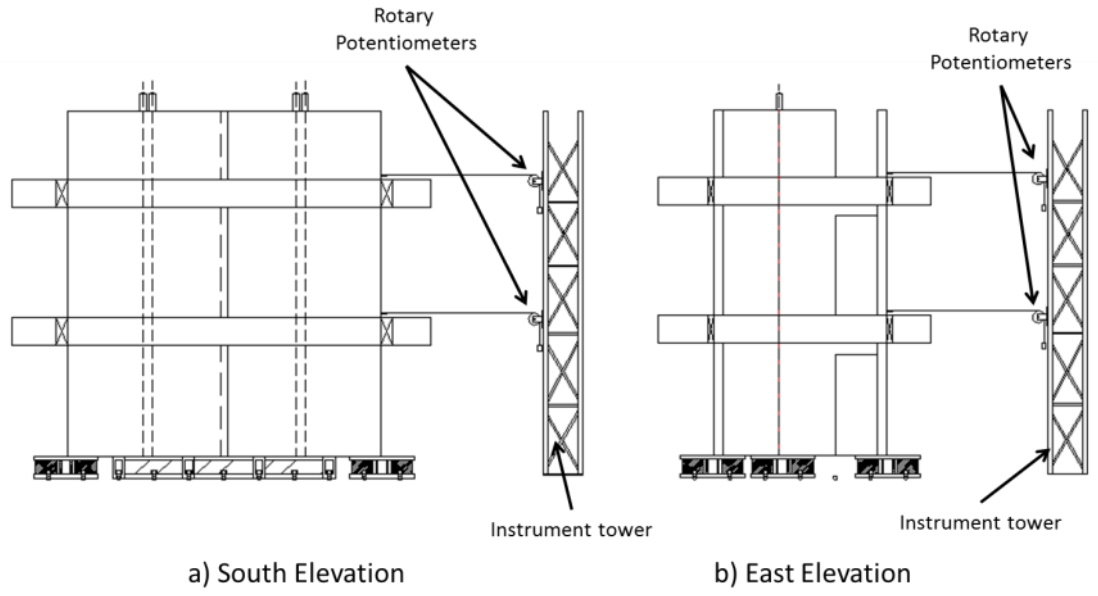

Figure B-1: Location of Rotary potentiometers measuring lateral displacements of the walls; a) South elevation, b) East elevation

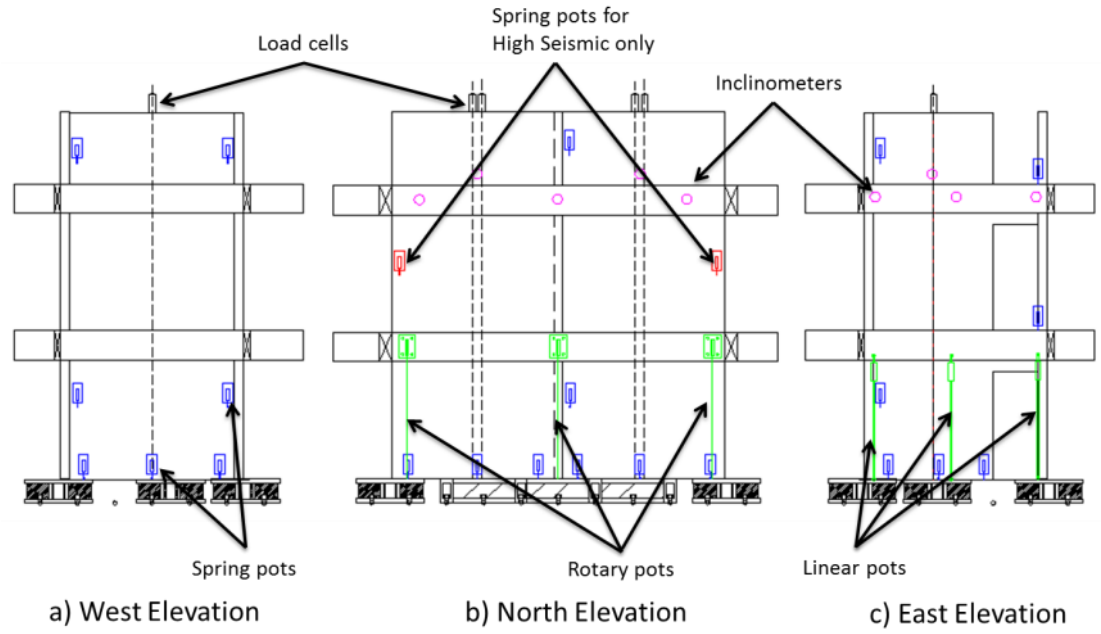

Figure B-2: Position of spring potentiometers, inclinometers and additional rotary potentiometers used during testing

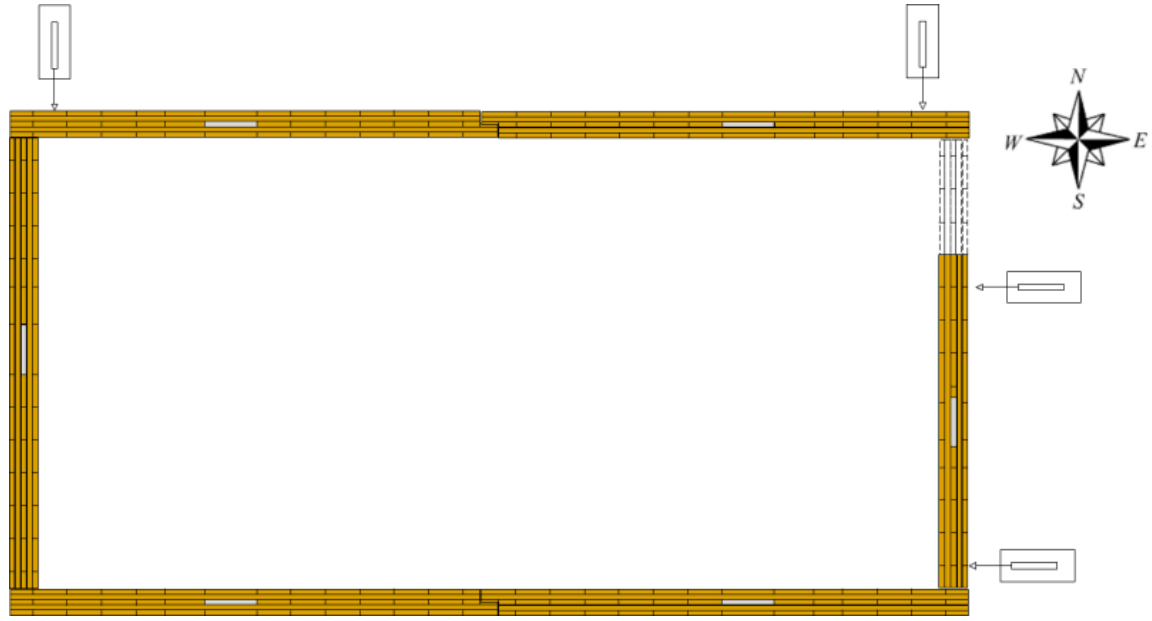

c) Original layout

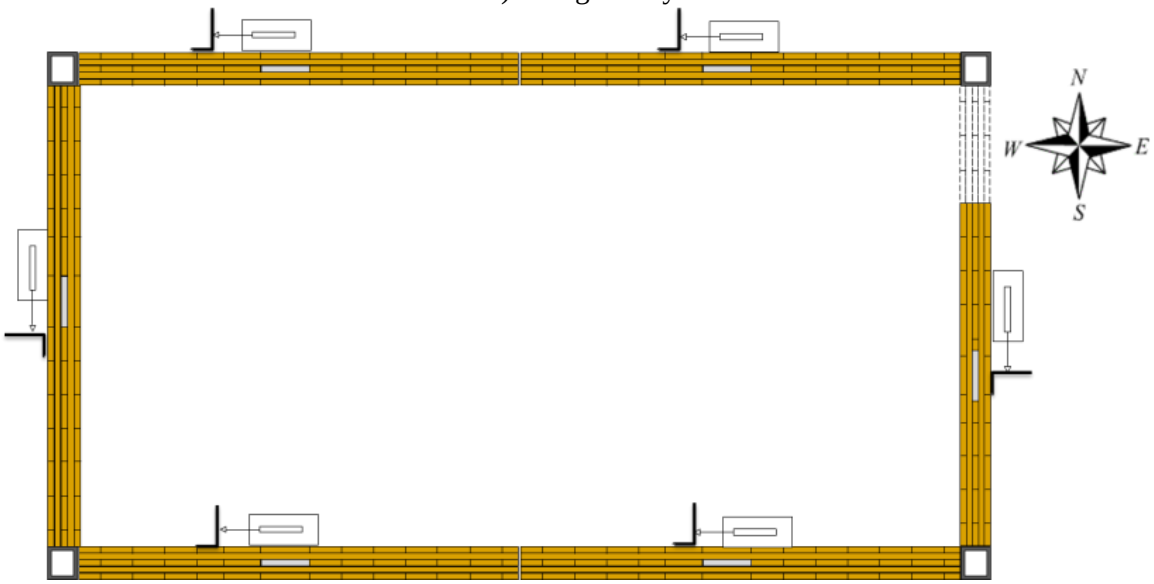

d) Modified layout

Figure 0-3: Position of spring potentiometers measuring slip

Figure 0-4: Instrumentation measuring uplift at the base of the East wall, with doorway openings

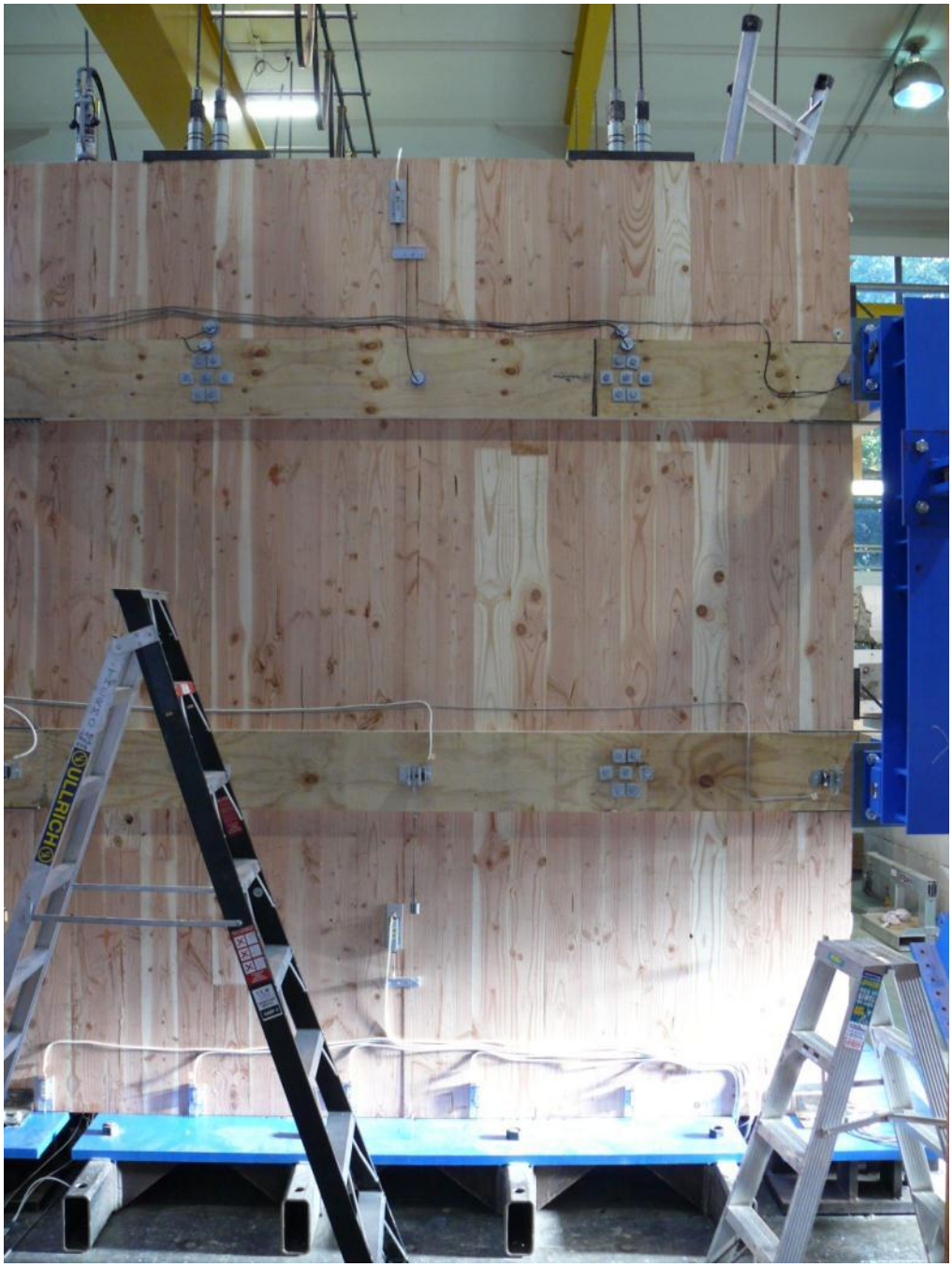

Figure 0-5: Instrumentation measuring uplift at the base of the South coupled walls and rotary potentiometers measuring beam deflection

a)

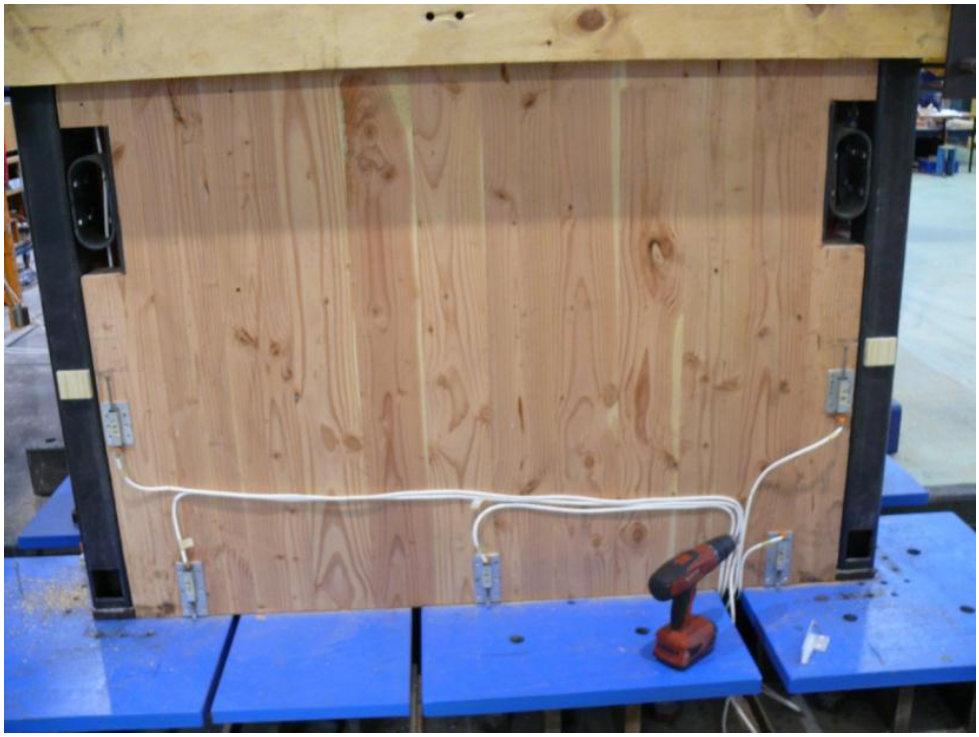

b)

Figure 0-6: West wall, a) potentiometers measuring relative movement at the top of the panels, b) uplift potentiometers

Figure 0-7: South coupled walls, a) uplift potentiometers, b) inclinometers measuring the rotation of the loading beam and walls

APPENDIX C: OBSERVED BEHAVIOUR

This Appendix shows typical behaviour of elements, for the Low Seismic and High Seismic specimens, during testing.

C.1. Low Seismic

C.1.1: Low Seismic Test 1: Low PT, 3 screws, max 1.5%

a)

b)

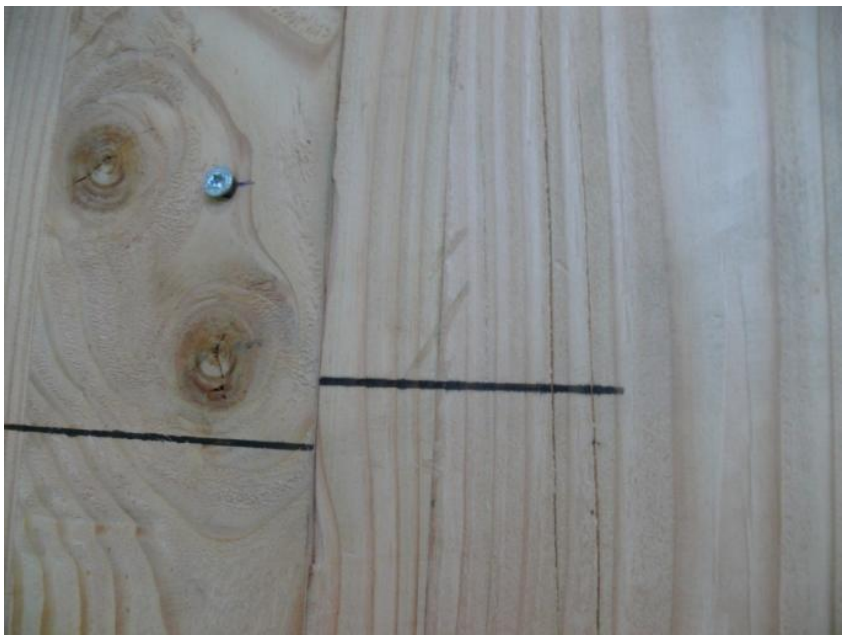

Figure C-25: Relative movement between coupled walls from Test 1 at 1.5% drift at a) the base of the walls, b) mid-height up the wall

Figure C-26: Behaviour of loading beams during Test 1 at 1.5% drift

C.1.2: Low Seismic Test 2: Low PT, 20 screws, max 0.5%

a)

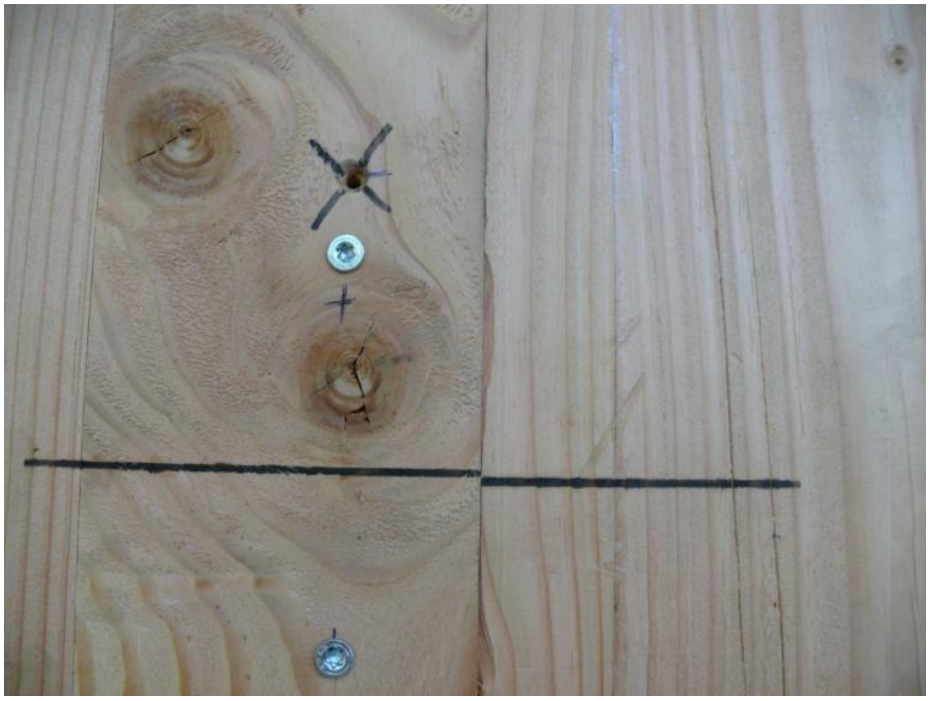

b)

Figure C-27: Rocking of walls during Test 2 for a) mid height between the coupled walls, b) uplift at the base of the East wall at 0.5% drift

C.1.3: Low Seismic Test 3: High PT, 3 screws, max 1.5%

a)

b)

Figure C-28: Test 3, a) uplift at the base of the coupled walls, b) deformation of shear key at the toe of the coupled walls at 1.5% drift

C.1.4: Low Seismic Test 4: High PT, 3 screws, bi-directional max 1.5%

a)

b)

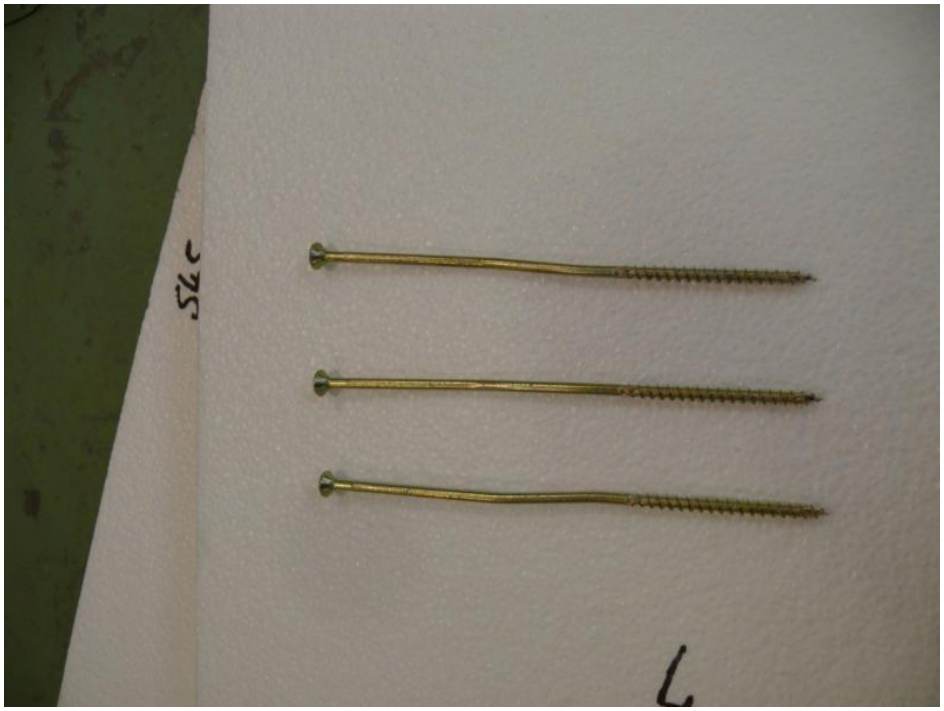

Figure C-29: a) Uplift of coupled walls during Test 4 at 1.25% drift, b) deformation of screws after Test 4

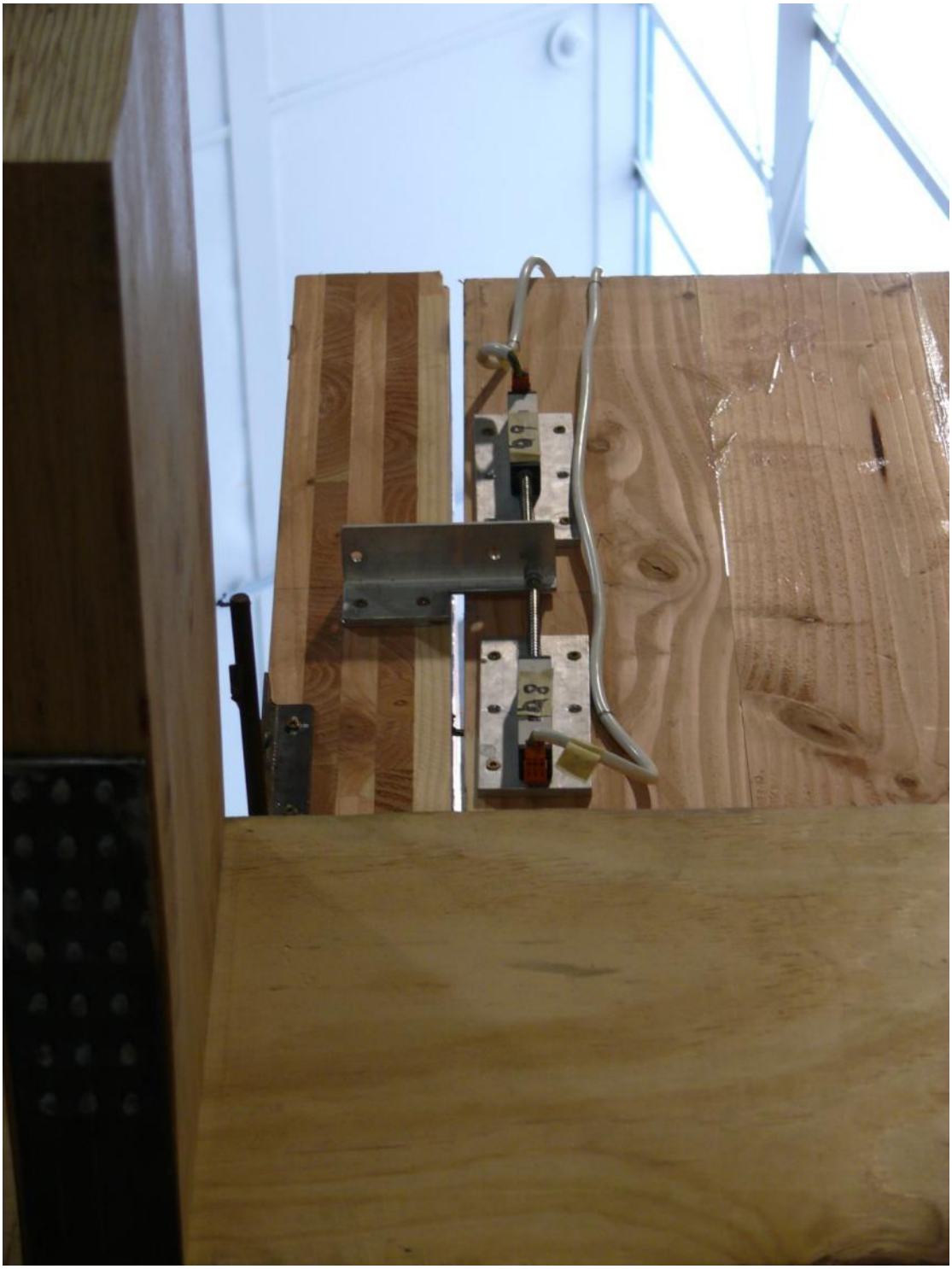

Figure C-30: Separation at the top of the walls in the South East corner of the stairwell during Test 4

C.1.5: Low Seismic Test 5: High PT, 20 screws, max 1.5%

Figure C-31: Sliding at the base of the coupled walls, leaving a gap between the edge of the wall and the shear key, during Test 5

Figure C-32: Cushing of the toe of the wall, and deformation of the shear key during Test 5

C.1.6: Low Seismic Test 6: High PT, 3 screws, bi-directional max 1.5%

Figure C-33: Separation of perpendicular walls during bi-directional clover-leaf from Test 6

Figure C-34: Gap behind the heel of the wall, between the wall and the shear key, due to sliding during Test 6

C.2. High Seismic

C.2.1. High Seismic Test 1: Low PT, 2 UFP's

Figure C-35: Uplift at the base of the West wall during Test 1 of the High Seismic Tests

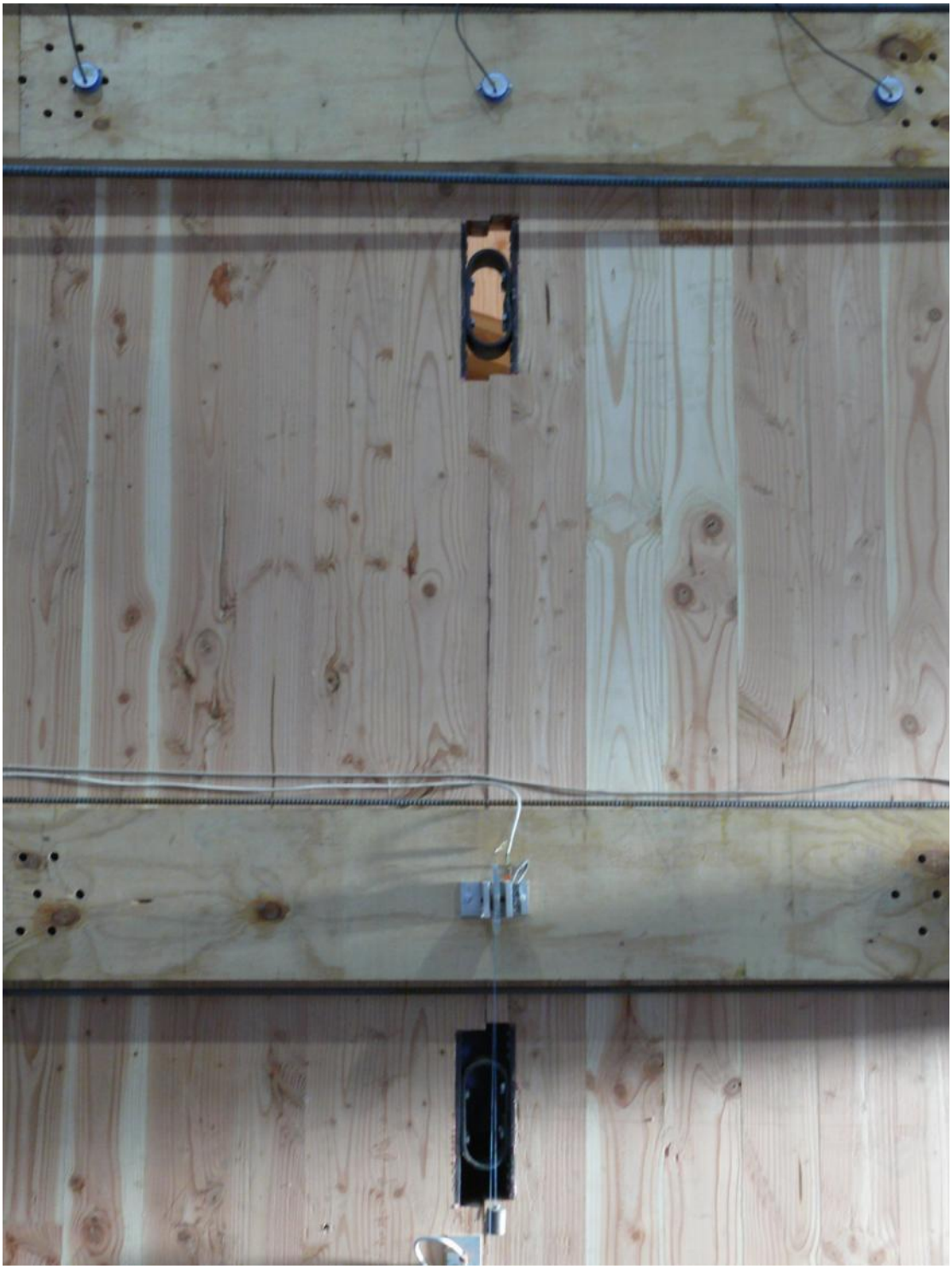

Figure C-36: Rocking of the coupled walls and deformation of the UFPs during Test 1

C.2.2: High Seismic Test 2, Low PT, 2 UFP's, Clover

Figure C-37: Gap between wall and corner column due to sliding of the foundation base block during Test 2

C.2.3: High Seismic Test 3, High PT, 2 UFP's

Figure C-38: Deformation of a UFP in the north coupled walls during Test 3

Figure C-39: Uplift at the base of the West wall during Test 3 at 1.25% drift

C.2.4: High Seismic Test 4: High PT, 1 UFP, X only

Figure C-40: Deformation of UFP during Test 4

C.2.5: High Seismic Test 5, High PT, 2 UFP's, Y direction only

Figure C-41: Uplift at the base of the West wall at 1.5% drift, during Test 5

Figure C-42: Deformation of a UFP on the West wall during Test 5 at 1.5% drift

C.2.6: High Seismic Test 6: High PT, no UFP's, Y only (slip measured)

Figure C-43: Uplift at the base of the West wall during Test 6 with the UFPs removed

Figure C-44: Global displacement of the West wall during Test 6. The loading beams remain approximately level at 3% drift

C.2.7: High Seismic Test 7: High PT, no UFP's, X direction only

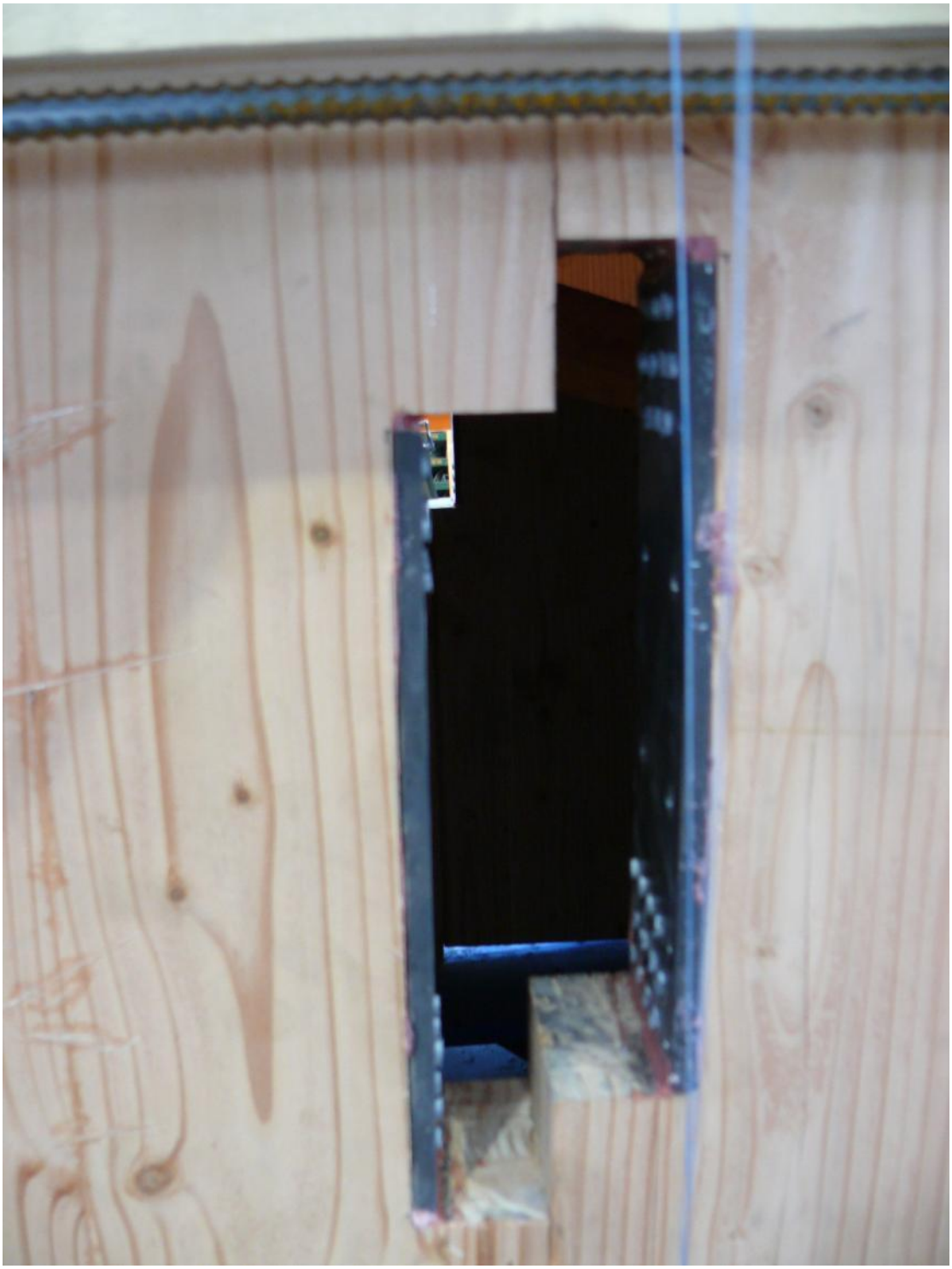

Figure C-45: Relative movement between the coupled walls during Test 7 at 3% drift

Figure C-46: Global displacement of the North coupled walls during Test 7. The loading beams remain approximately level at 3% drift

APPENDIX D: RAW TEST RESULTS

This Appendix shows the raw test results of the Low Seismic and High Seismic specimens. The main results considered, are the global hysteretic response.

D.1 Low Seismic Test Results

D.1.1 Test 1: Low PT, 3 screws, max 1.5%

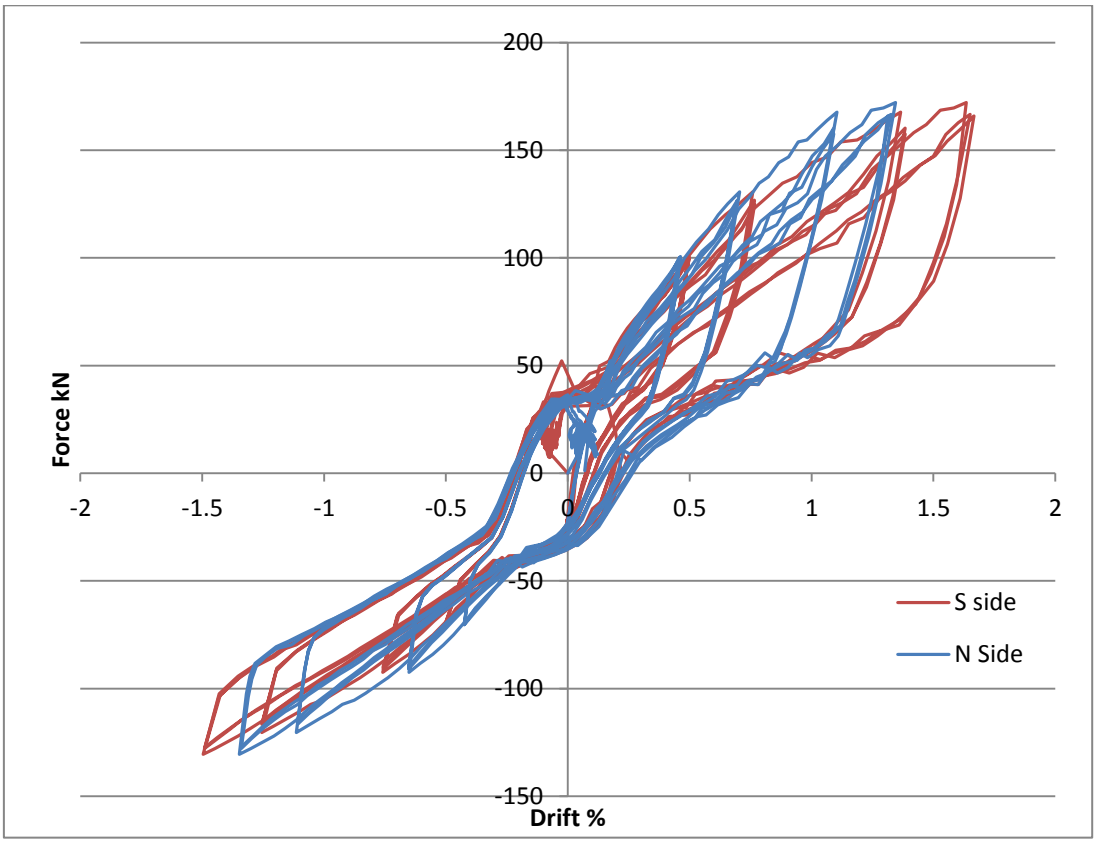

Figure D-1: Hysteretic behaviour of the North and South coupled walls from Test 1 (Low Seismic), un-adjusted

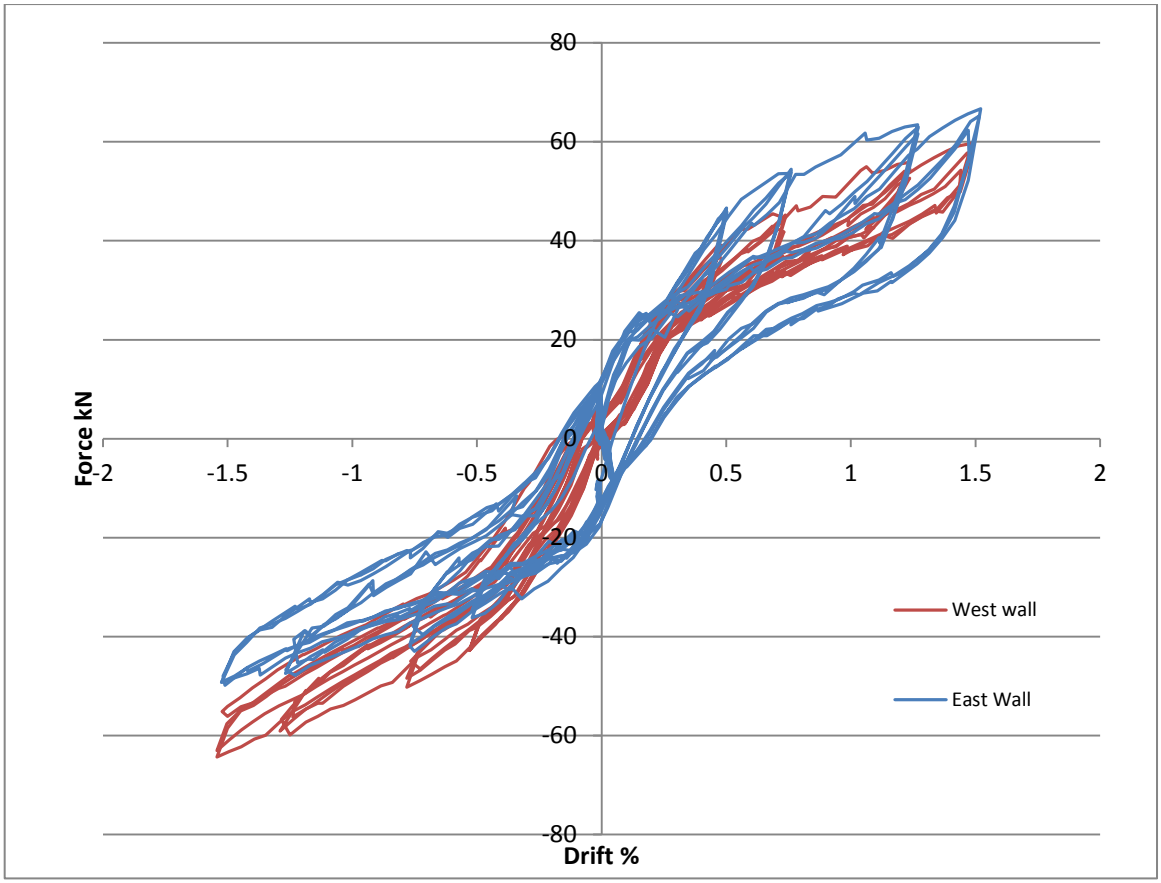

Figure D-2: Hysteretic behaviour of the East and West single walls from Test 1 (Low Seismic), un-adjusted

D.1.2 Test 2: Low PT, 20 screws, max 0.5%

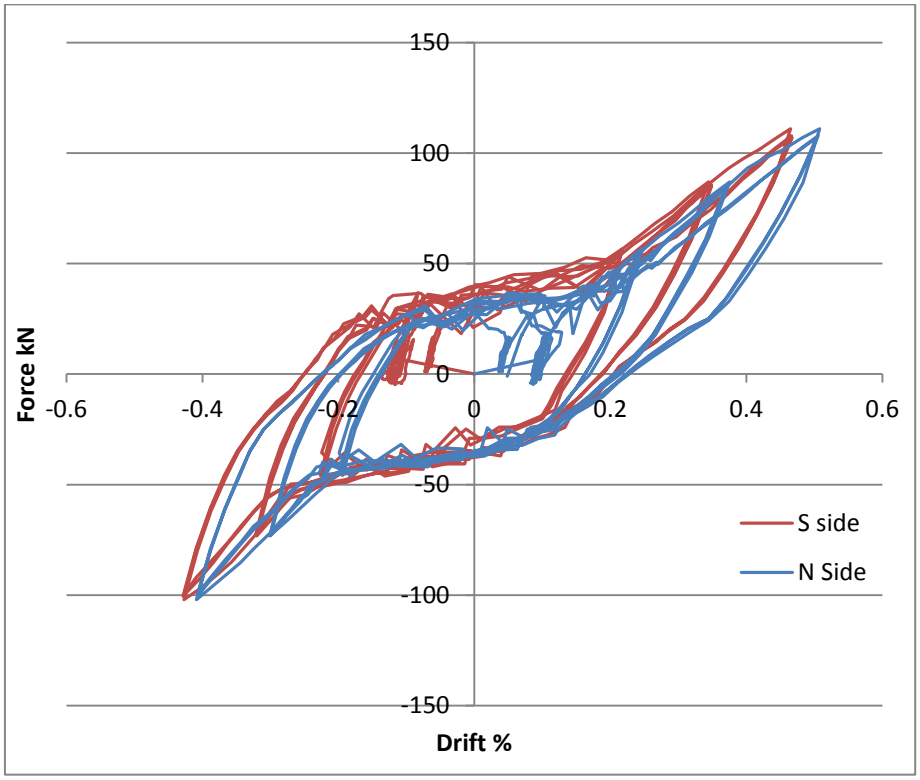

a)

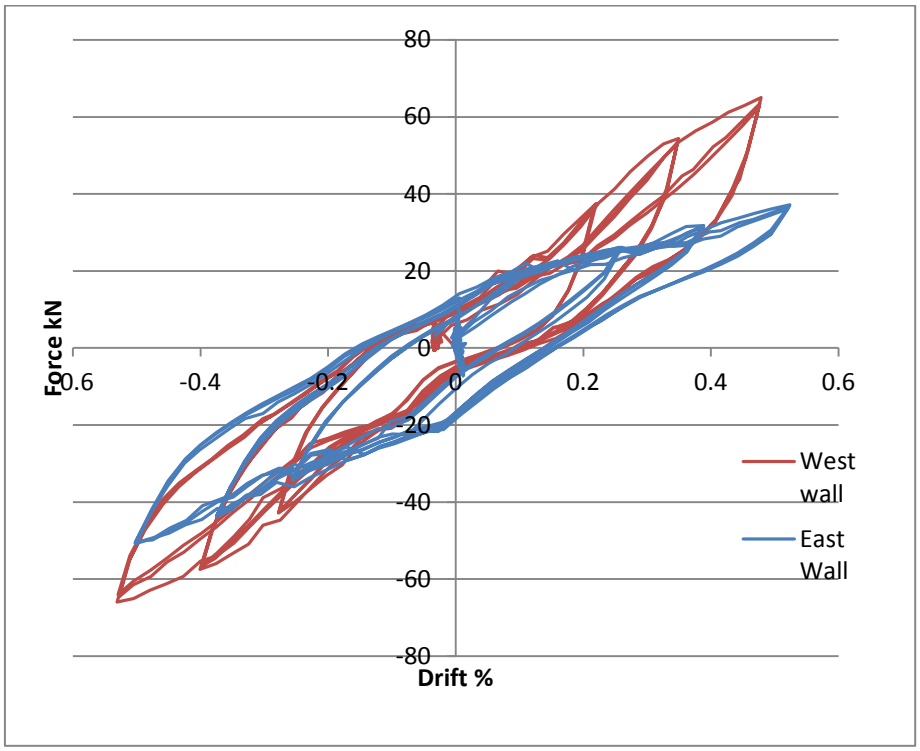

b)

Figure D-3: Un-adjusted hysteretic behaviour of a) the North and South coupled walls, b) the East and West single walls, from Test 2 (Low Seismic)

D.1.3 Test 3: High PT, 3 screws, max 1.5%

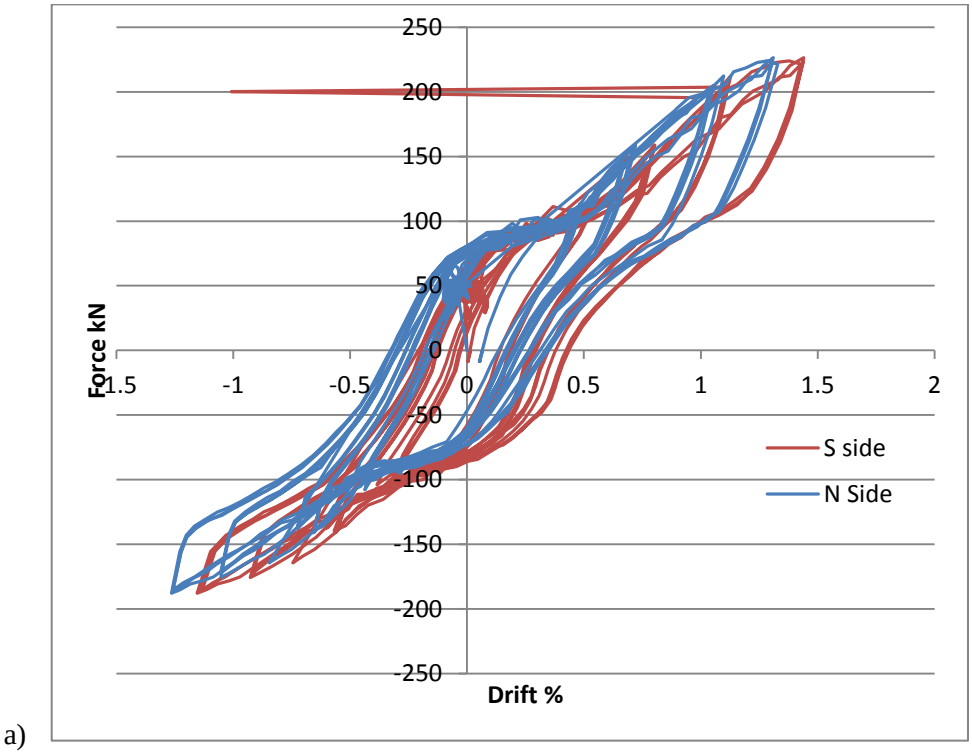

a)

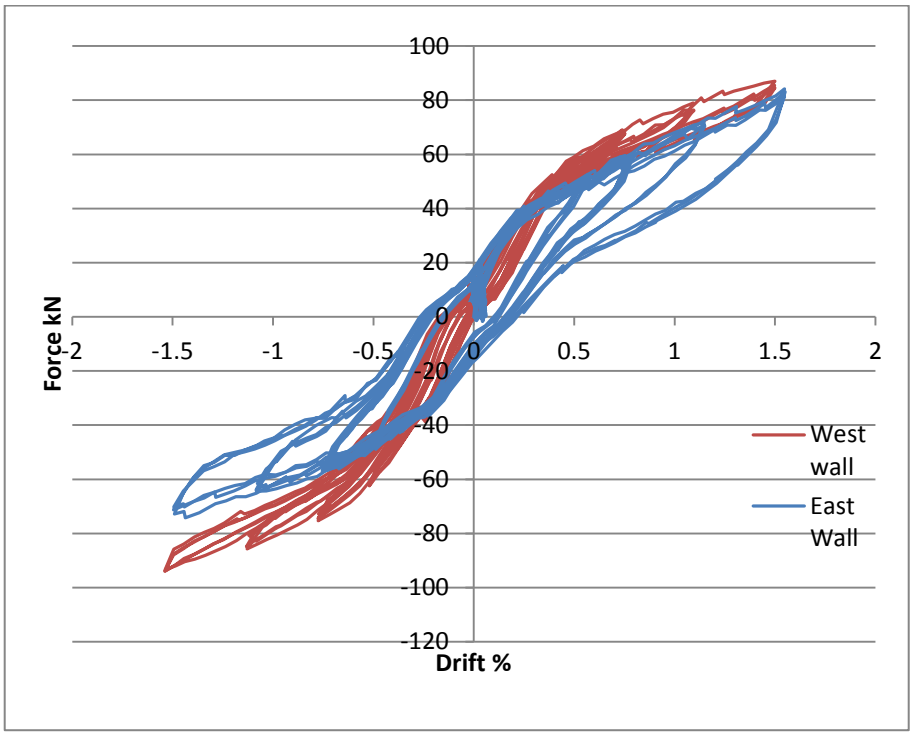

b)

Figure D-4: Un-adjusted hysteretic behaviour of a) the North and South coupled walls, b) the East and West single walls, from Test 3 (Low Seismic)

D.1.4 Test 4: High PT, 3 screws, bi-directional max 1.5%

a)

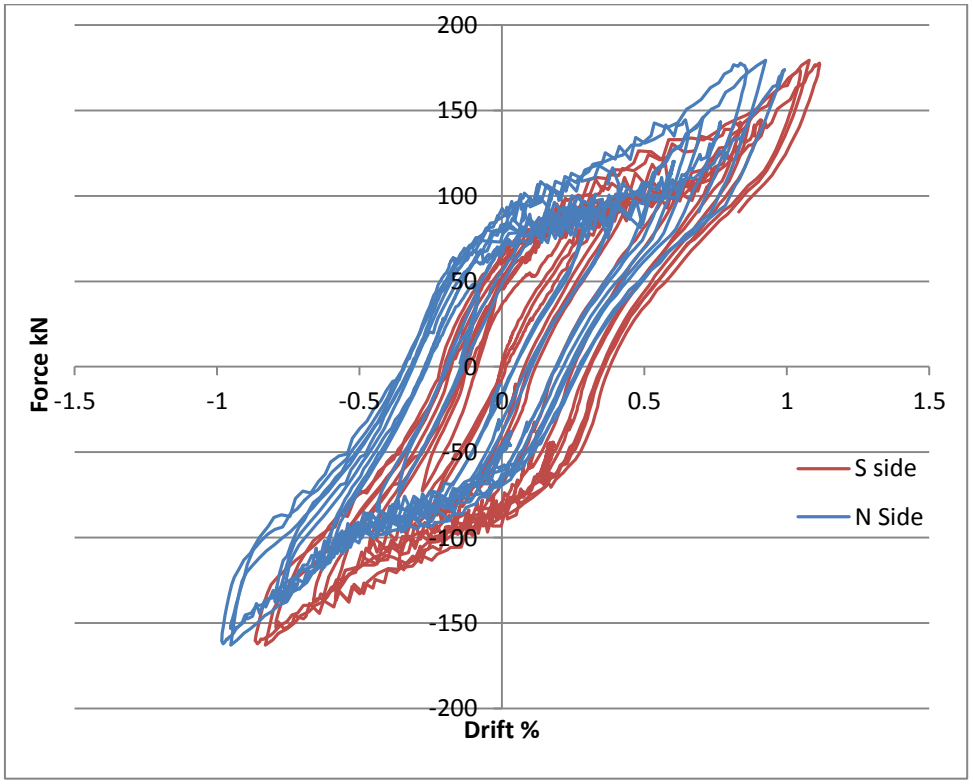

b)

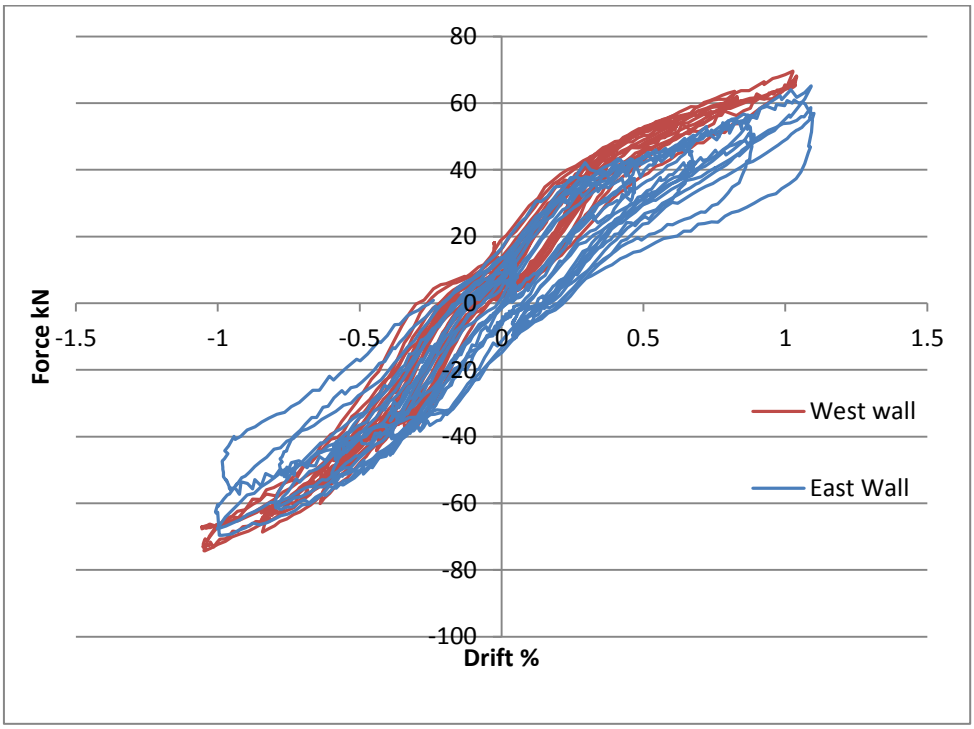

Figure D-5: Un-adjusted hysteretic behaviour of a) the North and South coupled walls, b) the East and West single walls, from Test 4 (Low Seismic)

D.1.5 Test 5: High PT, 20 screws, max 1.5%

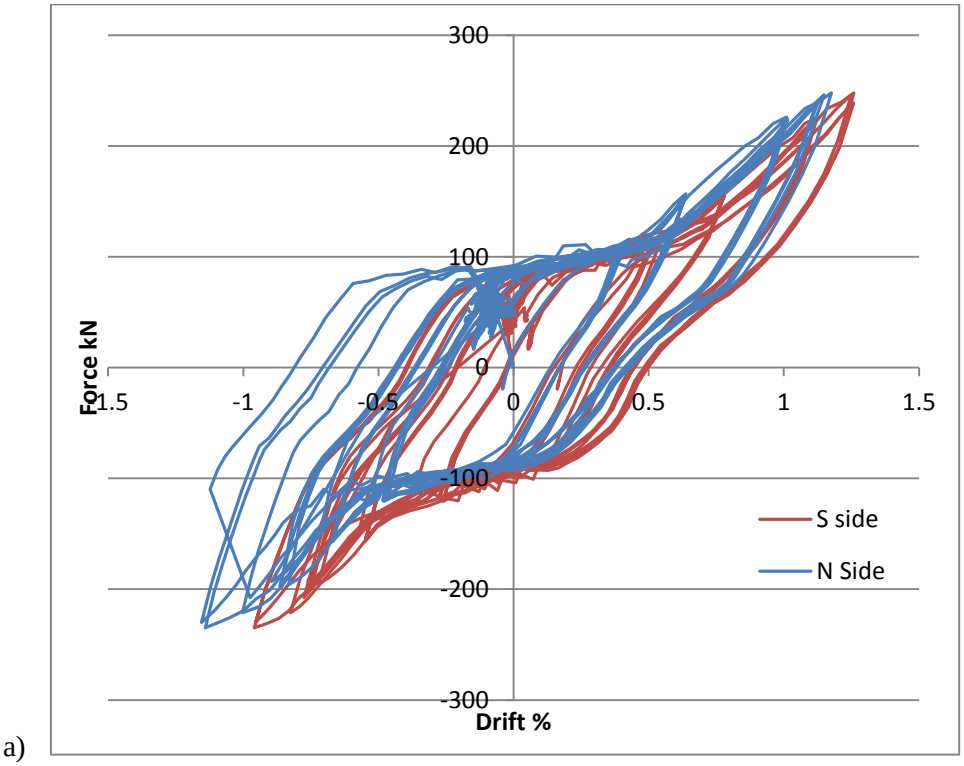

a)

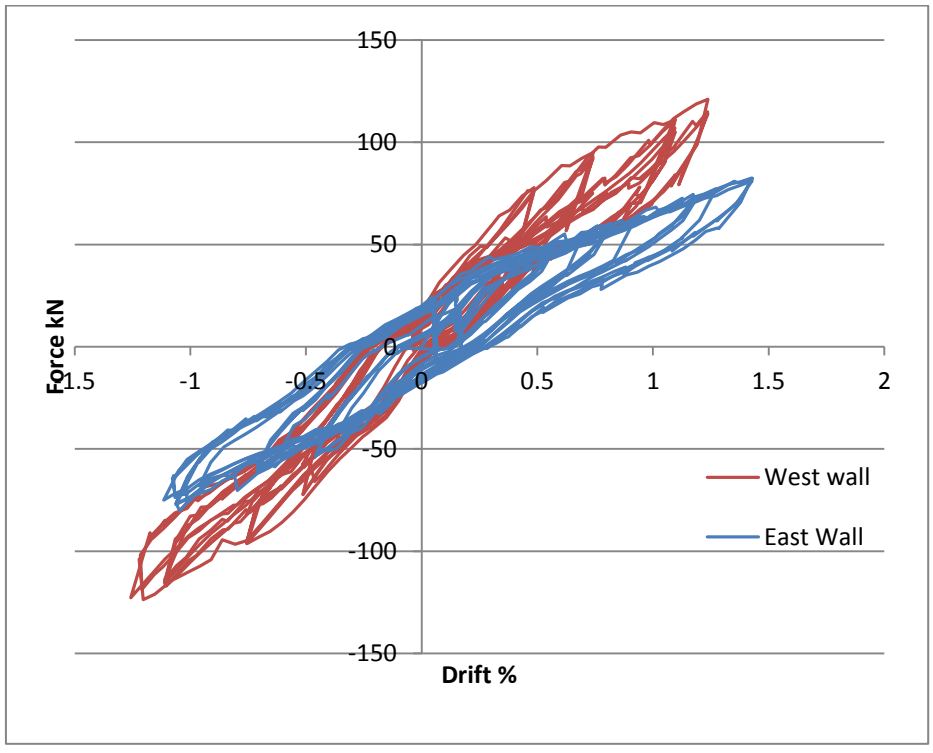

b)

Figure D-6: Un-adjusted hysteretic behaviour of a) the North and South coupled walls, b) the East and West single walls, from Test 5 (Low Seismic)

D.1.6 Test 6: High PT, 3 screws, bi-directional max 1.5%

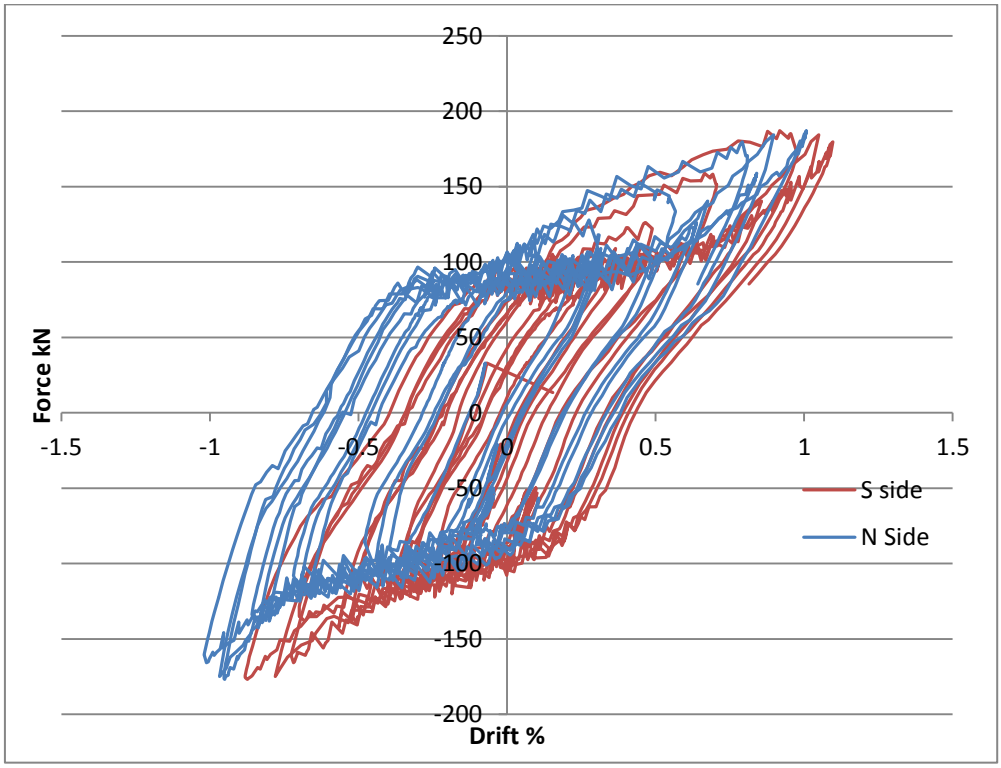

a)

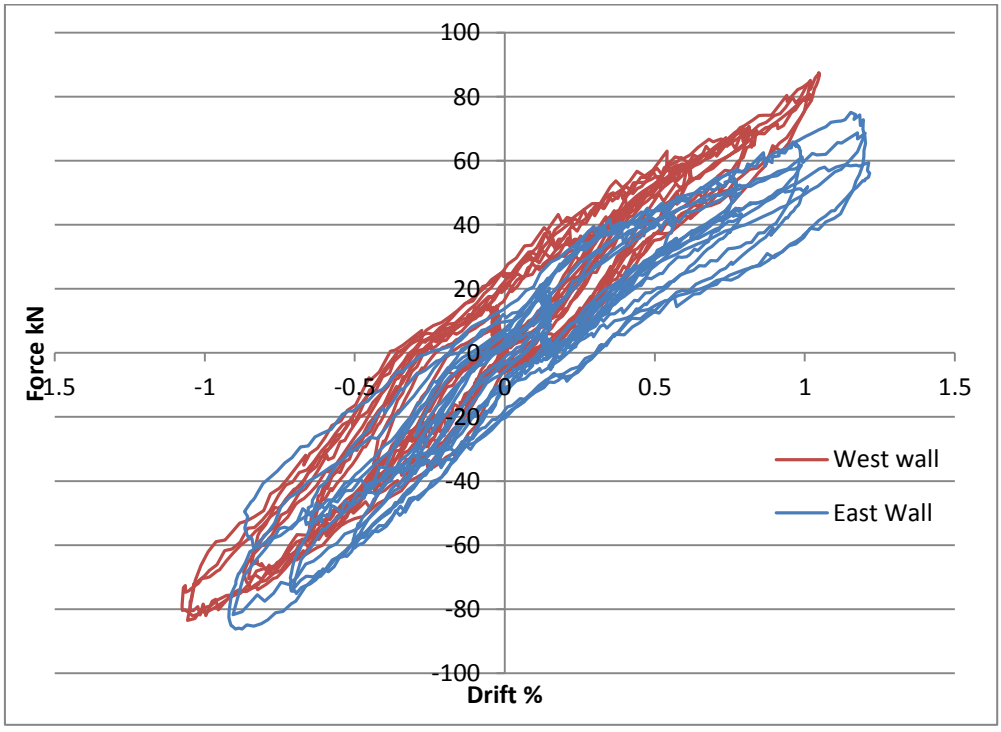

b)

Figure D-7: Un-adjusted hysteretic behaviour of a) the North and South coupled walls, b) the East and West single walls, from Test 6 (Low Seismic)

D.2 High Seismic Test Results

D.2.1 Test 1: Low PT, 2 UFP's, max 1.5%

a)

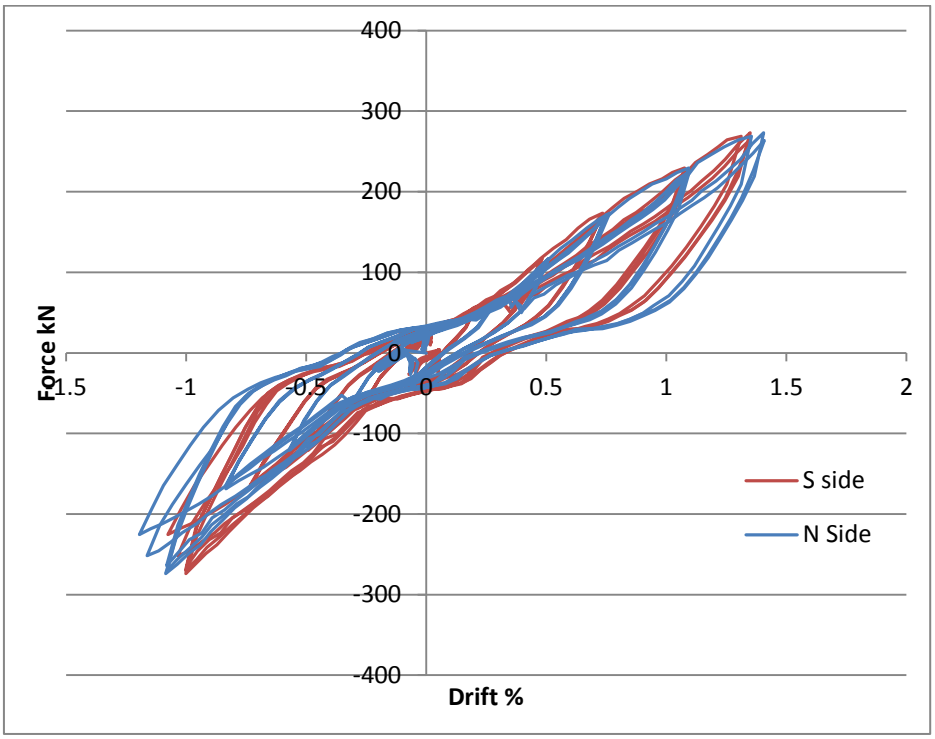

b)

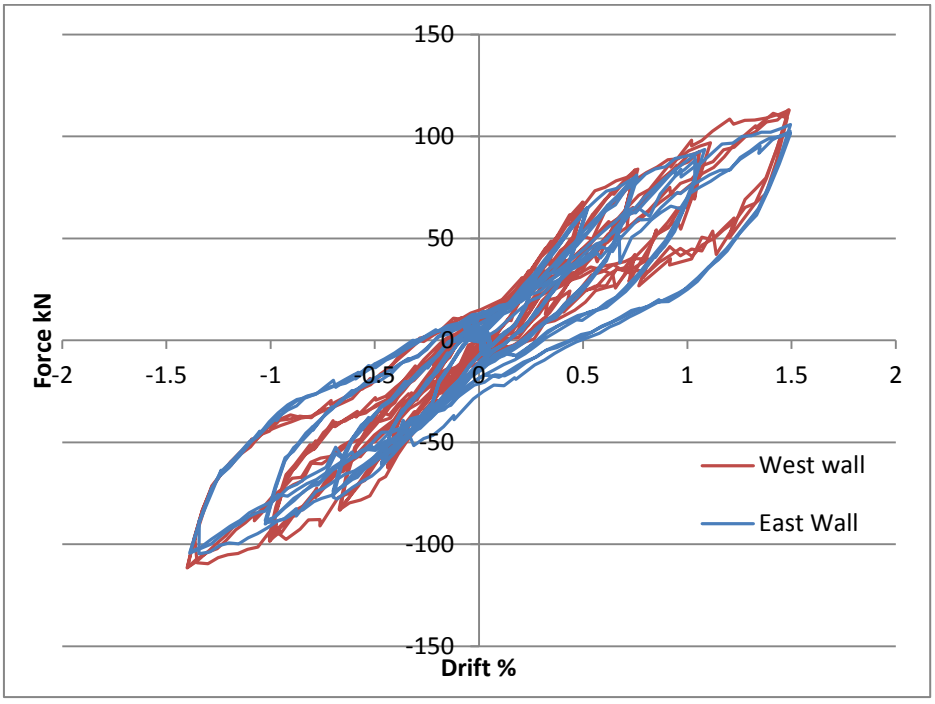

Figure D-8: Un-adjusted hysteretic behaviour of a) the North and South coupled walls, b) the East and West single walls, from Test 1 (High Seismic)

D.2.2 High Seismic Test 2: Low PT, 2 UFP's, bi-directional clover leaf, max 1.25%

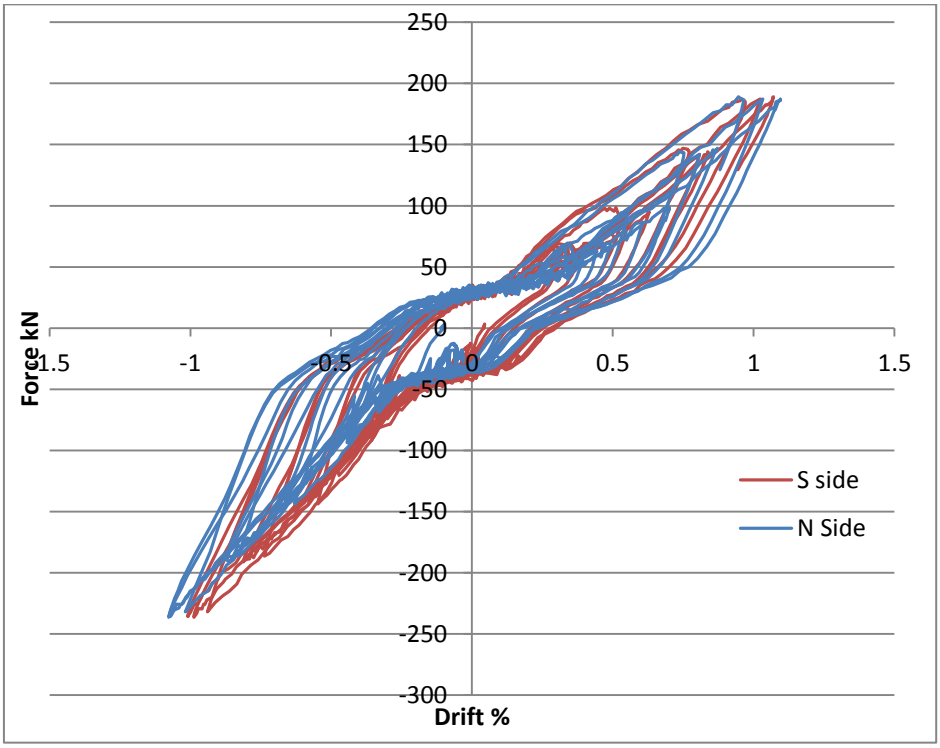

a)

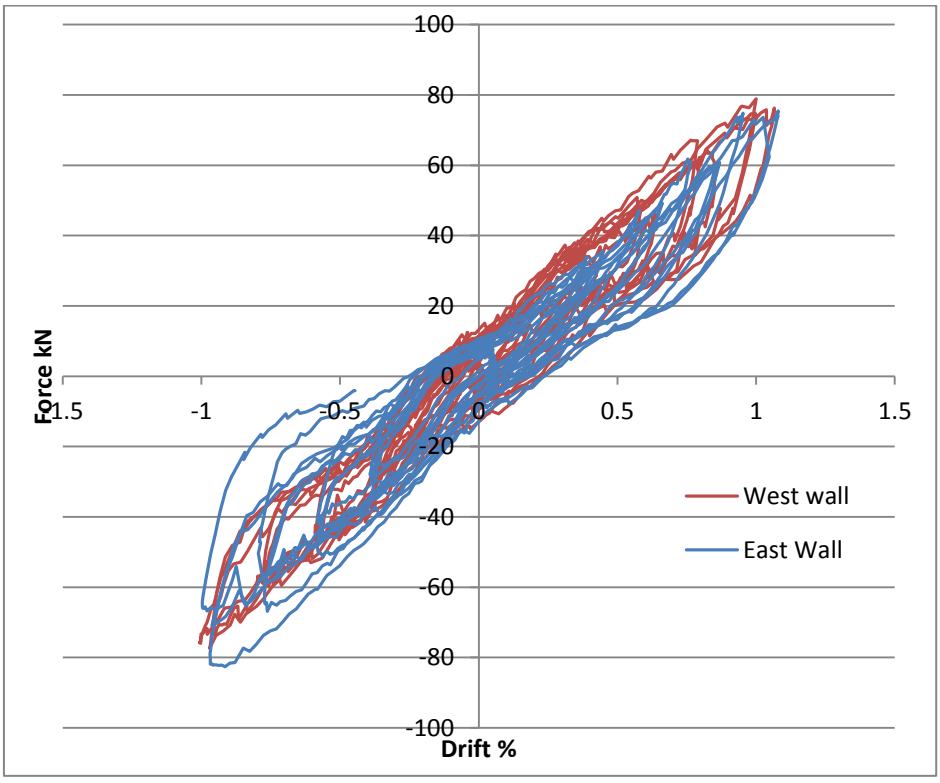

b)

Figure D-9: Un-adjusted hysteretic behaviour of a) the North and South coupled walls, b) the East and West single walls, from Test 2 (High Seismic)

D.2.3 High Seismic Test 3: High PT, 2 UFP's, max 1.25%

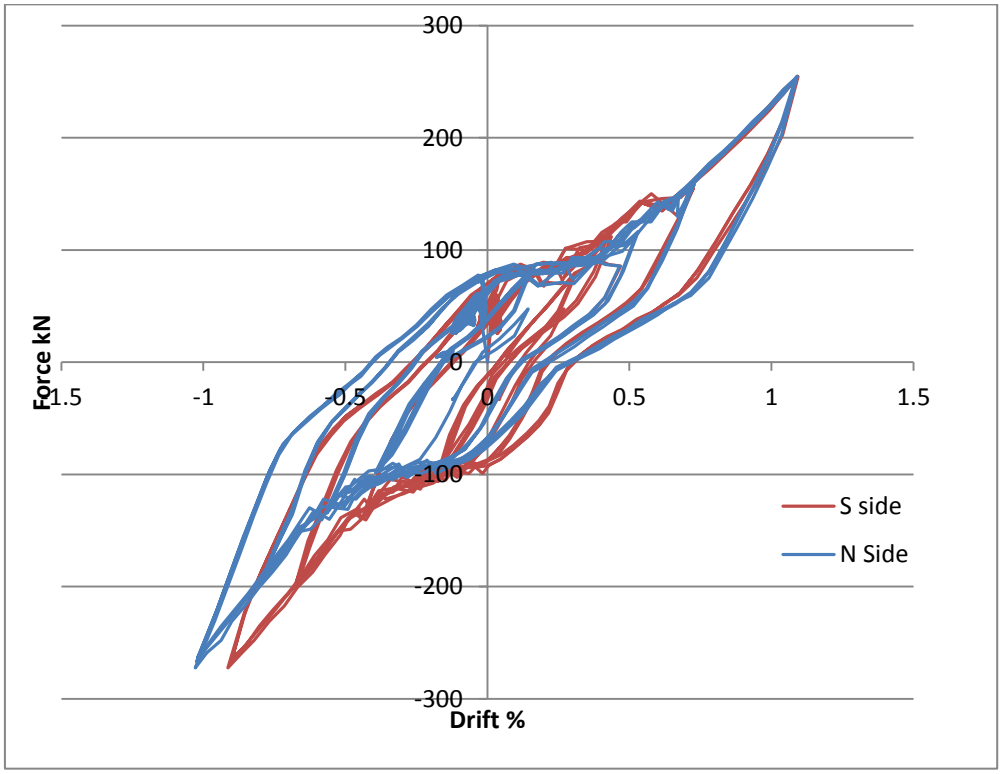

a)

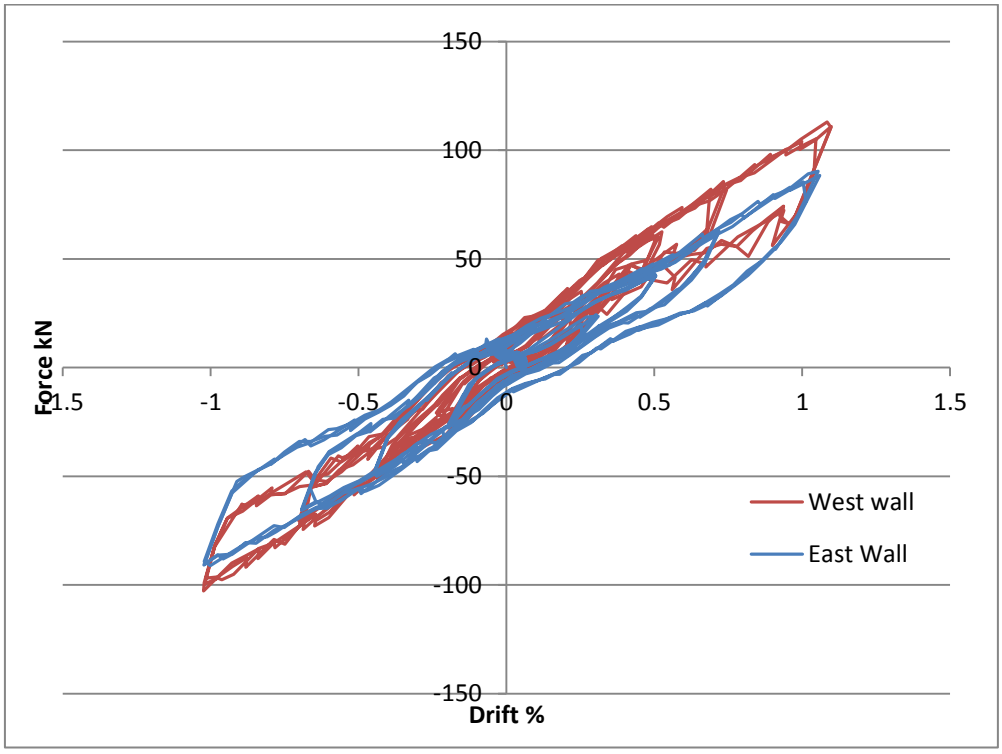

b)

Figure D-10: Un-adjusted hysteretic behaviour of a) the North and South coupled walls, b) the East and West single walls, from Test 3 (High Seismic)

D.2.4 High Seismic Test 4: High PT, 1 UFP, X only, max 1.25%

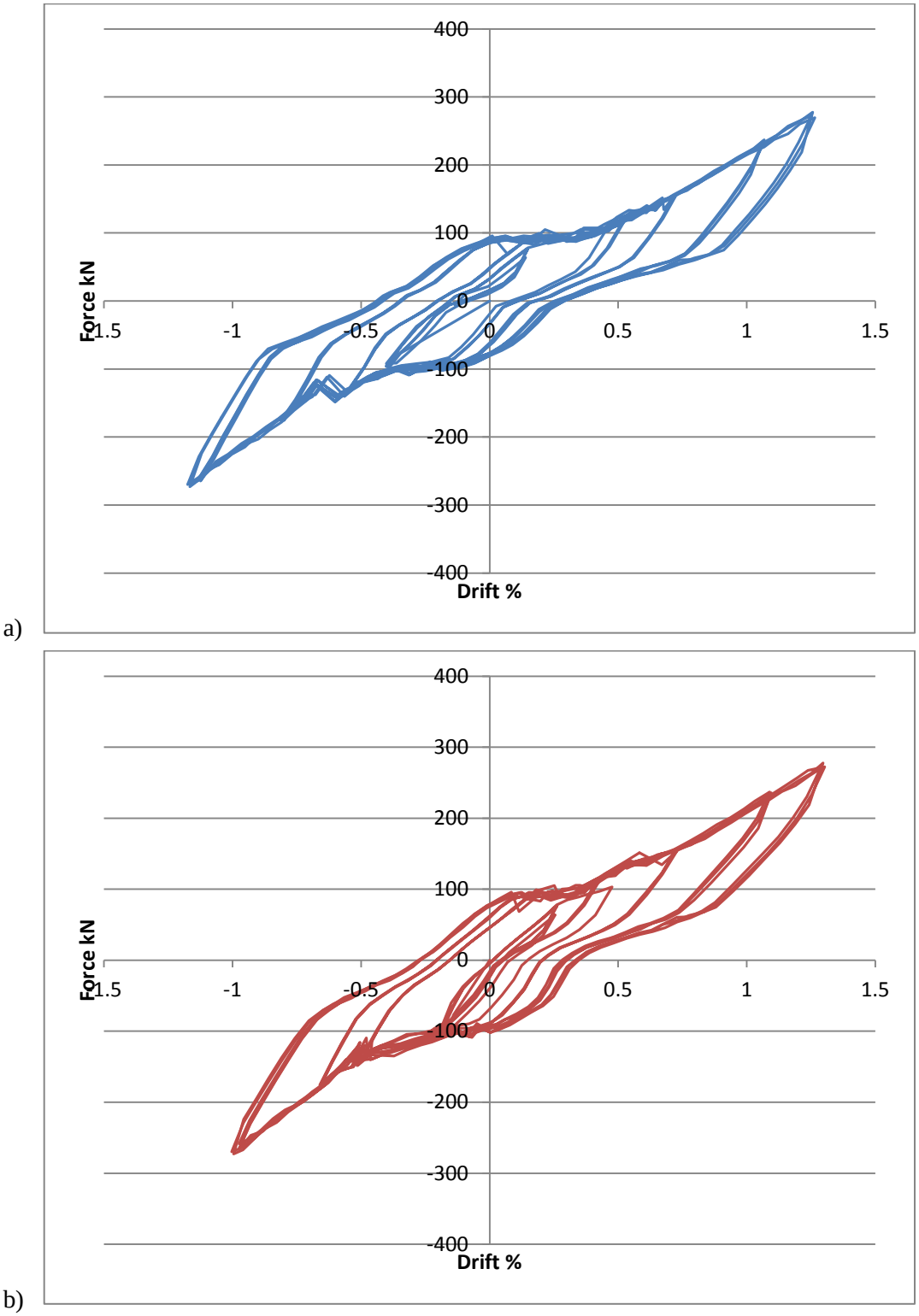

Figure D-11: Un-adjusted hysteretic behaviour from Test 4, X only (High Seismic) of a) the North coupled walls and b) South coupled walls

D.2.5 High Seismic Test 5: High PT, 2 UFP's, Y direction only, max 1.5%

a)

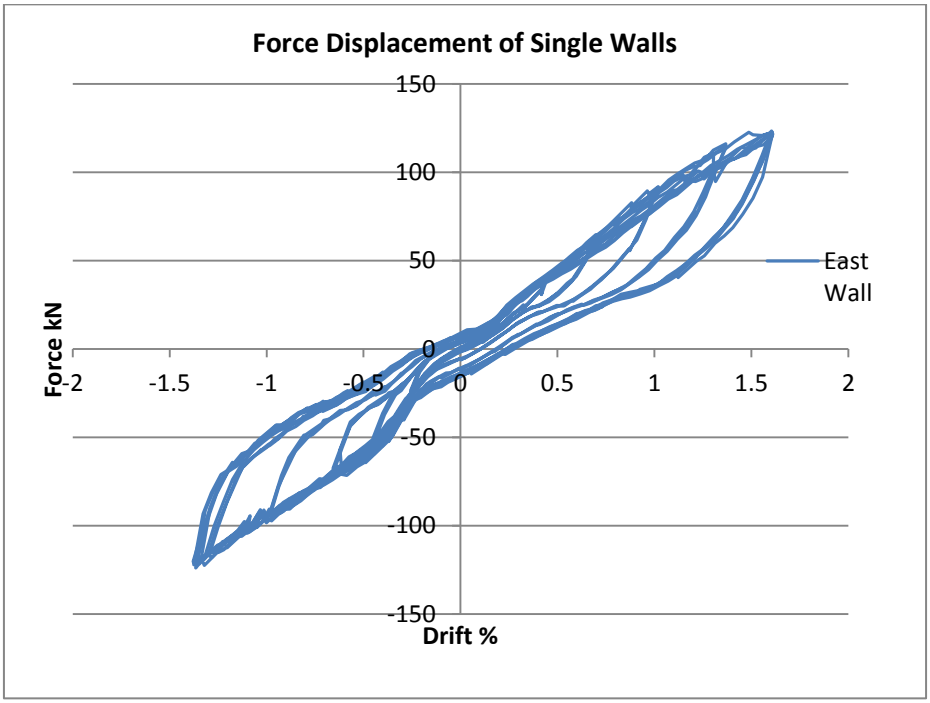

b)

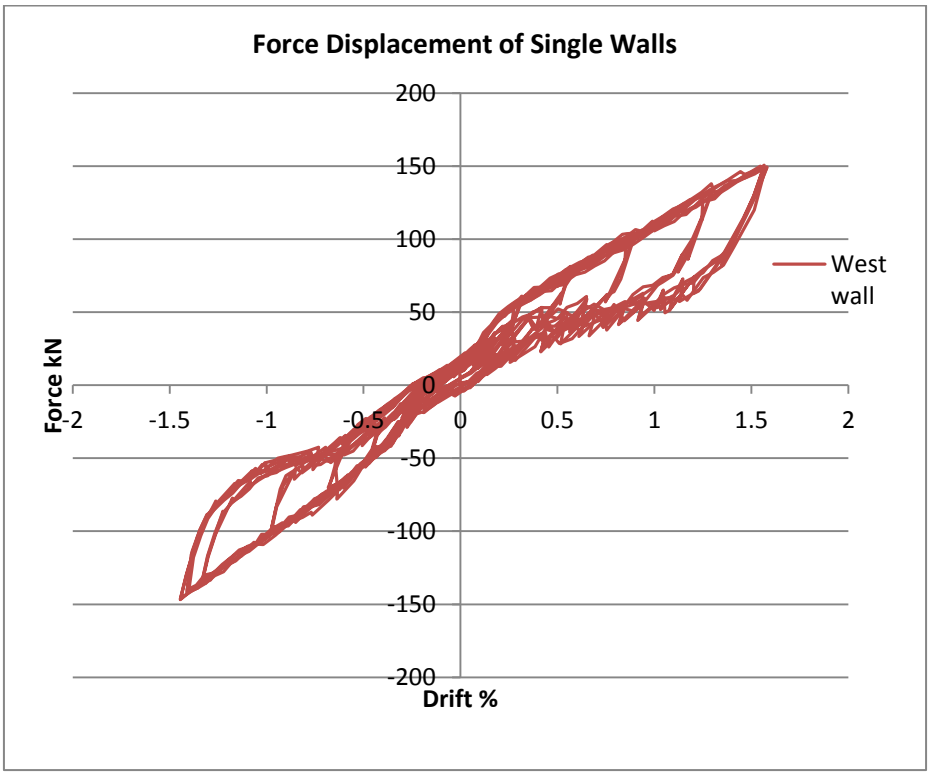

Figure D-12: Un-adjusted hysteretic behaviour from Test 5, Y only (High Seismic), of a) the East single wall and b) West single wall

D.2.6 High Seismic Test 6: High PT, no UFP's, Y only, max 3.5%

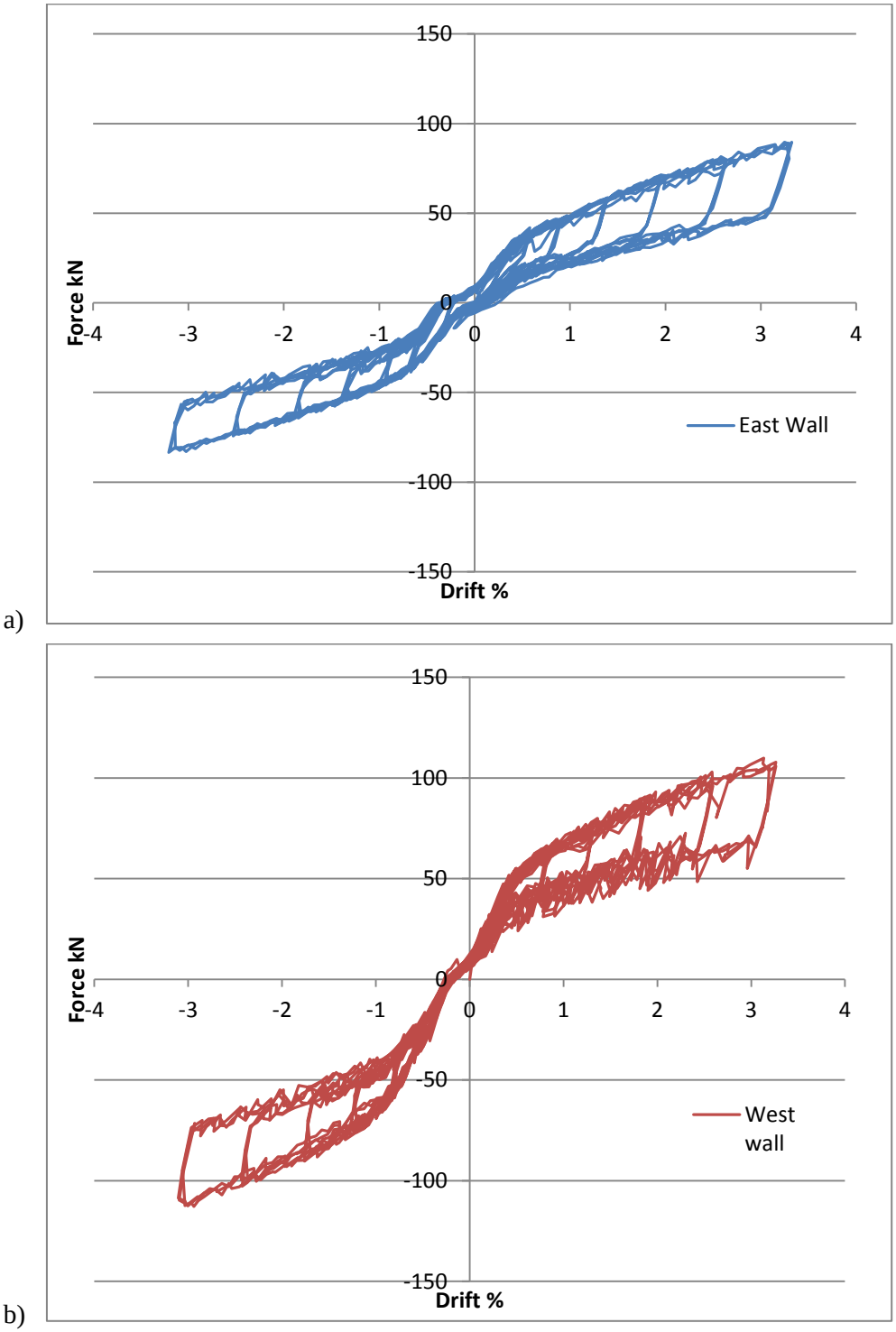

Figure D-13: Un-adjusted hysteretic behaviour from Test 6, Y only (High Seismic), of a) the East single wall and b) West single wall

D.2.7 High Seismic Test 7: High PT, no UFP's, X direction only, max 3%

a)

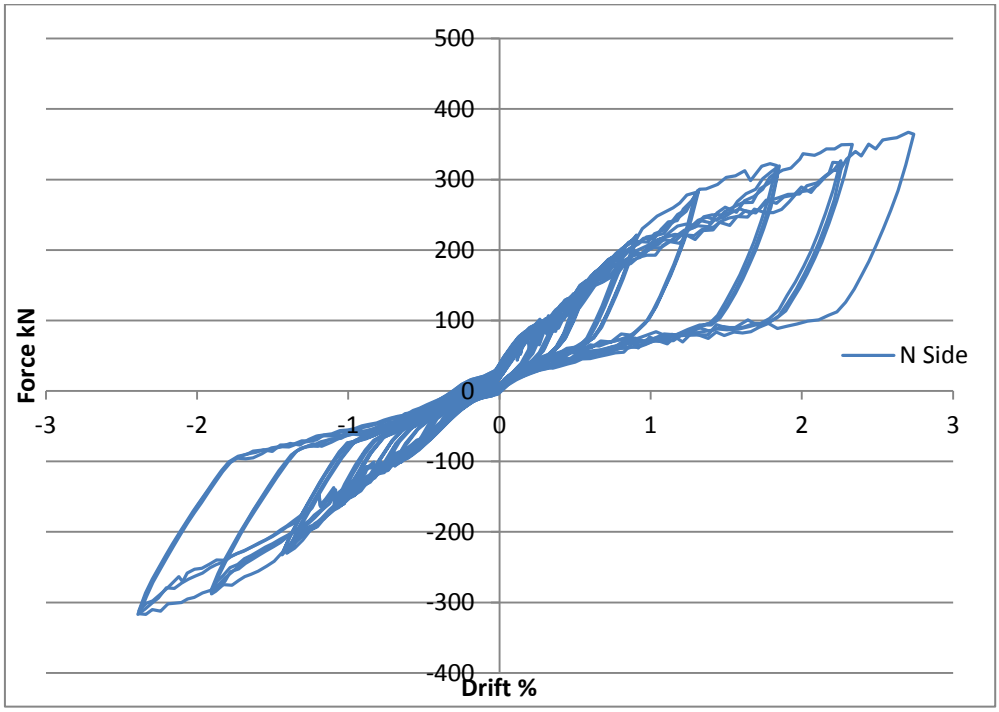

b)

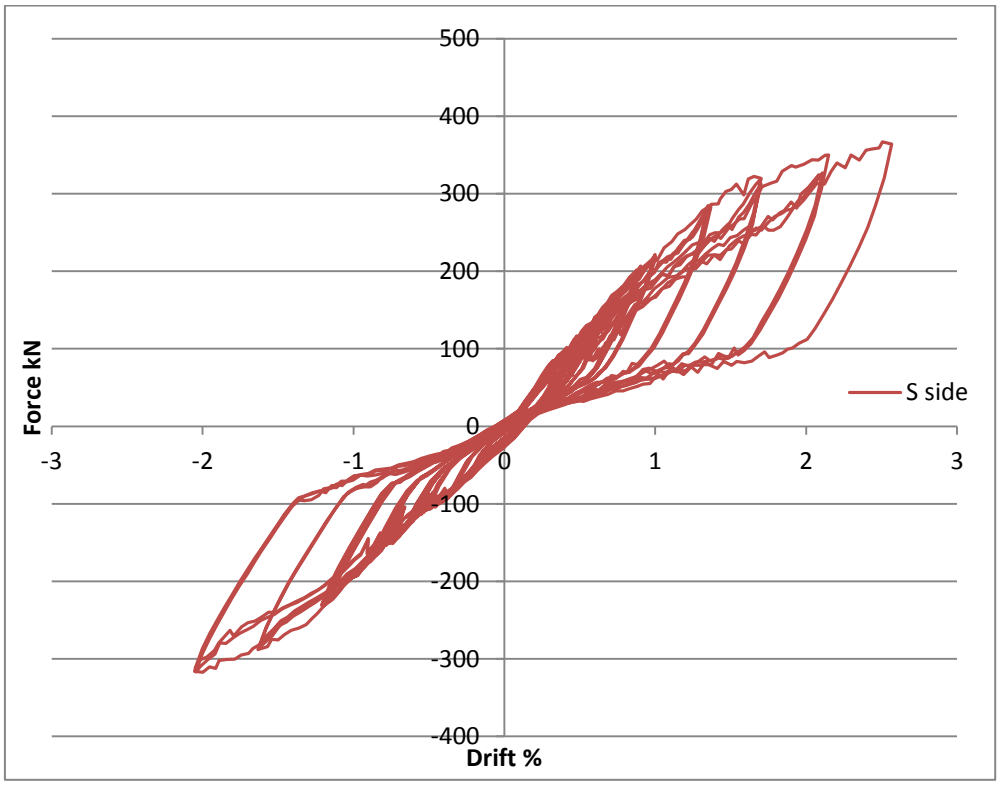

Figure D-14: Un-adjusted hysteretic behaviour from Test 7, X only (High Seismic), of a) the North coupled walls and b) South coupled walls